

Diss. ETH No. 14905

**Exhumation of the northern Sub-Andean Zone of Ecuador and  
its source regions: a combined thermochronological and heavy  
mineral approach**

A dissertation submitted to the  
SWISS FEDERAL INSTITUTE OF TECHNOLOGY ZURICH

For the degree of  
Doctor of Natural Sciences

Presented by

Geoffrey Modeste Henri, Ruiz  
D.E.A Tectonics, Université de Montpellier

Born May 8, 1973  
French

Accepted on the recommendation of

PD Dr. W. Winkler	ETH Zürich,	examiner
Dr. D. Seward	ETH Zürich,	co-examiner
Prof. J-P. Burg	ETH Zürich,	co-examiner
Dr. E. Jaillard	Université Grenoble-IRD	co-examiner

2002



# Table of contents

*Acknowledgments*

*Abstract*

*Resumen*

*Zusammenfassung*

## Chapter 1. Introduction

1.1. Geographical setting	15
1.2. Geological overview	17
1.3. Previous work and limitations	20
1.4. Scope of this study	21

## Chapter 2. Geological framework

2.1. The northern Ecuadorian Sub-Andean Zone	23
2.2. Lithostratigraphy and sedimentological observations	27
2.2.1. Basement of the northern SAZ	28
2.2.1.1. <i>The Abitagua batholith</i>	28
2.2.1.2. <i>The Misahualli volcanics</i>	29
2.2.1.3. <i>The Upano and Paradalarga units</i>	30
2.2.1.4. <i>The Pumbuiza Fm.</i>	31
2.2.2. Sedimentary series	
2.2.2.1. <i>Hollin Fm.</i>	33
2.2.2.2. <i>Napo Fm.</i>	37
2.2.2.3. <i>Tena Fm.</i>	41
2.2.2.4. <i>Tiyuyacu Fm.</i>	44
2.2.2.5. <i>Orteguaza Fm.</i>	49
2.2.2.6. <i>Chalcana Fm.</i>	51
2.2.2.7. <i>Arajuno Fm.</i>	52
2.2.2.8. <i>Chambira and Curaray Fms.</i>	54
2.2.2.9. <i>Mesa and Mera Fms.</i>	56
2.3. Tectonic subsidence analysis	58
2.3.1. Introduction/dataset	58
2.3.2. Localisation	75
2.3.3. Backstripping methodology	76
2.3.4. Results	78

## Chapter 3. Thermochronology of the northern SAZ

3.1. Introduction to Fission-track analysis	65
3.1.1. History of fission-track analysis	65
3.1.2. Temperature of closure ( $T_c$ ) and partial annealing zone (PAZ)	66
3.1.3. Annealing	66
3.2. Applications	67
3.3. Methodology	68

3.3.1. Sample preparation	68
3.3.2. Microscope analysis	70
3.4. Results and interpretation	72
3.4.1. Abitagua batholith or the Cordillera de Huacamoyos	72
3.4.1.1. <i>Apatite fission-track ages (AFTA) and track length measurements</i>	72
3.4.1.2. <i>Zircon fission-track (ZFT) ages</i>	72
3.4.1.3. <i>T-t modelling</i>	73
3.4.1.4. <i>Interpretation</i>	77
3.4.2. Misahualli Fm.	83
3.4.2.1. <i>Apatite fission-track (AFT) ages</i>	83
3.4.2.2. <i>Zircon fission-track (ZFT) ages</i>	84
3.4.2.3. <i>T-t modelling</i>	86
3.4.2.4. <i>Interpretation</i>	88
3.4.3. Others Formations	91
3.4.3.1. <i>Paradalarga and Upano units</i>	91
3.4.3.2. <i>Pumbuiza Fm.</i>	97
3.4.4. Reset detrital age	87
3.5. Synthesis	99
Chapter 4. Provenance	
4.1. Provenance of detrital grains (heavy minerals)	103
4.1.1. Introduction	103
4.1.2. Methodology	104
4.1.3. Results	105
4.2. Detrital Fission-Track analysis	110
4.2.1. Provenance role for detrital thermochronological ages	110
4.2.1.1. <i>Definitions</i>	110
4.2.1.2. <i>Assumptions</i>	115
4.2.1.3. <i>Empirical derivation (new methodology)</i>	117
4.2.2. Results	129
4.2.2.1. <i>Detrital zircon fission-track ages</i>	135
4.2.2.2. <i>Detrital apatite fission-track ages</i>	135
4.3. Interpretation	138
4.3.1. Stratigraphic ages	138
4.3.2. Provenance	144
Chapter 5. Geological evolution of the northern Ecuadorian Sub-Andean Zone and its source regions	155
Chapter 6. Future work	167
Chapter 7. Conclusions	169



References	171
Appendices	
3.1. Location and description of the samples	186
3.2. Radial plots for fission-track age determinations of the basement	188
4.1. Heavy mineral analyses	193
4.2. Radial plots for fission-track age determinations of the sediments	198
4.3. Individual fission-track grain-age analysis combined (sediments) with parameters and results for best-fit peaks from Binomfit's software (Brandon, 1992 & 1996).	203
Curriculum Vitae	260



# Acknowledgments

*(ik-'nä-lij-m&nt,ak-/Function: noun; Date: 1594): a thing done or given in recognition of something received.*

I am very grateful to Diane, Wilfried, Jean-Pierre who allowed me to complete this ultimate degree. It took us a while but at the end, and after all, will always remain that we did it, and that what is important. Thanks also to all my colleagues and especially Richard Spikings, Ph.D, researchers, post-docs, secretaries, technicians and diploma students, from Zürich to Quito through Paris and Montpellier, but also to Claude Jaupart and Jean Marcoux from Paris who transmitted to many of us in Paris their passion for geology.

To my mum go a lot of thanks and kisses: without her, her permanent support in any situation since I left home, none of these pages would have been filled. A lot of acknowledgments are for Martine, my lovely wife who came one month with me in Ecuador in a hostile region where she got the opportunity to meet both spiders and puma. Our situation was complicate, one in London, the other one in Zürich, or Ecuador but here it is, that's finished... every story has its end, even the nice one... but this will continue, together for sure, for our next project, in Amsterdam or/and Peru, in south of France. I love you.

Finally, I would like to dedicate this Ph.D to my grandfather Modeste who recently died and who will remain a, if not THE example to follow. Associated to him are (1) two women, his wife Marinette and my second grandmother Janine who always remain both so sweet and kind with the wild boy I was/am, and (2) my uncle Arnaud. Part of these last thoughts also go to 'Commando', a bright, young and enthusiastic student from the Escuela Politecnica Nacional de Quito, who drawn into a river of the northern Sub-Andean Zone while he was living intensively for Geology.



## Abstract

The Ecuadorian Andean Amazon Basin (AAB) developed along the eastern Andean margin as a response to the (1) interaction of the subducting Farallon/Nazca plates and the South American Craton, and (2) accretionary events since Early Cretaceous. The Aptian to Recent sediments contain clastic material which was eroded from the craton and its Paleozoic cover to the east as well as the rising Andean Cordilleras in the west. Previous work established a quantitative thermal history record of exhumation in the bounding orogen to the west although the depths of rock exhumed limit the temporal extent of this record. Often information cannot be continuously traced within the orogens because it has been removed by erosion or overprinted. Hence the details of source region tectonics can be recognized in sedimentary sequences using geochronology. An advanced thermochronological methodology based on pattern of changes in lagtime upwards in the stratigraphic column, combined with heavy mineral analysis, allowed events in the source regions of the AAB to be distinguished through dating of the eroded material present in the northern SAZ and Pastaza depression where uplift has exposed both the Jurassic basement and its Aptian to Recent sedimentary cover.

In a preliminary study, the thermal history of the northern SAZ was constrained using fission-track analysis on both zircon and apatite from 25 samples from the basement of the region. The results reveal that the basement of the sediments, dominantly Jurassic igneous sequences, has never undergone temperatures higher than 100°C since emplacement. Consequently, the region was never heated to temperatures that would have modified zircon detrital fission-track ages in the overlying sedimentary sequences (zircon has a closure temperature of  $\sim 270 \pm 40^\circ\text{C}$ ). Hence, the dated zircon fission-track ages from the Aptian to Recent siliciclastic sediments are true detrital ages and express the varied thermal histories of the source regions.

70 detrital zircon fission-track age populations were statistically extracted from 1082 zircon grains, and show a significant variation from  $579 \pm 65$  Ma to  $22.9 \pm 1.2$  Ma. The abundance of DZFT populations with Proterozoic to Early Cretaceous ages in the Aptian-Albian Hollin Fm. suggests that several distinct source regions, which may have been significantly geographically dispersed, contributed to the early infilling of the AAB. The old populations (600-250 Ma) indicate a probable sourcing in the Guyana-Brazilian Shield regions to the east. Early Cretaceous detrital zircon fission-track populations suggest a Late Jurassic-Early Cretaceous phase of exhumation along the Ecuadorian margin (Peltetec event?), which may be responsible for the 60 My hiatus observed in some locations between the Jurassic Misahualli volcanic arc and the overlying Aptian-Albian sediments (Hollin Fm.).

A rapid exhumation within the source region greater than 2mm/yr during the Coniacian/Santonian to Paleocene was recognised. This is most likely from within the Cordillera and may have been due to the accretion of an oceanic plateau, referred to as the Pallatanga Terrane, against the Ecuadorian margin. This is also manifested by the first appearance of metamorphic detritus into the Maastrichtian Tena Fm.

During the Eocene, distinct provenance changes were coeval with the deposition of proximal sedimentary facies in the AAB (Tiyuyacu Fm.), suggesting that the contemporaneous tectonic development along the Ecuadorian margin was more protracted. Rapid exhumation in the hinterland of the AAB was restricted to the Middle to Late Eocene, when lower crustal levels were eroded into the AAB. This phase probably ended with the final docking of the Macuchi oceanic island arc against the Ecuadorian margin where it currently constitutes part of the Cordillera Occidental.

A clear change of provenance, characterized by the introduction of a pyroxene-olivine dominated heavy mineral assemblage, is observed between the Late Miocene Chambira Fm. and the Pliocene-Pleistocene Mesa and Mera Fms. Rocks with an oceanic affinity, such as the basement of the Cordillera Occidental and parts of the Interandean region, must have been eroded into the AAB since the Pliocene suggesting that western, allochthonous Ecuador was eroding at this time.

Collectively, the combination of these techniques permit (1) an assessment of the thermal and tectonic history of the northern Sub-Andean Zone and Pastaza depression, (2) the identification of the source regions of the preserved western and proximal deposits of the AAB, and (3) a refinement of the exhumation histories of individual source regions. Knowledge gained from this study contributes to the understanding of the Jurassic - Recent active continental margin of Ecuador. Furthermore, the northern Sub-Andean Zone forms a relic part of the flat lying Andean Amazon Basin, which is a major, hydrocarbon contributor and an increased understanding of its evolution may enhance the productivity and economic prosperity of the area.

## Resumen

La Cuenca Andino-Amazónica (CAA) en Ecuador se formó a lo largo del margen andino oriental como respuesta a la interacción entre la subducción de la placa de Nazca bajo el cratón sudamericano y a los eventos acrecionarios ocurridos desde el Jurásico Tardío hasta el Cretácico Temprano. Esta cuenca ha ido acumulando, desde el Aptiense hasta el presente, sedimentos procedentes de la erosión del cratón y de su cobertera Paleozoica, situados hacia el Este, así como de las Cordilleras en elevación en el Oeste. En trabajos previos se ha establecido cuantitativamente el registro histórico térmico en orógenos limítrofes, aunque su extensión temporal está limitada por la profundidad de las rocas exhumadas. Con frecuencia, se pierde la continuidad lateral de este tipo de información dentro de los distintos orógenos debido a que ha sido eliminada por la erosión o retrabajada por eventos posteriores. No obstante, los detalles del área tectónica fuente se pueden reconocer en las secuencias sedimentarias utilizando técnicas geocronológicas. Una metodología termocronológica avanzada, basada en los modelos de cambio en intervalos de retrasos temporales ('lagtime') hacia arriba en la serie estratigráfica, combinada con el análisis de minerales pesados, permite distinguir eventos tectónicos en las áreas fuente de la CAA a través de la datación del material erosionado en el norte de la Zona Sub-Andina (ZSA) y la depresión de Pastaza, donde un notable levantamiento tectónico expone en superficie tanto el basamento Jurásico como su cobertera sedimentaria Aptiense-Presente.

En un estudio preliminar, la historia térmica del sector septentrional de la ZSA fue establecida utilizando análisis de trazas de fisión, tanto en zircón como en apatito, en 25 muestras procedentes del basamento. Los resultados revelan que este basamento, predominantemente formado por secuencias ígneas jurásicas, nunca ha estado sometido a temperaturas superiores a los 100°C desde su emplazamiento. De esta forma, la región nunca ha sido calentada a temperaturas que modificarían las edades de las trazas de fisión en zircones detríticos dentro de las secuencias sedimentarias suprayacentes (la temperatura de cierre de las trazas de fisión en el zircón es de  $\sim 270 \pm 40^\circ\text{C}$ ). Por tanto, los zircones datados por trazas de fisión en sedimentos siliciclásticos de edades comprendidas entre el Aptiense y el presente son edades detríticas reales y muestran la variedad de historias térmicas en las áreas fuente.

70 poblaciones de edades de trazas de fisión en zircones detríticos fueron extraídas estadísticamente de 1082 granos de zircón, mostrando una variación significativa en las edades, desde  $579 \pm 65$  Ma hasta  $22.9 \pm 1.2$  Ma. La abundancia de poblaciones de zircones detríticos con trazas de fisión (DZFT), con edades comprendidas entre el Proterozoico al Cretácico Temprano en la Formación Hollín (Aptiense-Albiense), sugiere que distintas áreas fuente, que pueden haber estado dispersas geográficamente, han contribuido al relleno temprano de la CAA. Las poblaciones viejas (250-600 Ma) indican probablemente procedencias de regiones situadas hacia el Este, en el cratón de Guyana-Brasil. Por otra parte, las poblaciones de zircones detríticos con trazas de fisión que datan del Cretácico Temprano,

sugieren una fase de exhumación Jurásico Tardío – Cretácico Temprano a lo largo del margen ecuatoriano (¿evento Peltetec?), que puede haber sido responsable del hiato estratigráfico de 60 Ma observado en algunas localidades entre el arco volcánico Jurásico de Misahualli y los sedimentos suprayacentes Aptiense-Albiense de la Formación Hollín.

Los resultados de zircones detríticos con trazas de fisión indican una rápida exhumación dentro de las áreas fuente con tasas que superan los 2 mm/año entre el Coniaciense-Santoniense y el Paleoceno. Esto puede haberse debido a la acreción al margen ecuatoriano de un 'plateau' oceánico, conocido como Terreno Pallatanga, que provocaría la exhumación y denudación de materiales en el área fuente occidental de la ZSA y condicionaría la aparición de detritos metamórficos dentro de la Formación Tena, de edad Maastrichtiense.

Durante el Eoceno, cambios en las zonas de aporte de material coexisten con el depósito de facies sedimentarias proximales en la CAA (Formación Tiyuyacu), sugiriendo que el desarrollo tectónico, contemporáneo a lo largo del margen ecuatoriano, fue más prolongado. La rápida exhumación de las zonas internas de la CAA se restringe al período Eoceno Medio-Superior, cuando los niveles de la corteza inferior son erosionados y depositados en la CAA.. Esta fase probablemente termina con la anexión final al margen ecuatoriano del arco de islas oceánico de Macuchi, que actualmente forma parte de la Cordillera Occidental.

Un cambio claro de la procedencia del aporte de materiales, caracterizado por la introducción de una asociación de minerales pesados dominada por piroxeno y olivino, se observa entre la Formación Chambira (Mioceno Tardío) y las Formaciones Mesa y Mera (Plioceno-Pleistoceno). Rocas que muestran una afinidad oceánica, tales como las presentes en el basamento de la Cordillera Occidental y en algunos sectores de la región interandina, deben de haber sido erosionadas y depositadas en la CAA desde el Plioceno, sugiriendo que el Ecuador alóctono occidental estaba siendo erosionado en ese momento.

En conjunto, la combinación de todas estas técnicas permiten: (1) una evaluación de las historias térmicas y tectónicas del sector septentrional de la Zona Sub-Andina y la depresión de Pastaza; (2) la identificación de áreas fuente de los depósitos occidentales preservados y los depósitos proximales de la CAA; y (3) un refinamiento en el establecimiento de historias de exhumación en áreas fuente individuales. El conocimiento que se adquiere con este estudio contribuye en gran medida al entendimiento geológico del margen continental de Ecuador, activo desde el Jurásico hasta el presente. Conviene añadir que una mejora en el conocimiento de la evolución de la región, en el sector septentrional de la Zona Sub-Andina, uno de cuyos sectores es relicto de la Cuenca Andino-Amazónica la cual constituye una reserva de hidrocarburos de importancia global, puede repercutir positivamente en la productividad y la prosperidad económica de la región.



## Zusammenfassung

Das andine Amazonas-Becken (AAB) von Ecuador entwickelte sich entlang des östlichen Randes der Anden als Reaktion auf die (1) Wechselwirkung der Subduktion der Farallon/Nazca Platten unter den südamerikanischen Kraton, und (2) die wiederholte Akkretion von pazifischen Terranen am westlichen südamerikanischen Kontinental-Rand seit der Kreidezeit. Die unterkretazischen bis rezenten Sedimente enthalten klastisches Material, welches einerseits vom Osten vom Kraton und dessen paläozoischer Bedeckung, und andererseits vom Westen von den sich hebenden Anden-Kordillern erodiert wurde. Bisherige Arbeiten haben eine quantitative thermische Geschichte der Exhumierung des Andenorogens im Westen geliefert, wobei die Tiefe der exhumierten Gesteine den zeitlichen Umfang dieses Datensatzes limitieren. Oft können diese Informationen nicht kontinuierlich in frühe geologische Zeit zurück verfolgt werden, da die Gesteine, welche die ältere Geschichte zeigen könnten, erodiert wurden. Daher können die Details der Tektonik in den Liefergebieten mittels geochronologischer Untersuchungen an detritischen Körnern in den Sedimenten des AAB besser identifiziert werden. In der vorliegenden Arbeit wurde eine erweiterte thermochronologische Methodik, basierend auf dem Prinzip der zeitlichen Verzögerung zwischen dem Alter der Exhumierung der detritischen Körner (im folgenden DZFT genannt; detrital zircon fission track age) und den Sedimentationsaltern angewendet. Zum besseren Verständnis der tektonischen Vorgänge in den Liefergebieten in der stratigraphischen Abfolge wurden auch die Schwermineralgehalte in den analysierten Sedimenten beigezogen. Wir haben in der vorliegenden Arbeit Material von der nördlichen SAZ und der Pastaza-Depression analysiert, wo das jurassische Grundgebirge und seine sedimentäre Bedeckung (Aptian bis Rezent) durch Hebung freigelegt worden sind.

In einer einleitenden Studie wurde die thermische Geschichte der nördlichen SAZ anhand von Spaltspur-Analysen an Zirkonen und Apatiten von 25 Proben aus dem Grundgebirge der Region abgeleitet. Die Resultate zeigen dass die jurassischen Vulkanite und Plutonite (Misahualli Fm. und Abitagua-Granit) unter den Sedimenten nie höhere Temperaturen als 100°C seit der magmatischen Abkühlung erfahren haben. Folglich wurden die Sedimente nicht auf Temperaturen geheizt, welche die Spaltspuren in den detritischen Zirkonen in den überliegenden Sediment-Sequenzen hätten modifizieren können (Zirkon hat eine Schliesstemperatur von  $270 \pm 40^\circ\text{C}$ ). Daher liefern die datierten Zirkone wahre Exhumierungs-Alter, welche die verschiedenartigen thermischen Entwicklungen in den Liefergebieten dokumentieren. 70 Populationen von Spaltspur-Altern detritischer Zirkone wurden statistisch aus 1082 Zirkon Körnern ausgewählt, und zeigen eine signifikante Streuung von  $579 \pm 65$  Ma bis  $22.9 \pm 1.2$  Ma. Das Vorhandensein von DZFT-Populationen mit proterozoischen bis unterkretazischen Altern in der Hollin Fm. (Aptian-Albian) deuten an, dass mehrere unterschiedliche Liefergebiete, welche geographisch deutlich voneinander getrennt sein mussten, zur frühen Füllung des AAB beigetragen haben. Die alten Populationen (600-250 Ma) weisen auf eine mögliche Lieferung aus der Schild-Region von Guyana

und Brasilien im Osten hin. Spaltspur-Populationen detritische Zirkone aus der frühen Kreide legen eine oberkretazische Exhumierungsphase entlang dem ecuadorianischen Kontinentalrand im Westen nahe, die mit dem Peltetec-Ereignis korreliert werden kann. Dieses tektonische Ereignis ist für die bis 60 Millionen Jahre ausmachende Schichtlücke zwischen dem jurassischen (Misahualli-) Vulkanbogen und der überliegenden Hollin Fm. verantwortlich.

Von Coniacian/Santonian bis Paleozän (Mittlere Napo. Fm. bis Tena Fm.) wurde eine schnelle Exhumierung (größer als 2mm/yr) in den Liefergebieten festgestellt. Ab dem Maastrichtian wird auch ein signifikanter Eintrag von metamorphen Mineralen registriert. Die Hebung und die anschließende Exhumierung von metamorphen Serien der frühen Cordillera Real im Westen wurde höchst wahrscheinlich durch die Akkretion eines ozeanischen Plateaus (Pallatanga Terran) am ecuadorianischen Kontinental-Rand verursacht.

Das Eozän war durch deutliche Herkunftsänderungen in den Ablagerung der proximalen Sedimentfazies der Tiyuyacu Fm. gekennzeichnet, was darauf hinweist, dass der ecuadorianische Kontinental-Rand einer weiteren signifikanten tektonischen Überprägung unterzogen wurde. Schnelle Exhumierung im Hinterland des AAB war beschränkt auf das mittlere bis späte Eozän, als auch vermehrt hochgradig metamorphe Krustenteile in der Cordillera Real erodiert wurden. Diese Periode korreliert vermutlich mit dem endgültigen Andocken eines ozeanischen Inselbogens (Macuchi Terran) an den ecuadorianischen Kontinental-Rand.

Ein deutlicher Herkunftswechsel wird durch den Eintragung von Pyroxen/Olivin-führenden Schwermineralparagenesen zwischen der obermiozänen Chambira Fm. und der plio-pleistozänen Mesa und Mera Fm. festgestellt. Gesteine mit ozeanischer Herkunft, wie sie im Grundgebirge der Cordillera Occidental und Teilen der Interandinen Region anstehen, müssen seit dem Pliozän detritisches Material in das AAB geliefert haben. Diese Periode korreliert mit der seit ca. 10-9 My in verschiedenen Teilen der ecuadorianischen Anden festgestellten Hebung.

Insgesamt ermöglichte die Kombination der Techniken (1) eine Abschätzung der thermischen und tektonischen Geschichte der nördlichen Sub-Andinen Zone und der Pastazza-Depression, (2) die Identifikation der Herkunftgebiete des detritischen Materials in den Ablagerungen des AAB, und (3) eine Verfeinerung der Exhumierungsgeschichte der Liefergebiete, wie sie durch grosstektonische Vorgänge im ecuadorianischen Subduktionsgürtel geleitet wurde. Die aus dieser Studie gewonnenen Kenntnisse leisten einen Beitrag zum Verständnis der jurassisch bis rezent Entwicklung der ecuadorianischen Anden. Darüber hinaus liefert sie ein verbessertes Verständnis der Entwicklung der Erdöl-produzierenden Sub-Andinen Zone und des Oriente-Beckens für die Exploration des Rohstoffes, der den Wohlstand des Landes erhöhen könnte.

# 1. Introduction

## 1.1. Geographical setting

Ecuador, on the western coast of South America, is bordered to the north by Colombia and to the east and south by Peru (Fig. 1.1). It is physiographically very varied and can be divided into five regions, which are from west to east (Fig. 1.1): (1) the coastal lowlands (*Costa*), (2) the Western Cordillera or *Cordillera Occidental*, (3) the Interandean region, (4) the Eastern Cordillera or *Cordillera Real*, and finally the (5) Ecuadorian upper Amazon region. Except for the *Costa*, young volcanoes form prominent features in the northern segment of the Ecuadorian Andes.

### *Study area*

The Ecuadorian upper Amazon region, herein referred to as the Andean Amazon Basin (AAB; Fig. 1.1) is in turn subdivided into two morphologically distinct areas (Fig. 1.1): (1) a flat-lying region to the east that is generally referred to as the Oriente region as in other parts of South and Central America, and (2) the Sub-Andean Zone (SAZ; Fig. 1.1) to the west. The latter region is made up of the Cutucú and Napo domes that are separated by the Pastaza depression (Fig. 1.1). In the Napo region and Pastaza depression the drainage, toward the east, consists of three main tributaries of the Amazon river, i.e. the Pastaza, Napo, and Aguarico rivers (Fig. 1.1). The altitude ranges from 3732 to ~900 meters in the northern SAZ (Napo region), to less than 400 meters in part of the Pastaza depression and Oriente region. Such difference in elevation is related to recent uplift but also to the presence of three volcanoes: the Sumaco (3732 m), Pan de Azúcar, and Reventador (3592 m; Fig. 1.2).

The mean annual rainfall in Puyo (Fig. 1.1), reaches 4632 mm/year (Litherland et al. 1994) while it approximates 5000-6000 mm/year in the immediate vicinity of the Andes to the west of the northern SAZ (Tschopp, H. J., 1953). Daily temperatures range from 20°C degrees to more than 35°C with 80-100% humidity. This tropical climate allows the growth of a luxuriant jungle (Fig. 1.2), which causes serious problems in locating outcrops that are also masked by recent lavas-flows.

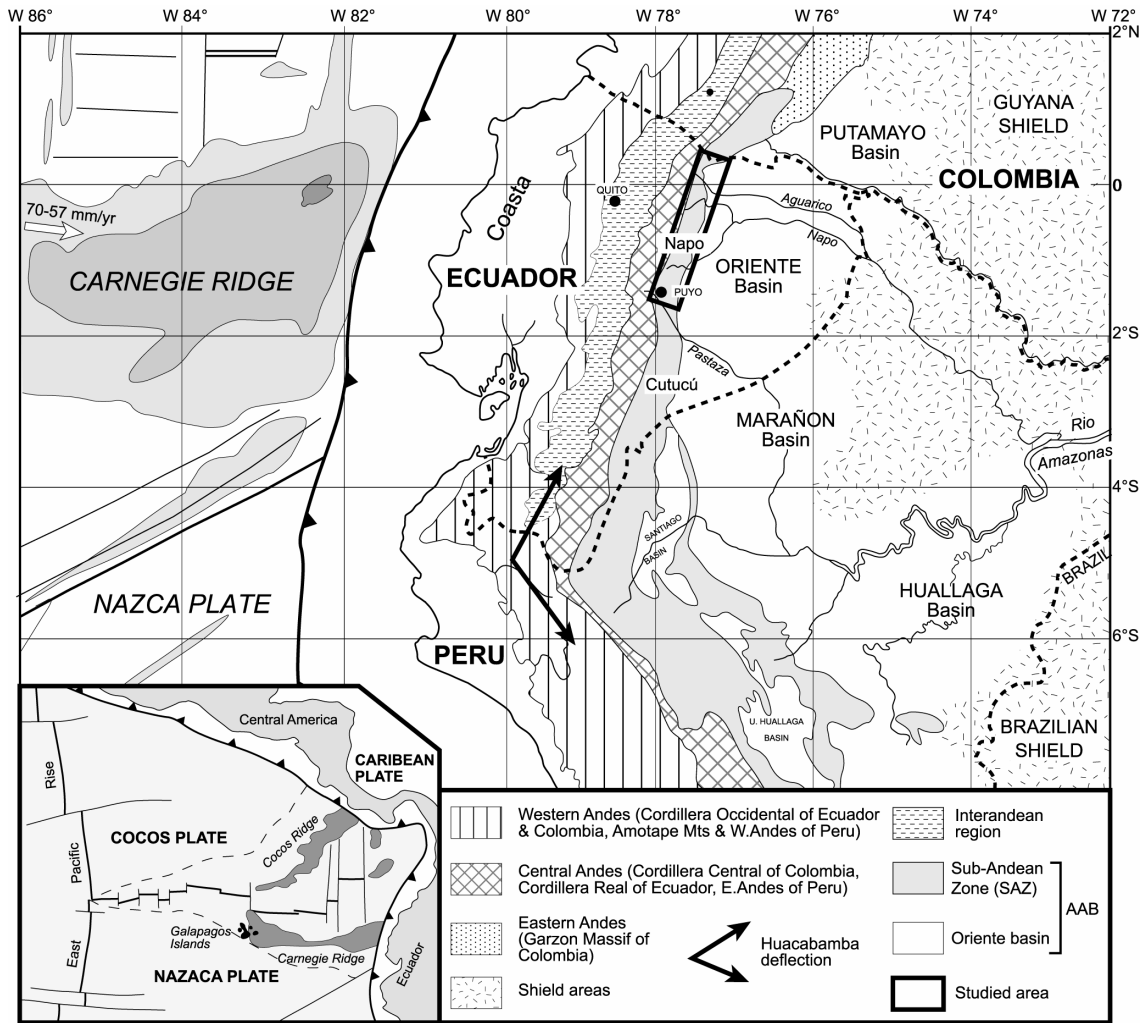


Figure 1.1: Morpho-tectonic sketch of part of the Northern Andes, with special references to Ecuador. Highlighted is the studied area, i.e. the northern Ecuadorian Sub-Andean Zone referred to as the Napo region and the Pastaza depression (adapted from Campbell, 1970; Spikings et al., 2001).

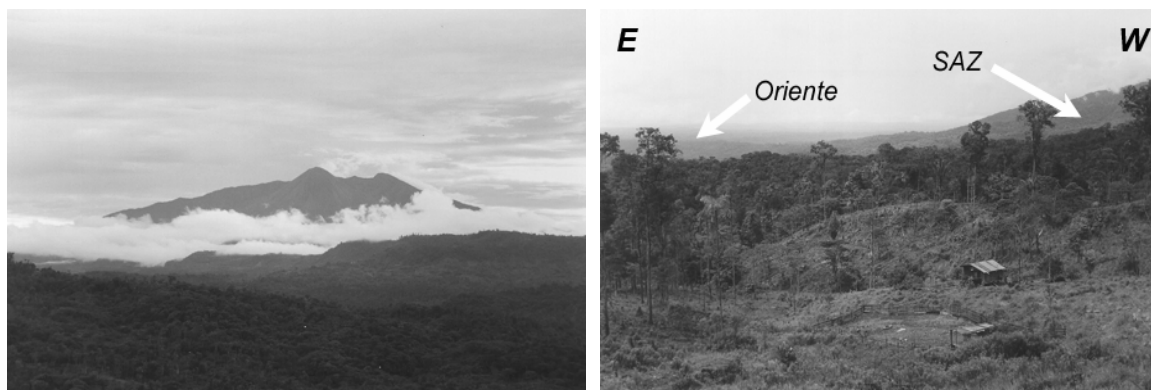


Figure 1.2: Landscape and volcanic activity in the northern Sub-Andean Zone (SAZ). Left: the Reventador volcano (3562 m) located in the center of the northern Ecuadorian Sub-Andean Zone (SAZ), and right: the eastern termination of the northern SAZ, to the left (east) is the Oriente region and to the right (west) the front of the northern SAZ.

## 1.2. Geological overview

The Ecuadorian continental margin is situated in the northern Andean segment (north of 5°S) and is separated from the central segment by a distinct change in the convergence angle between the oceanic Nazca and South American (SOAM) plates, otherwise referred to as the Huancabamba deflection (Gansser, 1973; Fig. 1.1). The Ecuadorian geology is essentially composed of parallel morpho-tectonic zones running approximately with the SSW-NNE strike of the coastal line (Fig. 1.1). Repeated accretions of oceanic plateau and island-arc terranes since the Mesozoic (Feininger and Bristow, 1980; Litherland et al., 1994) have contributed to the establishment of this composite NNE-oriented orogenic belt (Fig. 1.3). These characteristics distinguish the Northern Andes from the Central and Southern Andes that have not experienced such a history of terrane accretion.

Traversing from west to east, the geodynamic system can be resolved into several morpho-tectonic domains separated by suture zones, terrane boundaries or major fault systems: (1) an almost orthogonally subducting oceanic Nazca plate at a rate of 70-57 mm/y (Norabuena et al., 1999) including the thick and buoyant Carnegie Ridge (Fig. 1.1), (2) Paleocene to Miocene forearc basins lying on the Cretaceous oceanic plateau Piñon Terrane (e.g. Feininger and Bristow, 1980; Egüez, 1986; Daly, 1989; Bourgeois et al., 1990; Jaillard et al., 1995 and 1997a; Fig. 1.3), (3) the Cordillera Occidental composed of both an Eocene oceanic island arc sequence (Macuchi Terrane, Hughes and Pilatasig, 2002; Fig. 1.3) and a Cretaceous oceanic plateau referred to as the Pallatanga Terrane (Hughes and Pilatasig, 2002; Fig. 1.3), (5) the Interandean region which is a central depression filled by Late Miocene to Recent volcanosedimentary and volcanic rocks (Ego et al., 1996; Winkler et al., 2002), (6) the polydeformed, Paleozoic-Mesozoic, metamorphic rocks and intrusions of the Cordillera Real (Litherland et al., 1994), and (7) a retro-foreland basin (Jordan, 1995; DeCelles and Giles, 1996) herein referred to as the AAB (Fig. 1.3). The latter domain is part of an assemblage of basins that can be followed to the south of the northern Andes into the Marañón and Huallaga basins in Peru (Fig. 1.1), and into the Putamayo basin of southern Colombia (Fig. 1.1). Its western region is composed of (1) steeply west-dipping thrust slices (Sub-Andean Belt, Litherland et al., 1994) and (2) large antiforms within a series of foothill highs, which are commonly referred to as the Sub-Andean Zone (SAZ; Fig. 1.3). The studied area that comprises the Napo region and the Pastaza depression (Fig. 1.1) is bounded to the west by the Sub-Andean Fault from Paleozoic to Cretaceous metamorphic rocks defining the Eastern Cordillera (Fig. 1.3), and bordered to the east by the flat lying Oriente basin that is in turn limited to the east by the Guyana Shield (Fig. 1.1). Conspicuous tectonic uplift is evident in the Sub-Andean Zones, exposing the (1) Paleozoic to Mesozoic cover, and (2) Cretaceous to Recent basin formations (Fig. 1.3).

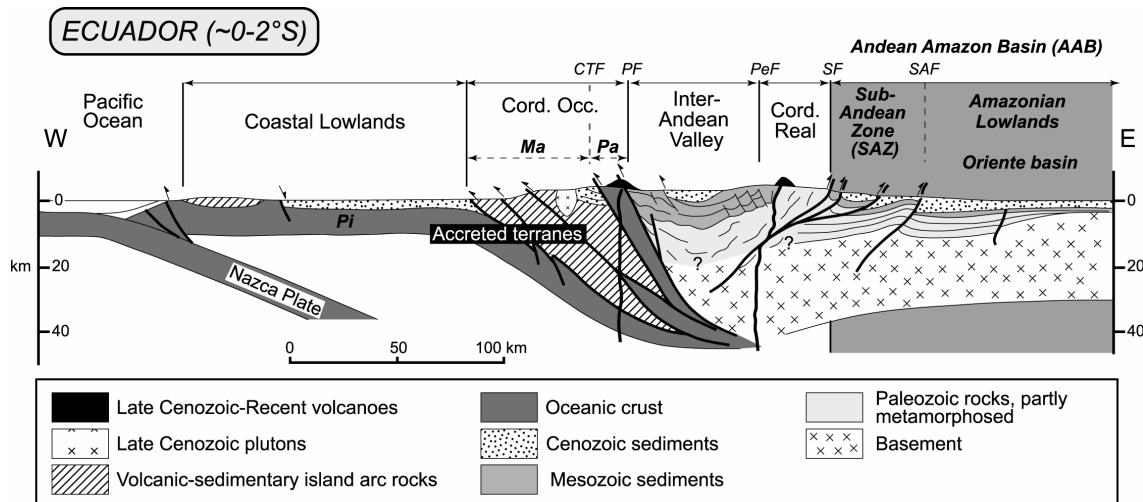


Figure 1.3: Cross-section through the Ecuadorian Andes at latitude of 2°S (adapted from Jaillard et al., 2002a). Pi, Ma, Pa: Piñon, Macuchi and Pallatanga Terranes. CTF, PF, PeF, SF, SAF: Chimbo-Toachi Fault, Pujili-Pallatanga Fault, Peltetec Fault, Sub-Andean Fault and Sub-Andean Front.

## Jurassic

The history of the Ecuadorian margin was mainly governed by subducting oceanic plates under the South American continent that was initiated in the Jurassic within the early Tethyan spreading, and continued afterwards in the eastern Pacific system (Pilger, 1984; Jaillard et al., 1990; Pindell and Tabbutt, 1995). This led to the NNE-oriented Misahualli continental arc in the present-day location of the northern SAZ (Aspden et al., 1987; Romeuf et al., 1995; Jaillard et al., 2000). Back-arc basins were probably present in the region of the Oriente basin of Ecuador (Chapiza Fm.; Tschopp, 1953; Jaillard et al., 2000) whereas forearc regions are unknown due to protracted and multiple tectonic developments since the Jurassic, which destroyed any evidence (Jaillard et al., 2000). Subduction ceased by the Peltetec tectonometamorphic event reported within the Cordillera Real region that is associated with the accretion of continental microplates along the northern segment of the Andes (Litherland et al., 1994). The unconformably overlying Aptian-Albian deposits (Hollin Fm.) that characterize the early development of the studied Ecuadorian AAB may provide a minimum age (120-110 Ma) for this event.

## Cretaceous

No Cretaceous subduction-related magmatism is known from the NE-oriented continental margin of Ecuador north of 3°S whereas spreading in the Pacific realm never stopped. The Peruvian subduction zone, which gave rise to the formation of a continental arc of Albian to Coniacian age to the south of Ecuador should have then extended north-westwards into the oceanic domain by means of intra-oceanic subduction zone (Jaillard et al., 1999). In the AAB an epi-continental depositional system prevailed from Middle to Late Cretaceous (Tschopp, 1953; Jaillard, 1997b).

Subsequently, the Ecuadorian margin underwent the accretion of an oceanic plateau referred to as the Pallatanga Terrane that constitutes today part of the Cordillera Occidental (Fig. 1.3). A minimum early Maastrichtian age (71-65 Ma) is attributed to this event through evidence of deposition in the Maastrichtian times on both sides of the exhuming Cordillera Real of the (1) red-beds of the Tena Fm. to the east in the AAB (Hughes and Pilatasig, 2002), and (2) marine turbidites of the Yunguilla unit to the west.

### *Tertiary*

Different oceanic provinces accreted along the western margin of the SOAM in Ecuador in the Tertiary. These are (1) the Eocene docking of the Macuchi island arc along the Chimbo-Toachi suture zone against the Pallatanga Terrane to the east (Hughes and Pilatasig, 2002), and (2) the Late Paleocene collision of the coastal Piñon block to the south of Ecuador (Jaillard et al., 2001).

Resuming volcanic arc activity probably occurred in the coastal region but was probably diachronous from south to north, i.e. 67 Ma to the south (Sacapalca Fm.; Hungerbühler et al., 2002), and 53-45 Ma to the north (Saraguro Group, Egüez, 1986; Jaillard et al., 2000; Hungerbühler et al., 2002). However, the geodynamic development of Ecuador during the Paleocene-Eocene is still debatable, because the relationships between these oceanic provinces defining today the Cordillera Occidental are not completely elucidated (Jaillard et al., 2001).

A major plate reorganization took place at ca. 28-26 Ma, when the oceanic Farallon plate broke into the (1) Cocos and Nazca plates to the south, and (2) Juan de Fuca Plate farther north (Fig. 1.1; Hey, 1977; Pilger, 1984; Pardo-Casas and Molnar, 1987). Due to differential stresses on the northeastward-subducting Cocos Plate and the eastward-subducting Nazca Plate, N-S spreading was initiated around 23 Ma between the two plates in the vicinity of the Galapagos hotspot (Lonsdale and Klitgord, 1978). Such a phase was associated with a change in convergence direction between the Nazca and SOAM plates from NNE-SSW to a more orthogonal E-W direction (Pilger, 1984; Pardo-Casas and Molnar, 1987).

The subduction of the buoyant Carnegie ridge under the SOAM plate with a flat slab configuration (Gutscher et al., 1999) may have played a major role in the geodynamic development of the Ecuadorian margin since the Middle Miocene (Spikings et al., 2001). Analysis of ages from the Carnegie Ridge basalts combined with plate reconstruction allowed Spikings et al. (2001) to suggest a 15 Ma age for the early stage of collision with the northern Ecuadorian margin. Increasing coupling of the Carnegie ridge with the upper plate since 9 Ma probably generated increased compression and exhumation rates in both the Cordillera Real (Spikings et al., 2001) and southern Ecuadorian forearc (Steinmann et al., 1999; Hungerbühler et al., 2002).

### 1.3. Previous work and limitations

Previous attempts to determine the sedimentary evolution of the Andean Amazon Basin of Ecuador have included geological explorations in the 30's (Wasson and Sinclair, 1927; Colony and Sinclair, 1932) that were followed by detailed lithostratigraphic descriptions from geologists of the Shell Company in the 50's (e.g. Tschopp, 1948 and 1953). Further work in the Oriente basin was done to characterize oil reservoirs (Feininger, 1975; Dashwood and Abbotts, 1990; White et al., 1995; Balkwill et al., 1995; Rivadeneira and Baby, 1999), while Jaillard (1997b) accurately synthesised the Cretaceous stratigraphy using fossils, micro-fossils and internal oil company reports. Subsidence analyses of the Oriente basin were also undertaken (Berrones, 1992; Thomas et al., 1995; Berrones and Cotrina, 1996) although since then the stratigraphic subdivision has significantly changed. Using seismic analyses in the Oriente basin, many authors (e.g. Balkwill et al., 1995; Rosero-Revelo, 1999, and Rivadeneira and Baby, 1999) identified compressive episodes that reactivated and inverted pre-Cretaceous extensional structures in the (1) Late Cretaceous-Maastrichtian, (2) Early Eocene, and most likely (3) during the Plio-Quaternary. Furthermore, Valdez-Pardo (1997) and Christophoul et al. (2002) compiled the Eocene to Oligocene stratigraphy of the AAB.

Within the northern SAZ, few additional and recent studies were undertaken: (1) paleo-stress measurements in the northern SAZ that led Pasquarè et al. (1990) to relate the Miocene to Recent tectonic evolution of the region with a change in plate convergence along the Ecuadorian margin, (2) detailed sedimentological and structural analysis of the region of Baeza in the northern SAZ (Buitron and Vallejo, 1999), and finally (3) deformation and uplift along the Pastaza alluvial fan (Bes De Berc, et al., 2002). The British Geological Survey published a memoir in 1994 (Litherland et al., 1994) that compiled almost ten years of intensive and multi-disciplinary work towards the understanding of the geology of the adjacent Cordillera Real. Within this report, the westernmost region of the SAZ referred to as the Sub-Andean Thrust Belt (see section 2.1) was briefly described including few K/Ar thermochronological ages.



## 1.4 Scope of this study

This study aims to understand the sedimentary and tectonic history of the Ecuadorian Andean Amazon Basin (AAB) since the Early Cretaceous, with a special emphasis on the western foothills of the Ecuadorian Andes in the Napo region referred to hereon as the northern Sub-Andean Zone (SAZ, Figures 1.1 and 1.3). The study was undertaken using fission-track analysis on the basement and sedimentary rocks of the northern SAZ. It forms a complementary study to those undertaken by Spikings et al (2000, 2001) who made thermochronological studies in the adjacent Cordillera Real to the west. The events seen in both these studies and from previous stratigraphic work (see overview in chapter 2) should be refined and is potentially more clearly seen in the sediments of the SAZ which were assumed to have been sourced, at least partly, from the Cordillera Real. The following approach was then applied:

(1) Determination of apatite fission-track ages on the basement sequences (Jurassic intrusives and extrusives) in order to determine the thermochronology of the basement, and particularly the maximum temperatures reached during burial by the overlying Mesozoic-Cenozoic sediments (chapter 3).

(2) Based on these results, which showed that the temperature attained was not greater than the closure temperature of zircon fission track ( $\sim 270^{\circ}\text{C}$ ), detrital zircon grain age studies were undertaken to determine (a) potential source regions, and (b) thermal histories within the source regions of these sediments. This latter goal required the development of a new method of interpreting detrital grain ages (chapter 4).

(3) The heavy mineral suites of the sediments were also analysed and later combined with the fission-track results to effectively increase the precision on the interpretation of source region identification (chapter 4).



## 2. Geological framework

In the present section is structurally defined the area of study (i.e. the Napo antiform and Pastaza depression), which is in turn a subdivision of the AAB (see section 1.2). Later, a detailed lithostratigraphic column is presented based on previous studies and field observations (section 2.2) that are followed by a revision of tectonic subsidence analyses (section 2.4; Berrones, 1992; Berrones and Cotrina, 1996).

### 2.1. The northern Ecuadorian Sub-Andean Zone

Both the northern SAZ and the Pastaza depression define the eastern foothills of the Ecuadorian Andes north of 2°S (Fig. 1.3). This region, which is approximately 250 km long and 60 km wide (Fig. 2.1), is limited to the west from the polydeformed rocks of the Cordillera Real by the Sub-Andean Thrust Fault (SF; Fig. 2.1), and to the east from the Oriente basin by the Sub-Andean Front (SAF; Fig. 2.1) that has a maximum vertical offset of 1000m (Rosero-Castillo, 1997; Baby et al., 1999).

Field evidence designates an additional and important regional fault: the Cosanga Fault (CF; Litherland et al., 1994, Fig. 2.2). It separates the steeply dipping Mesozoic to Paleocene series (Paradalarga unit, Hollin, Napo and Tena Fms., see 2.2) to the west from the low dipping Mesozoic to Neogene series to the east (Fig. 2.2). Hence, the area of study can be structurally sub-divided into (Litherland et al., 1994): (1) the 5-15 km wide Sub-Andean Thrust Belt (SATB; Fig. 2.2; Litherland et al., 1994), which is limited by the Sub-Andean Fault to the west and the Cosanga Fault to the east, and (2) the rest of the SAZ to the east towards the east (Figures 2.1 and 2.2).



Figure 2.1: Geological map of the northern Ecuadorian Sub-Andean Zone and Pastaza depression (after Litherland et al., 1993 and 1994).

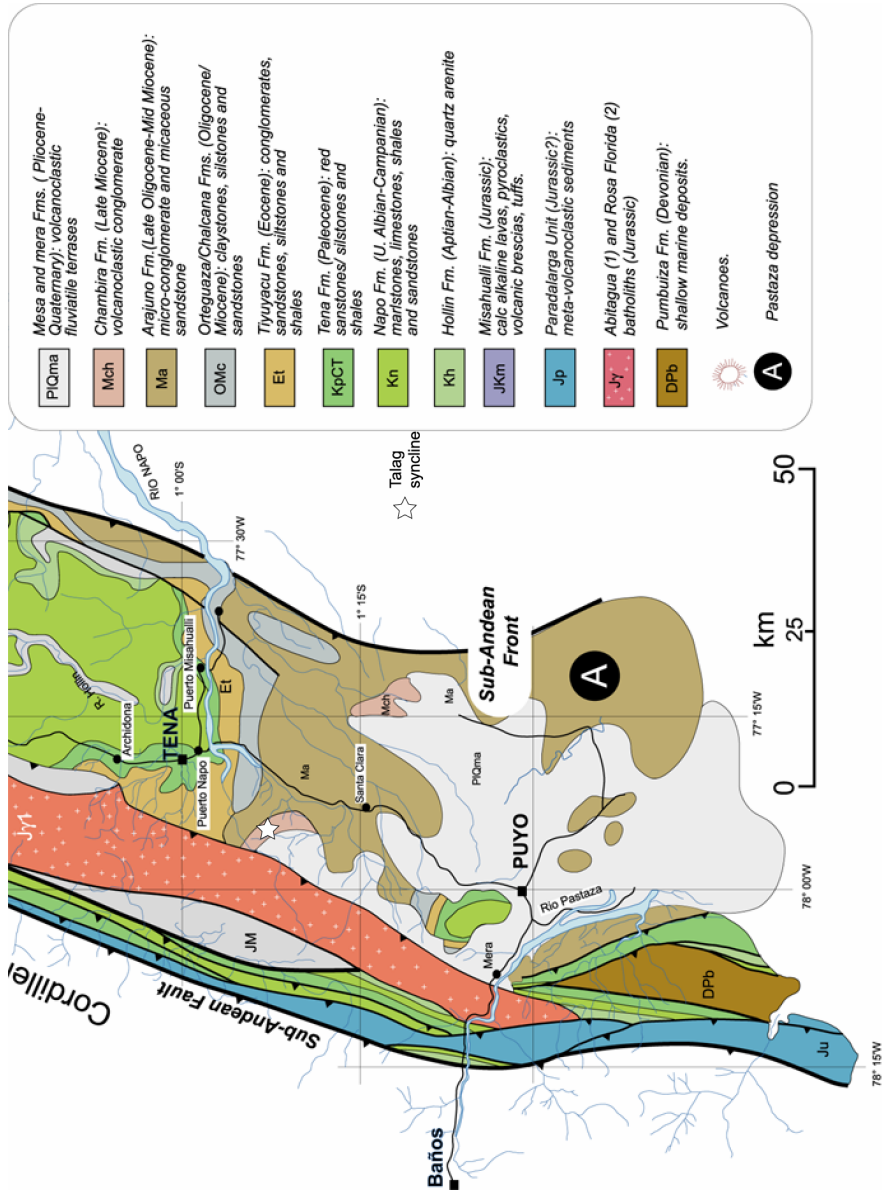


Figure 2.1 (Continued)

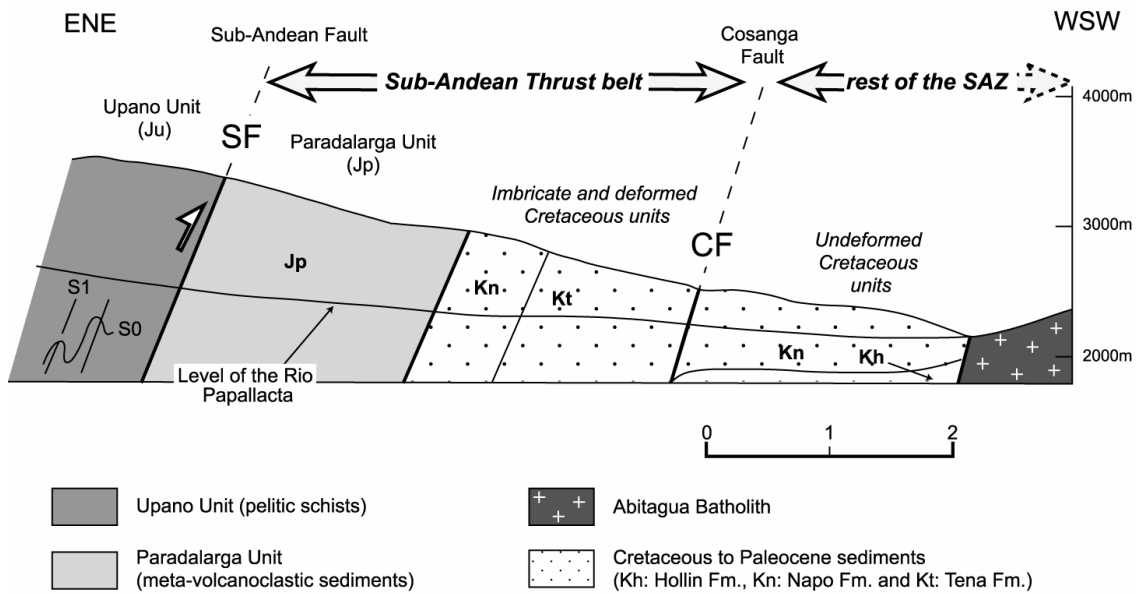


Figure 2.2: Section across the western edge of the northern Sub-Andean Zone (SAZ). See Figure 2.1 for localization (adapted from Litherland et al., 1994; Buitron and Vallejo, 1999). SF: Sub-Andean Fault; CF: Cosanga Fault. See text for lithological descriptions.

## 2.2. Lithostratigraphy and sedimentological observations

The stratigraphic column of the AAB from Early Cretaceous to Recent is summarized in Figure 2.3.

Formations	Remarks	Lithology	Chronostratigraphy	AGE
MERA	CONTINENTAL DEPOSITS		Pleistocene	1.75
MESA			Pliocene	5.3
CHAMBIRA				
CURURAY				
ARAJUNO			Miocene	
CHALCANA				23.8
ORTEGUAZA	BRACKISH TO MARINE		Oligocene	33.7
TIYUYACU	CONTINENTAL SS, CLAYST & CGL LOCALLY PRODUCTIVE		Eocene	
TIYUYACU				
TENA	SHALLOW MARINE TO CONT., MOSTLY CLAYSTONE. THINBASAL SAND FREQUENTLY OIL BEARING		Paleocene	55.7
TENA			Maastrichtian	66
eroded and/or non-deposited in the SAZ			Campanian	71.3
NAPO	MARINE SHALES, LIMESTONES AND SANDSTONES WHICH ARE FREQUENTLY OIL PRODUCTIVE ("U" & "T" SANDS)		Santonian	83.5
			Coniacian	85.8
			Turonian	89
			Cenomanian	93.5
HOLLIN	MOSTLY CONTINENTAL MAJOR OIL RESERVOIR		Albian	98.9
			Aptian	112.2
CHAPIZA/ MISAHUALLI	VOLCANICS & CONTINENTAL CLAYS, SILTS & SANDS		Barremian	121
			Hauteverian	127
			Valanginian	132
			Berrasian	137
			Tithonian	144.2
				Ju

Figure 2.3: Generalized stratigraphic column, Oriente basin, Ecuador (modified from Canfield et al., 1982; Christophoul et al., 1999; Rivadeneira et al., 1999)

### 2.2.1. Basement of the northern SAZ

Basement is understood in a pragmatic way, i.e. a complex of rocks that underlies the rocks of interest of the area.

In the present study this term comprises all formations that stratigraphically underlie the mid-Cretaceous to Quaternary (more or less continuous) sedimentary series of the Andean orogenic cycle in the SAZ and Oriente basin. These include the (1) underlying granitic and gneissic series of the Guyana Shield to the east in the Oriente region, (2) the Paleozoic Pumbuiza and Macuma sedimentary formations (Baldock, 1982), (3) the Late Permian to Lower Jurassic rift-related Mitu and Santiago Fms. (Baldock, 1982), and (4) the late Early to Late Jurassic continental arc Misahualli Fm. with the coeval volcanoclastic series of the Chapiza Fm. to the east in the Oriente region (Tschopp, 1953; Rivadeneira and Baby, 1999), and finally (5) the co-magmatic Abitagua and Zamora granites (Litherland et al., 1994).

The Misahualli Fm. is believed to have its equivalents in the Upano and Paradalarga units (Litherland et al., 1994; Buitron and Vallejo, 1999) across the Cosanga and Sub-Andean faults to the west. Because our interest is the reconstruction of the Andean Amazon Basin during the Cretaceous to Recent with special reference to the northern Ecuadorian Sub-Andean Zone, the basement of this region is restricted to: (1) the Abitagua batholith first described by Colony and Sinclair (1932), (2) the Misahualli Fm. (Wasson and Sinclair, 1927), (3) the Upano (Litherland et al., 1994) and Paradalarga (Buitron and Vallejo, 1999) units, and (4) the sedimentary Pumbuiza Fm. (Tschopp, 1953). In the northern SAZ rarely primary sedimentary contacts between the Abitagua-Misahualli volcanic arc complex and the mid-Cretaceous to Recent sediments are observed. However, the general stratigraphic pattern implies that the overlying mid-Cretaceous sediments sealed a continental arc that rimmed the South American continent to the west.

2.2.1.1. The **Abitagua** batholith is a 120 km long and up to 15 km wide body located to the west of the Cosanga Fault (Litherland et al., 1994). It defines the highest non-volcanic relief of the northern SAZ (~2700 m; Fig. 2.1), and is composed of pink, medium or coarse-grained biotite monzogranite to K-feldspar megacrystic biotite granite (Litherland et al., 1994). The Abitagua batholith is commonly correlated with two other important calc-alkaline plutonic bodies in Sub-Andean positions, the Zamora batholith to the south and the Rosa Florida batholith further north, close to the Colombian border (Fig. 2.1; Hall and Calle, 1982; Litherland et al., 1994). All three batholiths are voluminous elongate bodies located along the eastern flank of the Andes that were probably related to the same period of magmatism (Baldock, 1982). Because of two important road crosscuts, i.e. the Baeza-Tena and Baños-Puyo roads, the undeformed Abitagua batholith remains the best studied between all. The Abitagua batholith also crops out west of the Pastaza depression within the southern part of the northern SAZ (Fig. 2.1). Nonetheless, up to 500 m wide pods of the Abitagua batholith are also encountered further north in the bed of the Rio Quijos in the vicinity of the



Reventador volcano (Fig. 2.1), indicating that other parts of the Abitagua batholith probably remain buried below Jurassic volcanics and Cenozoic sediments (see below).

Prior to this study, the age of the Abitagua was constrained using Rb/Sr methodology. A three-point, whole rock, Rb/Sr isochron age of  $173 \pm 5$  Ma was obtained by Halpern (quoted in Hall and Calle, 1982). Samples in 100 km distance (i.e. west of Mera and south of Cosanga; see Fig. 2.1) gave a 16-point isochron with an age of  $162 \pm 1$  Ma (Aspden and Litherland, 1992; Litherland et al., 1994). A minimum Middle Jurassic crystallisation age is therefore assumed (Litherland et al., 1994). Few K/Ar ages between  $194 \pm 7$  and  $126 \pm 12$  Ma (Herbert, 1977; Pichler and Aly, 1983; Litherland et al., 1994) were also produced and will be discussed in chapter 3.

Xenoliths from the volcanic Misahualli Fm. are encountered within the Abitagua batholith in the Rio Gringo, an affluent of the Pastaza River west of Puyo (Figures 2.1 and 2.4). This infers a close relationship between the Abitagua batholith and the Misahualli volcanics and suggests a comagmatic origin (Aspden and Litherland, 1992; Litherland et al., 1994). The thrust and faulted contacts of the batholith with both the Misahualli Fm. and the Cenozoic sediments from the northern SAZ does imply that the emplacement of the Abitagua granite to its ultimate level was driven by Cretaceous to Recent tectonics as stated by Kennerley (1980).

2.2.1.2. The volcanic rocks of the **Misahualli** Fm. express a rich association of lithologies from volcanic tuff, trachytic lavas, rhyolitic welded tuffs, andesites, dacites to tuffaceous breccias in the northern Sub-Andean Zones (Fig. 2.4; Wasson and Sinclair, 1927; Hall and Calle, 1982; Baldock, 1982; Litherland et al., 1994; Romeuf et al. 1997). Tschopp (1953) and Hall and Calle (1982) previously attributed these igneous rocks to the upper member of the Jurassic volcano-sedimentary Chapiza Fm. (Tschopp, 1953). However, recent geochemical studies combined with  $^{40}\text{Ar}/^{39}\text{Ar}$  dating concluded that these volcanic levels have a characteristic calc-alkaline signature typical of a continental-type volcanic arc sequence that developed at least as early as  $172 \pm 2$  Ma (Litherland et al., 1994; Romeuf et al., 1995; Romeuf et al., 1997). Therefore, these levels are much older than expected, and their attribution to the Late Jurassic-Early Cretaceous as the upper member of the Chapiza Fm. was misleading (Hall and Calle, 1982). Volcanic rocks are reported above the Chapiza Fm. in a deep well of the flat lying Oriente region and were dated to the Early Cretaceous (132 Ma) using K/Ar (WR) methodology (quoted in Hall and Calle, 1982), and this age was mostly responsible for the misleading attribution of the complete volcanic sequences to the upper member of the Chapiza Fm. Because the Misahualli Fm. does not extend east of the Sub-Andean Front (Rivadeneira and Baby, 1999), where the Chapiza Fm. replaces it, this dated level of Early Cretaceous age is attributed to the Yaupi unit that overlies the Chapiza Fm. in the Oriente region (Jaillard, 1997b; Rivadeneira and Baby, 1999). In the present work, the Jurassic volcanics rocks in the Sub-Andean Zones were individualized from the Chapiza Fm., which represents the back-arc sediments, and ascribed to the Misahualli Fm.

### *- Localization*

Poorly dated volcanic rocks of the Misahualli Fm. are encountered within the northern SAZ in two main positions: (1) as imbricates with the metamorphosed rocks of the Paradalarga unit (Litherland et al., 1994; Buitron and Vallejo, 1999) and Cretaceous cover rocks to west of the Cosanga Fault in the Sub-Andean Thrust Belt (Fig. 2.1; Litherland et al., 1994), and (2) underlying the Hollin Fm. to the east but still in the SAZ. In the first position, the Misahualli Fm. can be metamorphosed as epidote and garnet appears, whereas no metamorphism is reported in the latter one (Litherland et al., 1994).

### *- Thickness and stratigraphic relationship*

The base of the Misahualli Fm. was never encountered in the northern SAZ but can be traced to interfinger with the uppermost deposits of the Triassic-Early Jurassic marine Santiago Fm. in the southern SAZ (Romeuf et al., 1997). Its upper limit with the Hollin Fm. is erosive (Tschopp, 1953; see Hollin section). The thickness of the Misahualli Fm. was never correctly estimated, because it was often confused with the Chapiza Fm. (Tschopp, 1953). A minimum thickness of 650 m was broadly approximated by Pasquarè et al. (1990) in the region of the Reventador volcano in the northern SAZ (Fig. 2.1).

### *- Age of the formation*

The Misahualli Fm. remained poorly dated with the exception of (1) the previously mentioned  $^{40}\text{Ar}/^{39}\text{Ar}$  age of  $172 \pm 2$  Ma (Romeuf et al., 1997), and (2) a  $^{40}\text{Ar}/^{39}\text{Ar}$  age of 162 Ma (Bt) from an imbricate rhyolite in the Sub-Andean Thrust Belt to the west of the village of La Bonita (Spikings et al., 2001; Fig. 2.1). A volcanic level of the northern SAZ yielded an additional age of 230 Ma using K/Ar (Hb) methodology that is quoted in Aspden and Litherland (1992) without more precision, which may indicate the existence of older material within the Misahualli Fm.

The present fission-track study on the Misahualli Fm. proposes a Middle Jurassic (190/180 Ma) to Early Cretaceous (130 Ma) eruption age, which is further discussed in section 3.4.

2.2.1.3. The pelitic schists of the **Upano unit** were never encountered in normal stratigraphic contact with the Cenozoic sediments of the northern SAZ and Pastaza depression (Litherland et al. 1994). However, because this unit is probably older than the Cretaceous (Litherland et al., 1994) and just outcropping to the west of the Sub-

Andean Fault (Litherland et al., 1994), it may have been part of the basement of the AAB in the Mesozoic to Cenozoic.

A recent study in the region of Baeza (Fig. 2.1) allowed Buitron and Vallejo (1999) to distinguish the metamorphosed volcanoclastic sediments from the rest of the unit that is mainly defined by pelitic schists (Litherland et al., 1994). As a result, the authors ascribed these green-schist metamorphosed volcanoclastic sediments to the new **Paradalarga unit**, whereas the Upano unit is reserved for the rest of the unit. The limit between both units was unfortunately not encountered in the field but is most likely represented by the Sub-Andean Fault (Fig. 2.1). The Paradalarga unit has a maximum thickness of 2 kilometers west of the village of Baeza, considering almost vertical bedding whereas no estimation can be made in the NE-SW oriented Rio Sardinas Chico and Rio Bermejo (respectively north and south of Baeza, Fig. 2.1) because the Upano unit further west could not be reached (Buitron and Vallejo, 1999).

The strongly probable common genetic history of the volcanoclastic sediments of Paradalarga unit and the Misahualli Fm. allowed Litherland et al. (1994) to assign a Jurassic age to the formerly undivided Upano unit even as no unambiguous age was ever provided (U/Pb?). Nevertheless, K/Ar ages of  $54 \pm 2$  Ma (Feininger and Silberman, 1982) and  $59.1 \pm 2.2$  Ma (Herbert and Pichler, 1983), an  $^{40}\text{Ar}/^{39}\text{Ar}$  age of  $61.5 \pm 0.6$  Ma (Spikings et al., 2001) on Biotite are associated with a zircon fission-track age of  $45 \pm 5$  Ma from the same sample to suggest that the Upano unit was totally reset. As a result, any possible information relative to its stratigraphic age was lost (see chapter 3).

ZFT ages from  $46 \pm 2.7$  to  $56 \pm 3$  Ma (see chapter 3) suggest that the Paradalarga unit underwent post-depositional resetting to temperatures higher than the zircon partial annealing zone, i.e. 230-310°C (Tagami et al., 1998; see chapter 3).

The transition from the Paradalarga unit toward the Upano unit across the Sub-Andean Fault is characterized by an increasing grade of metamorphism from a lawsonite-sericite-epidote association to a muscovite-garnet association toward the west (Litherland et al., 1994; Buitron and Vallejo, 1999). Furthermore, both units did not yield similar apatite fission-track ages (see section 3.4). This therefore reinforces the distinction of the volcanoclastic sediments of the Paradalarga unit from the pelitic schists of the Upano unit.

2.2.1.4. The Paleozoic **Pumbuiza Fm.** (Tschopp, 1953) was only observed outcropping in the Rio Gringo River west of Puyo and east of the Abitagua batholith (Fig. 2.1), where its lithology is dominated by strongly deformed muscovite rich graphitic schists. The quality of the very few outcrops is very bad because the region is covered by very dense vegetation, and the outcrops are almost inaccessible. The attribution of these levels to the Pumbuiza Fm. rather than to the Cretaceous Napo Fm., which is present in the northern SAZ, was based on their graphitic and mica-rich character that characterize the Pumbuiza Fm. further south in the SAZ (Tschopp, 1953). The Pumbuiza Fm. yielded a zircon fission-track age of  $461 \pm 32$  Ma that most likely

indicates that these levels are the oldest rocks dated in this study of the Andean Amazon Basin (see section 3.4.3).



Figure 2.4: (1) Volcanic xenoliths of the Misahualli Fm. within the Abitagua batholith (Rio Gringo, west of Mera; grid location: 149310-9836286); (2) ash-flows deposits of the Misahualli Fm., Rio Salado-Rio Quijos' junction, south of the Reventador volcano (grid location: 196723-9977438).

## 2.2.2. Sedimentary series

### 2.2.2.1. *Hollin Formation:*

#### *- Type region and extension*

This formation was first described by Wasson and Sinclair (1927) and named Hollin sandstone after its type locality along the Hollin River, in the southern part of the northern SAZ (Fig. 2.1). The Hollin Fm. is a main reservoir rock in the Oriente region where its occurrence is everywhere co-extensive with the overlying Napo Fm. (Tschopp, 1953). Equivalents of the Hollin Fm. are present throughout southern Colombia in the Putumayo Basin (the Caballos Fm.), and northeastern Peru in the Marañón Basin, i.e. the Cushabatay Fm. (Campbell, 1970; Dashwood and Abbotts, 1990; White et al., 1995; Balkwill et al., 1995; Higley, 2000).

Good exposures exist along most of the rivers that cut the northern SAZ. Hence, White et al. (1995) defined a representative stratigraphy of the Hollin Fm. along the Loreto road section where most of the dated Hollin Fm. samples were taken (Fig. 2.1 and 2.5). The westernmost occurrence of the Hollin Fm. is represented by quartzitic slivers situated in the Sub-Andean Thrust Belt along the Baños-Puyo road in the Rio Topo depression (Sauer, 1965; Litherland et al., 1994; Fig. 2.4).

#### *- Lithology*

The detailed stratigraphy of the Hollin Fm. is described elsewhere (Tschopp, 1953; Canfield, 1982; Dashwood and Abbotts, 1990; White et al., 1995; Shanmugam et al., 2000). In general, the Hollin Fm. comprises a blanket of generally coarse, white, porous, thick-bedded to massive, commonly tabular cross-bedded sandstone with sporadic ripple marks. Bedding planes are marked by thin intercalations of dark sandy, in many places micaceous shales and also black carbonaceous shales in the upper part of the section (Tschopp, 1953). Basal conglomerates, often with oil impregnation, are encountered in the central part of the Napo uplift where pebbles are mainly composed of sub-rounded volcanics (Misahualli Fm.?) and sandstones (Fig. 2.6). In the Rio Topo area in the Sub-Andean Thrust Belt (Fig. 2.4), quartz sandstones with frequent muscovite, chlorite and blue quartz characterize the Hollin Fm. (Fig. 2.6). Additionally, White et al. (1995) reported within the same region, isolated outcrops of the basal Hollin Fm. containing gravel-to cobble-size clasts of locally derived igneous rocks that were not studied in detail but possibly indicate a local sourcing from adjacent igneous levels of the Cordillera Real.

### *- Thickness and stratigraphic relationships*

In most of the locations within the northern SAZ, the Hollin deposits rest onto the Jurassic Misahualli Fm. with an angular unconformity (Tschopp, 1953; White et al., 1995; Shanmugam et al., 2000). A 40-60 My hiatus between these two formations, e.g. 4 km west of the Rio Hollin Chico along the Narupa-Loreto road (Fig. 2.6), has been dated in the present-study using fission-track methodology (see chapter 3). This important hiatus perfectly illustrates the commonly assumed truncation and peneplanation of the previously structured older rock units ranging from (probable) Precambrian to Late Jurassic-Early Cretaceous (Tschopp, 1953; Dashwood and Abbotts, 1990), prior to the deposition of the Hollin Fm. Furthermore, levels of the Hollin Fm. to the west of the Abitagua batholith in the region of Mera (Fig. 2.4) are also reported to have been unconformably deposited onto the Abitagua batholith (Litherland et al. 1994; Pratt et al., in press).

The maximum thickness of the Hollin Fm. has been estimated at 150 meters in the south-western AAB (Dashwood and Abbotts, 1990), whereas it gradually thins north-eastwards towards the Guyana Shield. An isopach map of the Hollin formation is here represented in Figure 2.7 indicating that the depocenter of the Hollin Fm. was to the southwest.

### *- Depositional environment*

White et al. (1995) divided the Hollin into two members, i.e. the Main Hollin Sandstone Mb. and the Upper Hollin Mb. characterized by a progressive change of the depositional environment from an alluvial valley fill to a shallow marine sequence (Fig. 2.5). The widespread deposition of the Hollin Fm. in the AAB was the result of an eastward marine transgression over the peneplaned, block faulted, 'pre-Cretaceous' structures (Tschopp, 1953; Dashwood and Abbotts, 1990) that can be correlated in seismic lines through the Oriente basin (Rosero, 1999; Rivadeneira and Baby, 1999). Internal and confidential reports of Oil companies indicate a clear sourcing of the detrital material from the shield regions to the east as also indicated by NW and WNW directed paleo-currents in the Rio Misahualli section in the northern Subandean Zone (Jaillard, 1997b). In the present study, some paleo-current indicators were measured in the westernmost part of the northern SAZ suggesting a slightly different current direction from the NNE to the WNW. However, such variations are common in alluvial plain depositional settings.

### - Age of the formation

Palynologic and paleontologic studies indicate an Albian age for the Hollin Fm. but it can probably be as old as Aptian like in the Putumayo Basin in Colombia (Marksteiner and Aleman, 1996; Balkwill et al., 1995). Balkwill et al. (1995) also reported (non-detailed, because confidential) biostratigraphic arguments indicating an eastward younging of the base of the formation.

Unfortunately, no tephra layer has ever been observed intercalated with the deposits of the Hollin Fm., which would have allowed the determination of an absolute stratigraphic age using an appropriate thermochronometer. Hence, this limits the present application of thermochronology (fission-track on zircons) to the attribution of a maximum stratigraphic age (see section 4.3).

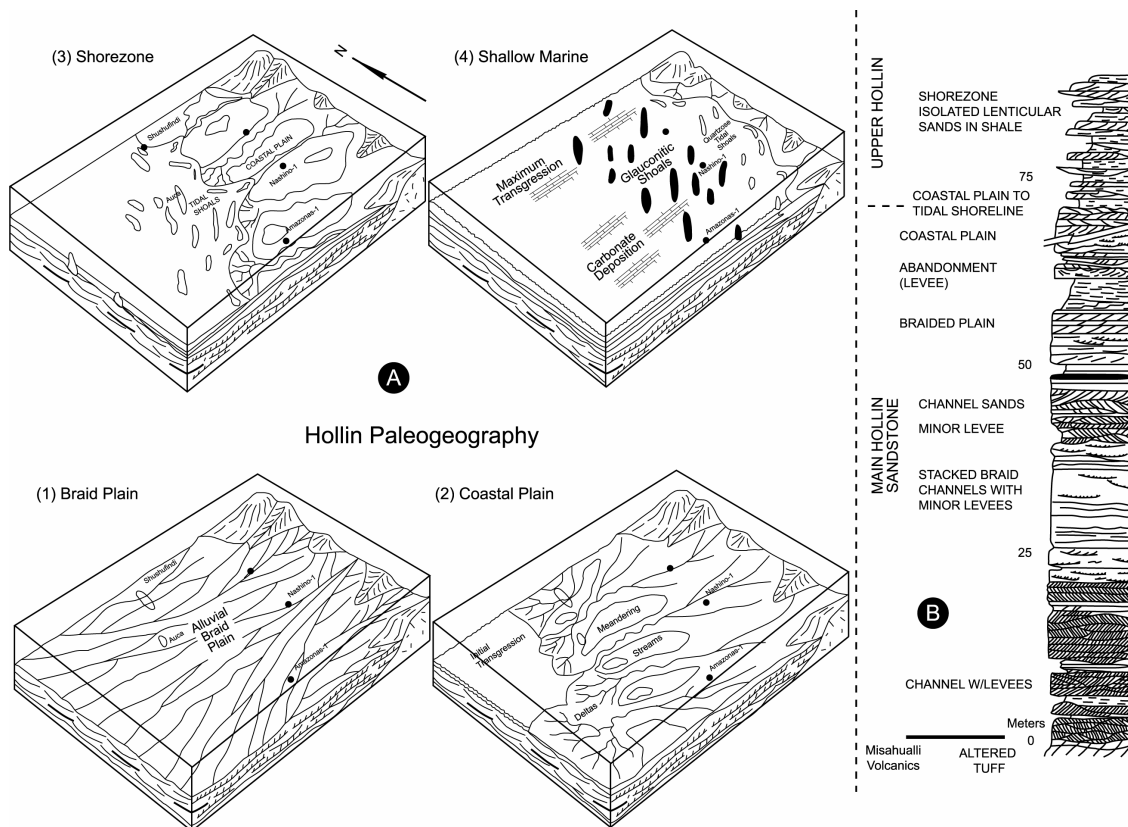


Figure 2.5: (A) Hollin paleogeography in Albian time (White et al., 1995) (1) Braided alluvial plain, (2) initial transgression during main Hollin coastal deposition, (3) Upper Hollin shore zone deposition in tidally influenced nearshore environments, (4) Open Marine sedimentation. (B) Composite sedimentological section of the Hollin Fm. as exposed along the Hollin-Loreto road in the northern SAZ (White et al., 1995).

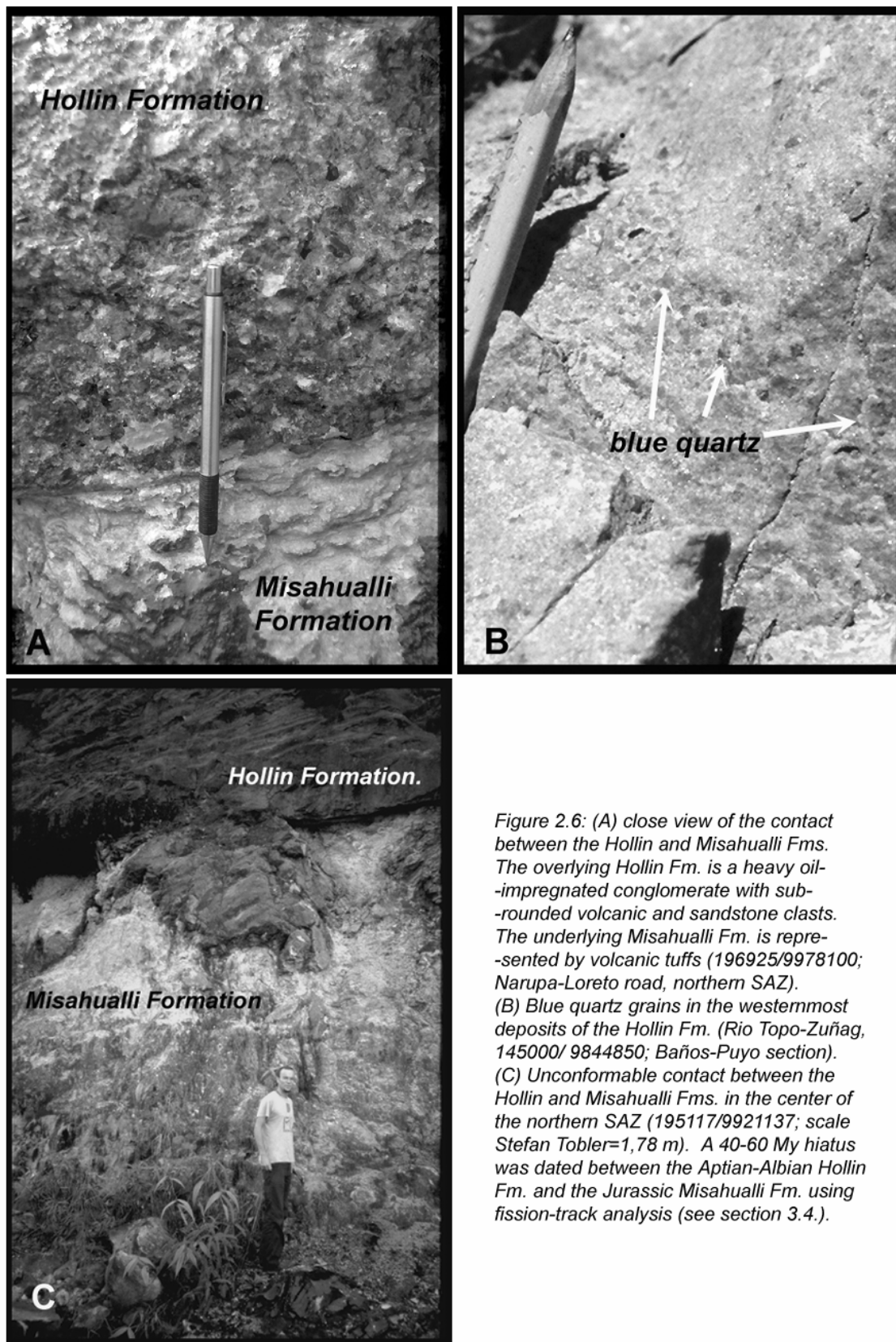


Figure 2.6: (A) close view of the contact between the Hollin and Misahualli Fms. The overlying Hollin Fm. is a heavy oil-impregnated conglomerate with sub-rounded volcanic and sandstone clasts. The underlying Misahualli Fm. is represented by volcanic tuffs (196925/9978100; Narupa-Loreto road, northern SAZ). (B) Blue quartz grains in the westernmost deposits of the Hollin Fm. (Rio Topo-Zuñag, 145000/ 9844850; Baños-Puyo section). (C) Unconformable contact between the Hollin and Misahualli Fms. in the center of the northern SAZ (195117/9921137; scale Stefan Tobler=1,78 m). A 40-60 My hiatus was dated between the Aptian-Albian Hollin Fm. and the Jurassic Misahualli Fm. using fission-track analysis (see section 3.4.).



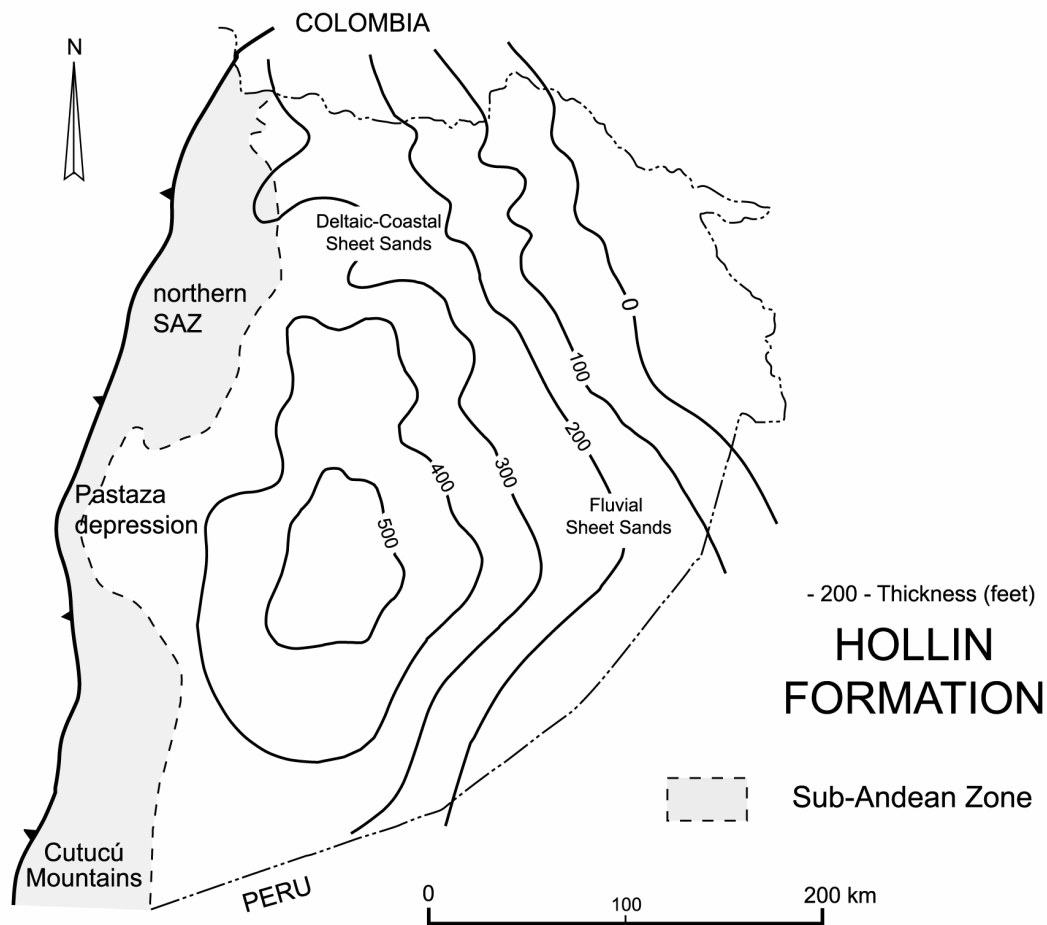


Figure 2.7: Isopach map of the Hollin Formation (adapted from Dashwood and Abbotts, 1990).

#### 2.2.2.2. Napo Formation:

##### - Type region and extension

The type locally was first described by Wasson and Sinclair (1927) along the Napo River in the southern part of the northern SAZ (Fig. 2.1). Several studies were carried out since then to constrain the development of this formation, because it is considered to represent the main hydrocarbon source rock and reservoir rock for the oil present in the Oriente region. Because this formation represents one of the main outcropping formations in the northern SAZ (Fig. 2.1), it gave its name to the northern SAZ in the literature, e.g. the 'Napo Uplift', 'Napo antiform' or 'Napo anticline'.

The known most western occurrence of the Napo Fm. is located in the Sub-Andean Thrust Belt, west of the Abitagua batholith along the Baños-Puyo road (see Fig. 2.1). The time equivalent of the Napo Fm. to the west is not precisely known, as Late Cretaceous to Recent Andean orogenic movements probably removed the westernmost deposits of the Napo Fm. A recent study (Pratt et al., 2002) suggests that the strongly deformed limestones of the Cerro Hermoso (i.e. a ~ 5000 metres summit in the present-day Cordillera Real) might represent relics of the westernmost Napo deposits as already proposed by other authors (e.g. Wolf, 1892; Tschopp, 1953; Kennerley, 1971; Baldock, 1982). Litherland et al. (1994) attributed a Jurassic age to the Cerro Hermoso unit because it is intruded by the Middle Jurassic Azafrán pluton. However, this contact may have occurred later than the Jurassic, i.e. when rocks of the Azafrán pluton were exhumed and brought toward the surface during an orogenic phase. To the east, in the Oriente region, the Napo Fm. conformably rests on the Hollin Fm. or on the basement of the AAB (Tschopp, 1953).

### *- Lithology*

The Napo Fm. consists of a variable succession of shallow marine sandstones, claystones and limestones. The two latter ones appear to be the main source rock while some of the sandstones bodies are significant oil reservoirs (the 'U' and 'T' members; White et al., 1995; Jaillard, 1997b). The shallow marine series of the Napo Fm. are fully described in more detail elsewhere (Tschopp, 1953; Canfield, 1982; Balkwill et al., 1995; White et al., 1995; Dashwood and Abbotts, 1990; Jaillard, 1997b; Vallejo et al., 2002).

### *- Volcanism*

Igneous bodies are intercalated within the Napo Fm. along NNE-SSW oriented pre-Cretaceous faults in the Oriente region (Barragan et al., 1997) that were reactivated in the Cretaceous in a right-lateral transpressive regime (Rivadeneira and Baby, 1999; Fig. 2.8). Some of these bodies of alkaline composition were dated using K/Ar methodology and range from 106 to 84 Ma (Barragan et al., 1997). Moreover, igneous bodies within the Napo Fm. are not restricted to the Oriente region but are also located within the northern SAZ, e.g. in the Bermejo Norte-16 well (Jaillard, 1997b), and Pungarayacu-30 well (Vallejo, pers. com.) where they are interbedded within the early-Middle Turonian 'A' limestone (Jaillard, 1997b). Additionally, volcanics bodies are also seen in the Napo Fm. in the southern SAZ (or Cutucú Mountains) in the Rio Upano and along the road Limón-Plan de Milagro where an Albian age is assumed (Jaillard, 1997b). All the igneous bodies in the Oriente and SAZ lie along a NNE-SSW trending direction that is parallel to the inverted pre-Cretaceous structures (Fig. 2.9). It is thus

reasonable to envisage that this NNE-SSW pre-structuration of the basin may have extended further to the west, at least in the area of the present-day location of the Ecuadorian Sub-Andean Zones.

#### *- Thickness and stratigraphic relationships*

The base of the Napo Fm. is characterized by the appearance of glauconitic sandstones conformably overlying the Hollin Fm. (Fig. 2.7) whereas it unconformably overlies the basement to the far-east in the Oriente region where the Hollin Fm. was not deposited. The thickness of the Napo Fm. varies from 200 metres to the ENE to up to 600 metres in the south-western part of the AAB, i.e. the southern SAZ or Cutucú Mountains (Baldock, 1982; Dashwood and Abbotts, 1990; Fig. 2.9). The axis of the depocenter is oriented NNW-SSE according to Dashwood and Abbotts (1990). However, this difference in thickness from northeast to southwest is probably minimized by the westward truncation of the Napo Fm. from the axial part of the basin prior to the deposition of the overlying Tena Fm. (Tschopp, 1953; Balkwill et al., 1995), indicating that the depocenter of the Napo Fm. was possibly differently oriented and located further west of the Sub-Andean Zone.

#### *- Age of the formation*

Very detailed studies of the Cretaceous-Paleocene stratigraphy in the AAB was carried out since 15 years by both the National Ecuadorian Oil Company (Petroproducción) and l'Institut de Recherche et Développement (IRD) using micropaleontology. The compilation of the data (Jaillard, 1997b) indicates a Middle Albian to Campanian age to the Napo Formation that is corroborated by a recent Palynologic study from the Pungarayacu well (Vallejo et al., 2002).

#### *- Depositional environment*

It is commonly accepted that the transgressive-regressive system tracts characterizing the shallow marine Napo Fm. took place in a broad, relatively stable epi-continental sea west of the Guyana Shield and east of a paleo-relief that might have been represented by the northward equivalent of (1) the Olmos Arch in northern Peru (Baldock, 1982; Jaillard, 1997b), and (2) the southern equivalent of the emergent Central Cordillera in Colombia (Rangel et al., 2000; Ramón et al., 2001). Moreover, the presence of local parasequences suggests that the Napo Formation was deposited above elongate, northward-trending paleostructural highs (Balkwill et al., 1995).

Moreover, the upper Napo deposits, e.g. the M1 member, which are most probably only preserved to the east of the Andean Amazon Basin are considered as deposited during compressional tectonic activity that developed to the west of the basin (Jaillard, 1997b; Rosero, 1997; Christophoul, 1999). This allowed Christophoul (1999) to suggest that the polarity of the sourcing probably changed from westward to eastward in the Turonian-Paleocene interval, and Jaillard (1997b) to correlate the onset of a foreland development of the Andean Amazon Basin to the Turonian-Coniacian boundary.

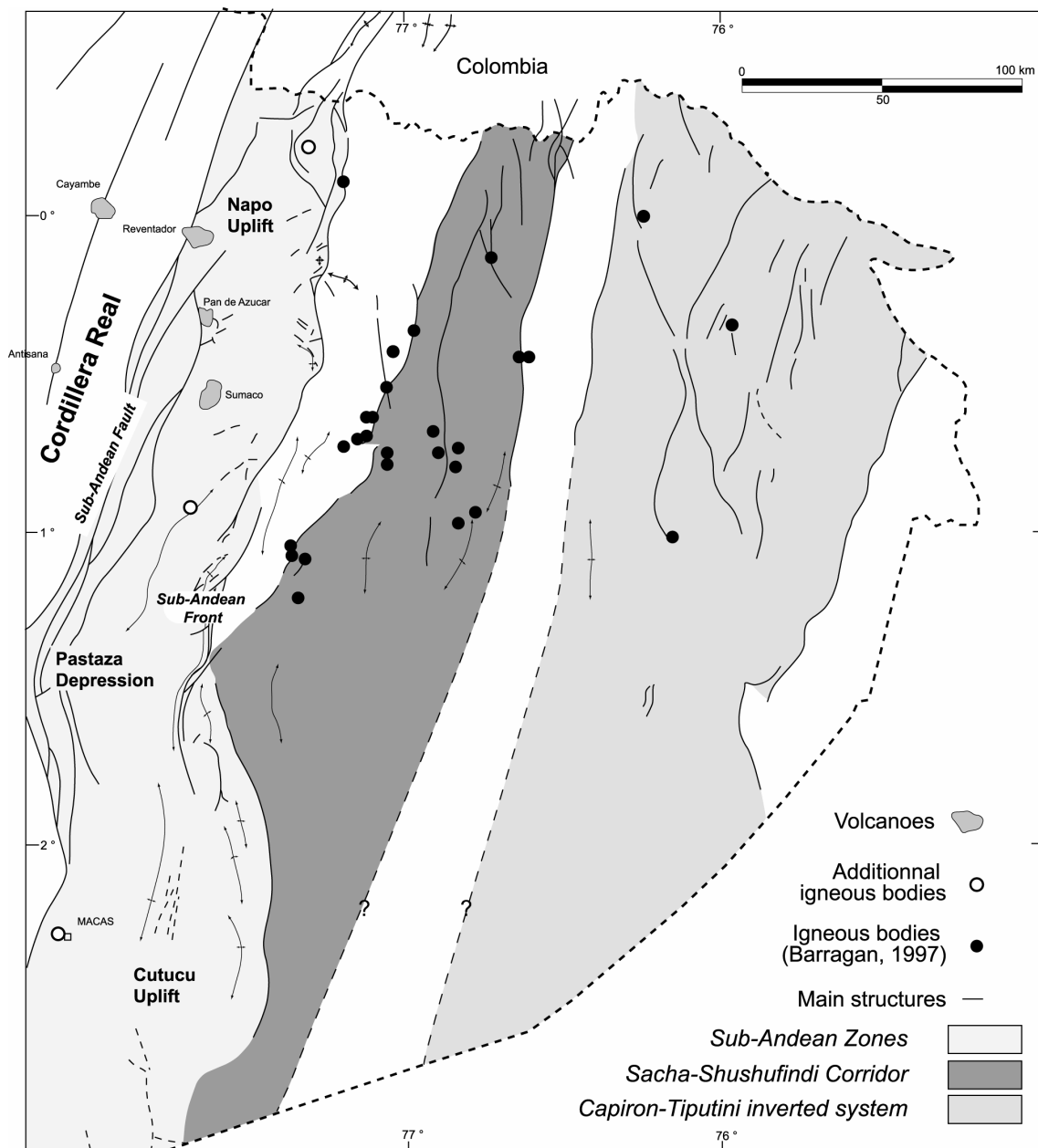


Figure 2.8: Localization of igneous bodies in the Andean Amazon Basin (Barragan, 1997; Rivadeneira and Baby (1999); Jaillard, 1997b; Vallejo, pers. com.). The AAB has been divided into three zones in which the inversion of the pre-existing Permo-Triassic and Early Jurassic structures occurred, i.e. the Sub-Andean Zone, the Sacha-Shushufindi corridor and the Capiron-Tiputini inverted system (Rivadeneira and Baby, 1999).

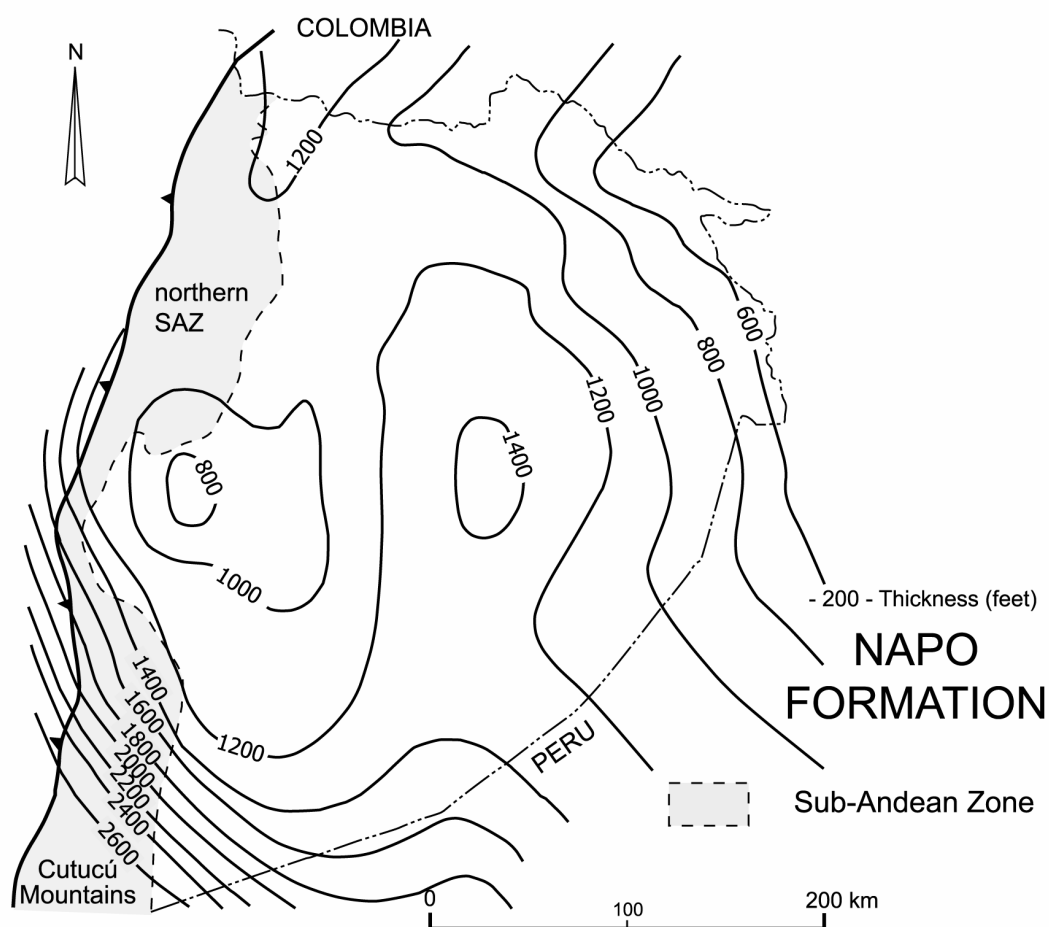


Figure 2.9: Isopach map of the Napo Formation (adapted from Dashwood and Abbotts, 1990).

#### 2.2.2.4. Tena Formation:

##### - Type region and extension

The name Tena Fm. was introduced in 1939 by Shell geologists (quoted in Tschopp, 1953) to series of red bed sediments encountered in the vicinity of the town of Tena in the northern SAZ (Fig. 2.1).

These characteristic continental series were deposited in the entire Ecuadorian Andean Amazon Basin (AAB), as they were penetrated in every drilled well in the Oriente region. Imbricate slivers in the Sub-Andean Thrust belt (Litherland et al., 1994), e.g. west of the Abitagua batholith in the Baños-Puyo section (Fig. 2.1) represent the westernmost occurrence of the Tena Fm. The Tena Fm. can be correlated with the

Olini Gp. and Rumiyaco Fm. in the Putumayo Basin in southern Colombia (Higley, 2000), and with the upper formations of the Vivian group and the Yahuarango Fm. (Tschopp, 1953; Jaillard, 1997b; Higley, 2000) in the Marañon Basin of northern Peru.

### *- Lithology*

The Tena Fm. is dominated by red shales with numerous intercalations of sandstones and sparse conglomerates, particularly in the lower 200 m and the upper 150 m (Baldock, 1982). The colour of the Tena Fm. varies from brick red to purple toward greenish to brown sandstones in the lower part (Tschopp, 1953). These different colours are largely due to surface weathering, because the sediments are black, grey or greenish when sampled from quite fresh outcrops (Baldock, 1982).

Recent reports (Jaillard, 1997b; Rivadeneira and Baby, 1999) and study (Christophoul, 1999) suggest that the Tena Fm. can be divided into two members, which are probably separated by a Late Maastrichtian-Early Paleocene hiatus. In the northeast of the Oriente region, this hiatus is indicated by a conglomerate at the base of the upper member. To the southwest, the boundary is indicated by clear differences in the gamma ray and spontaneous polarisation sonic logs (Jaillard, 1997b). The upper member in few locations is characterized by coarsening upward cycles (Tschopp, 1953).

### *- Thickness and stratigraphic relationships*

The transition from the Napo Fm. to the Tena Fm. marks a prominent change in the type of sedimentation that since prevailed in Ecuador. As mentioned earlier, the upper Napo Fm. to the west of the AAB was truncated prior to the deposition of the Tena Fm. resulting in a hiatus between the formations (Tschopp, 1953; Canfield et al., 1982; Balkwill et al., 1995; Jaillard, 1997b; Christophoul, 1999).

Well data and seismic lines allowed Dashwood and Abbotts (1990) to document an isopach map of the Tena Fm. (Fig. 2.10) but that did not take into account the new subdivision of the Tena Fm. into two members. Considering the entire Tena Fm., a general decrease in thickness is observed in the Oriente basin towards the east where the Tena Fm. was not deposited or completely eroded. In the Sub-Andean Zone, the thickness of the Tena Fm. is traceable with difficulty, because (1) it shows general sub-horizontal bedding, and (2) both contacts with the underlying Napo Fm. and the overlying Tiyuyacu Fm. are traceable with difficulty. This thus renders the estimation of its thickness impossible. Furthermore, the probable uplift of the Sub-Andean Zone in the Early Eocene possibly generated the erosional truncation of the Tena deposits in the region prior to the deposition of the overlying Tiyuyacu Fm. (Christophoul et al., 2002).

However, the thicknesses of Tena Fm. preserved in the SAZ and in the westernmost proximal wells in the Oriente region, indicate that the Tena Fm. may have reached 900-1000 meters in the present-day location of the northern Subandean Zone (Dashwood and Abbotts, 1990).

#### *- Age of the formation*

The Tena Fm. is poorly dated as observed fossils are very scarce and may be also the results of reworking from previously deposited sedimentary formations (Baldock, 1982). Nevertheless, Jaillard (1997b) suggests that the age of the Tena Fm. is not restricted to the Maastrichtian as previously assumed (Faucher and Savoyat, 1973) but probably extended into the Paleocene.

A detrital zircon fission-track grain age population of  $63 \pm 3$  Ma was obtained from a level in the upper member (see section 4.2). This age is a maximum stratigraphic age for these terms of the Tena Fm., and thus validates the extension of the Tena Fm. into the Early Paleocene.

Further south in the Subandean Zone (Cutucú Mountains), another group of poorly studied sediments (the Limon Group) is observed and correlated with the Maastrichtian (Faucher and Savoyat, 1973; Jaillard, 1997b). This would indicate that the Limon Group could be an equivalent of the Lower Tena member (Christophoul, 1999).

#### *- Depositional environment*

The Tena Fm. was deposited mainly in a fresh water environment (Tschopp, 1953); brief marine incursions occurred in the lower part (Tschopp, 1953). Therefore, a significant change of the depositional environment occurred in the Andean Amazon Basin from a shallow marine to continental basin. Since the first investigations in the Andean Amazon Basin (Tschopp, 1953), the deposits of the Tena Fm. are assumed to represent the first sediments in the AAB to be supplied to from the west in response to uplift and erosion of a nascent Andean orogenic belt (Baldock, 1982; Jaillard, 1997b). Furthermore, the contemporaneous increase of the tectonic subsidence during time of deposition of the Tena Fm. suggests the presence of an orogenic load onto the South American Plate in the Maastrichtian-Paleocene that was located to the W of the basin (Jaillard, 1997b). Asymmetrical deposits of the Tena Fm. (without additional precisions) are reported above Pre-Cretaceous structures in the Oriente basin (Rivadeneira and Baby, 1999). This allowed the authors to conclude that the distal part of the AAB experienced compressive phases after the deposition of the Tena Fm. (Maastrichtian-Paleocene).

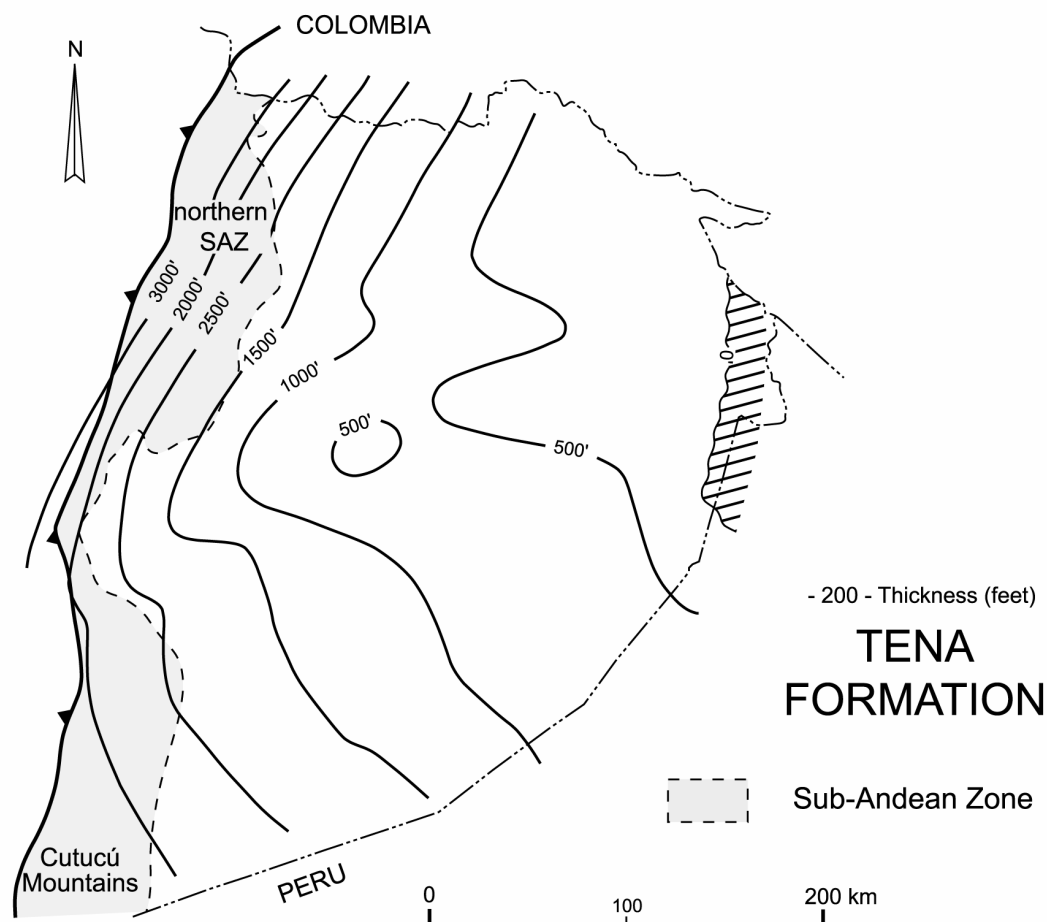


Figure 2.10: Isopach map for the Tena Formation (adapted from Dashwood and Abbotts, 1990).

#### 2.2.2.5. Tiyuyacu Formation:

##### - Type region and extension

The Tiyuyacu Fm. was named by geologists from the Texaco and Shell Oil Companies (Hess, P., 1939 quoted in Tschopp in 1953). The type locality of the Tiyuyacu Fm. is at Tiyuyacu creek, 8 km E/SE of the village of Puerto Napo (Fig. 2.1) in the southern part of the northern Sub-Andean Zone.

The geographic distribution of the Tiyuyacu Fm. is not much different from the underlying Tena Fm. to the east, in the Oriente region (Dashwood and Abbotts, 1990). In contrast, in the Sub-Andean Thrust Belt, or generally to the west of the Cosanga Fault (Fig. 2.1), the Tiyuyacu Fm. is absent (Fig. 2.1). The Tiyuyacu Fm. outcrops in



the (1) southern and northern parts of the northern SAZ (Fig. 2.1), (2) the Pastaza depression (Fig. 2.1), and (2) vicinity of the Sub-Andean Front where it defines an almost continuous outcrop (Tschopp, 1953; Fig. 2.1).

The Tiyuyacu Fm. can be broadly correlated with the Rentema and Pozo Fms. to the south in northern Peru (Naeser et al., 1991; Jaillard et al., 2000), and with the Rumiayaco Fm. to the north in Colombia (Higley, 2000).

### *- Lithology*

The Tiyuyacu Fm. was recently studied in details and divided into two members following sedimentological and seismic arguments that are detailed in the publications of Valdez-Pardo (1997), Rivadeneira and Baby (1999), and Christophoul et al. (2002). The lithologies of both members are briefly summarized here:

*Lower Tiyuyacu Mb.:* the Lower Member correlates with a major regional erosive unconformity that has removed part and possibly the totality of the underlying Tena Mb. (Rivadeneira and Baby, 1999). The deposits of the Lower Tiyuyacu Mb. are represented by up to 10 metre thick sequences of conglomerates grading upward into coarse and fine sandstones. The conglomerates are composed of 80% to 90% of reddish cherts and 10% to 20% of white vein quartz and metamorphic pebbles (Campbell, 1970; Rivadeneira and Baby, 1999; Christophoul, et al., 2002). However, personal observations in a similar level of the Lower Tiyuyacu Mb. in the Cerro Lumbaqui area to the west of the village of Lumbaqui (Fig. 2.1) show that the composition is more variable. We encountered: (1) anchizonal metamorphic black shale pebbles up to 3 cm long, (2) 2-4 cm sized micaceous greywacke clasts, and (3) up to 10-12 cm large sub-rounded clasts of black radiolarian cherts (Fig. 2.11).

The matrix of these conglomeratic levels is partly composed of devitrified volcanic ash whereas the bulk of the clasts is in agreement with other described outcrops.

*Upper Tiyuyacu Mb.:* the main difference between the two members is the lithologic composition of the conglomerates (Rivadeneira and Baby, 1999). Conglomerates of the upper member are composed of 90% well sorted to very well sorted clasts of white vein quartz; the matrix being scarce and composed of blue to green sandstone (Fig. 2.11; Christophoul et al., 2002).

### *- Thickness and stratigraphic relationships*

Both Members are unconformably overlying the preceding deposits in a remarkable and sharp contact observed both in the field (Fig. 2.11), and in seismic lines (Tschopp, 1953; Campbell, 1970; Christophoul et al., 2002). Christophoul et al. (2002) proposed

that the Lower Tiyuyacu Mb. may have been completely removed in the south-western part of Oriente region.

The thickness of the Tiyuyacu Fm. was estimated in 1953 (Tschopp) using both the well data and photo-geologic studies. Later, the first isopach map of this formation was produced in 1990 by Dashwood and Abbott. Collaboration between the National Oil Company (Petroproducción) and the IRD (Institut Français de Recherche pour le Développement) enabled Christophoul et al. (2002) to compile more than 200 well data and present isopach maps respecting the most recent sub-division of the AAB sedimentary units.

The NE 10° striking depocenter of the lower Tiyuyacu Mb. is situated on the eastern side of the Sacha-Shushufindi corridor where a maximum thickness of 450 metres is observed (Fig. 2.12). However, it should be noted that the thickness of the Lower Tiyuyacu Mb. is only a minimum thickness estimate as part of the deposits were eroded prior to the deposition of the upper member (Christophoul et al., 2002). Very few wells were drilled in the Sub-Andean Zone; the thickness of the Tiyuyacu Fm. is estimated there in the field with difficulty because the formation is not always preserved. The isopach lines presented in Figure 2.12 in the Sub-Andean Zone are therefore very poorly constrained and cannot be used for interpretation.

Unfortunately, the Upper Tiyuyacu Mb. deposits were not distinguished from the overlying Orteguzza Fm. in Christophoul et al. (2002). Hence, no clear estimates concerning the Upper Tiyuyacu Mb. can be made.

#### *- Age of the formation*

Faunal and palynological evidence indicate a maximum Early Eocene age for the Tiyuyacu Fm. (Faucher and Savoyat, 1973; Bristow and Hoffstetter, 1977). However, Christophoul et al. (2002) recently dated using  $^{40}\text{Ar}/^{39}\text{Ar}$  thermochronology on biotite from an interbedded tuff layer in the basal conglomerates of the Upper Tiyuyacu Mb. in the Napo Uplift that is elsewhere reported in the Napo Uplift (Valdez-Pardo, 1999 quoted in Christophoul, 1999). The age of  $46.0 \pm 0.4$  Ma correlates the Upper Tiyuyacu Mb. with the Middle Eocene.

Indirect dating of the formation is provided by the youngest detrital zircon fission-track population (see section 4.3.1). A detrital zircon fission-track population of  $61 \pm 5$  Ma therefore ascribed a minimum Early Eocene age to the base of the Tiyuyacu Fm., whereas the extension of the upper member probably reaches the Late Eocene, as a population of  $36 \pm 4$  Ma was dated in the uppermost sampled level (see 4.3.1).

#### *- Depositional environment:*

Fluvial deposits characterize the facies of the Eocene Tiyuyacu Fm. The sediments of the Lower Tiyuyacu Mb. are organized in typical channel filling, fining-upward

sequences (Christophoul et al., 2002). Each base of sequence corresponds to conglomerates deposited in gravel bars grading upward into flood plain deposits of a meandering system (Christophoul et al., 2002). Facies associations of the Upper Member are quite similar to the Lower Tiyuyacu Mb. but show a stacking of channel filling sequences as typical for braided river deposits.

Data from 70 wells were compiled to map the sediment grain-size/thickness ratio in the Lower Tiyuyacu Mb. deposits (Christophoul et al., 2002). The authors concluded that two trenches of coarse sediments with a N135 strike were present to the west of the AAB during time of deposition of the Lower Member. Both trenches and paleocurrents directions clearly indicate that the Tiyuyacu Fm. was sourced in the west (Christophoul, 1999).

Syn-sedimentary growth along reactivated pre-Cretaceous faults generated local progressive unconformities in the Lower Tiyuyacu Mb. in the Oriente region (Rivadeneira and Baby, 1999; Christophoul et al., 2002). This is combined with the absence of the Tiyuyacu Fm. in the Sub-Andean Thrust Belt to the west to suggest that a major compressive phase occurred prior or during deposition of the Tiyuyacu Fm. imbricating the preceding deposits of the Hollin, Napo and Tena Fms.

Similar re-activation is not reported from the Upper Member, which was characterized by a high mineralogical maturity of the conglomeratic clasts (Christophoul et al., 2002). Furthermore, Spikings et al. (2000) reported rapid exhumation in the Cordillera Real during deposition of the Upper Tiyuyacu Mb. that allowed Christophoul et al. (2002) to invoke an isostatic readjustment of the Cordillera Real in the Middle to Late Eocene. According to the authors, this would have permitted the (1) deposition of the homogenous Upper Tiyuyacu blanket over the entire AAB (Rivadeneira, pers. com.).

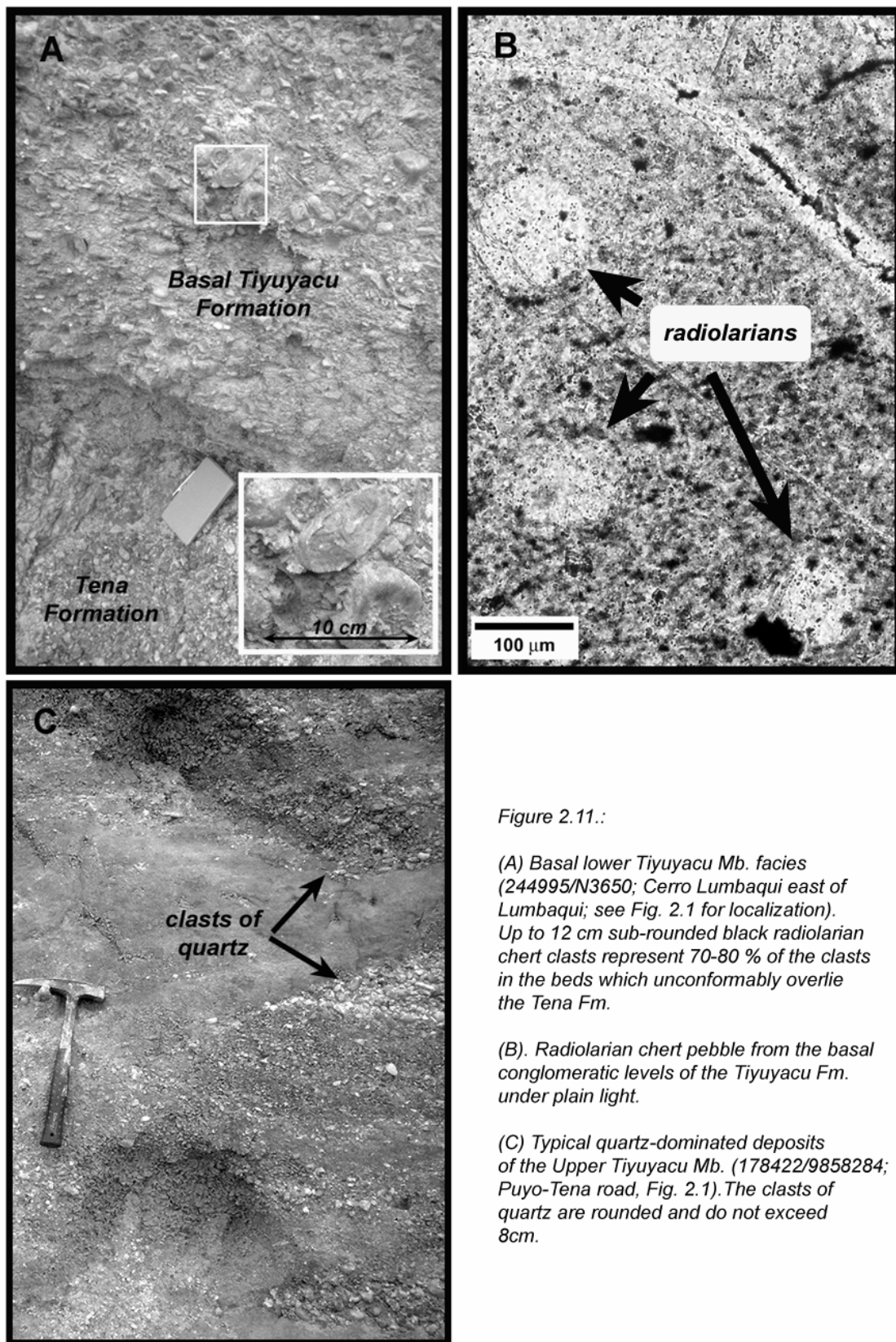


Figure 2.11.:

(A) Basal lower Tiyuyacu Mb. facies (244995/N3650; Cerro Lumbaqui east of Lumbaqui; see Fig. 2.1 for localization). Up to 12 cm sub-rounded black radiolarian chert clasts represent 70-80 % of the clasts in the beds which unconformably overlie the Tena Fm.

(B). Radiolarian chert pebble from the basal conglomeratic levels of the Tiyuyacu Fm. under plain light.

(C) Typical quartz-dominated deposits of the Upper Tiyuyacu Mb. (178422/9858284; Puyo-Tena road, Fig. 2.1). The clasts of quartz are rounded and do not exceed 8cm.

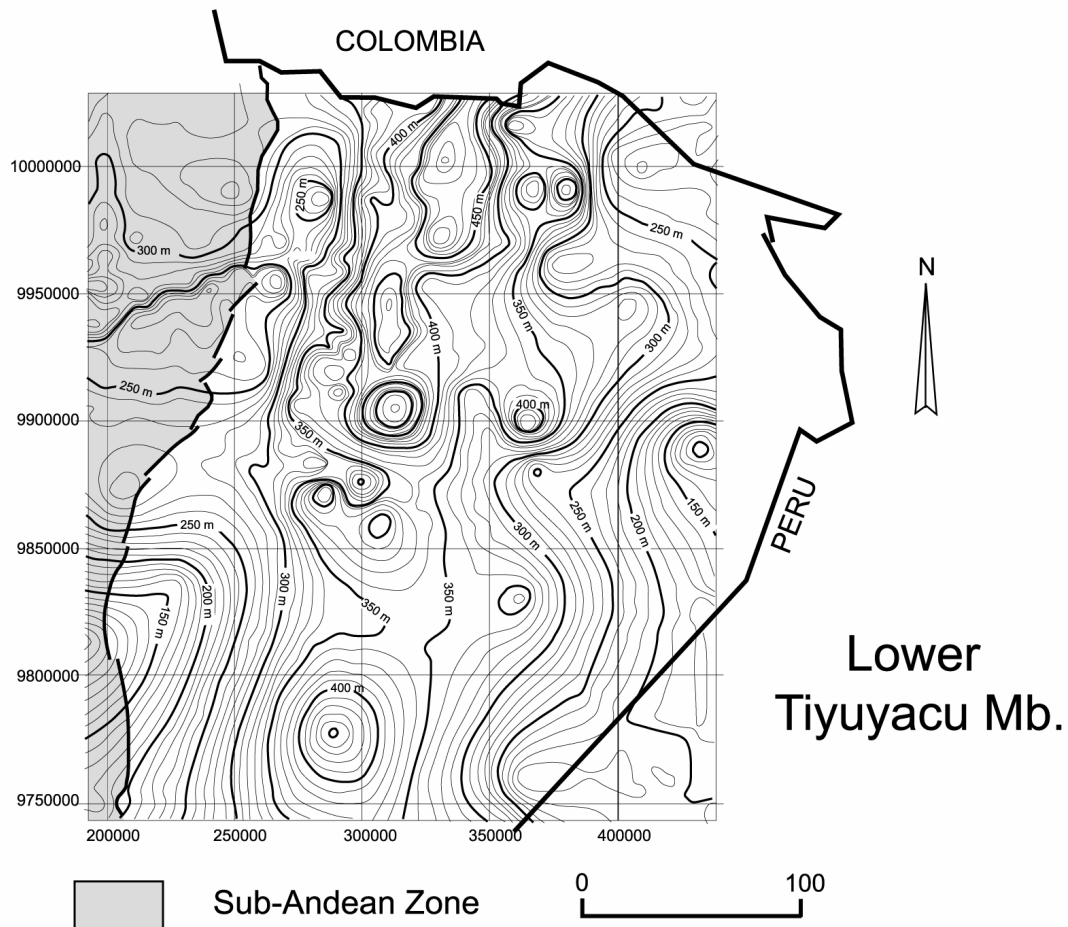


Figure 2.12: Isopach map of the Lower Tiyuyacu Mb. (Christophoul et al., 2002).

### 2.2.2.6. Orteguaza Formation

#### - Type region and extension

Outcrops of the Orteguaza Fm. are limited to the Aguarico River in the northern part of the Napo Uplift (Fig. 2.1). Based on well data Christophoul et al. (2002) indicate that the Orteguaza Fm. was deposited in the entire AAB. The Orteguaza Fm. can be traced from the Putumayo Basin in Colombia from which its name is derived (Baldock, 1982).

### *- Lithology*

The Orteguzaza Fm. consists of fine fluvial deposits similar to the overlying Chalcana Fm. (Baldock, 1982), which were not yet individualized from the Tiyuyacu Fm. and Chalcana Fm. by Tschopp in 1953. Further to the east, the Orteguzaza Fm. consists of shallow marine deposits composed of greenish shales and medium to coarse, locally glauconitic, sandstones (Rivadeneira and Baby, 1999; Christophoul et al., 2002).

### *- Thickness and stratigraphic relationships*

The Orteguzaza Fm. para-conformably overlies the Upper Tiyuyacu Mb. Its base corresponds to a regional onlap surface that can be traced in most of the Oriente region (Christophoul et al., 2002). As previously discussed in section 2.4.2.5, the Upper Tiyuyacu Mb. and the Orteguzaza Fm. were combined in one isopach map (Christophoul et al., 2002). However, Rivadeneira and Baby (1999) estimated the maximum thickness of the Orteguzaza Fm. to 250 m in the northern part of the Oriente region, and to 40 m in the northern part of the Napo Uplift.

### *- Age of the formation*

An Internal reports from the Ecuadorian State Oil Company (Petroproduccion) attributed a Mid-Eocene-Oligocene age to the Orteguzaza Fm. using unknown criteria (quoted in Rivadeneira and Baby, 1999). However, a recent palynologic study correlates the Orteguzaza Fm. with the Early Oligocene with a possible extent to the Late Eocene age (Zambrano, 1999 quoted in Christophoul et al., 2002).

### *- Depositional environment*

The deposition of the Orteguzaza Fm. occurred within beach to marginal marine environments (Christophoul et al., 2002). Well log data indicate that the Orteguzaza Fm. is composed of two transgression–regression cycles (Christophoul et al., 2002), the first one being possibly isochronous along the northern Andean segment, i.e. Colombia (Christophoul, 1999).

### *2.2.2.7. Chalcana Formation:*

#### *- Type region and extension*

Earlier, the Chalcana Fm. represented the middle member of the Pastaza Fm. of Tschopp (1953) that was individualized and named Chalcana Fm. in 1982 by Baldock. The Chalcana deposits are encountered in the Napo Uplift only along its eastern flank where it shows together with the Tiyuyacu Fm. an almost continuous outcrop (Fig. 2.1). The Chalcana Fm. is buried by younger deposits in the Pastaza depression (Fig. 2.1), and is continuously traced in the Oriente region by well log analysis (Tschopp, 1953).

#### *- Lithology*

The Chalcana Fm. comprises a thick and monotonous sequence of red to green spotted marlstones, with sandstones intercalations (Baldock, 1982). Sediments are bioturbated and exhibit rooted muds (paleosols), silts and laminated sandstones. Gypsum is also observed (Christophoul et al., 2002). Along the Rio Napo river, the formation is constituted of a succession of micaceous marlstone and sandstone levels, with a maximum 1-2 m thickness for the later ones (Fig. 2.13).

#### *- Thickness and stratigraphic relationships*

The depositional hiatus between the underlying Orteguzza Fm. and the Chalcana Fm. (Baldock, 1982) is strongly marked (high contrast in seismic records) in the Oriente region (Christophoul, 1999). An isopach map of the Chalcana Fm. is not available. However, Christophoul et al. (2002) calculated the thickness of the Chalcana Fm. in three locations of the Oriente region. It ranges from 250 meters to the west, to more than 450 meters in the center part, and 310 m to the east.

#### *- Age of the formation*

A palynologic analysis suggests a Late Oligocene-Early Miocene age of the Chalcana Fm. (Zambrano, 1999 quoted in Christophoul et al., 2002) that is in agreement with the age correlation provided by Bristow and Hoffstetter (1977) using faunal evidences.

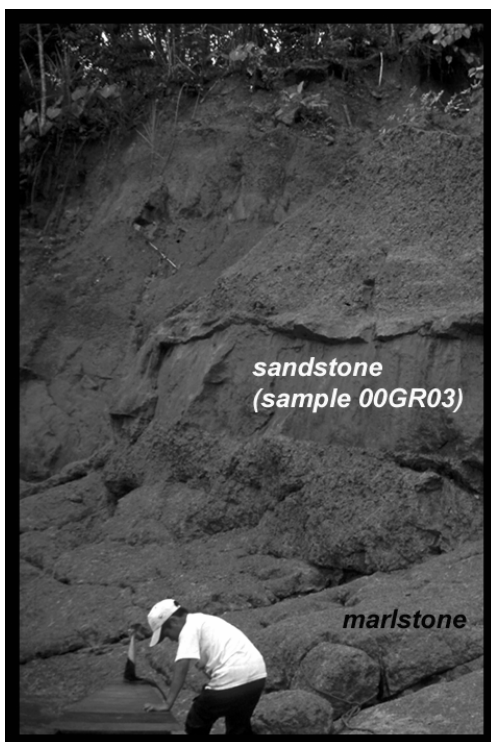


Figure 2.13: Outcrop of the Chalcana Fm. along the Napo River (212561/9886172). The formation is constituted of a succession of micaceous marlstone and sandstone levels, with a maximum 1-2 m thickness for the later ones.

### - Depositional environment

The Chalcana Fm. consists of fine-grained sediments represented mainly by overbank and floodplain deposits in an alluvial plain environment (Christophoul et al., 2002). Intercalated sandstone beds are laterally continuous indicating the presence of a meandering fluvial system.

### 2.2.2.8. Arajuno Formation:

#### - Type region and extension

The Arajuno Fm. was introduced by Hess in 1939 (reported in Tschopp, 1953) from outcrops along the Arajuno tributary of the Napo River southeast of the village of Puerto Napo (Fig. 2.1).

In the lithologic scheme of Tschopp (1953), the Arajuno Fm. represented the upper member of his Pastaza Fm. In the Oriente region, its geographic extension remains poorly constrained (Baldock, 1982), because the Neogene series commonly have not been differentiated in well logs. To the west, in the Pastaza depression (Fig. 2.1) the Arajuno Fm. is limited by the Abitagua batholith but is not reported elsewhere in the Napo Uplift with the exception of outcrops located to the west of the Sub-Andean Front between Loreto and Puerto-Misahualli (Fig. 2.1).



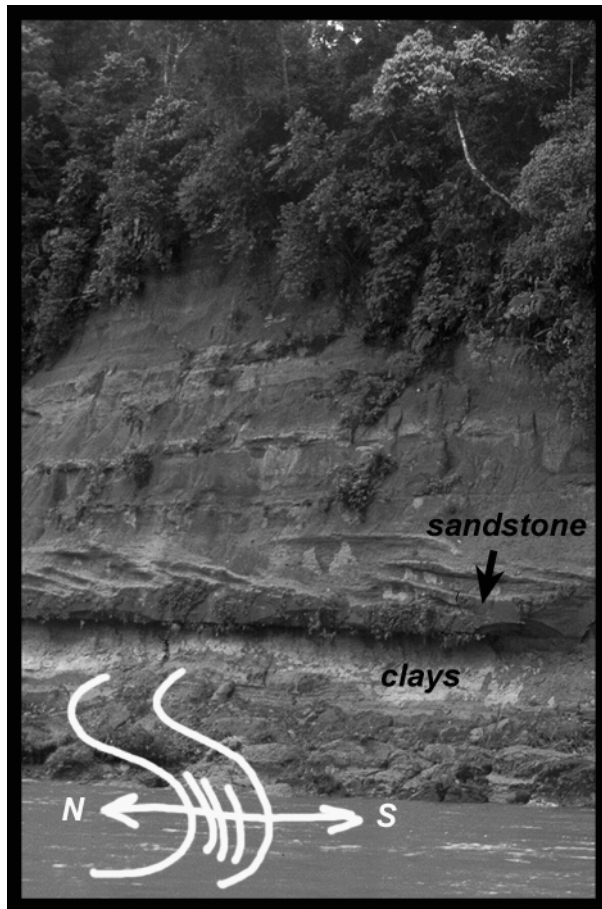


Figure 2.14: succession of silts and sandstones levels of the basal (?) Arajuno Fm. along the Rio Napo (216517/9882580) in the vicinity of the village of Puerto Misahualli (Fig. 2.4). The lee-side channel facies are dipping toward the south indicating a W-E orientation of transport.

### - Lithology

The Arajuno Fm. has been divided into two informal units (Tschopp, 1953; Baldock, 1982): a lower sandstone unit with conglomeratic and bentonite clay intercalations (Fig. 2.14), and an upper unit of reddish gypsiferous clays at the base and tuffaceous clays upwards. It is interesting to note that Tschopp (1953) observed in the lower unit a remarkable amount of hornblende.

### - Thickness and stratigraphic relationships

Following Baldock (1982), the Arajuno Fm. is at least 1000 m thick. The transition from the Chalcana Fm. to the Arajuno Fm. was reported as conformable along the Puyo-Tena road (Campbell, 1970; Fig. 2.1) whereas it was qualified as 'clear' (?) by Baldock (1982). However, a recent study on the Neogene sequences of the Ecuadorian AAB (Rosero-Revelo, 1999) suggests that the contact between the Chalcana and Arajuno formations is most likely slightly unconformable.

### - Age of the formation

In the present study we can provide a chronostratigraphic dating of a level in the basal Arajuno Fm. near the village of Puerto Misahualli (Fig. 2.4). The heavy mineral analysis of this sample (00GR04) suggest a coeval volcanic contribution to the analysed sandstone that can be correlated with the abundance of hornblende that was already observed in the basal unit by Tschopp in 1953. (see section 4.1). The youngest

(euhedral) detrital apatite and zircon fission-track populations yielded identical populations of ~21-22 Ma old (see section 4.3.1). This therefore correlates this level to the Early Miocene. With regard to the great thickness of the Arajuno Fm., an Early to Middle Miocene age can be assumed for this formation.

#### *- Depositional environment*

The Arajuno Fm., as most of the Neogene series of the AAB, was never really investigated in detail. The Arajuno Fm. was deposited in a fluvial environment, with a meandering rivers system that is consistent with the few observations of this study. The high percentage of metamorphic minerals in the heavy mineral fraction suggests the erosion of metamorphic sources in the Cordillera Real to the west of the basin. Both the volcanic contamination in the sampled level of the Lower Arajuno Fm. and the tuffaceous Middle Member (Tschopp, 1953) suggest that volcanic activity prevailed during the Lower and Middle (?) Miocene and partly supplied the Andean Amazon Basin.

#### *2.2.2.9. Chambira and Curaray Formations:*

##### *- Type region and extension*

The Curaray Fm. was firstly correlated with upper unit of the Arajuno Fm. (Tschopp, 1953). However, possible seismic evidence (Christophoul, 1999) would preferably correlate the Curaray Fm. with the Chambira Fm. and suggests that the Curaray Fm. is the distal (eastern) and lateral equivalent of the Chambira Fm.

The Chambira formation was first identified in the Oriente area by Haus (1940). The Chambira Fm. is absent in the Napo Uplift but is present in the Pastaza depression, e.g. the Talag syncline southwest of Tena (Fig. 2.1; Campbell, 1970; Christophoul, 1999). The geographic extension of the Chambira Fm. is loosely constrained but it is at least present into the proximal wells of the Oriente basin (e.g. the Oglan, Villano, Cangaima, Macuma, Coca wells; Tschopp, 1953). On the other hand, the Curaray Fm. was firstly recognized in sporadic outcrops in the Curaray River 60 kilometres east of Puyo, east of long. 76° 30' W (Dozy, 1943).

### *- Lithology*

Two main sections are described in the Chambira Fm.: (1) the Rio Uchuculin section (Christophoul, 1999), and (2) the Rio Bobonaza section (Tschopp, 1953). In the first section, the base of the formation is represented by metric to multimetric conglomerate levels that are mainly composed of up to 8 cm quartz (90%) and black schist pebbles. The series shows several fining-upward sequences topped by red claystones. The here dated sample of the Chambira Fm. was taken in this section (see section 4.3).

The Curaray Fm. was not investigated in this study. According to Tschopp (1953), the Curaray Fm. mostly consists of well-bedded light grey to blue-green or reddish, in some locations gypsiferous clays that alternate with fine to medium grained sandstones. Tuffaceous horizons, lignitic seams, and carbonaceous black clays are common in the upper part.

### *- Thickness and stratigraphic relationships*

The base of the proximal Chambira Fm. unconformably overlies the Arajuno Fm. as suggested by its erosional base in the Rio Uchuculin in the Pastaza depression (Christophoul, 1999) whereas the transition from the Arajuno Fm. to the of the Curaray Fm. in the Oriente region is not documented.

The thicknesses of these two formations have never been appropriately calculated. However, field mapping combined with well-log data suggests an increase of the thickness of the Chambira Fm. from 100 meters in the Pastaza depression to 1500 meters in the Oriente region east of the Cutucú Mountains (Tschopp, 1953). The maximum thickness of the Curaray Fm. is indicated in Baldock (1982) to reach 750 m but without further explanation.

### *- Age of the formation*

On grounds of characteristic mollusc faunas Tschopp (1953) suggested a Miocene age to the Curaray Fm., whereas the Chambira Fm. remains un-dated. Intercalated tephra layers are documented in the Chambira Fm. (Tschopp, 1953) but were never dated. The here proposed Early to Middle Miocene age for the Arajuno Fm. would imply that the Chambira Fm. has an approximate Middle to Late Miocene age that is in agreement with the Miocene age of the time equivalent Curaray Fm. in the Oriente region to the east (Tschopp, 1953).

### *- Depositional environment*

The Chambira Fm. was deposited on a proximal alluvial fan system whereas the Curaray Fm. represents the distal deposits (Christophoul, 1999). The characteristic faunal content of the Curaray Fm. (e.g. fishes, crustaceans, turtles, crocodiles) is combined with plants remnants, carbonaceous clays to suggest a low energy depositional system (Tschopp, 1953).

The strong erosion of the Arajuno Fm. before the deposition of the Chambira Fm. indicates increased tectonic activity in the foothills of the Cordillera Real (Tschopp, 1953), which is also corroborated by the increasing thickness of the Chambira Fm. towards the SE. The Chambira Fm. also forms a progressive unconformity with the Abitagua batholith in the Talag syncline region to the west of the Pastaza depression (Christophoul, 1999). This implies that the deposition of Chambira Fm. and the exhumation of the Abitagua batholith probably occurred coevally (Christophoul, 1999).

#### *2.2.2.10. Mesa and Mera Formations:*

The Mesa Fm. corresponds to the Rotuno Fm. of Parsons (1942) and Tschopp (1953) whereas the youngest Mera Fm. was previously named the 'Mesa of Mera' by Tschopp in 1953. The most recent descriptions of these formations (Faucher and Savoyat, 1973; Baldock, 1982; Christophoul, 1999) follow more or less the descriptions of Tschopp (1953).

Both formations occur in proximal positions with respect to the Andean chain (Fig. 2.1):

- The Mesa Fm. is encountered east of the Sub-Andean Front and in the Pastaza depression (Tschopp, 1953; Litherland et al., 1993). Highly dissected terraces composed of medium to coarse clastic deposits that were derived from continued erosion of the orogen, define the Mesa Fm. in the Pastaza depression (Baldock, 1982).

The formation is probably thicker in the range of 1000 m to the west of the Pastaza depression near the Cordillera Real, whereas it is only 100 m thick to the east of the Sub-Andean Front in the Oriente region (Baldock, 1982). The terraces show evidence of faulting and uplift; paleo-current directions indicate a sourcing from the WNW (Deniaud, 2000). This supply from the Cordillera Real to the west is corroborated by the occurrence of (1) large sub-rounded clasts (up to 1.0 m across) of probably derived from the Abitagua and Azafrán granites, and (2) the presence of strongly foliated schist pebbles in the vicinity of the Rio Alpayacu close to the village of Mera (Figs. 2.1 and 2.15).



*Figure 2.15: Conglomeratic Mesa Fm. in the vicinity of the Rio Alpayacu east of the village of Mera (0822317/9837582). Boulders up to 1m across of granitic origins are present with indeterminate schist pebbles.*

- The Mera Fm. consists of younger, because stratigraphically higher, deposits in the region of Vuano-Cangaime east of the Cutucú Mountains (Tschopp, 1953). These are typical terrace deposits that are composed of piedmonts fans, tuffs and clays that post-date the last major period of faulting and uplift (Tschopp, 1953; Baldock, 1982). Just to the east of the Abitagua batholith in the region of Mera, the Mera Fm. can be situated topographically lower than the Mesa Fm., because important exhumation occurred in the region and uplifted the older terraces of the Mesa Fm. In the Pastaza depression, the terraces of the Mera Fm. are located along the Pastaza River where they are less dissected than the remnants of the Mesa Fm. (Baldock, 1982). Eastwards the terrace sediments eventually grade into the Quaternary alluvium of the present-day drainage system (Baldock, 1982).

## 2.4. Tectonic subsidence analysis.

The exercise of partitioning the subsidence due to tectonics from that due to sediment loading within a given sedimentary basin is termed *backstripping* (Steckler and Watts, 1978). If the lithosphere is considered in a local Airy isostasy model, the decompacted subsidence, corrected for paleobathymetric and eustatic variations, can be used to calculate the tectonic component (Allen and Allen, 1990), and thus the geodynamic development of the studied basin can be constrained.

### 2.4.1. Introduction/dataset

In the Ecuadorian Andean Amazon Basin (AAB), very few backstripping studies were carried out (Berrones, 1992; Thomas et al., 1995; Berrones and Cotrina, 1996). Thomas et al. (1995) combined data from nine wells in one to sketch a general tectonic subsidence curve for the entire basin. Because the goal of the present work is to discuss possible variations in tectonic subsidence across the basin, the study of Thomas et al. (1995) was therefore not re-compiled.

The adjustment of two studies (Berrones, G., 1992; Berrones and Cotrina, 1996) required (1) to update the chronostratigraphy and lithostratigraphy the AAB (see section 4.3.1), and (2) the application of modern geological time scales (Gradstein et al., 1995, and Berggren et al., 1995). In addition, one single well-log located in the Capirón-Tiputini Corridor (AMO-1 well; see Fig. 2.16), was decompacted using (1) well data from the Argentinean YPF oil company, and (2) a software of l'Institut Français du Pétrole or IFP called *Genex*.

### 2.4.2. Localisation

The different wells (Berrones, 1992; Berrones and Cotrina 1996) are located in the northern part of the Oriente region, with the exception of the (1) Pungarayacu and Bermejo sites, which are both situated in the northern Sub-Andean Zone, or Napo Uplift (Fig. 2.16), and (2) Amo-1 well that is located in the southern area of the Capirón-Tiputini inverted system (Fig. 2.16).

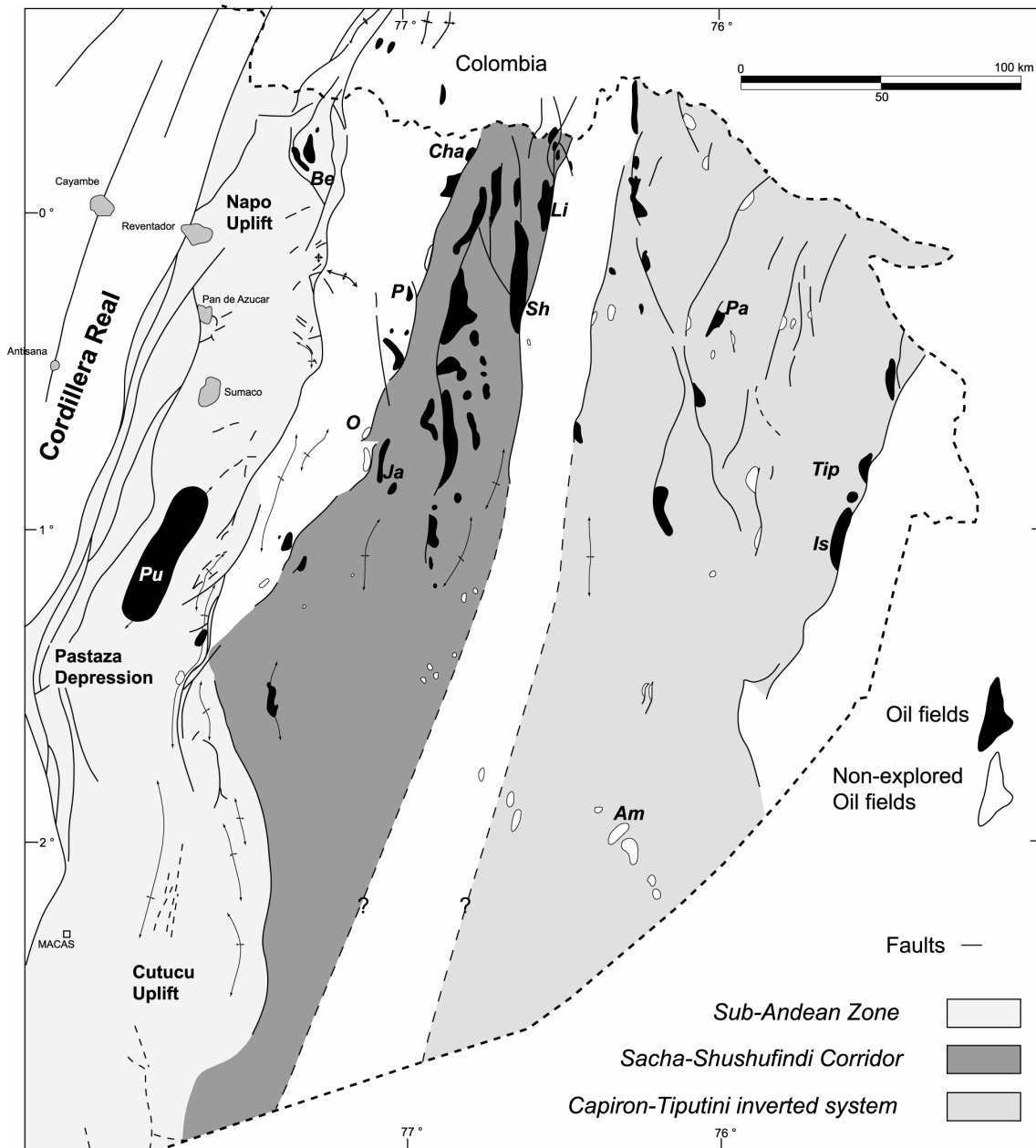


Fig. 2.16: Morpho-structural map of the Ecuadorian Andean Amazon Basin (Rivadeneira and Baby, 1999). The decompacted well logs (Berrones 1992; Berrones and Cotrina, 1996) are located in the vicinity of productive oil fields: Am: Amo-1, Be: Bermejo, Cha: Charapa, Is; Ishpingo, Ja: Jaguar, Li: Libertador, O: Oso, P: Pucuna, Pu: Pungarayacu, Pa: Pañacocha, Sh: Shushufindi, Tip: Tiputini.

### 2.4.3. Backstripping methodology

#### - Porosity

The authors used:

(1) An exponential relationship for the porosity of the form:  $\Phi = \Phi_0 e^{-cz}$ , where  $\Phi$  is the porosity at any depth  $z$ ,  $\Phi_0$  the primary or surface porosity and  $c$  is a coefficient that is dependent of the lithology.

(2) The DEPOR and BURSUB programs (Stam et al., 1987).

The porosity parameters for the different lithologies were obtained using electric logs analysis (sonic, density or gamma ray, and neutron) and are listed in Table 2.1 (Berrones, 1992). These parameters were also used for the decompaction of the Amo-1 well.

Lithology	Surface porosity $\Phi_0$	$c$ ( $\text{km}^{-1}$ )
Shale	0,6903	0,7629
Sandstone	0,4048	0,3658
Siltstone	0,4048	0,3658
Limestone	0,4300	0,1290

*Table 2.1: Porosity-lithology parameters as applied in the Ecuadorian Andean Amazon Basin by Berrones (1992).*

Moreover, because the young formations of the AAB are still poorly investigated (Berrones, 1992), a linear porosity relationship was considered for the post-Chalcana formations, i.e. post-Oligocene, see 2.2.2.7):

$\Phi = 0,4 - (0,0837)z$  with depth ( $z$ ) in kilometers (Berrones, 1992).

#### - Stratigraphic column

Recent biostratigraphic (Zambrano et al., 1999 quoted in Christophoul et al. 2002) and  $^{40}\text{Ar}/^{39}\text{Ar}$  data (Christophoul et al. 2002) are combined with detrital fission-track ages to refine the stratigraphic column of the AAB (see section 4.3.1) according to time scales of Berggren et al. (1995) and Gradstein et al. (1995). The necessary modifications of the two previous correlations charts (Berrones, 1992; Berrones and Cotrina, 1996) are shown in Figure 2.17.



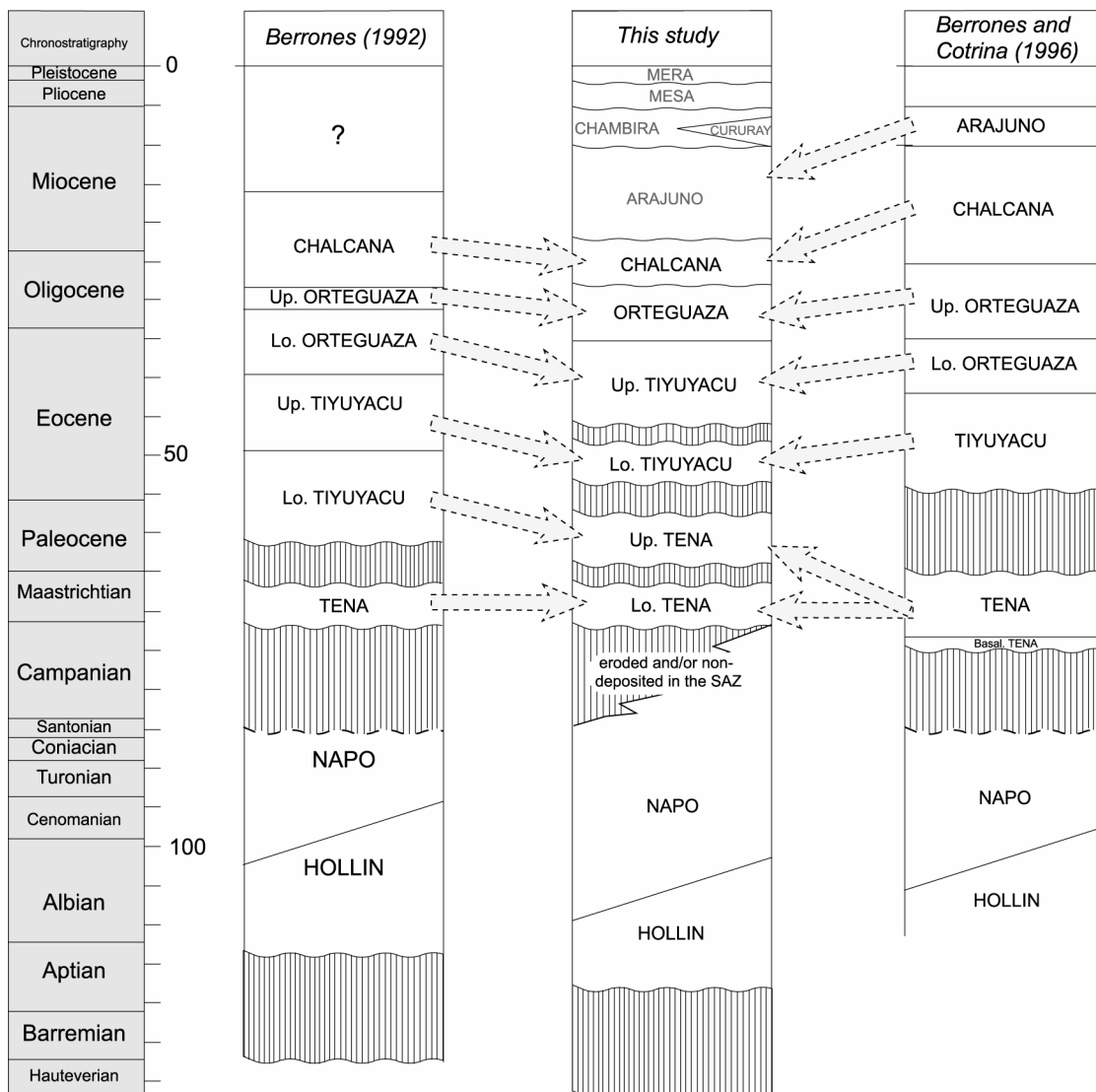


Figure 2.17: Comparisons of the stratigraphic correlation charts used in previous backstripping studies (Berrones, 1992; Berrones and Cotrina, 1996) with the one applied in the present study; some lithostratigraphic intervals were reinterpreted according to recent data (Rivadeneira and Baby, 1999; Christophoul et al., 1999; Christophoul et al. 2002); time scales: Berggren et al. (1995) and Gradstein et al. (1995).

#### 2.4.4. Results

Four zones have been separated according to the subdivisions of the Andean Amazon Basin (Rivadeneira and Baby, 1999; Fig. 2.16):

(1) The western side of the Sacha-Shushufindi corridor with the Oso-1, Jaguar, Puma-1 and Charapa-1 wells (Fig. 2.16).

(2) The eastern side of the Sacha-Shushufindi corridor with 6 wells of the Libertador oil field (Pacayacu-1, Shushuqui-1, Shuara-4, Secoya-24, Pichincha-1, Carabobo-1; Fig. 2.16).

(3) The inverted Capirón-Tiputini corridor with 7 wells (Tiputini-1, Tambococha-1, Ishpingo-1/2, Panacocha-2, Paujii-1, Panacocha-B1 and Amo-1 wells; Fig. 2.16).

(4) The Northern SAZ or Napo Uplift penetrated the Bermejo and Pungarayacu wells (Fig. 2.16).

An increase of the tectonic subsidence in the Sub-Andean Zone is observed in the Aptian-Albian (Fig. 2.18, D) during the deposition of the Hollin Fm. Because the Hollin Fm. becomes thinner towards the east (see section 2.2), it was then probably not always decompacted in the most distal wells of the Andean Amazon Basin and consequently no variation of the tectonic subsidence can be reported (Fig. 2.18). The Napo Fm. records the onset of weak tectonic subsidence in the three other zones of the Oriente region (Fig. 2.18; A, B, C). Interestingly, this increase of 270 m (from 30 to 300 m) is recorded in the Campo Libertador at ~90-85 Ma (Fig. 2.18, B) that may have occurred slightly earlier in the most proximal Oriente area along the western flank of the Sacha-Shushufindi corridor (Fig. 2.18, C). It is in fact tempting to distinguish a diachronous increase of the tectonic subsidence in the AAB from west to east in the mid-Cretaceous. However, this should be taken with a lot of care since none of the tectonic subsidence curves was re-compiled from any location of the AAB for the time of deposition of both the Hollin and Napo Fms. because of the low precision in the dataset (Berrones, 1992; Berrones and Cotrina, 1996).

A period of tectonic quiescence is everywhere observed until the deposition of the lower Tena member in the Maastrichtian with the exception of the Bermejo well (Fig. 2.18, D) where significant tectonic subsidence from 230-250 to 470m is observed during the Campanian. This relative quiescence was possibly related to the non-deposition or erosion of the Upper Napo Fm. prior to the deposition of the Tena Fm. (see section 2.2.2).

The lower Tena Fm. is characterized by a significant increase in tectonic subsidence of (1) ~380 m in the proximal part of the Oriente area in the western area of the Sacha-Shushufindi corridor (Fig. 2.16 and 2.18, C), and (2) ~220 m further east in the Campo Libertador (Fig. 2.16 and 3, B). Coevally, the tectonic subsidence did not much vary in the distal part of the basin (Fig. 2.16 and 2.18, C). This may indicate the presence of an orogenic load to the west of the Andean Amazon Basin in the Maastrichtian that probably generated the flexure of the South-American continental Plate (Jaillard, 1997b). However, such a situation probably developed earlier (Santonian? Campanian?) as recorded in the northern area of the northern Sub-Andean Zone where contemporaneous deposits are preserved and indicate rapid tectonic subsidence. This probably cannot be traced today in the other regions of the AAB because erosion may have occurred prior to the deposition of the Tena Fm. (see section 2.2.2).

The deposition of the Upper Tena Mb. is characterized by the almost absence of tectonic subsidence in the whole AAB (Fig. 2.18). This period of quiescence is also difficult to reconcile, because the distinction between the two Tena members did not exist yet when these backstripping studies were realized (see section 2.2.2.). Therefore, the differentiation between the two Tena members is based on (1) the observation of inflexion points along the tectonic subsidence curve within the Tena Fm. for the latest study (Berrones and Cotrina, 1996; Fig. 2.17), and (2) the correlation of the Lower Tiyuyacu of Berrones (1992) with the Upper member of the Tena Fm. However, the Tena Fm. was truncated prior to the deposition of the Tiyuyacu Fm. (see section 2.1.2) that does not permit today any clear interpretation for the Upper Tena Mb.

The time of deposition of the Lower Tiyuyacu Mb. is marked by a relatively homogeneous augmentation of 250 m of the tectonic subsidence along both flanks of the Sacha-Shushufindi corridor (Fig. 2.18, B & C). During the same period of time (56-46 Ma; see section 2.4.2), the easternmost part of the Ecuadorian AAB, which is represented by the Pañacocha-Tiputini zone (C, Fig. 2.16), underwent a weaker (50-150 m) increase of the tectonic subsidence. Similarly with the Maastrichtian, the Early to Middle Eocene was characterized by a noticeable increase of the tectonic subsidence that can be seen across most of the basin. This was probably related to an increase of the orogenic load onto the South-American continental Plate. However, the Sub-Andean Zone does not provide any data because the information (deposits) was partly removed since.

The deposition of the Upper Tiyuyacu Member was, as the Upper Tena and Napo Fms., characterized by the absence of tectonic subsidence across the basin with the exception of the distal Capirón-Tiputini corridor (Fig. 2.18, A). This can be correlated with the possible isostatic readjustment of the Cordillera Real (Christophoul et al., 2002) according to the model of Heller et al. (1988) and DeCelles and Giles (1996), which was most probably associated with a decrease of the orogenic load onto the South American plate.

Tectonic subsidence slightly increased of 200 m to the east of the AAB toward 100 m or less to the west of the Oriente region (Fig. 2.18) during the deposition of the Orteguaza Fm. (Oligocene; see section 2.2.2). The Oligocene-Early Miocene, which correlates with the deposition of the Chalcana Fm. (see sections 2.2 and 4.3.1) in the AAB was characterized by important tectonic subsidence in the distal zones (Fig. 2.18, A and B) while the proximal region may have experienced an exhumational phase (Fig. 2.18, C). The westernmost region of the ABB, which is represented by the Sub-Andean Zone cannot provide any additional information because the Chalcana Fm. is there not preserved. However, the imbrication of levels of the Chalcana Fm. along the thrust system of the Sub-Andean Front but not from the stratigraphically younger Arajuno Fm. (see Fig. 2.1) suggests that the Sub-Andean Front structure was (re-)activated in the Early Miocene. Hence, this would corroborate with the exhumation of the westernmost region of the AAB in the Early Miocene that was evidenced using apatite fission-track modelling on the basement of the Napo Uplift (see section 3). Further investigations are unfortunately impossible because the Neogene series were not differentiated.

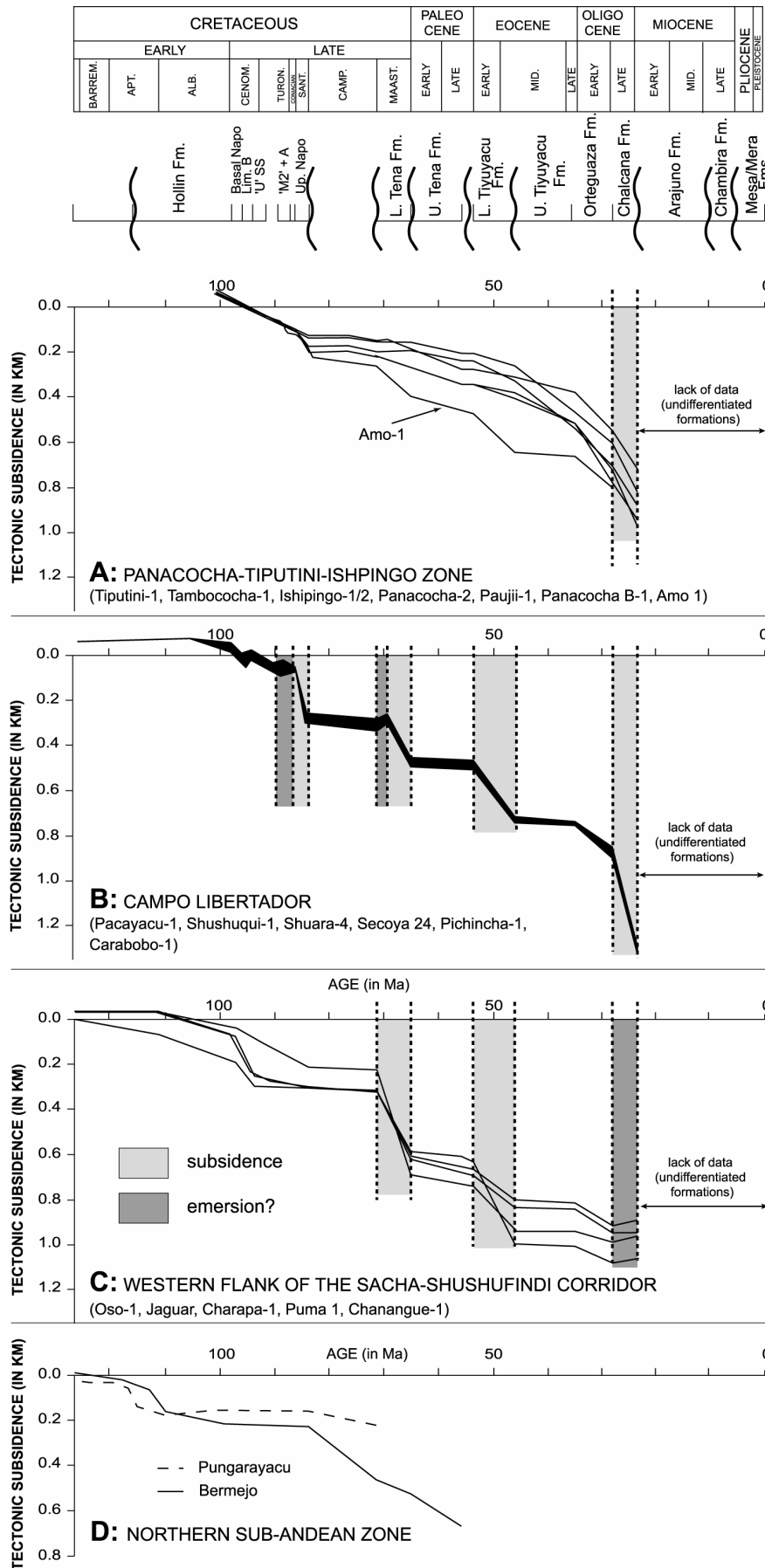


Figure 2.18: Tectonic subsidence curves across the Ecuadorian Andean Amazon Basin. From east to west: (A) the Panacocha-Tiputini-Ishpingo zone, (B) the Campo Libertador region along the eastern side of the Sacha-Shushufindi corridor (Fig. 2.16), (C) the western flank of the Sacha-Shushufindi corridor, and (D) the Pungarayacu and Bermejo wells in the northern Sub-Andean Zone, or Napo Uplift (Fig. 2.16). The dataset is a compilation of previous studies (Berrones, 1992, and Berrones and Cotrina, 1996) using an updated stratigraphic column (Fig. 2.17) and geological time scales of Gradstein et al. (1995) and Berggren et al. (1995). One well (Amo-1) was decompacted using well data from the Argentinean YPF Oil Company and the Genex software from l'Institut Français du Pétrole (IFP). For localization of the four regions see Figure 1. In light grey are the periods of noticeable increase of the tectonic subsidence, whereas the periods of non-deposition or erosion (emersion?) are in darker grey.

## 3. Thermochronology of the northern SAZ

### 3.1. Introduction to Fission-track analysis

#### 3.1.1. History of fission-track analysis

During the late 1950's and 1960's it was discovered that charged particles from the spontaneous fission of  $^{238}\text{U}$  nuclei in minerals and in natural and synthetic glasses leave a trail of metamict damage as they pass through a solid medium (Silk and Barnes, 1959; Price and Walker, 1962a). These trails are known as 'fission tracks' and they result from the transfer of energy from the fission fragments to the atoms of the medium.

Fission-track analysis is applicable to those geological, non conducting, crystalline materials which possess a reasonable trace quantity of uranium (1 to >100 ppm). In practice, this limits the method to the minerals zircon, apatite, titanite and certain glasses, partly also because they are common accessory minerals in many rock types.

These latent fission tracks are meta-stable, and, given that a particular activation energy barrier is crossed, the host material will repair itself (or anneal) over a period of time and the tracks will fade via atomic translational processes. However, Price and Walker (1962b) discovered that the fission tracks could be enlarged by a laboratory process of chemical etching until visible under an optical microscope. This method of visualising radioactive decay within natural materials initiated the development of the fission-track dating technique (Fleischer et al., 1975) as well as many other applications.

The spontaneous fission of an individual  $^{238}\text{U}$  nucleus creates a single etchable straight track because the two largest fission fragments are repelled from each other at angles very close to  $180^\circ$  in order to conserve momentum. The result is a continuous straight line of disruption within the host material. The length of the disruption depends on the amount of energy transferred from the fission fragments to the host material and hence, for fission of a given nucleus the length of the resulting track will depend on the nature of the host material. Counting the number of fission tracks on a chemically etched surface gives a quantitative measure of the number of fission events that have occurred if the uranium content is known. Therefore, the number of spontaneous fission tracks is proportional to the time over which the tracks have been accumulating in the material. This, if the spontaneous fission decay rate of the  $^{238}\text{U}$  nucleus and the uranium concentration of the material are known, the number of spontaneous tracks can be used to calculate a geological age.

### 3.1.2. Temperature of closure ( $T_c$ ) and partial annealing zone (PAZ)

For fission-track systems, there are no discrete "closure" temperatures as in other isotope systems, but rather a transition zone where tracks are essentially unstable is recognized. This transition zone is termed the partial annealing zone, and it is defined by upper and lower temperature limits. The effective closure lies within these bounds and is dependent on cooling rates.

The partial annealing zone for apatite (APAZ) lies between 60°C to 120°C (Green et al., 1989). Hence, apatite fission-track analysis is particularly useful for evaluating low temperature thermal histories, i.e. those affecting the upper 3-4 km of the crust, depending on the geothermal gradient.

Based on experimental studies extrapolated to the geological time scale, current estimates for the partial annealing zone of zircon range from 310°C to 230°C, depending on the type of model used (Tagami et al., 1998). These authors defined the lower temperature limit as that needed for 5% age reduction, whereas the upper limit is essentially total resetting to zero age. Many additional factors such as rates of cooling and chemical composition may also come into question.

Recent studies attempted to constrain the temperature of closure of zircon and apatite by varying the duration of the thermal event (Brandon et al., 1998; Garver et al., 1999). However, since this variable cannot be estimated with precision within the bedrocks of the SAZ, the effective closure temperature for zircons is taken here as 270°C  $\pm$  40°C (Tagami et al., 1998). A lower limit of 230°C is taken for initiation of annealing.

### 3.1.3. Annealing

Annealing of the fission tracks results in a reduction of their lengths (Laslett et al., 1987), which in turn relates to changes in track density and hence fission-track age which defines an invisible 'stratigraphy', in otherwise homogeneous rock masses. The annealing characteristics of fission tracks and thus the track density and length of tracks in apatite and zircon grains is a function of the thermal history (e.g. Green et al., 1986 and 1989), which can be attributed to tectonic and erosional events.

Since fission tracks are produced continuously, each track in a sample will have been exposed to a different portion of the time and temperature history of its host rock. The distribution pattern of confined fission track lengths in apatite is therefore an integrated cooling history. The time taken for a rock to pass through the partial annealing zone is reflected in the track-length distribution. Furthermore, if a rock undergoes burial and/or heating, pre-existing tracks are shortened to a length determined by the maximum temperature and the duration of burial. At temperatures greater than the upper limit of the partial annealing zone, all tracks are erased and the "clock" is reset when the rock cools again through the partial annealing zone. Using the

random Monte Carlo and Genetic Algorithm approach (Gallagher, 1995), the sample age and the track-length parameters are compared to those determined through experimental annealing in order to assess some possible temperature-time (T-t) paths. The 'Monte Trax' program (Gallagher, 1995) was used for modelling T-t paths with an initial  $L_0$  of 15.5  $\mu\text{m}$  in this study. Envelopes of temperature-time paths consistent with the data are useful for identifying periods of accelerated cooling and heating, which can then be used to constrain geological processes.

## 3.2. Applications

Tectonic activity at or near plate margins results in orogenic uplift and exhumation of rocks in the Earth's crust by various processes. This links the dynamics and origins of surficial processes, such as geomorphic and climatic evolution, with lithospheric plate motions and their large-scale origins and influences. Detailed knowledge of the timing and rate of orogenic activity thus provides important links between a wide range of Earth processes.

As a rock cools during exhumation (England and Molnar, 1990), the most direct links between tectonic and geomorphic processes are provided by low-temperature thermochronometers, because of their sensitivity to the movement of rocks through the uppermost crust. The  $\sim 310\text{-}60^\circ\text{C}$  closure temperatures of apatite and zircon fission-track thermochronometers are particularly useful for these purposes.

### *The northern Ecuadorian Sub-Andean Zone (SAZ)*

The northern Ecuadorian SAZ, also called the Napo "Uplift" or "antiform" is the only region of the Ecuadorian Amazon Basin (AAB), with its southern equivalent the Cutucú 'Uplift', where the Aptian to Recent basin fill series and their basement are together encountered at outcrop. Fission-track methodology was thus applied to rocks defining the northern SAZ to quantify the exhumation in this region, and subsequently to constrain the evolution of the whole Ecuadorian AAB from the Jurassic to Recent.

Initial results forced the direction of the project to diverge: the apatites within the sedimentary sequences had not been reset since deposition; they had not reached temperatures over  $100^\circ\text{C}$  during burial (see section 4.2.2). Hence they yielded no thermal history relating to burial and later basin inversion. These results highlighted the detrital character of fission-track ages from the sediments and subsequently supplied information regarding the cooling/exhumation/orogenic phases in the source region of the northern Ecuadorian SAZ (Fig. 3.1).

Finally, applying fission-track analysis to the northern Ecuadorian SAZ allowed constraints to be made on the exhumation of both (1) the source regions of the Andean Amazon Basin, and (2) the northern SAZ as well as (3) the burial history of the region

(Fig. 3.1). These are respectively presented in chapter 3 and section 4.2; the detrital character of the second section required the development of a new interpretative method to better understand the significance of such ages (see section 4.2.1.3).

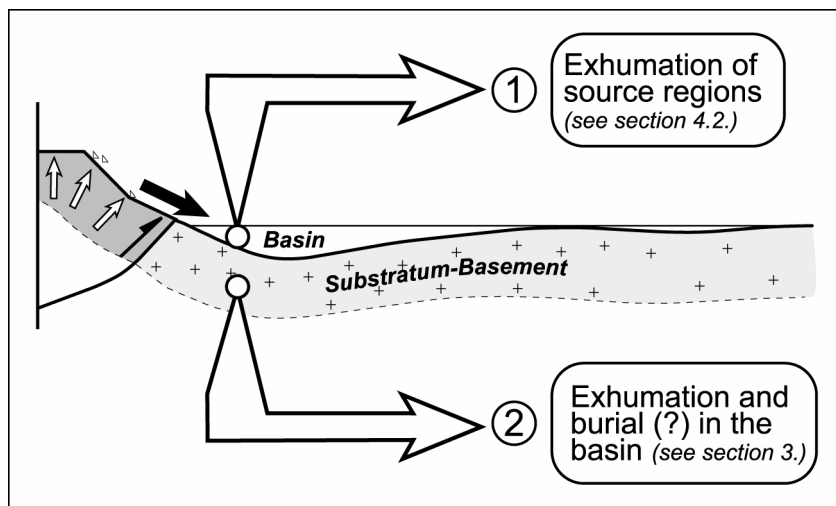


*Figure 3.1: Fission-track applications. If the detrital character of the fission-track ages is preserved in the basin fill series, i.e. post-depositional resetting of the thermochronometer can be excluded, then the exhumation history in the source region(s) can be investigated through the basin fill series (1). The exhumation and burial histories of the basin may still be traced by applying fission-track analysis to the basement series (2).*

### 3.3. Methodology

#### 3.3.1. Sample preparation

##### - Separation

Samples were crushed and wet sieved. The resulting 63-250  $\mu\text{m}$  fraction was processed through a crude magnetic separation, i.e. between 0.1 and 0.2 Ampère to decrease the size of the residues. The resulting non-magnetic residue was further separated by density using firstly bromoform with a density of 2.85, and secondly methylene-iodide with a maximum density of 3.35. Bromoform was preferred to Sodiumpolytungstate, or SPT ( $\text{Na}_6(\text{H}_2\text{W}_{12}\text{O}_{40})\text{H}_2\text{O}$ ) because of its low viscosity, even though the former is more toxic.

Two fractions were obtained, these are the 3.1-3.3 density fraction and the >3.3 density fraction. The first hosts apatites and the second zircons and sphenes. These two fractions were often not pure. They were then further processed using a Frantz magnetic separator until sufficient amounts of the required minerals were present. Different acids (e.g. aquaregia:  $\text{HNO}_3/\text{HCl}$ ) were also used to remove non-desired minerals such as pyrite from the zircon fraction.



Because sediments may host grains of different origins, large, representative samples of the required minerals were separated from very large samples (>5 kg) with care in order not to bias potential provenance information. As expected, detrital zircon grains have different shapes, colors and sizes, indicating a possible multi-sourcing (Fig. 3.2). Different methods were then applied to separate and characterize the diverse detrital zircon populations because of the possibility of different ages and the fact that etching time of zircons is proportional to the age (Naeser et al., 1979; Cervený et al., 1988). Separating by size and magnetic susceptibility helped to split the various populations. Thus, the >3.3 density fraction (zircon) was later processed through (1) the horizontal magnet using different slope angles and magnetic field intensity, and also through (2) sieves with different mesh sizes (from 70 to 110  $\mu\text{m}$ ). Hand picking was rarely necessary. Detrital apatites do not need such a procedure, as etching time is not dependent on the age.

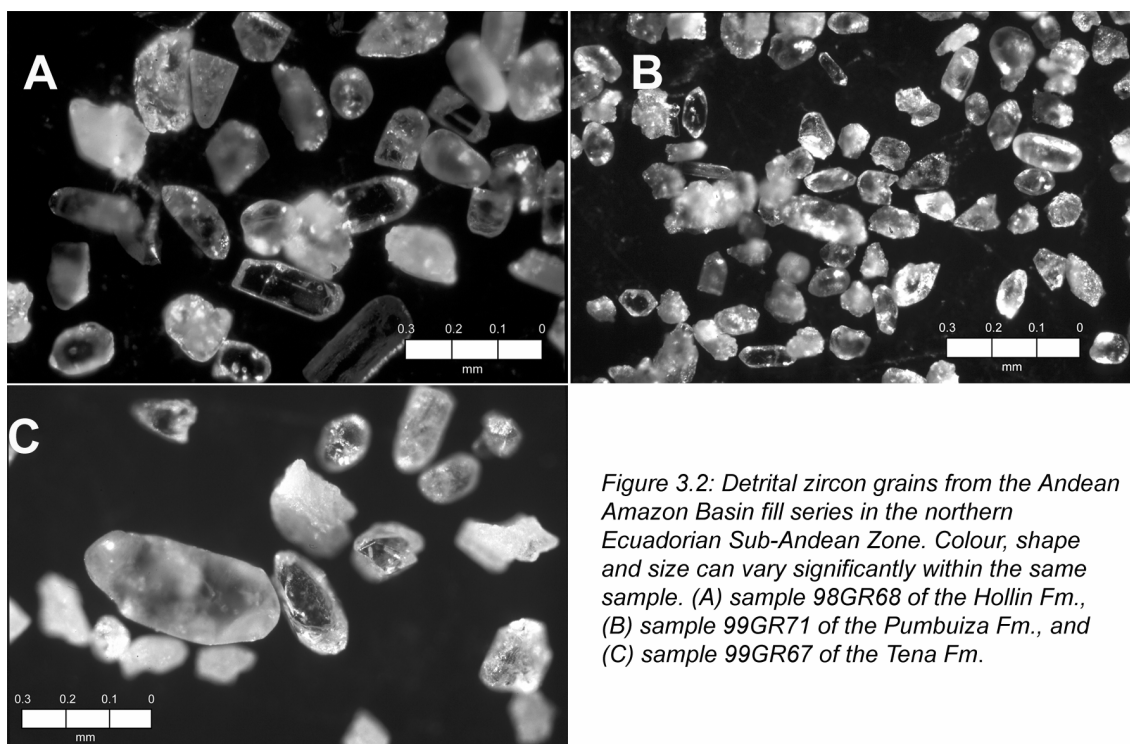


Figure 3.2: Detrital zircon grains from the Andean Amazon Basin fill series in the northern Ecuadorian Sub-Andean Zone. Colour, shape and size can vary significantly within the same sample. (A) sample 98GR68 of the Hollin Fm., (B) sample 99GR71 of the Pumbuiza Fm., and (C) sample 99GR67 of the Tena Fm.

#### - Mounting and polishing

Apatite and zircon were differently mounted; apatite simply in epoxy-resin on glass, whereas zircons were pressed into PFA-Teflon sheet on a hot plate at a temperature of 260°C. Mounts were cut with a 1000  $\mu\text{m}$  carbide paper and polished with 0.05  $\mu\text{m}$  aluminium oxide powder to expose inner crystal surfaces. As previously discussed,

sediments necessitate a longer procedure in that multiple mounts are necessary to reveal the different possible populations. Therefore, the number of zircon mounts reached up to 8 per sample.

#### *- Etching*

Apatite were etched in 7% HNO<sub>3</sub>, at 21°C for 50 seconds, whereas zircons were etched in a eutectic melt of NaOH - KOH, at 220°C (Gleadow et al., 1976). The various zircon mounts from the same sediments were etched using a one to two hours incrementation until most of the zircons were etched. Within the same sample, etching time varied from 5 to more than 40 hours for the different populations.

After etching mounts were covered for neutron irradiation with a uranium free muscovite external detector. Samples were sent for irradiation at the ANSTO facility Lucas Heights, Australia together with age standards (e.g. Fish Canyon tuff, Durango, Tardree) and different dosimeters, i.e. CN1 for zircon and CN5 for apatite, with a nominal total integrated flux of  $1 \times 10^{15}$  neutrons.cm<sup>-2</sup> for zircons, and  $1 \times 10^{16}$  n.cm<sup>-2</sup> for apatites. After irradiation, the external detector, i.e. muscovite, was etched for 40 minutes in 40% HF.

### 3.3.2. Microscope analysis

Microscopic analyses were carried out using an optical microscope with a computer driven stage ('Langstage' software from Dumitru, 1993). All ages were determined using the zeta approach (Hurford and Green, 1983), with a zeta value of  $359 \pm 11$  for CN5 and  $121 \pm 3$  for CN1 (Table 3.1). They are reported as central ages (Galbraith and Laslett, 1993) with a 1-sigma error (Table 3.1). Where possible, 20 crystals of each sample were counted from the bedrocks of the northern Ecuadorian Sub-Andean Zone (SAZ). However, fission-track analysis on sediments requires a representative number of grains for each population within the same rock sample. As a result, the number of grains counted reached 60 where possible. The magnification used was x1250 for apatite and x1600 (oil) for zircon. Horizontal confined track lengths were measured at x1250 within apatite and x1600 within zircons.

Age standard	N	Dosimeter glass	$\rho_d$ x $10^4$ cm $^{-2}$	$\rho_s$ x $10^5$ cm $^{-2}$	$\rho_i$ $10^5$ cm $^{-2}$	U (ppm)	$P\chi^2$	Zeta $\pm 1 \sigma$
Zircon			(counted)	(counted)	(counted)			
FCT	14	CN1	42.00 (2508)	35.1 (673)	34.1 (655)	324.9	42.6	132.3 $\pm$ 8.1
FCT	16	CN1	40.25 (2542)	54.5 (867)	47.7 (759)	473.8	98.3	119.1 $\pm$ 6.7
FCT	16	CN1	42.10 (2562)	44.9 (1244)	44.3 (1228)	421.3	96.9	129.4 $\pm$ 6.3
FCT	14	CN1	39.98 (2475)	45.9 (1274)	40.7 (1131)	407.7	49.7	121.0 $\pm$ 5.9
FCT	11	CN1	41.60 (2578)	34.7 (378)	35.6 (388)	342.3	99.4	139.9 $\pm$ 10.8
FCT	20	CN1	53.20 (2583)	40.0 (1539)	54.3 (1672)	408.1	26.8	112.1 $\pm$ 5.0
Weighted Mean								121 $\pm$ 3
Apatite								
FCT	12	CN5	105.00 (5440)	2.4 (183)	14.6 (1095)	17.4	99.8	317.7 $\pm$ 26.4
Durango	16	CN5	110.60 (10917)	1.4 (154)	8.2 (920)	9.2	97.0	334.9 $\pm$ 29.8
Durango	13	CN5	124.40 (8048)	1.8 (146)	13.5 (1096)	13.7	92.3	380.5 $\pm$ 34.3
Durango	8	CN5	102.70 (5137)	2.1 (134)	13.0 (844)	15.9	76.5	383.1 $\pm$ 36.5
Durango	10	CN5	118.70 (3703)	2.2 (83)	12.9 (481)	13.7	92.1	304.6 $\pm$ 36.9
Durango	9	CN5	118.90 (11913)	1.9 (173)	12.7 (1141)	13.3	67.4	348.1 $\pm$ 29.1
Durango	18	CN5	88.35 (10114)	2.3 (578)	12.1 (3089)	17.1	0.2	391.0 $\pm$ 19.2
Durango	14	CN5	120.90 (3772)	1.8 (157)	13.3 (1158)	13.7	100.0	384.7 $\pm$ 31.9
Weighted Mean								359 $\pm$ 11

Table 3.1: Data used for the generation of the author's zeta values for both zircon and apatite analysis (Hurford and Green, 1983) as used throughout the thesis. These zeta values were derived from standard samples, Durango and Fish Canyon tuff (FCT). The weighted mean zeta values are  $359 \pm 11$  for CN5 standard glass (apatite) and  $121 \pm 3$  for CN1 standard glass (zircon). N represents the number of counted grains whereas numbers in parentheses are the counted tracks.  $\rho_d$ ,  $\rho_s$ , and  $\rho_i$  represent the density of the dosimeter, spontaneous and induced tracks of the samples.  $P\chi^2$  is the probability of obtaining  $\chi^2$  values for  $\nu$  degrees of freedom, where  $\nu$ =number of crystals minus 1. The samples with a  $P\chi^2 < 5$  did not pass the  $P\chi^2$ -test and therefore age populations can be discriminated using different statistical treatments. Samples were sent for irradiation at the ANSTO facility Lucas Heights, Australia.

## 3.4. Results and interpretation

Approximately 40 fission-track ages were obtained from the basement of the Andean Amazon Basin (AAB) in the northern Ecuadorian Sub-Andean Zone (SAZ; Fig. 3.3). The complete dataset, from both apatite and zircon is presented with 1-sigma error and interpreted in detail. Sample localities are given in Appendix 3.1 and radials plots in Appendix 3.2.

### 3.4.1. Abitagua batholith or the Cordillera de Huacamoyos

#### 3.4.1.1. Apatite fission-track ages (AFTA) and track length measurements

Apatite fission-track ages from the Abitagua batholith range between  $1.4 \pm 1.0$  Ma and  $160 \pm 24$  Ma (Table 3.2). Four young apatite fission-track ages (AFTA), i.e.  $1.4 \pm 1.0$  (99GR66),  $5.0 \pm 0.9$  Ma (98RS08),  $7.2 \pm 2.4$  Ma (98RS41) and  $9.9 \pm 1.2$  Ma (99GR17) were produced from samples taken along (1) both sides of the batholith in the region of Mera, and (2) its eastern flank in the region of Tena to Narupa (Fig. 3.3, Table 3.2). The measured  $11.71 \pm 0.49$   $\mu\text{m}$  apatite mean track length (MTL) in sample 99GR17 is short, suggesting that cooling through the apatite fission-track annealing zone (APAZ;  $120\text{-}60^\circ\text{C}$ ) may have occurred slowly but cannot be clearly resolved due to the low number of track lengths (6) (Table 3.2). The two measured track lengths from the youngest sample (99GR66) are long, i.e.  $14.25$   $\mu\text{m}$  (Table 3.2) suggestive of rapid cooling, which one must expect from such a young age. Sample 99GR14, from a less accessible part of the eastern flank of the Abitagua pluton (Fig. 3.3) yielded an  $82 \pm 7$  Ma AFT age with 57 track length measurements ( $9.85 \pm 0.33$   $\mu\text{m}$ ; Table 3.3), which allowed T-t modelling discussed in section 3.4.1.3.

Two samples, i.e. 98GR03 and 98GR53 (Table 3.2) yielded almost identical AFT ages:  $161 \pm 15$  Ma (98GR03) and  $160 \pm 24$  (98GR53) with short track lengths for both, i.e.  $10.29 \pm 1.13$   $\mu\text{m}$  (10) and  $10.50 \pm 0.34$   $\mu\text{m}$  (39) respectively (Fig. 3.3 and Table 3.2). These two samples were taken from locations approximately 50 km apart with an 800 m vertical variation between the two locations (Fig. 3.3). Data from sample 98GR53 permitted T-t modelling.

#### 3.4.1.2. Zircon fission-track (ZFT) ages

Seven zircon fission-track ages from the Abitagua batholith range from  $113 \pm 6$  Ma to  $176 \pm 19$  ( $\pm 1\sigma$ ; Table 3.2). Notably, the three sample sites located along the eastern flank of the batholith (Fig. 3.3) yielded ZFT ages between 113 and 157 Ma (Table 3.2);

the youngest age of  $113 \pm 6$  Ma is derived from a level of the same flank where the topography is the lowest, i.e. 580 m (Fig. 3.3; Table 3.2). The two oldest ages of  $176 \pm 19$  and  $175 \pm 19$  Ma (Table 3.2) were also those that yielded the two oldest apatite fission-track ages (98GR03 and 98GR53, Table 3.2).

### 3.4.1.3. T-t modelling

Two samples (98GR53 and 99GR14) from the Abitagua batholith allowed T-t modelling (Fig. 3.4):

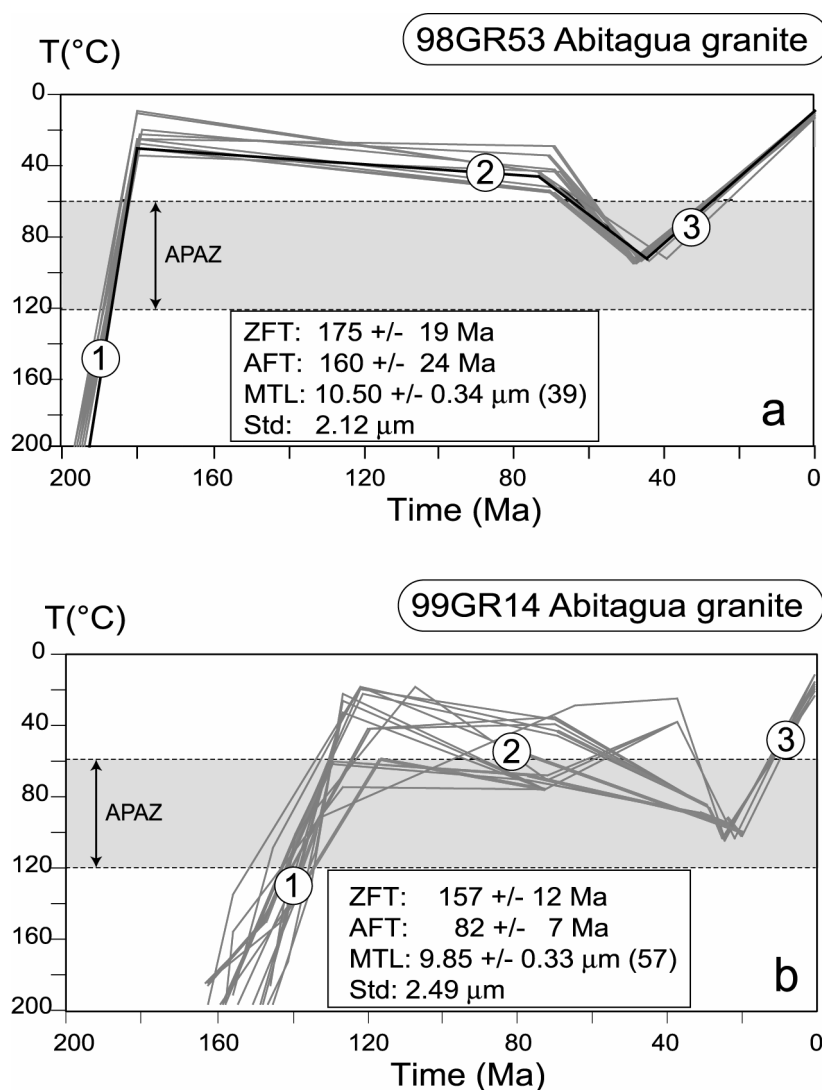
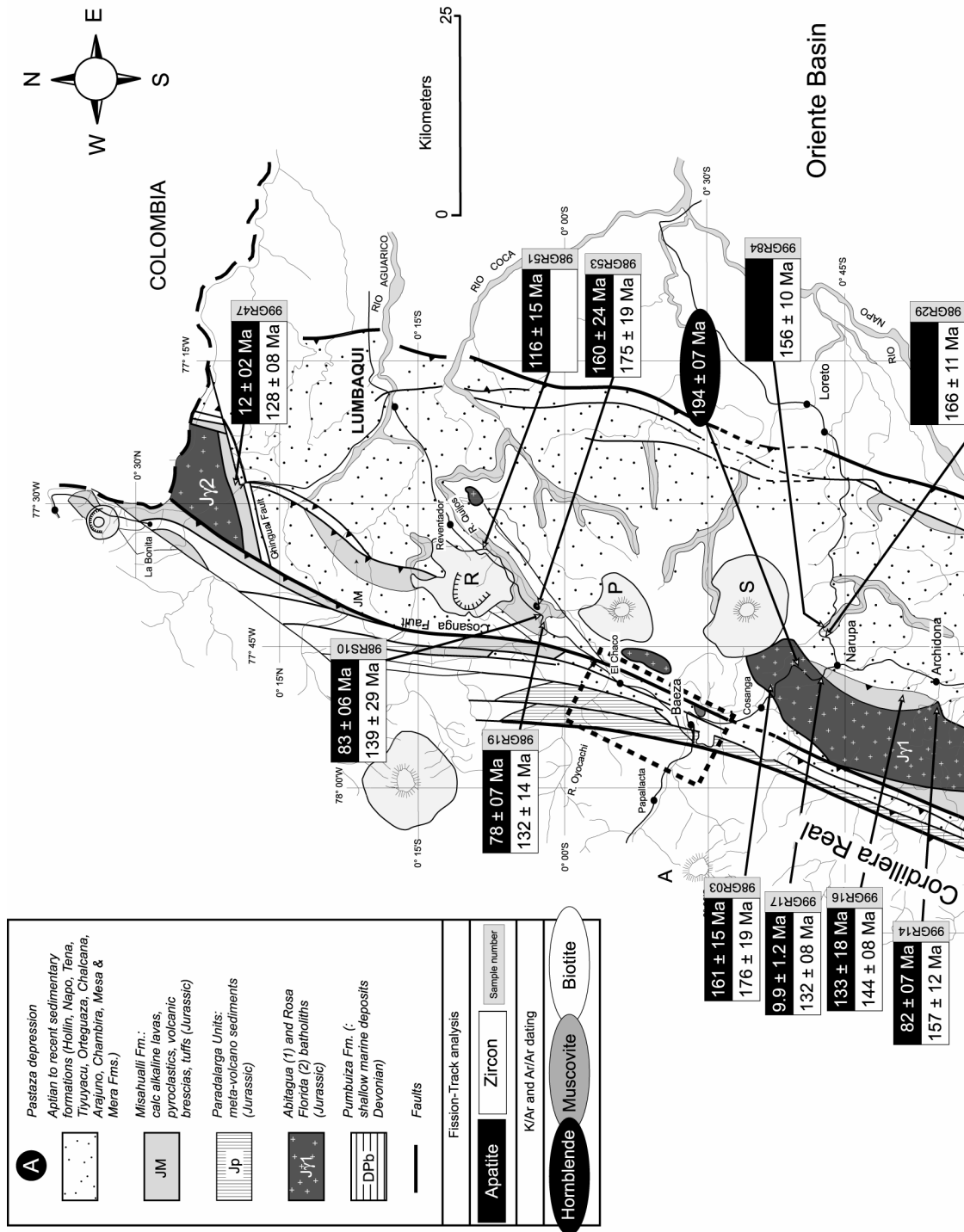


Figure 3.4: Temperature-time modelling of two samples from the Abitagua batholith. See Figure 3.3 for localities. All T-t modelling was completed following procedures described in Gallagher (1995), using Kolmogorov-Smirnov (K-S) test, an initial track length of  $L_0=15.5 \mu\text{m}$ , and 6000 simulation runs. The 20 best T-t paths fitting both AFT age and track length distribution within 95% confidence are used, the best run being indicated by a bold curve. Numbers indicate the corresponding path discussed in the text. APAZ: apatite partial annealing zone. AFT: apatite fission-track; ZFT: zircon fission-track; MTL: mean track length; Std: standard deviation (Table 3.2).



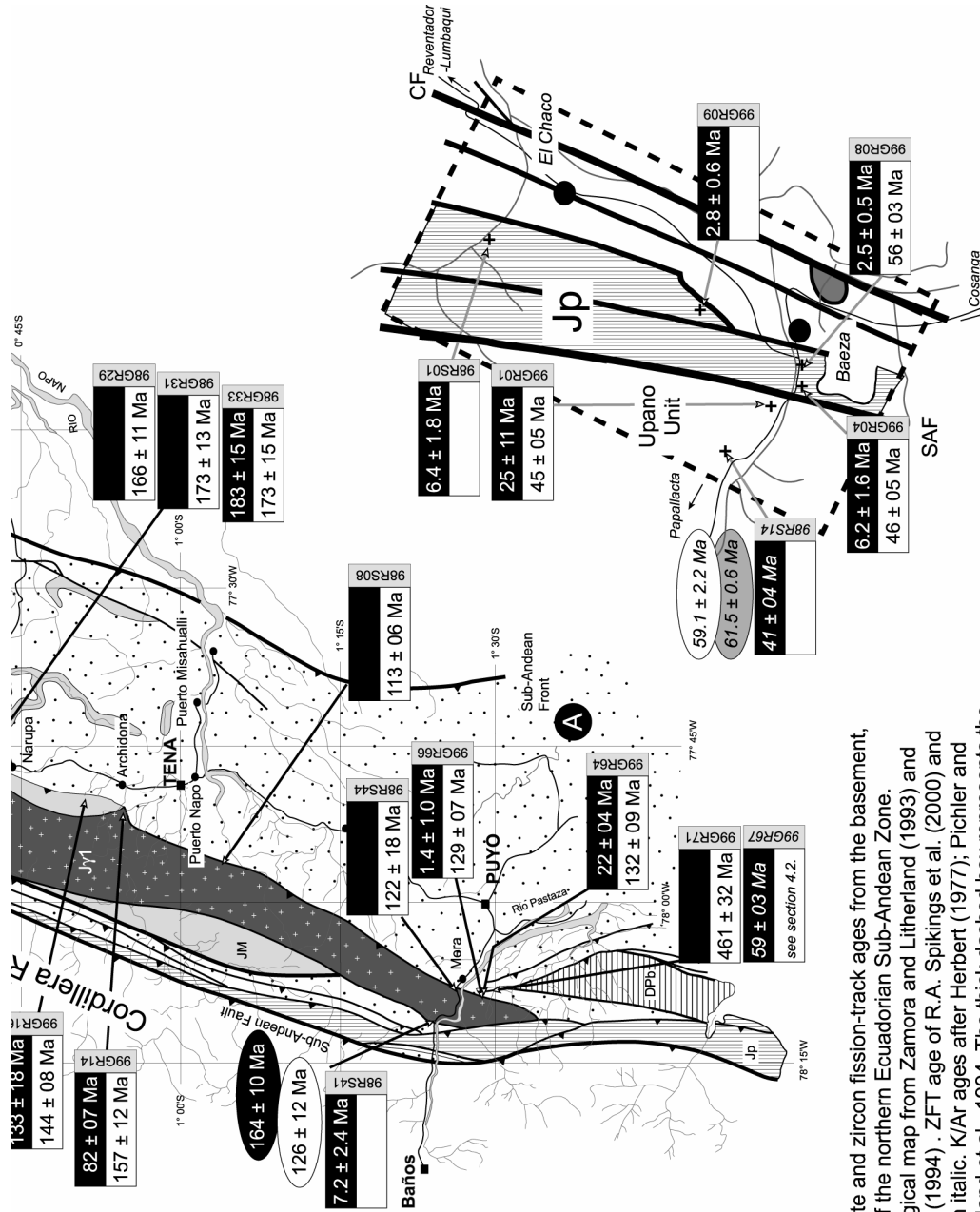


Figure 3.3: Apatite and zircon fission-track ages from the basement, or reset series of the northern Ecuadorian Sub-Andean Zone. Simplified geological map from Zamora and Litherland (1993) and Litherland et al., (1994). ZFT age of R.A. Spikings et al. (2000) and D. Seward are in italic. K/Ar ages after Herbert (1977); Pichter and Aly, 1983; Litherland et al., 1994. The thick dashed box represents the zoomed Baeza region from where both the Paradalarga and Upano Units were dated using fission-track methodology. SAF: Sub-Andean Fault; CF: Cosanga Fault.

Sample number	Alt. m	N	$A_g \times 10^4 \text{ cm}^{-2}$ (counted)	$A_s \times 10^5 \text{ cm}^{-2}$ (counted)	$A \times 10^5 \text{ cm}^{-2}$ (counted)	U ppm	$P\chi^2$	MTL $\mu\text{m}$ (N)	Std $\mu\text{m}$	Etch pit diameter $\mu\text{m}$	Central age $\pm 1\sigma$
					<b>Apatite</b>						
98GR03*	2150	32	115.1 (3553)	2.75 (233)	3.49 (294)	4.5	99.5	10.29 $\pm$ 1.13 (10)	3.57	-	161 $\pm$ 15
98RS08*	590	17	116.0 (5249)	0.68 (31)	28.69 (1302)	31.1	95.1	12.06 $\pm$ 0.52 (11)	1.71	-	5.0 $\pm$ 0.9
98RS41	1270	10	150.0 (6725)	0.32 (9)	11.90 (332)	10.0	87.8	-	-	-	7.2 $\pm$ 2.4
98GR53*	1350	13	116.4 (5440)	1.90 (80)	2.52 (106)	2.7	83.1	10.50 $\pm$ 0.34 (39)	2.34	-	160 $\pm$ 24
99GR14*	700	20	125.9 (7083)	2.21 (176)	6.03 (480)	5.8	9.1	9.85 $\pm$ 0.33 (57)	2.49	-	82 $\pm$ 7
99GR17*	1330	34	133.7 (7083)	0.60 (76)	14.47 (1846)	14.8	97.0	11.71 $\pm$ 0.49 (6)	1.20	-	9.9 $\pm$ 1.2
99GR66*	1400	10	120.7 (7083)	0.12 (2)	18.61 (302)	20.6	20.1	14.24 $\pm$ 0.84 (2)	1.18	-	1.4 $\pm$ 1.0
					<b>Zircon</b>						
98GR03*	2150	11	40.4 (2504)	136.70 (767)	18.71 (105)	196.8	98.0	-	-	-	176 $\pm$ 19
98RS08*	590	25	44.7 (2504)	192.38 (2746)	45.46 (648)	449.8	73.0	-	-	-	113 $\pm$ 6
98RS44	1200	6	32.0 (2063)	58.90 (521)	9.27 (82)	123.6	10.3	-	-	-	122 $\pm$ 18
98GR53*	1350	14	37.4 (2475)	237.43 (831)	30.29 (106)	325.3	100.0	-	-	-	175 $\pm$ 19
99GR14*	700	13	41.7 (2504)	153.30 (1375)	24.31 (217)	231.1	64.1	-	-	-	157 $\pm$ 12
99GR17*	1330	18	38.7 (2504)	117.98 (2411)	20.70 (423)	216.9	82.6	-	-	-	132 $\pm$ 8
99GR66*	1400	25	43.4 (2504)	240.30 (2492)	48.35 (501)	475.3	99.7	-	-	-	129 $\pm$ 7

Table 3.2: Apatite and zircon fission-track ages from the Abitagua batholith. For localities see Fig. 3.3 and Appendix 3.2. Track length measurements for both apatites and zircons are also indicated when completed; asterisks correspond to samples that yielded both AFT and ZFT ages. Numbers in parentheses, as N indicate the number of counted tracks and grains, respectively. Alt.: altitude in meters. All zircon and apatite separates were counted by G.M. Ruiz using zeta calibration of  $121 \pm 3$  (zircon analysis, CN1 standard glass) and  $359 \pm 11$  (apatite analysis, CN5 standard glass). Sample 98RS41 in italics, was counted by D. Seward using a zeta value of  $355 \pm 5$  for apatite analysis (CN5). Samples were irradiated at the ANSTO facility Lucas Heights, Australia



#### - 98GR53

AFT modelling combined with ZFTA indicate that cooling from the ZPAZ, i.e. 310-230°C (Tagami et al., 1998) towards a temperature lower than 60°C occurred between 195 and 180 Ma (Fig 3.4a, period 1). A long period of quiescence followed until ~50-45 Ma by which time the sample had been reheated to 90°C (period 2, Fig. 3.4a). From this time onwards, sample 98GR53 cooled towards the surface temperature (period 3, Fig. 3.4a) where it is encountered today in the bed of the Rio Quijos, south of the Reventador volcano (Fig. 3.3).

#### - 99GR14

From 160 Ma to 120 Ma cooling from 310-230°C temperatures (Tagami et al., 1998) towards  $60 \pm 20^\circ\text{C}$  took place (period 1, Fig. 3.4b). The further thermal history of this sample from 120 Ma to 25 Ma is less clear. However, sample 99GR14 was heated to temperatures of 95-100°C by 25 Ma (period 2, Fig. 3.4b) before undergoing an unequivocal period of cooling (period 3) until today (period 3, Fig. 3.4b).

#### 3.4.1.4. Interpretation

Firstly, the fission-track ages of the Abitagua batholith are, as expected identical to or younger than the few previously determined K/Ar ages on both biotite and hornblende from the same batholith that range from  $194 \pm 7$  Ma to  $126 \pm 12$  Ma (Herbert, 1977; Pichler and Aly, 1983; Litherland et al., 1994; Fig. 3.3). In addition Kennerley (1980) also reported a single  $87 \pm 7$  Ma K/Ar age on biotite from the western side of the batholith in the southern region that will not be considered here, as a more recent study in the same location produced much older ages (Litherland et al., 1994). These few K/Ar ages indicate cooling through the retention zones of biotite and hornblende that correspond to temperatures between 360-295°C and 545-500°C, respectively (McDougall and Harrison, 1999). Where possible, they will be combined with this fission-track data to constrain the thermochronology of the Abitagua batholith from temperature comprised between ~550°C and 60°C (Fig. 3.5). In the following section it is assumed that cooling represents exhumation whereas heating correlates with burial; the rates at which both occurred are investigated using a mean geothermal gradient of 30°C/km.

### *- Intrusion (190-170 Ma)*

Twenty-nine K/Ar ages from the Zamora pluton reported in Litherland et al. (1994) allowed them to conclude that this batholith, located 150 kilometers further south in the southern SAZ or Cutucú region, underwent its major phase of cooling at ~190-170 Ma. T-t envelopes from sample 98GR53 from the Abitagua batholith are here combined with both the fission-track ages from the highest sampled site of the batholith (98GR03, Fig. 3.3 and Table 3.2) and a  $194 \pm 7$  Ma K/Ar biotite age reported by Pichler and Aly (1983) from almost the same location (Fig. 3.3) to suggest rapid cooling between ~190-180 Ma through temperatures between 500 and 60°C for the Abitagua pluton (Fig. 3.5). Such a period of cooling is slightly older than the commonly assumed earliest stage of intrusion of the Abitagua batholith, i.e. 170-160 Ma (Litherland et al., 1994; see section 2.3.1.1). As a result, both batholiths from the Sub-Andean regions may have been intruding at relatively shallow depths (<10 kms) since 190-170 Ma.

### *- Late Early Jurassic-Early Cretaceous exhumation (180-115 Ma)*

A positive age-altitude linear relationship is observed for the ZFT ages of the Abitagua batholith (Fig. 3.6a) with the exception of two samples. The first one of these two samples (98GR53) is derived from a gabbroic pod encountered in the bed of the Quijos River further north in a region where the Abitagua batholith is not exposed on a large scale (Fig. 3.3). The second sample (99GR14) was extracted from a wedge along the eastern flank of the batholith west of the town of Archidona (Fig. 3.3). The five other ZFT ages exhibit a linear relationship with altitude (Fig. 3.6a) demonstrating that the differences in the cooling ages are only related to differences in elevation. Consequently, it implies that the batholith in general cooled as a whole block through temperatures corresponding to the ZPAZ (310-230°C, Tagami et al., 1998) at least since  $176 \pm 19$  Ma, which is the oldest ZFT age belonging to this correlation line (98GR03, Fig. 3.6a). A mean exhumation rate of 0.02 to 0.04 mm/year can be deduced for the period using both the differences in (1) altitude (1560 m, Fig. 3.6, Table 3.2) and (2) age ( $63 \pm 25$  My, Fig. 3.6a, Table 3.2) between the two extreme points of this correlation line. A similar pattern is not observed in the age-altitude plot of the apatite fission-track ages (Fig. 3.6b) implying that the Abitagua batholith did not undergo a homogeneous phase of cooling through the 120-60°C isotherms. Some fragmentation and hence differential cooling of the Abitagua batholith occurred some time after the youngest sample passed through the ZPAZ, i.e.  $113 \pm 6$  Ma (98RS08; Fig. 3.6a).

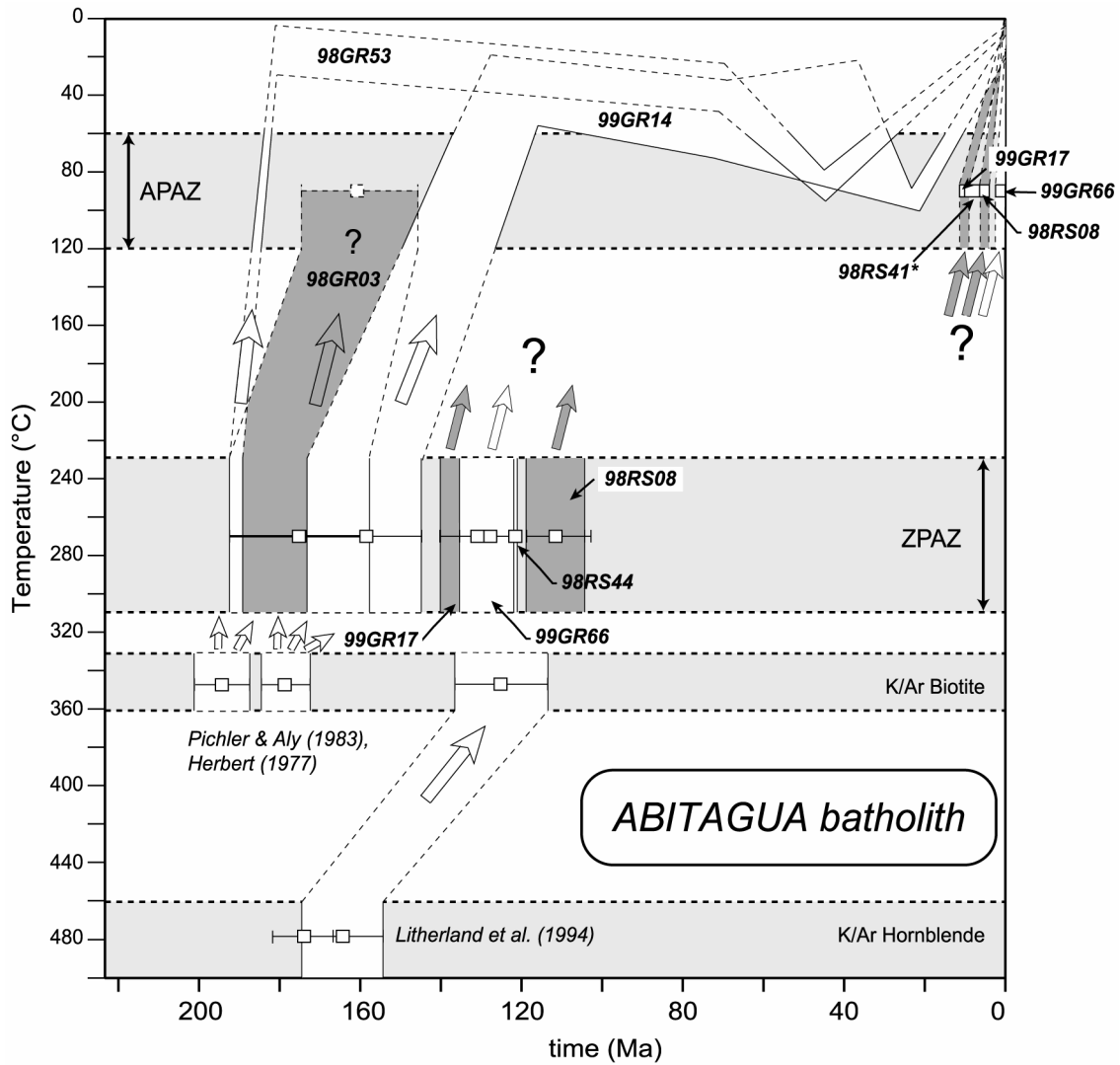


Figure 3.5: Thermochronology of the Abitagua batholith. *T-t* envelopes were obtained from both apatite modelling, and pairs of ZFT-AFT ages when track length measurement on apatite could not be completed (Table 3.2). See Figure 3.3 for sample localities. K/Ar and  $^{40}\text{Ar}/^{39}\text{Ar}$  ages from previous studies are also presented (Herbert, 1977; Pichler and Aly, 1983; Litherland et al., 1994; Romeuf et al., 1995; Spikings et al., 2001). Asterisks after sample 98RS41 indicate sample counted by D. Seward. Arrows indicate the most probable *T-t* paths whereas plain lines delimit constrained *T-t* envelopes and the dashed lines interpolated paths. APAZ: Apatite Partial Annealing Zone; ZPAZ: Zircon Partial Annealing Zone.

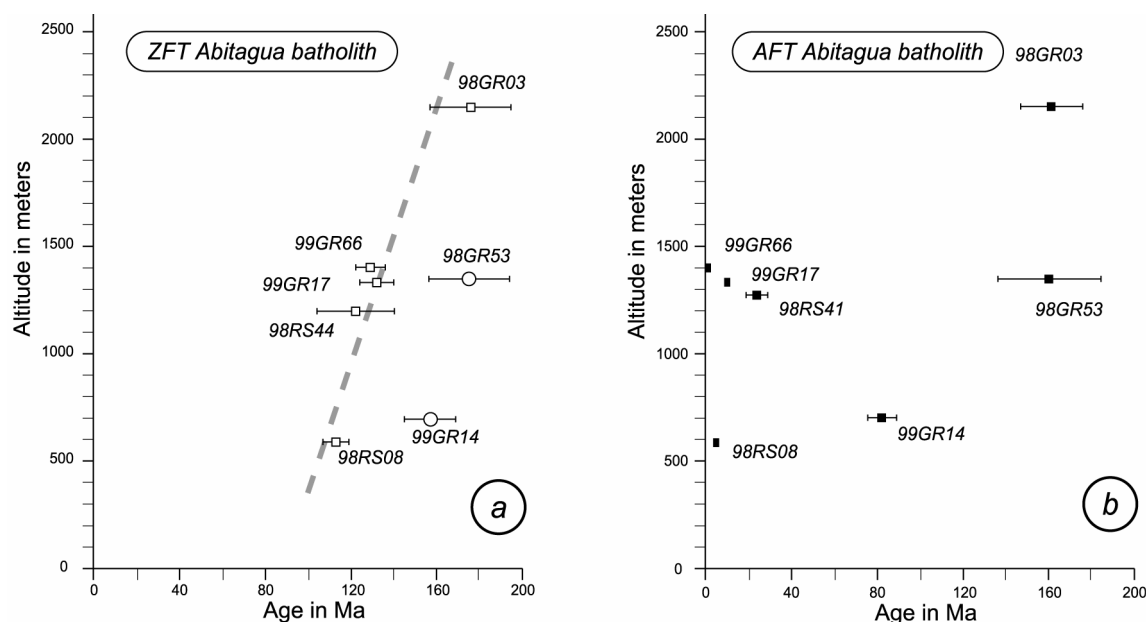


Figure 3.6: Age-altitude representation of the fission-track ages from the Abitagua batholith (Table 3.2). (a) zircon, (b) apatite. The two plain circles correspond to two excluded samples from the ZFTA-altitude correlation line as discussed in the text.

### - Periods of burial

Heating events can be identified using fission-track modelling on apatites and are interpreted as the result of either tectonic or sedimentary burial.

Only two relatively clear phases of heating are identified within the T-t envelopes of samples from the Abitagua batholith (Fig. 3.5): these are (1) from ~70 Ma to 50-45 Ma when sample 98GR53 reached a temperature of ~95°C, and (2) also a less constrained phase of heating from 115 Ma to 25 Ma when sample 99GR14 reached temperatures of 100°C (Fig. 3.5).

(1) Sample 98GR53 underwent a constrained increase in temperature of ~35°C during until the Early Eocene period (50-45 Ma, Fig. 3.5). Using a normal geothermal gradient of 30°C/km, this can be converted into a minimum paleo-burial of ~1 kilometer which is in the range of the minimum cumulate thickness of the Maastrichtian to Early Eocene continental series from the Tena Fm. and the lower Tiyuyacu Mb in the northern SAZ (see 2.3.2).

(2) Burial is less clear but emphasis can be made on both its cessation at ~25-20 Ma, and the maximum temperature attained, ~100°C using the thermal modelling of sample 99GR14 (Fig. 3.5). As discussed above, this phase of heating is used to estimate the increase in the thickness of the overlying sedimentary pile. Using a 30°C/km geothermal gradient, this implies that the thickness of the sedimentary pile of Aptian to

Early Miocene age (i.e. Hollin, Napo, Tena, Tiyuyacu, Orteguzaza, and Chalcana (?) Fms.; see section 2.2) did not exceed 3 to 4 kilometers in the region of Archidona (Fig. 3.3).

#### *- Mid-Early Eocene to Early Miocene and Late Miocene exhumation periods*

T-t envelopes from sample 98GR53 indicate a phase of cooling that began at ~50-45 Ma and has at 60°C at ~33-25 Ma when sample 98GR53 left the APAZ (Fig. 3.5). Using a normal geothermal gradient of 30°C/km, this corresponds to a mid-Middle to Late Eocene phase of exhumation at a low rate of 0.06 mm/y. This phase of exhumation was synchronous with the deposition of the Upper Tiyuyacu Mb. in the Ecuadorian Amazon Basin, which is derived from sedimentary to upper crustal sources (see sections 2.3.2.4 and 4.1). As a result, the slow exhumation of part of the substratum of the northern SAZ during the mid-Middle to Late Eocene may have contributed to the erosion of the overlying sedimentary cover, which was reworked into the Upper Tiyuyacu Mb.

Similarly, sample 99GR14 underwent renewed cooling that started at ~25-20 Ma with a mean cooling rate of 3.5°C/my (Fig. 3.5). The deduced mean rate of exhumation is approximately 0.12 mm/y (Fig. 3.5), which does not suggest an important phase of exhumation but can be correlated with the reported periods of cooling that prevailed in the northern Cordillera Real to the west of the northern SAZ in the Early Miocene (Spikings et al., 2000).

Along the faulted contact of the Abitagua batholith with the adjacent sediments to the east, and to the west in the region of Mera, four samples (98RS41, 98RS08, 99GR17, 99GR66) yielded AFT ages ranging from 10 to 1 Ma (Figs. 3.3 and 3.5). Because none of these samples produced sufficient number of apatite track length (Table 3.2), no T-t path within the 60-120°C temperature window could be modelled (Fig. 3.5). However, such a set of young ages clearly suggests that the Abitagua batholith underwent a phase of exhumation since the Late Miocene that would be contemporaneous with the unconformable deposition of the alluvial fan deposits of the Chambira Fm. of probable Late Miocene age over the Arajuno Fm. (see section 2.2.9).

#### *- Recent*

Interestingly, two samples from the Abitagua batholith (98GR03 and 98GR53) provide almost identical fission-track ages and mean-track lengths (Table 3.2). Though, these two samples probably had similar thermal histories through the ZPAZ and APAZ, i.e. between 310°C and 60°C. The difference in altitude (~800m; Fig. 3.6) observed today between these two regions is then probably related to recent exhumation in the region

of the Cordillera de Huacamoyos (sample 98GR03), which did not yet generate sufficient erosion because identical ages are still preserved.

### 3.4.2. Misahualli Fm.

Samples of the Misahualli Fm. were taken from east to west: (1) in the 'core' of the northern Ecuadorian SAZ, i.e. along the Narupa-Loreto road (samples 98GR29-31-33 and 99GR84, Fig. 3.3), (2) just east of the Abitagua batholith, west of Archidona (99GR16, Fig. 3.3), (3) south and east of the Reventador volcano (98GR19, 98RS10, 98GR51, Fig. 3.3), and finally (4) from the westernmost imbricate deposits with the Cordillera Real, i.e. in the Chingual river northwest of Lumbaqui (99GR47, Fig. 3.3), and in the Gringo river south-west of Mera (99GR64, Fig. 3.3).

Some localities, where the Misahualli Fm. is also present are missing in the sample dataset because it could not be reached without advanced field expeditions. These are (1) west and north of the Reventador volcano, (2) along the eastern side of the northern SAZ just west of the Sub-Andean Front (SAF, Fig. 3.3), and south-west of Cosanga (Fig. 3.3)

#### 3.4.2.1. Apatite fission-track (AFT) ages

AFT ages of the Misahualli Fm. range from west to east from  $12 \pm 2.4$  Ma to  $183 \pm 15$  Ma ( $\pm 1\sigma$ , Table 3.3). The oldest age, i.e.  $183 \pm 15$  Ma is derived from a sample taken in the 'core' of the northern SAZ (98GR33, Fig. 3.3, Table 3.3) that is directly overlain by the Aptian-Albian Hollin Fm. (see section 2.3.2.1). A mean track length of  $11.86 \pm 0.24$   $\mu\text{m}$  from 59 track lengths was measured in this sample (Table 3.3), which allowed T-t modelling within the 120-60°C isotherms (Fig. 3.8).

Sample 99GR16 is located in an affluent of the Rio Misahualli, i.e. west of Narupa (Fig. 3.3) at an altitude of 1020 m (Table 3.3). It yielded an AFT age of  $133 \pm 18$  Ma with a relatively short mean track length of  $11.78 \pm 0.45$   $\mu\text{m}$  (Table 3.3), suggesting a protracted geothermal history that unfortunately cannot be modelled due to the low number of track lengths (N=12).

From further north in the northern SAZ two samples were dated, i.e. 98GR19 and 98RS10 (Fig. 3.3), which yielded statistically identical AFT ages of  $78 \pm 7$  Ma and  $83 \pm 6$  Ma, respectively, with a mean track length (MTL) of  $10.81 \pm 0.32$   $\mu\text{m}$  for 98GR19 (Table 3.3). The northernmost sample from the Misahualli Fm. (Fig. 3.3) produced a  $12.0 \pm 1.4$  Ma AFT age with a MTL of  $11.78 \pm 0.45$   $\mu\text{m}$  from 11 measurements (99GR47, Table 3.3).

A second western sample (99GR64) located southwest of Mera where the southern Ecuadorian SAZ passes into the Pastaza depression yielded a  $22.0 \pm 3.7$  Ma AFT age (Table 3.3). These igneous levels are there intensively imbricate with quartz-arenite deposits attributed to the Hollin Fm. (Fig. 3.3). The presence of imbricate igneous levels within this section may be correlative of the dioritic and syenitic intrusions reported (1) along the eastern edge of the batholith, and (2) also within the Hollin Fm. in an identical position further south (1:100 000 scale Baños geological map

of Ecuador, 1980; Edición Provisional). Sample 99GR64 was preferentially ascribed to the volcanic Misahualli Fm. and discussed in this section, rather than to the Abitagua batholith because basaltic glass and zoned plagioclase were observed in thin section demonstrating a volcanic origin.

Furthermore, there is no AFT age-altitude correlation (Fig. 3.7a) indicating that the different AFT ages can be individually interpreted.

#### 3.4.2.2. Zircon fission-track (ZFT) ages

Nine ZFT ages from rocks of the Misahualli Fm. range from  $173 \pm 15$  Ma to  $128 \pm 8$  Ma (Table 3.3). The oldest ages, i.e.  $173 \pm 13$  Ma,  $173 \pm 15$  Ma,  $156 \pm 10$  Ma and  $166 \pm 11$  Ma (Table 3.3) are from samples taken in the 'core' or center of the northern SAZ (Fig. 3.3). The ZFT ages like the AFT ages decrease westwards (Fig. 3.3). However, in contrast to the ZFT ages from the Abitagua batholith, and similarly to the AFT ages, there is no clear age-altitude relationship for the ZFT ages of the Misahualli Fm. (Fig. 3.7a).

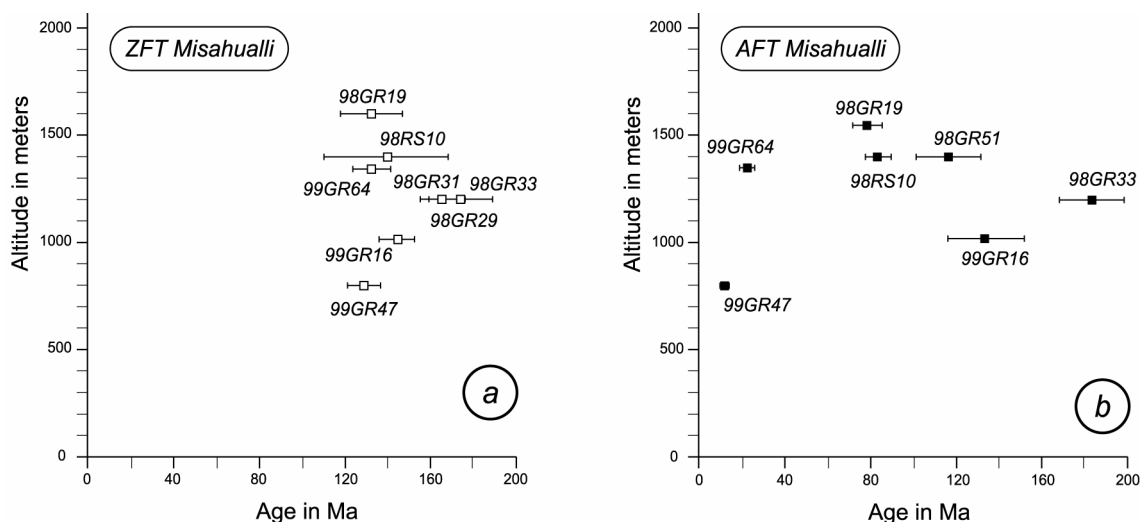


Figure 3.7: Age-altitude representation of the fission-track ages from the Misahualli Fm. (Table 3.2). (a) zircon and (b) apatite.



Sample number	Alt. m	N	$A_0 \times 10^4 \text{ cm}^{-2}$ (counted)	$\rho_s \times 10^5 \text{ cm}^{-2}$ (counted)	$A \times 10^5 \text{ cm}^{-2}$ (counted)	U ppm	$P\chi^2$	MTL $\mu\text{m}$ (N)	Std $\mu\text{m}$	Central age $\pm 1\sigma$
					<b>Apatite</b>					
98RS10*	1400	24	113.9 (5249)	3.11 (276)	7.66 (679)	8.6	100.0	9.56 $\pm$ 0.25 (25)	1.26	83 $\pm$ 6
98GR19*	1550	18	120.2 (5440)	1.99 (170)	5.41 (465)	5.4	100.0	10.81 $\pm$ 0.32 (59)	2.21	78 $\pm$ 7
98GR33*	1200	23	127.8 (5440)	2.42 (299)	2.99 (369)	3.1	82.9	11.86 $\pm$ 0.24 (59)	1.85	183 $\pm$ 15
98GR51	1400	24	120.1 (3553)	1.84 (92)	3.39 (170)	3.9	100.0	6.99 (1)	-	116 $\pm$ 15
98GR52	1375	28	127.5 (3553)	8.10 (30)	57.95 (215)	6.5	22.3	6.20 (1)	-	32 $\pm$ 6
99GR16*	1020	23	128.5 (7083)	2.34 (87)	4.01 (149)	3.8	100.0	11.78 $\pm$ 0.45 (12)	1.56	133 $\pm$ 18
99GR47*	800	31	105.0 (7083)	0.21 (27)	3.34 (422)	4.1	87.8	12.39 $\pm$ 0.46 (15)	1.77	12.0 $\pm$ 2.4
99GR64*	1350	11	112.8 (7083)	1.28 (41)	11.75 (377)	12.5	53.4	-	-	22.0 $\pm$ 3.7
					<b>Zircon</b>					
98RS10*	1400	2	40.0 (2504)	98.97 (163)	17.00 (28)	279.1	52.3	-	-	139 $\pm$ 29
98GR19*	1550	10	45.5 (2504)	165.90 (577)	34.23 (119)	312.6	98.6	-	-	132 $\pm$ 14
98GR29	1200	13	46.3 (2515)	208.90 (2075)	34.83 (346)	273.1	99.9	-	-	166 $\pm$ 11
98GR31	1200	17	46.8 (2515)	103.81 (1609)	16.77 (260)	138.2	55.8	-	-	173 $\pm$ 13
98GR33*	1200	16	35.7 (2475)	114.86 (1389)	14.14 (171)	172.3	99.8	-	-	173 $\pm$ 15
99GR16*	1020	35	32.4 (2485)	147.74 (3713)	19.81 (497)	270.8	100.0	-	-	144 $\pm$ 8
99GR47*	800	22	32.7 (2157)	95.79 (2910)	14.71 (447)	221.7	100.0	-	-	128 $\pm$ 8
99GR64*	1350	16	33.4 (2485)	101.02 (1788)	15.34 (271)	201.2	98.9	-	-	132 $\pm$ 9
99GR84	1040	19	42.1 (2504)	106.63 (2335)	17.26 (378)	172.4	92.7	-	-	156 $\pm$ 10

Table 3.3: AFTA and ZETA from the Misahualli Fm. For localities see Figure 3.2 and Appendix 3.2. Track length measurements for both apatites and zircons are also indicated when completed; asterisks correspond to samples that yielded both AFT and ZFT ages. Numbers in parentheses, as N indicate the number of counted tracks or grains, respectively. All zircon and apatite separates were counted by G.M. Ruiz using zeta calibration of  $121 \pm 3$  (zircon analysis, CN1 standard glass) and  $359 \pm 11$  (apatite analysis, CN5 standard glass).  $\rho_b$ ,  $\rho_s$  and  $\rho_i$  represent the density of the dosimeter, spontaneous and induced tracks of the samples. Samples were irradiated at the ANSTO facility Lucas Heights, Australia.

### 3.4.2.3. *T-t* modelling

Because the number of apatite track length measurements in most of the dated Misahualli Fm. samples did not exceed twenty-five (Table 3.3), T-t modelling was limited to two samples, i.e. 98GR33 and 99GR19 (Fig. 3.8).

#### - 98GR33 (Fig. 3.8a)

After extrusion at 190-175 Ma (period 1, Fig. 3.8a), a period of progressive heating towards a maximum temperature of 75°C is seen in the model of sample 99GR33 until the Late Jurassic-Early Cretaceous (period 2, Fig. 3.8a). Sample 98GR33 subsequently underwent cooling during the following ~30-20 My at a rate of 1.6°C/my until it reached surface temperatures (period 3, Fig. 3.8a) that is confirmed by the observed unconformable deposition of the Aptian Hollin Fm. immediately above sample 98GR33 (see section 2.3.2.1). A second period of heating towards ~70°C took place until 25-20 Ma (period 4, Fig. 3.8a; with a possible additional change at 90-80 Ma), when it left the APAZ, and cooled to its present position (period 5, Fig. 3.8a).

#### - 98GR19 (Fig. 3.8-b)

The Temperature-time modelling of sample 98GR19 can be divided into 3 periods over the last 140-130 Ma, with as for sample 98GR33 a possible additional change at ~90-80 Ma (Fig. 3.8b). The first period corresponds to rapid cooling at ~130-120 Ma from the ZPAZ, i.e. 310-230°C (Tagami et al., 1998) towards temperatures lower than 60°C (period 1, Fig. 3.8b). This is followed by heating towards maximum temperatures of ~90-100°C until 30-25 Ma (period 2, Fig. 3.8b) when cooling began at a rate of a 2.6°C/my (period 3, Fig. 3.8b).

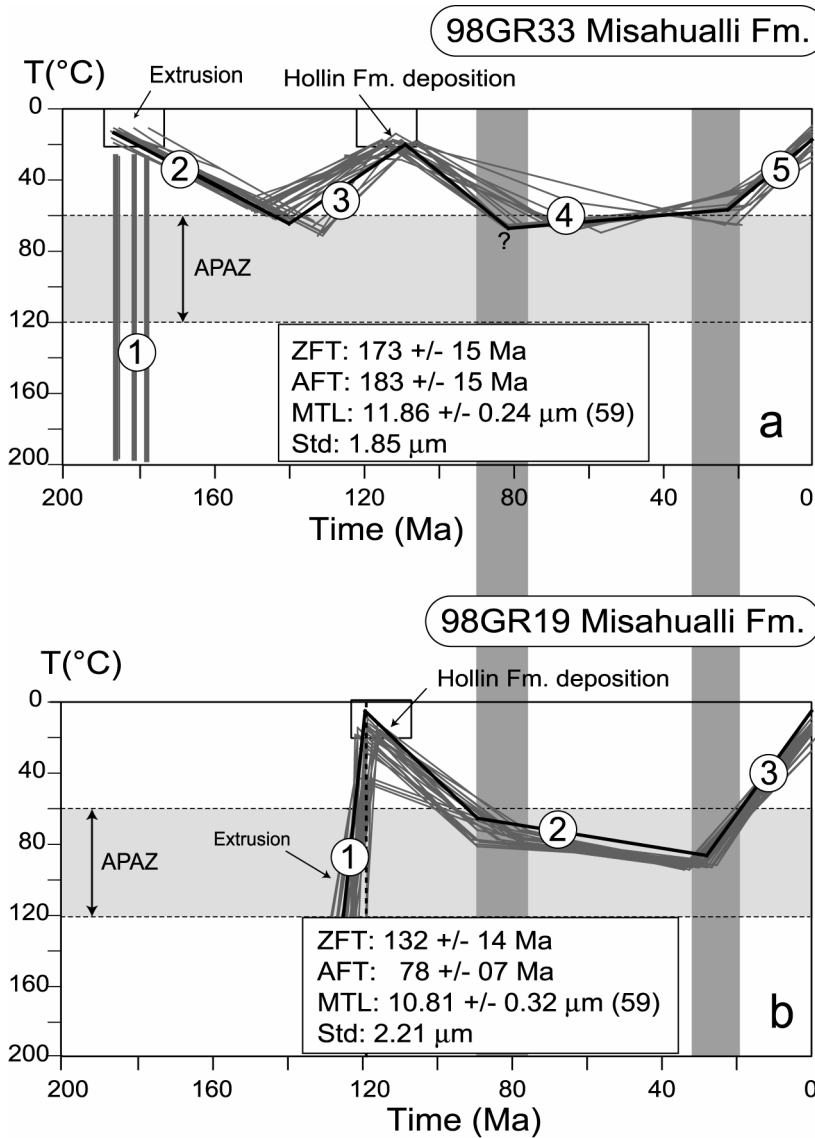


Figure 3.8: Temperature-time modelling of two samples from the Misahualli Fm. See Figure 3.3 for localities. All T-t modelling was completed following procedures described in Gallagher (1995), using Kolmogorov-Smirnov (K-S) test, an initial track length of  $L_0=15.5 \mu\text{m}$ , and 6000 simulation runs. The 20 best T-t paths fitting both AFT age and track length distribution within 95% confidence are used, the best run being indicated by a bold curve. Numbers indicate the corresponding path discussed in the text. APAZ: apatite partial annealing zone. AFT: apatite fission-track; ZFT: zircon fission-track; MTL: mean track length; Std: standard deviation (Table 3.2).

#### 3.4.2.4. Interpretation

In the following section it is again assumed that cooling represents exhumation whereas heating correlates with burial; the rates at which both occurred are investigated using a mean geothermal gradient of 30°C/km.

##### - Extrusion (190-130 Ma)

Sample 98GR33 has similar zircon fission-track ages to  $^{40}\text{Ar}/^{39}\text{Ar}$  ages from volcanics encountered along the southern Flank of the Napo Uplift ( $172 \pm 2$  Ma on Hornblende; Romeuf et al., 1995; Fig. 3.9), and far north close to the Colombian border within the Cordillera Real, i.e.  $162 \pm 2$  Ma (biotite, Spikings et al., 2001; Fig. 3.9). Combined with the modelling of sample 98GR33, this suggests rapid cooling from 480°C to above 60°C at 190-170 Ma that most likely attributes a mid-Early Jurassic age for the earliest extrusion of the Misahualli volcanics and would be coeval with the earliest stage of intrusion of the Abitagua batholith (see section 3.4.1.4), which is considered to have the same magmatic origin (see section 2.1.1).

The duration of the Misahualli arc remains uncertain but the zircon fission-track ages spread from  $173 \pm 15$  Ma to  $128 \pm 8$  Ma (Fig. 3.9 and Table 3.3). Because there is no argument for any resetting to temperatures higher than the ZPAZ, it thus suggests that the Misahualli arc was active until the Early Cretaceous (~130 Ma).

##### - Late-Early Jurassic-Early Cretaceous burial (180-140 Ma, Fig. 3.9)

Apatite fission-track ages vary widely from 183 Ma to 12 Ma, indicating a polyphased thermal history of the Misahualli Fm. at temperatures lower than the ZPAZ.

The post-extrusion heating of sample 98GR33 towards 70°C until 140 Ma (Fig. 3.9) can probably be related to burial by continued deposition of volcanic products from the Jurassic Misahualli-Colán arc. If this is correct, the thickness of the overlying volcanic pile above sample 98GR33 can be estimated, dividing the associated increase of temperature (~from 20°C to 70°C) by a 30°C/km geothermal gradient, to ~1.5-2.0 km before the Early Cretaceous exhumational phase (Fig. 3.9).

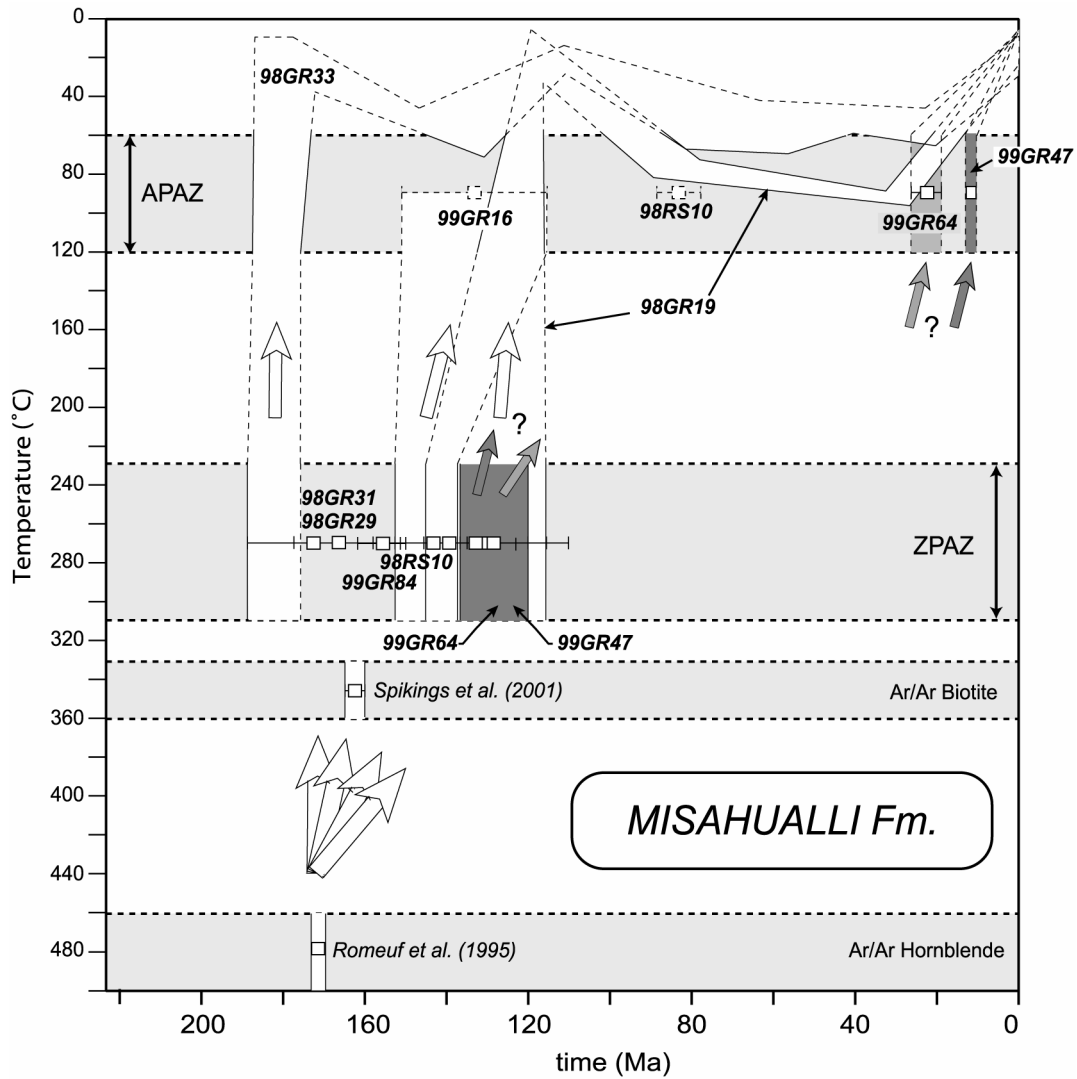


Figure 3.9: Thermochronology of the Misahualli Fm. T-t envelopes were obtained from both apatite modelling, and pairs of ZFT-AFT ages when track length measurement on apatite could not be completed (Table 3.2). See Figure 3.3 and 3.2 for sample localities.  $^{40}\text{Ar}/^{39}\text{Ar}$  age on hornblende (Romeuf et al., 1995) and biotite (Spikings et al., 2001) are also presented. Plain arrows indicate the most probable T-t paths whereas plain lines delimit constrained T-t envelopes and the dashed lines are interpolated paths. APAZ: Apatite Partial Annealing Zone; ZPAZ: Zircon Partial Annealing Zone.

### - Early Cretaceous exhumation and associated Jurassic hiatus

Sample 98GR33 underwent a phase of cooling during the Early Cretaceous from 70°C towards the surface at a rate of 1.6°C/my (Fig. 3.9). Using a geothermal gradient of 30°C/km, it suggests that part of the northern SAZ underwent a phase of exhumation at a mean rate of 0.05 mm/y during the Early Cretaceous. As a result, the above-discussed 1.5-2.0 km thick volcanic pile was eroded prior to the deposition of the Aptian-Albian Hollin Fm. and generated an important hiatus of ~ 40 to 60 My between both formations in this location (see section 2.1.2).

#### *- Albian-Campanian burial*

T-t envelopes of samples 98GR33 and 98GR19 indicate that they coevally underwent heating from ~110 Ma to 80 Ma (Fig. 3.9). This was most likely related to the burial of the northern SAZ by the contemporaneous basin fill series of the Hollin and Napo Fms., because both samples represented the basement of the basin by this time. The maximum temperature reached by sample 98GR19 (80°C) suggests that the thickness of the overlying sedimentary pile at ~90-80 Ma (Fig. 3.9) was of the order of 2 kilometers. Identically, T-t envelopes of sample 98GR33 points to a maximum cumulate thickness of 1.5-1.7 kilometers.

#### *- Mid-Campanian to Oligocene burial*

From possibly middle Campanian (90-80 Ma) until the Late Oligocene (i.e. 30-25 Ma), sample 98GR19 continued being buried at a rate of 0.01-0.02 mm/y (Fig. 3.9). Christophoul et al. (2002) estimated the average sedimentation rates during deposition of the Tiyuyacu and Orteguaza Fms. (Early Eocene to Oligocene) for 3 points located in the Oriente basin. In the westernmost site, which is the closest to the northern SAZ, a mean sedimentation rate of ~0.02 mm/y was calculated (~525m in ~27 My). This value is consistent with the above-calculated rate of burial for a longer period that also comprises the time of deposition of the Tena Fm. (Maastrichtian-Paleocene, see section 4.3.1). Hence, it suggests that sedimentation rates (within error) were about similar in both the western part of the Oriente region and the northern SAZ from Middle Eocene until the Oligocene.

#### *- Late Oligocene-Early Miocene exhumation*

T-t envelopes of sample 98GR19 suggest that a phase of exhumation started at ~30-25 Ma at a rate of ~0.1 mm/y (98GR19, Fig. 3.9). A similar change is also recorded in the T-t envelopes of sample 98GR33, but may have started later (~25-20 Ma). Such a phase of exhumation seems to have affected greater parts of the northern SAZ, because a similar phase is also seen within the Abitagua batholith further south (99GR14, Fig. 3.5) during the Early Miocene.

#### *- Late Miocene exhumation*

The AFT age of  $12 \pm 2.4$  Ma from sample 99GR47 (Table 3.3) located along the western side of the Rio Chingual Fault in the SAZ (Fig. 3.3), suggests that the

far northwest part of the northern SAZ underwent continued exhumation that started at least by the Late Miocene.

### 3.4.3. Other Formations

Here are presented the fission-track ages from various series that are today in tectonic contact with the Aptian to Recent basin fill series of the Ecuadorian AAB to the west of the northern SAZ in the Sub-Andean Thrust Belt, but which may have constituted part of the basement of the AAB between the middle Cretaceous to Recent. These are the (1) Paleozoic (?) sedimentary series of the Pumbuiza Fm. (see section 2.1.1), (2) meta-volcanic sediments of the Paradalarga unit to the east of the Sub-Andean Fault, and (3) the pelitic schist of the Upano unit to the west of the same fault (section 2.1.1).

#### 3.4.3.1. *Paradalarga and Upano units*

a- Results:

- Paradalarga unit:

This recently defined unit in the Sub-Andean Thrust Belt, i.e. between the Sub-Andean and Cosanga Faults (Buitron and Vallejo, 1999; Fig. 3.3) has never been dated.

Four AFT ages were obtained ranging from  $2.5 \pm 0.5$  to  $6.4 \pm 1.8$  Ma whereas two ZFT ages are much older, between  $46 \pm 5$  Ma and  $56 \pm 5$  Ma (Table 3.4). Only two single apatite track lengths, i.e. 14.35 and 15.07  $\mu\text{m}$  were measured due to both the low Uranium content and the young ages (Table 3.4). However, the fact that these two track lengths are long together with the youthfulness of the ages suggest rapid cooling between 2 to 6-8 Ma (Table 3.4). Twenty-seven track lengths within zircons from sample 99GR04 point to a mean track length (MTL) of  $9.54 \pm 0.18$   $\mu\text{m}$  with a standard deviation of 0.91  $\mu\text{m}$ . T-t modelling using zircon track lengths is unfortunately not yet possible; however, such a MTL is quite long for zircons (Hasebe et al., 1994), thus indicating rapid cooling through the ZPAZ at  $\sim 46 \pm 5$  Ma (Table 3.4).

- Upano unit:

This unit of the Salado Terrane from the Cordillera Real (Litherland et al., 1994) is of prime interest in understanding and interpreting the development of the Sub-Andean Zone as it outcrops on the western side of the Sub-Andean Fault, which is the western boundary of the SAZ with the Cordillera Real (Litherland et al., 1994; Fig. 3.3). A pair of AFT and ZFT ages, respectively  $25 \pm 11$  Ma and  $45 \pm 5$  Ma (sample 99GR01; Table 3.4), is here combined with three  $^{40}\text{Ar}/^{39}\text{Ar}$  and K/Ar ages to constrain the thermochronology of the Upano unit west of Baeza (Fig. 3.10), these are: (1) a K/Ar age of  $54 \pm 2$  Ma (mineral?) (Feininger and Silberman, 1982) in approximately the same location as sample 98RS13 (Spikings et al., 2000; Fig. 3.3), (2) a K/Ar age of  $59.1 \pm 2.2$  Ma on muscovite (Herbert and Pichler, 1983), and (3) a  $^{40}\text{Ar}/^{39}\text{Ar}$  age of  $61.5 \pm 0.6$  Ma on biotite (Fig. 3.3; Spikings et al., 2001). The latter two ages were produced from almost the same levels of the Upano unit (Fig. 3.3). Additionally, a ZFT age of  $39 \pm 2$  Ma age was obtained from the Upano unit located much further south in the Cordillera Real (Spikings et al., 2001) that is in complete agreement with the ZFT age of  $45 \pm 5$  Ma in this region (Table 3.4). However, the site of this southern sample is considered too distant from the Baeza region (>300 kms) to be included in the thermochronological dataset of the Upano unit for further interpretation.



Sample number	Alt. m	N	$A_0 \times 10^4 \text{ cm}^{-2}$ (counted)	$A_s \times 10^5 \text{ cm}^{-2}$ (counted)	$A \times 10^5 \text{ cm}^{-2}$ (counted)	U ppm	$P\chi^2$	MTL $\mu\text{m}$ (N)	Std $\mu\text{m}$	Etch pit diameter $\mu\text{m}$	Std $\mu\text{m}$	Central age $\pm 1\sigma$
<b>Paradalarga Unit</b>												
98RS01	1650	23	134.0 (5269)	0.21 (13)	7.80 (485)	7.1	99.3	14.35 (1)	-	2.78 $\pm$ 0.19 (10)	0.62	6.4 $\pm$ 1.8
99GR04*	2015	30	130.1 (5269)	0.12 (15)	4.560 (566)	4.8	42.0	-	-	2.58 $\pm$ 0.11 (10)	0.30	6.2 $\pm$ 1.6
99GR08*	1880	36	97.6 (6472)	0.12 (29)	8.31 (2052)	10.8	73.6	15.07 (1)	-	3.11 $\pm$ 0.23 (06)	0.55	2.5 $\pm$ 0.5
99GR09	2120	30	100.0 (6472)	0.09 (21)	5.75 (1331)	7.3	99.0	-	-	3.20 $\pm$ 0.08 (24)	0.35	2.8 $\pm$ 0.6
<b>Zircon</b>												
99GR04*	2015	19	36.1 (2199)	98.05 (2219)	46.49 (1052)	499.2	27.3	9.54 $\pm$ 0.18 (27)	0.91	-	-	46 $\pm$ 2.6
99GR08*	1880	24	33.4 (2157)	85.56 (2782)	30.79 (1001)	388.7	42.4	-	-	-	-	55.7 $\pm$ 2.7
<b>Upano Unit</b>												
99GR01*	2040	6	118.2 (5269)	0.43 (6)	3.62 (51)	3.8	85.1	14.66 (1)	-	-	-	25 $\pm$ 11
<b>Zircon</b>												
99GR01*	2040	13	34.1 (2157)	87.73 (594)	36.04 (244)	424.4	3.0	-	-	-	-	45 $\pm$ 5
<b>Others</b>												
99GR71 (Pb)	1220	19	35.8 (1875)	313.17 (6094)	14.21 (276)	176.5	100.0	-	-	-	-	461 $\pm$ 32

Table 3.4: AFTA and ZFTA from the Paradalarga and Upano units, the Pumbaiza Fm. (Pb) and also from one reset level from the Tena Fm. For localities see Fig. 3.3 and Appendix 3.2. Track length measurements for both apatites and zircons are also indicated when completed, whereas asterisks correspond to samples that both yielded AFT and ZFT ages. All zircon and apatite separates were counted by G.M. Ruiz using zeta calibration of  $121 \pm 3$  (zircon analysis, CN1 standard glass) and  $359 \pm 11$  (apatite analysis, CN5 standard glass).  $\rho_0$ ,  $\rho_s$ , and  $\rho_i$  represent the density of the dosimeter, spontaneous and induced tracks of the samples. Samples were irradiated at the ANSTO facility Lucas Heights, Australia.

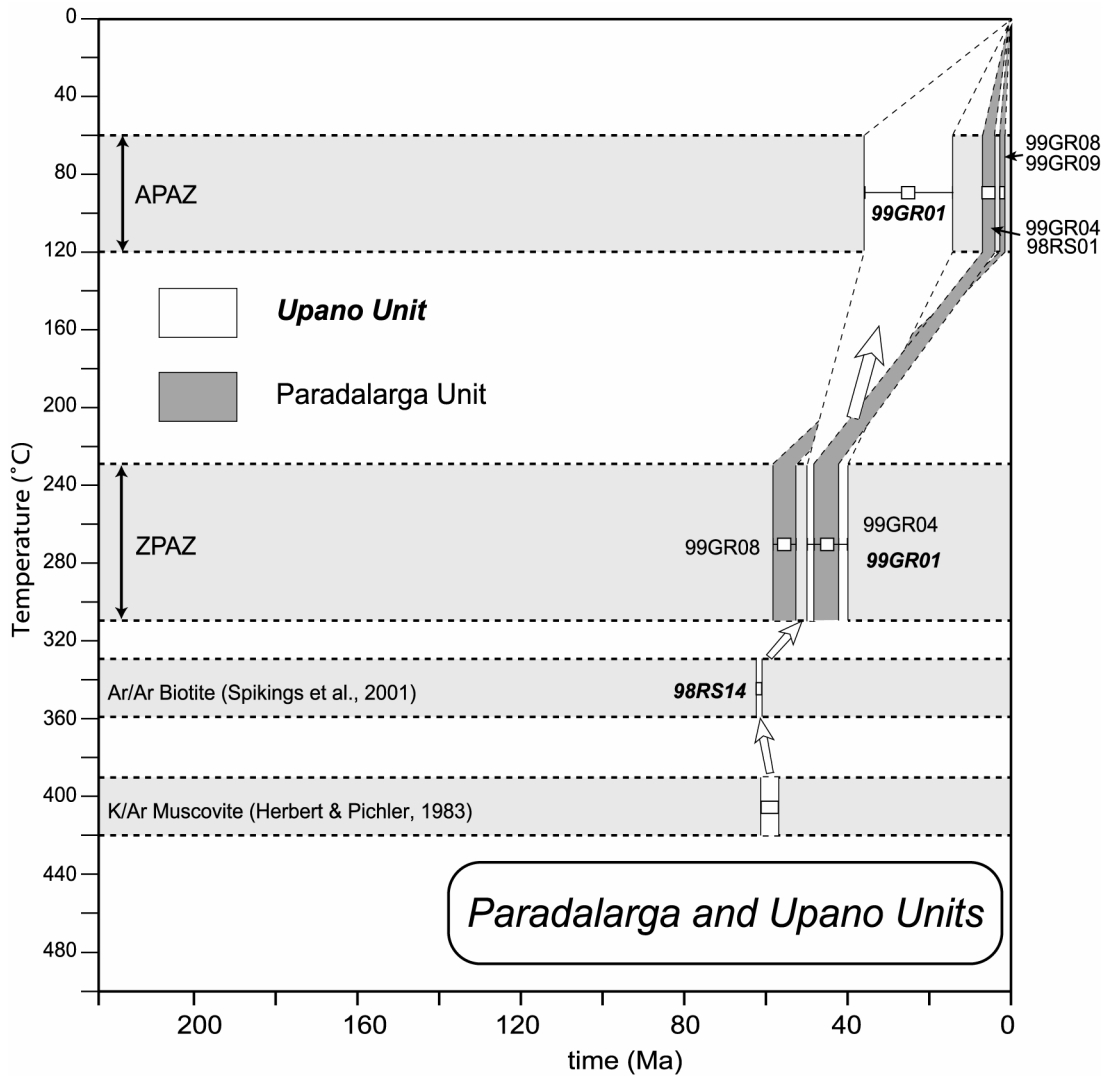


Figure 3.10: Thermochronology of the Paradalarga and Upano units. K/Ar and  $^{40}\text{Ar}/^{39}\text{Ar}$  ages from previous studies are also presented (Herbert and Pichler, 1983; Spikings et al., 2001). Plain arrows indicate the most probable and simplest T-t paths whereas plain lines delimit constrained T-t envelopes and the dashed lines are interpolated paths. APAZ: Apatite Partial Annealing Zone; ZPAZ: Zircon Partial Annealing Zone.

## b- Interpretations

Because lithologies of the Upano and Paradalarga units are internally homogeneous and the distance across strike does not exceed 2-3 kilometers, it is then possible to group all ages to obtain relevant Temperature-time envelopes (Fig. 3.10). In contrast to the Misahualli Fm. and Abitagua batholith that both have Jurassic formation ages constrained by Rb/Sr, K/Ar,  $^{40}\text{Ar}/^{39}\text{Ar}$ , and fission-track analyses, the formation ages of the Paradalarga and Upano units cannot be revealed by any thermochronological method because resetting at temperatures higher than 450°C probably occurred as

suggested by the K/Ar and  $^{40}\text{Ar}/^{39}\text{Ar}$  ages. Therefore, inferred phases of cooling and heating from the Late Paleocene to Recent are only related to post-formational exhumation or burial experienced by the Paradalarga and Upano units.

The T-t path from the Upano unit indicate rapid cooling at a rate of 7 to 10°C/my from 62 to ~30-25 Ma, which corresponds to an exhumation rate of 0.2 to 0.3 mm/y (considering a 30°C/km geothermal gradient) from the Paleocene to the Early Miocene. Since then, rocks of the Upano unit were probably never sufficiently heated to significantly modify their fission-track ages. Moreover, rocks of the Paradalarga unit also exhibit ZFT ages, i.e.  $56 \pm 3$  Ma and  $46 \pm 3$  Ma with relatively long track lengths (Table 3.4) indicating that the Paradalarga unit underwent a phase of exhumation from the Late Paleocene to the Middle Eocene. Because ZFT ages are almost identical in both units (Fig. 3.10), they were most likely commonly exhumed between ~60 Ma and 45-40 Ma. However, it is relevant to notice that AFT ages are different from one unit to the other across the Sub-Andean Fault, suggesting heterogeneous thermal histories below the partial annealing zone of zircons (Fig. 3.10).

Considering this, two possibilities are then envisaged to explain heterogeneous T-t envelopes across the Sub-Andean Fault (Fig. 3.11):

(1) Both units synchronously exhumed and passed through both the ZPAZ (310-230°C) and later the APAZ (120-60°C) during the Late Paleocene to Early Miocene period (~62-25 Ma; path 1 Fig 3.11). Subsequently the Paradalarga unit was heated (buried?) towards temperatures between 120°C and 230°C and later exhumed during the Late Miocene to Recent (8-0 Ma).

(2) The Upano and Paradalarga units have cooled differently below the 230°C isotherm since they commonly passed through the ZPAZ at ~62-40 Ma (path 2 Fig 3.11). The Upano unit alone exhumed during the Late Eocene (45-25 Ma) whereas the Paradalarga unit underwent exhumation since the Late Miocene.

Both solutions can be envisaged but the second one (Fig. 3.11) is preferable, because it does not necessitate any additional phase of heating for the Paradalarga unit that cannot be traced through fission-track analysis.

The Sub-Andean Fault (SAF) system was studied by Litherland et al. (1994) who concluded that this is a steep east-vergent reverse fault system that may also accommodate strike-slip movement. Eocene-Oligocene apatite fission-track ages are today present at the surface in the so-called hanging wall (Upano unit). Pure reverse displacement should have generated much younger ages in the hanging wall, which is not the case for the Sub-Andean Fault system in the region of Baeza. This therefore suggests that such component is not accommodated anymore by the Sub-Andean Fault system. It is rather suggested that the Sub-Andean Thrust Belt, which is defined as the area between the Sub-Andean and Cosanga Faults (Litherland et al., 1994; see

section 2.), may accommodate right-lateral sense of movement since ~8-6 Ma in a transpressive regime as suggested by Pasquarè et al. (1990) for the complete northern SAZ. Hence, this drives cooling and exhumation in the tectonically slice wedge of the Paradalarga unit in the region of Baeza.

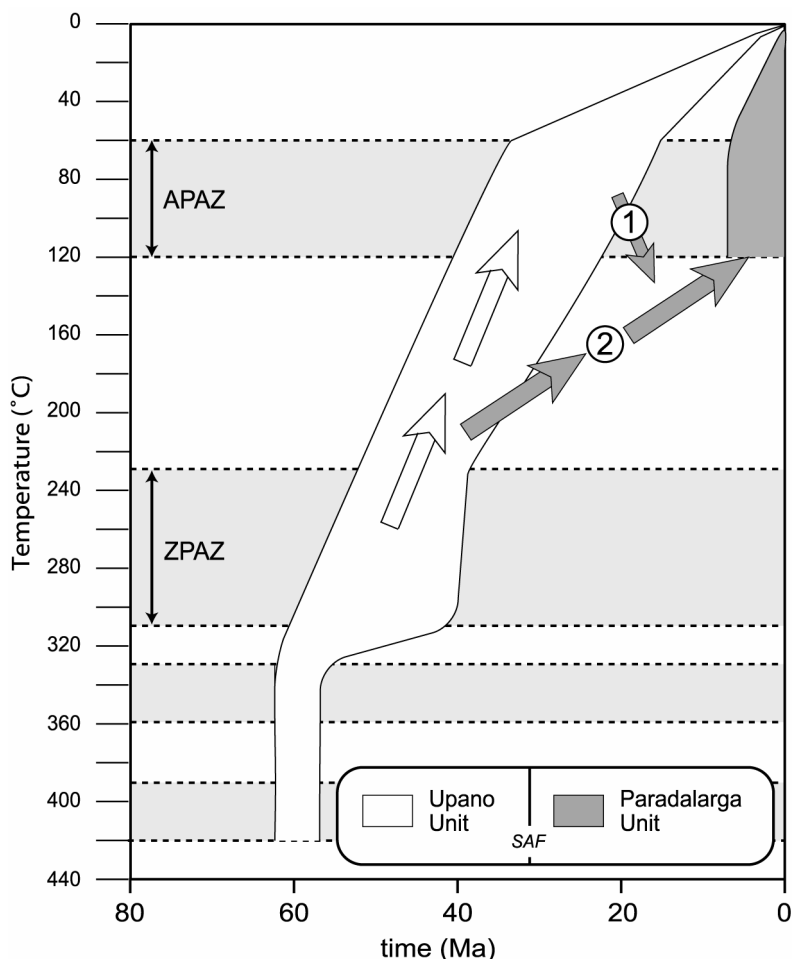


Figure 3.11: Possible T-t paths of the Paradalarga and Upano units across the Sub-Andean Fault (SAF) in the region of Baeza and El Chaco (Fig. 3.3) with the two possible scenarios for the Paradalarga unit. APAZ: apatite partial annealing zone; ZPAZ: zircon partial annealing zone.

These young AFT ages are localized in the region of Baeza in the vicinity of active volcanoes. Therefore, one may argue that partial, or total resetting of the apatite fission-track ages was driven by thick and hot cover of ignimbrites encountered today in the bed of the Rio Quijos, which was later removed by erosion. However, a young AFT age (i.e.  $2.8 \pm 0.6$  Ma; Table 3.4) was also produced from a level of the Paradalarga unit taken in an incised valley further north where no ignimbrites are reported (sample 99GR09; Fig. 3.3). This therefore confirms that the young AFT cooling ages from the Paradalarga unit are clearly related to recent activity along the Sub-Andean Fault system.

### 3.4.3.2. Pumbuiza Fm.

Mica-rich sandstones of the Devonian (?) Pumbuiza Fm. (see section 2.3.2.3) were encountered west of the Abitagua batholith, southwest of Mera (99GR71; Fig. 3.3). This level did not yield any apatite but a single population of zircons gave an age of  $461 \pm 32$  Ma (Table 3.4).

If post-depositional resetting is envisaged, one can conclude that this is an exhumation age of the Pumbuiza Fm., and as a result that the stratigraphic age of Pumbuiza Fm. is older than  $461 \pm 32$  Ma. If resetting did not occur, this is the reverse and the Pumbuiza cannot be older than the Ordovician.

### 3.4.4. Reset detrital age

Only one apatite fission-track age from the basin fill series located to the east of the Abitagua batholith was partially or totally reset. This is an AFT age of  $59 \pm 3$  Ma from a basal Tena Fm. level taken southwest of Mera (99GR67; Fig. 3.3) in a zone where recent tectonic development is evidenced by a very young AFT age of  $1.4 \pm 1.0$  Ma from the nearby eastern edge of the Abitagua batholith (99GR66; Fig. 3.3).

Zircon fission-track analysis from the same sample revealed three different populations; the youngest or  $P_1$  population yielded an age of  $72 \pm 3$  Ma that may correspond to the maximum stratigraphic age of sample 99GR67 (section 4.2). Sixty-seven measured track lengths (Table 3.4) allowed T-t modelling between the 120-60°C isotherms (Fig. 3.12). Two clear thermal phases are observed therein (Fig. 3.12): (1) heating towards temperatures in the range of 85-60°C from the time of deposition until ~57-50 Ma, and (2) a subsequent slow cooling until today.

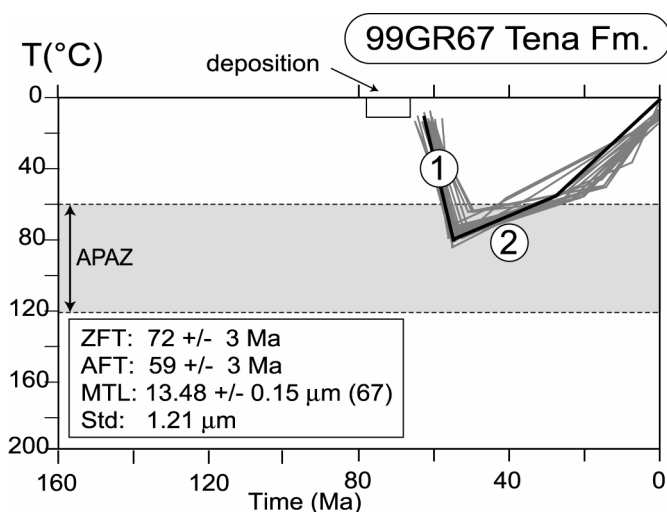


Figure 3.12: Temperature-time modelling of sample 99GR67 from the Tena Fm. See Figure 3.3 for locality. T-t modelling was completed following procedures described in Gallagher (1995), using Kolmogorov-Smirnov (K-S) test, an initial track length of  $L_0=15.5 \mu\text{m}$ , and 6000 simulation runs. The 20 best T-t paths fitting both AFT age and track length distribution within 95% confidence are used, the best run being indicated by a bold curve. Numbers indicate the corresponding path discussed in the text. APAZ: apatite partial annealing zone.

*- Interpretation*

Since deposition in the Maastrichtian, sample 99GR67 from the Tena Fm. probably underwent a phase of burial until the Late Paleocene-Early Eocene, that was contemporaneous with the deposition of the Tena Fm. in the Ecuadorian AAB. A rapid calculation using a geothermal gradient of 30°C/km suggests that its maximum thickness should not have exceeded 1.5-2 kilometers in the region of Mera (Fig. 3.3). In the Early Eocene sample 99GR67 ceased being buried and was exhumed towards the surface at a low rate of ~0.03 mm/y. Hence, the inception of this phase corroborates with the hiatus between the upper Tena Fm. of Paleocene age and the Early Eocene Tiyuyacu Fm. (see section 2.2.2.4) that was probably the result of the exhumation of the northern SAZ.

### 3.5. Synthesis

1- Cooling ages and T-t modelling from the Abitagua batholith and the Misahualli volcanics suggest coeval formation and a genetic relationship from the Jurassic (190-180 Ma) until the Early Cretaceous (130 Ma; Fig. 3.13). Both are probably also genetically related to the Zamora batholith in the southern SAZ (190-180 Ma).

2- If the zircon fission-track ages of the Misahualli Fm. are considered as eruption ages (Fig. 3.13), the continental Misahualli volcanic arc activity continued until the Early Cretaceous (~128 Ma). This is a long time span; contemporaneous sedimentation along the Ecuadorian margin may thus be represented by the volcanoclastic sediments of the Chapiza Fm., and the Upano and Paradalarga units.

Following heating, probably due to burial until ~140 Ma, the center of the Napo Uplift experienced an exhumational phase during the Early Cretaceous (140-130 Ma) that subsequently generated a 40-60 My hiatus between the Misahualli volcanics and the Aptian-Albian Hollin Fm. However, this phase was not recognized everywhere because the eruption ages had been reset later on, removing the identification of this event completely.

3- From the Aptian onward (110-0 Ma), no sediments other than along the Sub-Andean Thrust Belt have undergone temperatures greater than 100°C as evidenced from the 'basement' fission-track ages and the modelling of these. This therefore indicates that the zircon fission-track ages from the overlying Aptian to Recent basin fill series present in the northern SAZ sediments have an explicit detrital character that allows the exhumation in the source regions to be studied (section 4.2; Fig. 3.1).

4- Some events are seen through the modelling: these are a) burial at ~150 Ma from the overlying Jurassic volcano-sedimentary pile, and b) an Early to Middle Eocene (~55-45 Ma; Fig. 3.13) exhumation of the SAZ that may have been preceded by burial from 70 to 60 Ma (Fig. 3.13) that would correspond to the deposition of the Tena Fm.

A major, because extensive phase of exhumation prevailed during the Early Miocene (25-20 Ma) in the northern SAZ (Fig. 3.13) that can be correlated with an Early Miocene phase of exhumation that affected the Cordillera Real (Spikings et al., 2000). Hence, both the Cordillera Real and the northern SAZ appear to have undergone synchronous exhumation during the Early Miocene with similar rates, i.e. 0.1-0.3 mm/y.

5- Because young (reset) apatite fission-track ages of 6-8 to 2 Ma are located along the narrow Sub-Andean Thrust Belt, this region has most probably accommodated transpressional movement since the Late Miocene that localized exhumation.

Moreover, Late Miocene (12-10 Ma) to Pliocene (1.4 ± 1.0 Ma) apatite fission-track ages were also produced on both sides of the Abitagua batholith, and in the northernmost foothills of the Cordillera Real (Rio Chingual Fault; Fig. 3.3). This

explicitly indicates that the Abitagua batholith has been exhuming since at least the Late Miocene (Fig. 3.13), which was possibly coeval with the development of the Rio Chingual Fault to the north of the Napo Uplift. However, this period of exhumation is not restricted to the northern SAZ but was also affecting the Cordillera Real to the west as indicated by cooling in AFT modelling (Spikings et al., 2000), thus indicating that both the Cordillera Real and the northern SAZ have been exhuming since the Late Miocene.



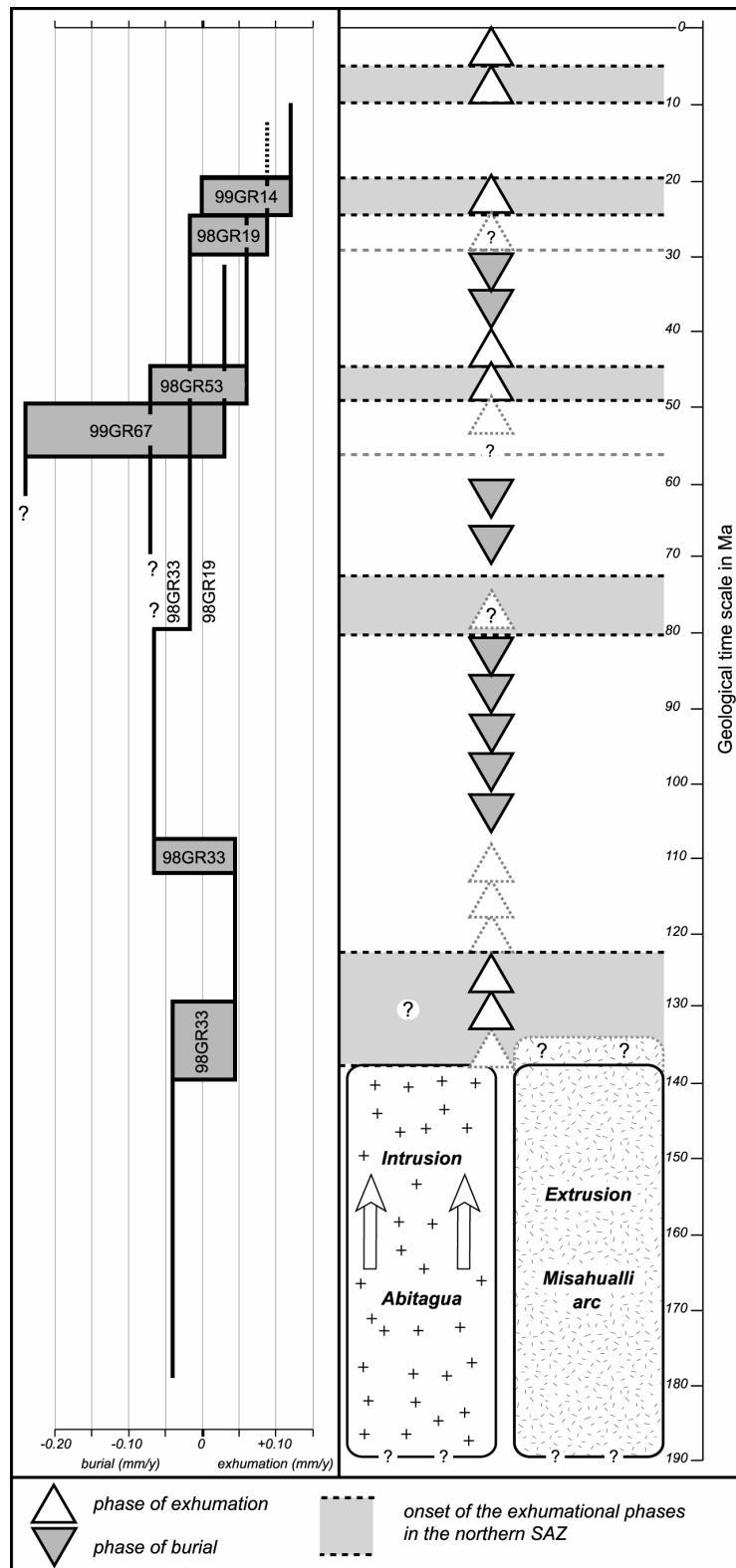


Figure 3.13: Exhumational and burial phases that can be traced using fission-track analysis in the substratum series of the northern SAZ. To the left are the associated rates considering a 30°C/km geothermal gradient for the modelled samples. This figure does not imply that all phases were present at all localities.



## 4. Provenance

### 4.1. Provenance of detrital grains (heavy minerals)

Accessory minerals of sandstones are marked by their higher than average density. These minor constituents rarely exceed more than 1% of the whole rock. However, they hold much information regarding the source region of the sediment. They are derived from the major but also often accessory minerals of the parent rock. They are the minerals that have survived weathering, erosion and chemical and physical abrasion during transport and interstratal solution (Morton, 1984; Johnsson, 1993). Thus the composition and abundance is dependant on many factors such as the source rocks, the climate, the type of transport, and the depositional and diagenetic environment (Morton and Johnsson, 1993).

In the present study, the heavy mineral suites of all the samples taken for thermochronological analysis were studied in order to assess: (1) the lithology of the source material of the sediments of the AAB deposited in the northern Ecuadorian SAZ (section 4.1), (2) to assess the variation of the source materials with any changes in the detrital thermochronology (section 4.2), and (3) to identify any major input of volcanic material which may have an influence on the pattern of the thermochronological data sets (section 4.2).

#### 4.1.1. Introduction

Heavy mineral suites can often be related to different groups of parent materials, such as plutonic, metamorphic and volcanic rocks which in themselves contain specific mineral associations. Reworked sedimentary rocks are more difficult to identify, but are generally characterized by the abundance of the more resistant heavy minerals such as the zircon, tourmaline and rutile associations (Mange and Maurer, 1992). In the following paragraphs the various associations commonly found are presented.

Zircon, tourmaline, rutile (commonly referred to as the ZTR assemblage) with additional brookite, anatase and titanite have their provenance mostly in granitic to dioritic and very low-grade (ortho)-gneissic terranes. Their occurrence may be correlated with the presence of shallow continental crustal elements (with possible sedimentary cover) in the source terrane.

Apatite is a commonly associated mineral. As inclusion rich and idiomorphic/prismatic form, it is just one possible indicator of the presence of a (possibly coeval) volcanic source. Similarly, a high abundance of idiomorphic zircons may point to an acidic volcanic source.

Mineral grains of different metamorphic grades can be observed in the separates. In order of increasing metamorphic grade these are pumpellyite (low grade), epidote, clinozoisite, chloritoid, zoisite (medium grade, ECCZ). The phyllosilicates, as muscovite, biotite and chlorite belong also to this group but are commonly only qualitatively registered during the counting, because of unusual enrichment or impoverishment during sedimentation due to variable hydrodynamic behaviour of the grains. Sillimanite, staurolite, andalusite and kyanite are high-grade minerals that define the GSSAK pole with garnet. Garnet may be derived from both medium and high-grade metamorphic source rocks. Minerals from the amphibole group can be derived from a wide range of magmatic and regional metamorphic successions.

Optical distinction of different amphibole species is often very difficult and only a broad scheme may be applied. So-called green and brown hornblendes occur in intermediate and acidic alkaline intrusive rocks and volcanics, and are also a main constituent in amphibolite (high grade) metamorphic rocks as blue amphibole for metamorphic blueschist (high pressure-low temperature) facies for source rocks. Tremolite is often the product of regional metamorphism of siliceous dolomites.

A similar problem of limited recognition under the petrographic microscope is also encountered in the group of pyroxenes. However, augite and hypersthene can be identified and indicate the presence of ultramafic to intermediate magmatic source rocks (basalts, andesites, gabbros, dolerites), but they are less frequent in metamorphic rocks (e.g. gneiss, granulites). Hypersthene occurs also in some granites and syenites. Diopside is indicative of alkaline basalts, andesites and some sub-alkaline magmatic rocks, but the presence in regional and contact metamorphic Ca-rich rocks (skarns) is also known. Olivine is a typical constituent of basic magmatic rocks and chromite is an accessory mineral in peridotites and serpentinites. Cassiterite is an important hydrothermal mineral in granites (in pegmatites and dykes).

#### 4.1.2. Methodology

Rocks were crushed and the carbonate fraction dissolved in acetic acid (10%). The density separation was carried out on the grain fraction 0.063-0.4 mm in bromoform (density 2.88-2.9). The heavy mineral residues were made into two permanent mounts for examination under the optical microscope. The counting was realized in mineral mounts in piperin (refraction index 2.67) under the petrographic microscope (e.g. Winkler, 1988). About 200 grains were statistically counted in each sample, when possible. This number provides a reliable estimate of the frequency proportions of the various heavy minerals (HM).

### 4.1.3. Results

The variable heavy mineral compositions of the sandstones of the northern Ecuadorian SAZ (Appendix 4.1) are summarized in Figure 4.1, where the samples are shown in stratigraphic order, from the base to the top.

#### - *Pumbuiza Fm. (Paleozoic)*

A sample, from the Paleozoic Pumbuiza Fm. (Baldock, 1982) was encountered in the Rio Gringo region, south of Mera and east of the Cordillera Real (Fig. 4.14). A ZTR representation dominates (Fig. 4.1) the heavy mineral suite with abundant muscovite (Appendix 4.1).

#### - *Hollin and Napo Fms. (Aptian/Albian-Campanian)*

Zircon is the main constituent (40 to 90%) in the Hollin and Napo Fms. (Figure 4.1) and is associated with variable amounts of tourmaline and the titanium-bearing minerals like rutile, brookite, anatase and sphene. Cassiterite and diopside are minor constituents. Epidote (1.0%) occurs rarely (Appendix 4.1). Muscovite, biotite and chlorite, which were not counted (see above), are present in few quantities only in the westernmost Hollin sample (99GR73, Fig. 4.1 and Appendix 4.1). Diopside occurs in a few samples (1.5-3.0%) of the Hollin and Napo sandstones in the center part of the northern SAZ, i.e. samples 98GR50, 99GR09, and 98GR41 (Fig.4.1, see Fig. 4.14 for sample localities). Several samples bear a moderate amount of monazite (1-5%), which was rarely found in the younger basin formations.

A Coniacian-Santonian (89-84 Ma) Napo Fm. sample adjacent to the Cordillera Real (98RS06, 'Mirador anticline', Jaillard, 1997b) hosts the first metamorphic mineral grains represented by 1% garnet that is associated with frequent muscovite, biotite and chlorite (Fig. 4.1 and Appendix 4.1).

#### - *Tena Fm. (Maastrichtian-Paleocene)*

The lower Tena Mb. is characterized by a high abundance of apatites (50% to 68.5%; Fig. 4.1) at the expense of the stable minerals (ZTR). In sample 98GR37, the apatites are often prismatic. The Tena Fm. is particularly characterized by the incoming of metamorphic minerals as garnet, clinozoïte and chloritoid, which were not found in the formations below (Fig. 4.1).

- *Tiyuyacu Fm. (Eocene)*

The Tiyuyacu Fm. samples are characterized by variable assemblages of stable (ZTR) and metamorphic minerals. A basal sample (99GR36) is mainly represented by the ZTR pole (96.2%; Fig. 4.2), where zircons are partly idiomorphic; phosphate and volcanic tuff cement compose part of the matrix. In contrast, the upper part of the Lower Tiyuyacu Member is dominated by chloritoid (75.5%; Fig. 4.1) at the expense of the ZTR group (Fig. 4.2). The base of the upper Tiyuyacu Mb. is mainly represented by the ZTR pole (Fig. 4.2). Upwards in the formation a low to medium grade metamorphic mineral group represented by clinozoisite and garnet (3%, Fig. 4.1 and 4.2) grades into a high-grade association of kyanite-sillimanite (23%, Fig. 4.1 and 4.2).

- *Orteguaza and Chalcana Fms. (Oligocene)*

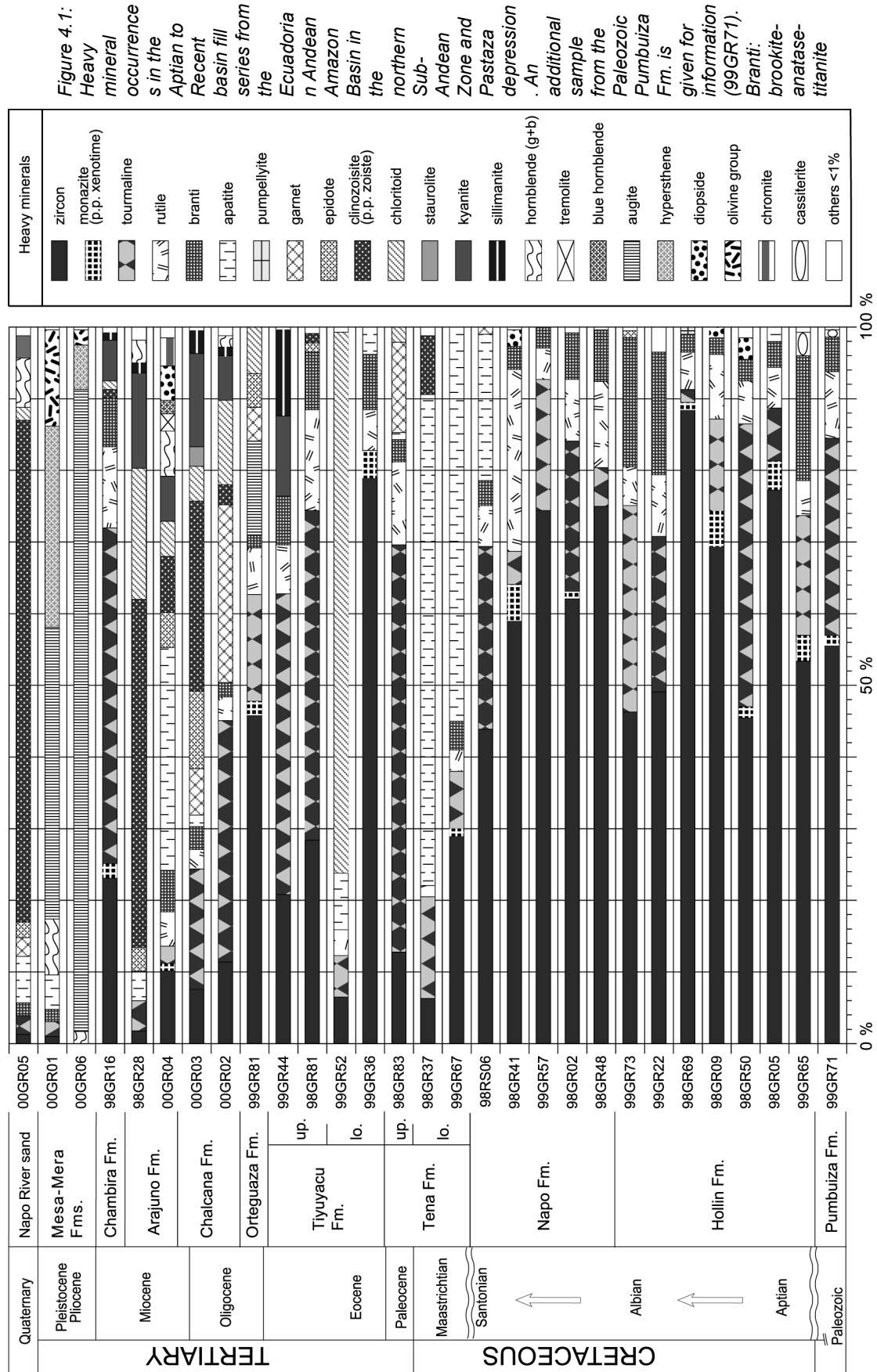
The Orteguaza and Chalcana Fm. formations yield a decreasing abundance of ZTR (from 70 to 25%) upward with a concurrent increase in metamorphic components, of both low to medium and high-grade (Fig. 4.2).

- *Arajuno and Chambira Fms. (Miocene)*

The heavy mineral content of a lower Arajuno sample (00GR04; Fig. 4.1) is characterized by the presence of (1) many euhedral, prismatic and inclusion rich apatites, (2) idiomorphic zircons, and (3) pseudo-hexagonal biotites, which are all suggestive of a volcanic input. The remaining fraction is very heterogeneous and comprises medium to high-grade metamorphic grains (including some green, brown and blue hornblende), diopside and chromite (Fig. 4.1). Upward in the Arajuno Fm. (98GR28; Fig. 4.1), the metamorphic component is dominated by high to medium-grade metamorphic associations (Fig. 4.1 and 4.2). The Chambira Fm. is characterized by the ZTR association with a slight percentage of high-grade metamorphic minerals (5.7% kyanite and 1% sillimanite, Fig. 4.1).

- *Mesa and Mera Fms. (Pliocene-Pleistocene)*

The Mesa and Mera Fms. are characterized by the absence of metamorphic minerals but augite, hypersthene and olivine dominate the heavy mineral spectra (95.8%, Fig. 4.1).



*- Quaternary*

A medium-grade metamorphic association (clinozoisite, epidote, chloritoid, garnet) strongly dominates (~77%; Fig. 4.1 and 4.2) the heavy mineral content of the modern-river sand from the Rio Napo in the Puerto Misahualli area (00GR05, Fig. 4.14). The remainder part is shared by amphibole (7%), the ZTR minerals (6%), augite (3%) and apatite (6%, Fig. 4.1).



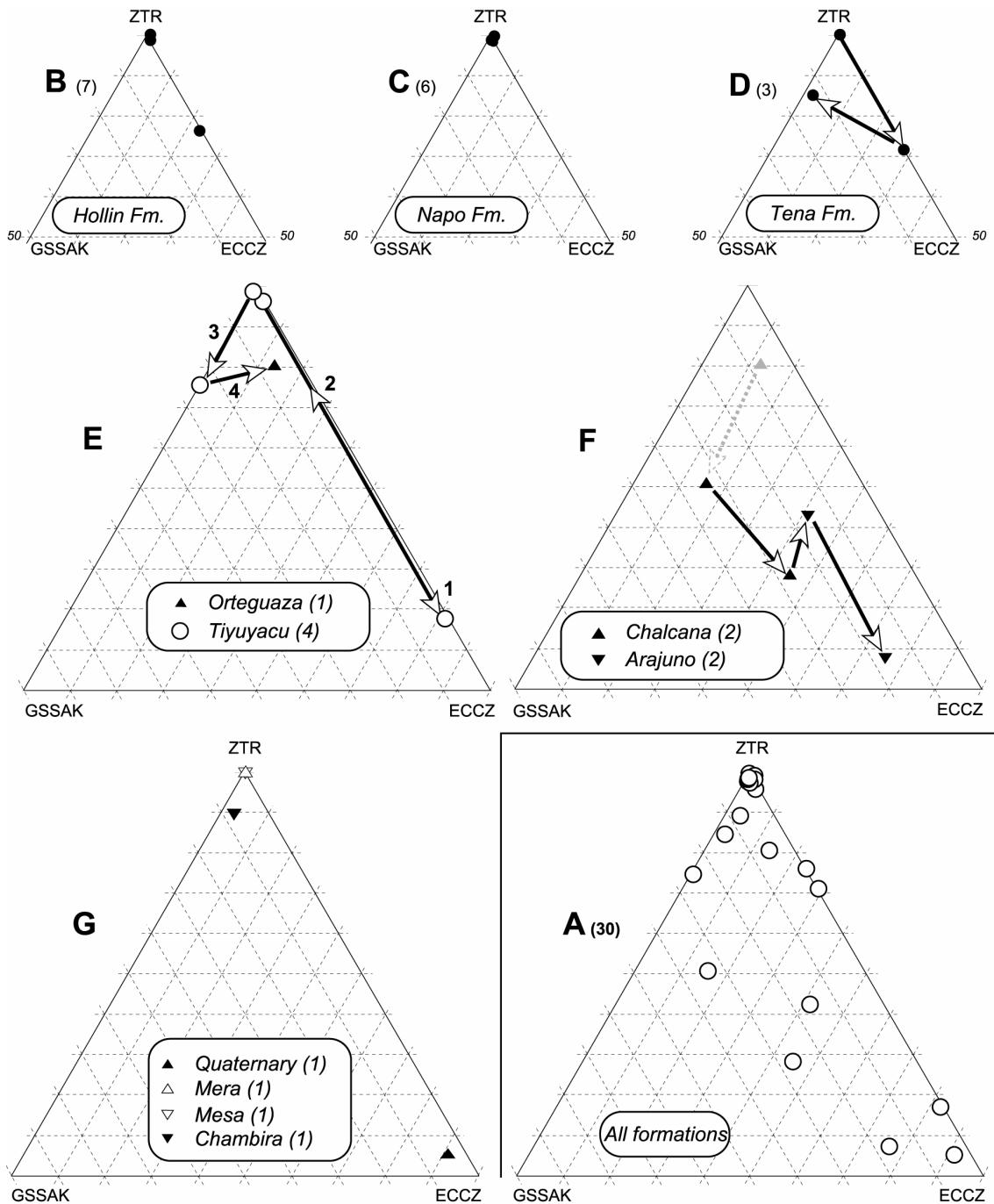


Figure 4.2: (A) Ternary plots of the relative abundance of garnet + staurolite + sillimanite + andalusite + kyanite (GSSAK), epidote + chloritoid + clinozoisite + zoisite (ECCZ) and zircon + tourmaline + rutile (ZTR) in samples, showing the differences in provenance of Aptian to Recent sediments from the Ecuadorian AAB (A). Six other ternary plots depict the relative abundance within the different formations. These are: the Hollin Fm. (B), the Napo Fm. (C), the Tena Fm. (D), the Tiyuyacu and Orteguaza Fms. (E), the Chalcana and Arajuno Fms. (F) and, the Chambira, Mesa, Mera Fms. (G) that are here drawn with a Quaternary river deposit from the Napo River in the vicinity of the village of Puerto Misahualli (see Fig. 4.14 for sample localities). Numbers in brackets indicate the number of samples whereas arrows indicate the younging direction in the stratigraphic column. A detailed list of analyses is given in Appendix 4.1.

## 4.2. Detrital Fission-Track analysis

Siliciclastic sediments generally contain grains derived from more than one source region. Hence, the varied thermal histories experienced by the source regions will be reflected in the distribution of the cooling ages of detrital grains (e.g. FT and  $^{40}\text{Ar}/^{39}\text{Ar}$ ) recorded through detrital grains in a sedimentary basin (Naeser, 1979). Several workers (e.g. Hurford et al., 1984; Zeitler et al., 1986, Cervený et al., 1988; Hurford and Carter, 1991; Brandon and Vance, 1994; Najman et al., 1997; Brandon et al., 1998; Carter, 1999; Carter and Moss, 1999; Garver et al., 1999; Bernet et al., 2001; Spiegel et al., 2001) attempted to use changes in detrital fission-track grain ages through time to reconstruct the geodynamic development of the hinterland/source region (Fig. 3.1). This was a major innovative development because the source region has itself been eroded or overprinted yet, information was obtained on the tectonic development of the hinterland through the sedimentary deposits.

The purpose of this section is to present (1) some clear definitions and concepts regarding detrital thermochronology, (2) new theoretical models which are discussed with special reference to their common geodynamic implication, and (3) the results from fission-track analysis on the Aptian to Recent basin fill series of the northern Ecuadorian Sub-Andean Zone, before being interpreted in section 4.3 using both the advanced detrital thermochronological methodology (point 2) and the heavy mineral analyses (section 4.1).

### 4.2.1. Provenance role for detrital thermochronological ages

#### 4.2.1.1. Definitions:

##### a) Temperature and time of closure (see also section 3.1):

The age ( $t_c$ ) yielded by any radiogenic decay sequence is a function of several variables including the phase composition and the temperature (T)-time (t) path that the sample experienced. The closure temperature is a function of the cooling rate.

The kinetics of the daughter isotopes for uranium fission in apatite is well constrained but in other systems, such as zircon, not so. Several authors have made assessments of the range of temperatures covered by the partial annealing zone for fission in zircon and even though they disagree on the width of the band, there is broad agreement that the midpoint lies somewhere between 310 and 230°C (Tagami et al., 1998). Using the concept of isotopic closure of Dodson (1973), we assume in this study that the FT ages of detrital zircon populations correspond to the time since they were

last at a temperature of  $270 \pm 40^\circ\text{C}$  (e.g. Tagami et al., 1998), and at  $90 \pm 30^\circ\text{C}$  for apatite (Green et al., 1989).

b) Detrital age populations:

Detrital ages from a sedimentary rock are usually composed of several groups rather than a single population. The  $P(\chi^2)$  value is used to distinguish the possible presence of multi-components. When the distribution of detrital cooling ages from a particular sedimentary rock yields a  $P(\chi^2)$  value of less than 5% (Galbraith, 1981), it is assumed that more than one age population is present. Subsequently, detrital age populations are extracted when necessary from individual grain age datasets using statistical techniques (Galbraith and Green, 1990; Sambridge and Compston, 1994; Brandon, 1992 and 1996).

The populations are classified in increasing ages from  $P_1$ ,  $P_2$ , ... to  $P_n$ , where  $P_1$  is the youngest population and  $P_n$  the oldest (Fig. 4.3; Garver et al., 1999; Bernet et al., 2001).

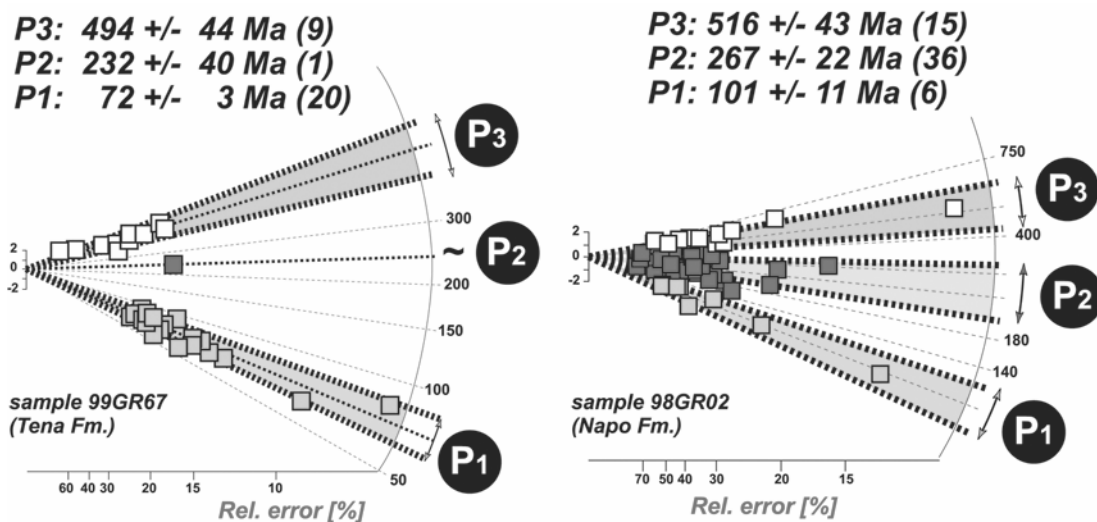


Figure 4.3: Detrital age populations on a radial plot representation (Galbraith, 1990). Both radial plots represent zircon fission-track ages from two sedimentary horizons from the northern Ecuadorian Sub-Andean Zone, i.e. sample 98GR02 (Napo Fm.) to the right and 99GR67 (Tena Fm.) to the left. The different age populations, labelled as  $P_1$ ,  $P_2$  and  $P_3$  were extracted from the raw dataset using statistical techniques (Galbraith and Green, 1990; Sambridge and Compston, 1994; Brandon, 1992 and 1996). Numbers in parentheses indicate the number of grains that are attributed to each population. Ages are presented with a  $1\sigma$  error.

## c) Lagtime:

Sedimentation is the end product of an exhumation process whereby source rocks were brought to the surface, eroded, and transported to a site of deposition. Detrital thermochronology permits investigations of sedimentary horizons to be extended further back in time than the age of the sedimentary sequence, i.e. when the source rocks cooled through a given isotherm ( $T_c$ ). From these ideas was developed the concept of lagtime ( $L_g$ ), which was first used by Zeitler et al. (1986) and Cervený et al. (1988). The lagtime ( $L_g$ ) of a particular detrital population is defined as the difference between the time of closure in the source region ( $t_c$ ) and the time of deposition in the basin ( $t_d$ ):

$$L_g = t_c - t_d \text{ in My} \quad (\text{Zeitler et al., 1986; Cervený et al., 1988}) \quad (1)$$

As a rock cools during exhumation (England and Molnar, 1990), the lagtime thus corresponds to the time taken for the source rock to reach the surface after cooling through the closure temperature of the mineral phase and subsequently transported to its site of deposition. Assuming that the time span between erosion, transport and sedimentation is negligible ( $t_e - t_d \sim 0$  My; Fig. 4.4), then the measured lagtime corresponds to the time taken to cool a grain, from the closure temperature ( $T_c$ ) to the surface temperature ( $T_s$ ; Zeitler et al., 1986; Cervený et al., 1988; Burbank and Anderson, 2001; Fig. 4.4).

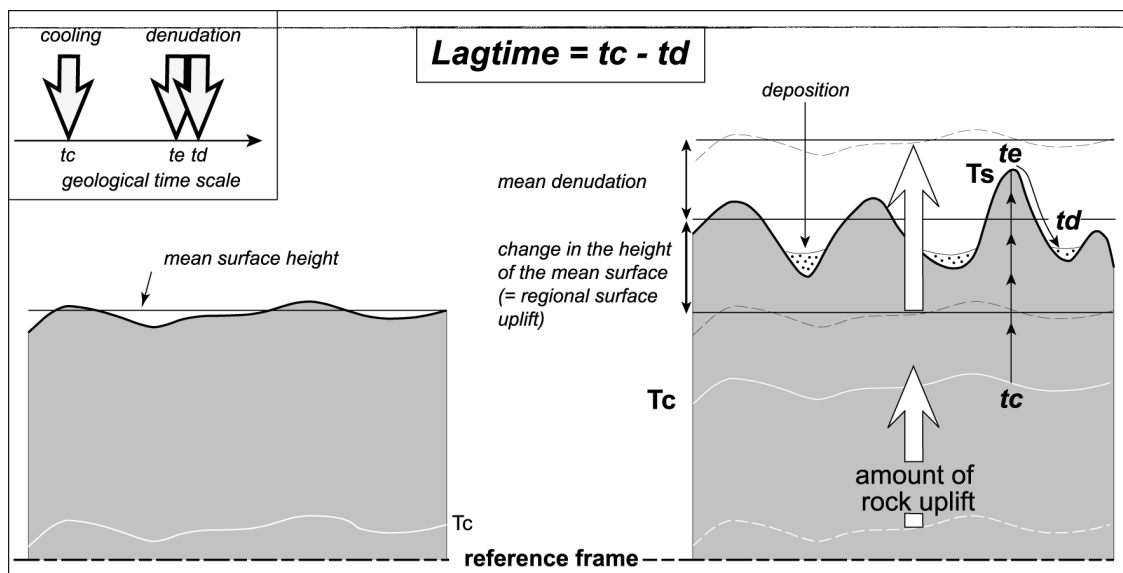


Figure 4.4: The notion of lagtime as introduced by Zeitler et al. (1986) includes the time taken for a mineral to cool through the specific closure temperature ( $T_c$ ), brought to the surface, where the temperature is  $T_s$ .  $t_c$ ,  $t_e$ ,  $t_d$ : times of closure, erosion and deposition (modified after Burbank and Anderson, 2001).

Moreover, between the time of cooling ( $t_c$ ) in source regions and time of deposition ( $t_d$ ) in the basin, source region(s) possibly underwent a polyphased thermal history that cannot be investigated if source rocks remained at temperatures higher than the closure temperature ( $T < T_c$ ). This is not true for thermochronometers permitting T-t modelling, e.g. fission-track analysis on apatites (see section 3.1) as Temperature-time modelling is possible for temperature comprised from 60 to 120°C defining the partial annealing zone, and  $^{40}\text{Ar}/^{39}\text{Ar}$  on K-feldspar.

First, cooling occurs at  $t_c$  in the source region at the temperature for closure of the applied thermochronometer ( $T_c$ ) and defines the onset of exhumation (Fig. 4.4). Later, these rocks were exposed to the surface at time  $t_e$  (Fig. 4.4) and eroded into the basin fill series by time  $t_d$  (Fig. 4.4). Both  $t_e$  and  $t_d$  characterized the second or at least ultimate phase of exhumation in source region (Fig. 4.4). The lagtime, i.e. the time difference between  $t_c$  and  $t_d$ , may be the result of a simple or multiple pulses hidden within the  $[T_c - T_s]$  temperature range. The shorter the lagtime, the more likely single pulsed was the exhumation (Fig. 4.4). This is also probably the case when dealing with thermochronometers with lower temperature of closure ( $T_c$ ), e.g. U-Th/he on apatite where  $T_c \sim 70^\circ\text{C}$  (Reiners, 2002).

Long lagtimes either suggest that the source regions underwent (1) a very slow exhumation since it passed through  $T_c$ , or (2) that exhumational history was polyphased below the temperature of closure of the applied thermochronometer. Hence, such lagtimes cannot be used to calculate any syn-orogenic exhumation rate in a source region. Application of thermal modelling of AFT data is one way to overcome this problem as well as the newly defined methodology (section 4.2.1.3.).

A combination of various lagtimes ( $Lg_1, Lg_2, Lg_3 \dots Lg_n$ ) is possible using different thermo-chronometers from within the same sedimentary layer, e.g.  $^{40}\text{Ar}/^{39}\text{Ar}$  on muscovite and fission-track analysis on zircons. However, the combination of all should be interpreted with care, as it is almost impossible to definitely state that one detrital mineral population is derived from the same source as another mineral population.

#### d) From 'cooling' to exhumation:

Cooling for a given particle in a reference frame is accommodated either by movement of lower temperature isotherms towards the particle (*conduction*) or by movement of this particle through lower temperature isotherms (*advection*). These 2 processes are respectively interpreted in geology as cooling following metamorphism or magmatism, and as movement of rock masses towards cooler zones (Burbank and Anderson, 2001). Rock uplift and associated denudation are the two driving forces for rock mass movements towards lower temperature isotherms closer to the surface. Cooling within a source region is thus a function of the linked rock uplift and denudation processes (Fig. 4.4), and hence the accurate record looking towards exhumation processes.

## e) Exhumation rate:

If assuming negligible transport time from source region to the basin and considering the above assumptions carefully, then the lagtime can be interpreted as an exhumation rate in the hinterland after a further series of assumptions concerning the depth of closure.

Garver et al. (1999) for example investigated depths of closure ( $Z_c$ ) for both zircon and apatite fission-tracks taking into direct consideration that they vary with the duration of the thermal event. Dividing then the depth of closure ( $Z_c$ ) by the time needed for the exhuming rock to reach the surface (i.e. the lagtime  $L_g$ ), still considering a negligible transport time, brings an estimation of the mean exhumation rate within the investigated source region for the considered period ( $[t_c; t_d]$ ) (Fig. 4.5):

$$Exh = \frac{Z_c}{L_g} \quad \text{in mm / y} \quad (2)$$

Thus by dating detrital grains from a sedimentary unit, and assuming negligible time of transport, which is most certainly true in orogenic belts, the exhumation within the source region can be assessed if this occurred rapidly.

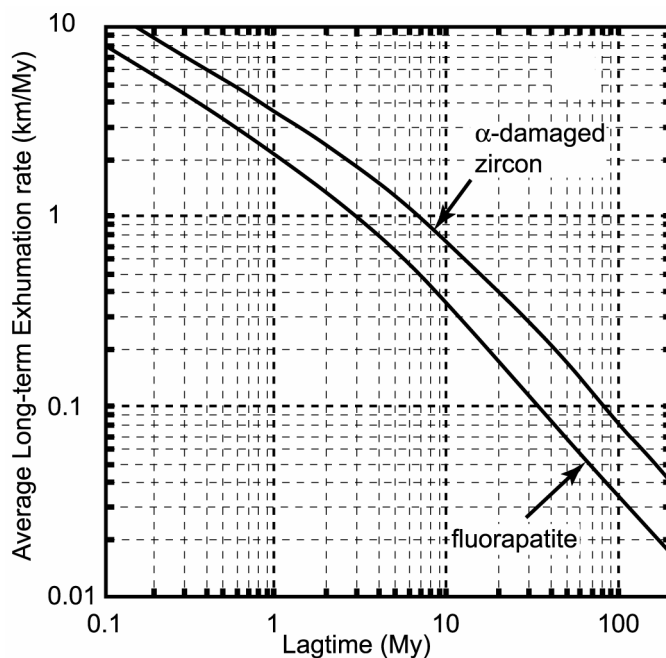


Figure 4.5: The lagtime shown as a function of exhumation rates (and reverse) using fission-track methodology (apatite and zircon; Garver et al., 1999).

#### 4.2.1.2. Assumptions:

Several assumptions are essential in this type of study, these are:

a)  $L_g > 0$ : the lagtime must be positive. If the lagtime is negative, then the dated sediment has experienced temperatures higher than the mineral closure temperature since deposition. Hence, information relative to the exhumation of the source region has been obliterated and can no longer be constrained.

However in special cases, lagtime can possibly remain positive when resetting was not complete. Therefore, an additional thermochronological analysis with a lower temperature of closure is strongly recommended, at least within the basement of the studied basin.

b) The time taken for transport is negligible. This is generally an accepted assumption where orogenic belts and associated basins are concerned (small  $L_g$  values); this is not the case for mature river system transport (high  $L_g$  values), e.g. erosion of the Andean material transported via the Amazon River and shed into the Atlantic Ocean.

c) In an exhuming source region, ages decrease with depth because those rocks higher in the sequence were the first to pass through the temperature of closure ( $T_c$ ), those lower down followed later. Hence, eroding a single tectonic unit or source region, which underwent a common geothermal history, one should expect to see a younging upwards in the detrital grain age populations deposited in the adjacent basins (Fig. 4.6; Garver et al., 1999).

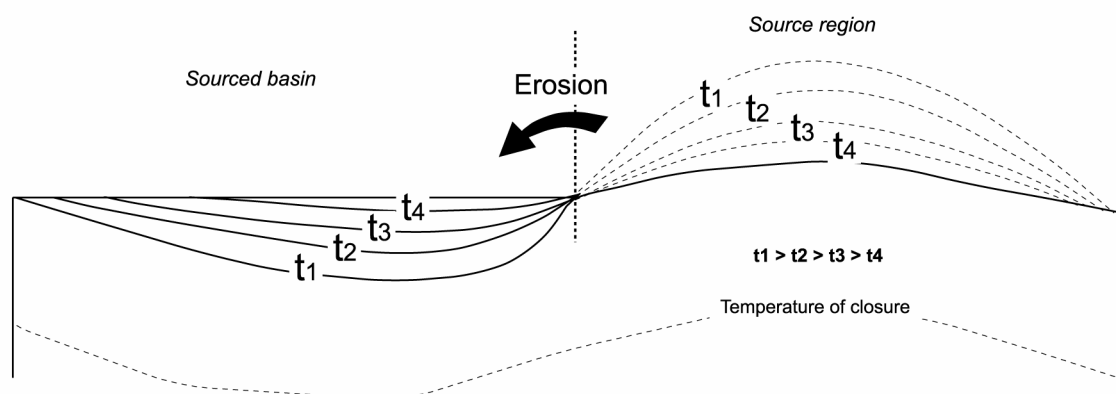


Figure 4.6: Conceptual diagram showing the development of an exhumational sequence through time. In this simple case, a source is progressively unroofed and the sedimentary detritus is deposited in an adjacent basin (modified from Garver et al., 1999). Time slices ( $t_1$ - $t_4$ ) correspond to four progressive and continuous intervals of erosion and deposition in the basin.

d) Cooling rates are not expected to be constant over geological time, but rather verify the relation:

$$\int_t^{t+Lg} V_i(t) \times dt = Tc - Ts = \bar{V} \times Lg \quad (3)$$

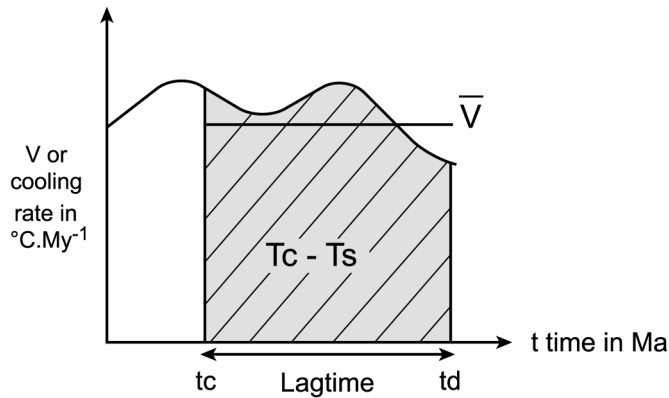


Figure 4.7: relationship between the lagtime (Lg), the cooling rate (V), and the closure and surface temperatures (Tc, Ts). The x-axis is the geological time scale (tc and td are respectively times of closure and deposition) whereas the y-axis represents the cooling rate.

where the amount of cooling during a period of time equal to the lagtime (Lg) is equal to the difference between closure (Tc) and surface (Ts) temperatures ((3) and Fig. 4.7). For convenience, a mean cooling rate (Fig. 4.7) is preferably used for a given Lg value. This is clearly theory but one should not forget the possibilities of variation particularly in the case of longer lagtimes (see c).

e) Possible contemporaneous volcanic contamination generating zero lagtime must be identified using lithologic and/or heavy mineral analysis because it would otherwise misleadingly imply very high cooling rates in the source region.



#### 4.2.1.3. Empirical derivation (new methodology):

##### a) Detrital age populations:

Because of possible variable exhumation histories within source regions, detrital grain age populations, i.e.  $P_1$ ,  $P_2$ , ...  $P_n$  are plotted against the stratigraphic age of the hosting sediments (Fig. 4.8A; Carter, 1999; Garver et al., 1999) to investigate information yielded by the lagtime from any particular detrital age population.

##### b) Detrital $D_n$ curves:

The various detrital grain age populations from all horizons are joined together per rank (Fig. 4.8B), e.g. all  $P_1$  populations are linked together, generating as a result the detrital  $D_1$  and  $D_2$ ... to  $D_n$  curves while the 1/1 line is the graphical representation of detrital grain age populations equal to the stratigraphic age ( $t_c = t_d$ ; Fig. 4.8B). It should not be forgotten that the populations are not linked per rank because they are genetically related, but rather the reverse, i.e. they are linked together per rank to investigate (1) the exhumation history of the source region(s), and (2) whether they can be genetically related or not (see section c).

The area to the right of the 1/1 correlation line (Fig. 4.8) corresponds to the resetting zone ( $L_g = t_c - t_d < 0$ ), i.e. a zone where the detrital grains have been heated after sedimentation to temperatures greater or in the range of the temperature of closure ( $T_c$ ). This might, in rare cases, point to an inaccurate stratigraphic age determination.

The youngest detrital curve  $D_1$  is the easiest to interpret, as it represents the shortest lagtime and consequently the most probable rapid cooling histories in the source regions. Hence, it is very relevant to the exhumation history of the immediate hinterland. Interpretation of the other detrital curves ( $D_2$ ,  $D_3$ ...  $D_n$ ) may require more thoughtful investigation. Further, in fission-track analysis there is a limit above which ages cannot be produced. This limit is a function of both the uranium concentration and the age of the grain. Hence, in general one can say that populations older than 500 Ma are unusual in FT analysis on zircons. This in turn leads thus to the possibility of missing an older group.

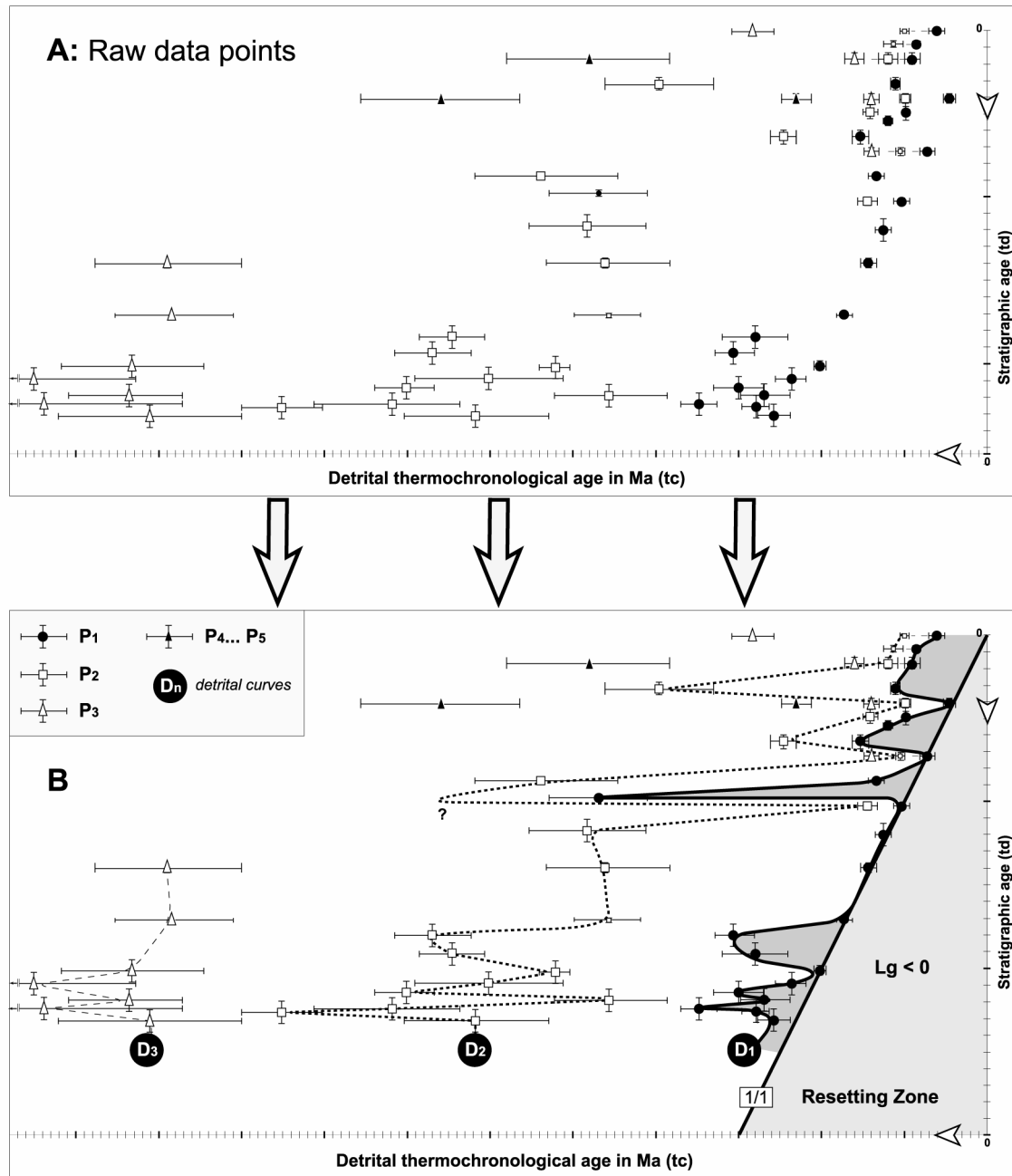


Figure 4.8: Detrital thermochronological age populations versus the stratigraphic column. The y-axis represents the stratigraphic age (td) of the hosting sediment and the x-axis is the thermochronological age of the detrital population (tc). (A) Raw data; (B) within this example, some sediments yielded up to 5 populations but because all did not, only three detrital curves  $D_1$ ,  $D_2$  and  $D_3$  linking the respective  $P_1$ ,  $P_2$  and  $P_3$  detrital age populations are drawn where possible. The area (in light grey) to the right of the 1/1 correlation line ( $tc=td$ ) corresponds to the resetting zone ( $Lg = tc - td < 0$ ), i.e. a zone where grains, in this case zircons, have been heated after sedimentation to temperatures greater or in the range of the temperature of closure ( $T_c$ ). The area between the 1/1 correlation line and the  $D_1$  curve (in dark grey) represents the evolution of the lagtime using all  $P_1$  populations (see section 4.2.1.1).

## c) Paths:

Because detrital fission-track ages vary upward within the stratigraphic column with conspicuous patterns (Fig. 4.8, B), and because detrital ages cannot merely be restricted to the determination of single temporal exhumation rates in the source region using individual lagtime values (see 4.2.1.1), the theory and thus the interpretation of such patterns along the  $D_n$  curves has been investigated. What is the significance of inflexion points along the different  $D_n$  curves, and especially along the  $D_1$ ? What are the possible patterns produced by an evolving exhuming landscape in the source region? Could these yield tectonic events associated with variable exhumation?

Any extensive detrital curve  $D_n$  (see section b) is composed of successive paths, or segments that can be individually investigated (Fig. 4.8). Five characteristic  $D_n$  paths are therefore described on the basis of variations in the two variables (1) the lagtime (Lg), and (2) the time of closure or mineral age (tc) (Fig. 4.9).

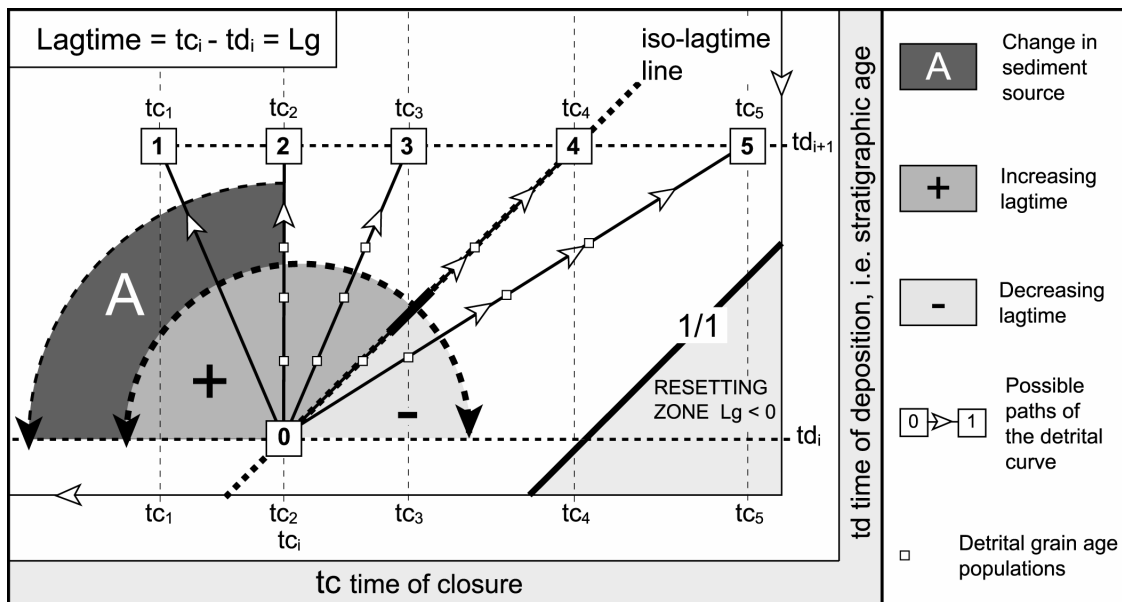


Figure 4.9: Possible paths upward in the stratigraphic column along a detrital curve  $D_n$ . Five paths are defined on the basis of variations in lagtime (Lg) and time of closure (tc). 0 [ $tc_i$ ;  $td_i$ ] is the starting point of all the paths that have the same incrementation within the stratigraphic column ( $td_{i+1}$ ) to facilitate comparison. The y-axis represents the stratigraphic age (td) of the hosting sediment whereas the x-axis is the thermochronological age of the detrital population (tc). Note the directions of both axes, particularly the y-axis which corresponds to a younging upward direction in the stratigraphic column.

## - Inflexion points

Inflexion points along a  $D_n$  curve (Figure 4.8B) may indicate some change in the exhumation of the source region. As explained below the inflexion point itself alone, does not record the event. It is only an indication that a change occurred. However, is

the timing of this possible change constrained by the x-axis (the thermochronological age,  $t_c$ ; Fig. 4.8) or the y-axis (stratigraphic age of the hosting sediment,  $t_d$ ; Fig. 4.8)?

The onset of a thermal phase affecting the source region and recorded in the dated basin fill series, started somewhere between the two first populations along this path ( $t_{c_i} > t > t_{c_{i+n}}$ ; Fig 4.9). Its end is by definition pre-dated by the time of deposition of the last detrital population along the path. However, this record is also dependent on the surface processes acting in the source region, shedding detritus into the basin at time  $t_d$ . To emphasise, it is very difficult to decipher which axis and thus which process (last cooling? Last denudational phase?), is specifically investigated through detrital thermochronology (see section 4.2.1.1). Therefore, each situation, or path must be considered individually.

### - Regression line

The possible different paths upward with time on the  $D_n$  curves are best considered in their simplest forms as segmented lines:

$$t_c = f(t_d) \text{ with } t_c = a \times t_d + b \quad (\text{Bernet et al., 2001}) \quad (4)$$

$$\text{since } Lg = t_c - t_d \quad (1) \Leftrightarrow Lg = (a - 1) \times t_d + b$$

When studying long segments with many data points, and considering uncertainties on both stratigraphic ages ( $t_d$ ) and detrital grain age populations ( $t_c$ ), a regression line specifies the appropriate ( $a$ ,  $b$ ) values (Bernet et al., 2001).

### - Increasing lagtime

i) **Type 1**, the path [0-1] is characterized by increasing lagtime and time of closure [ $a < 0$ ;  $b$ ], (Fig. 4.9).

As mentioned above in the assumptions, the exhumation of a single and homogeneous source region would under normal conditions, produce younger detrital grain ages over time into the basin. However, a type 1 path is the opposite to such, i.e. there is a detrital age increase upwards in the stratigraphic sequence (Fig. 4.9). Source rocks with a different thermal history must be invoked. This requires a change in source that can be on a regional scale, with rivers sourcing new regions due to larger scale tectonics, or local, such as erosion of stratigraphic “unreset” sedimentary series.

Examples of possible scenarios are illustrated in Fig. 4.10. A major change in source region to one of new active tectonic activity would yield old ages in the first instance assuming that the new source was an older stable block before reactivation (Fig. 4.10a). From a renewed block that had been stable over for example 100 My the

initial detrital ages coming from this unit are old and it will be some time before a “new” set of ages with syn-orogenic signatures are exposed at the surface. Depending on the distribution of the cooling ages within this block, and the rate of erosion, the type 1 path can vary in length. However, in general this part should be relatively short because the resumption to normal exhumation and transport of younger ages must take place. Such a path can represent a major change in regional tectonics (e.g. in the Miocene sediments of Pakistan, Ruiz and Seward, in prep) or many local events where the source is changed locally by vertical movements along fault systems.

The second example of common occurrences of path 1 would be cannibalisation of zircons from older sedimentary sequences that had not experienced temperatures great enough to anneal the zircons during burial (Fig. 4.10c). This represents simple erosion through a stratigraphic sequence. Furthermore, the cessation of exhumation can also generate type 1 path due to the cannibalisation of the proximal deposits (Fig. 4.10b). Other examples and combinations can be described, such as the erosion of long-term volcanic sequences that had never been buried to depths of closure.

Finally, surface rocks possibly reflect ages with a pre-orogenic thermal history that is possibly seen in the first erosion products by older ages upwards into the stratigraphic column (Fig. 4.10). Once exhumation is sufficient to expose reset thermochronometers, the cooling ages will reflect syn-orogenic (1) temperatures and (2) exhumation rates (Fig. 4.10). Thus, by the onset a major tectonic event that drives rock uplift and denudation within source region, the record of the event is probably seen in the first erosion products by older ages upward within the stratigraphic column (Zeitler et al., 1986), i.e. a type 1 path (Fig. 4.9). This timing of the inferred change of provenance is dated by the change to a negative gradient ( $td_i > t > td_{i+1}$ ) (Fig. 4.9).

ii) **Type 2**, the path [0-2] is characterized by a constant time of closure ( $t_c$ ) and increasing lagtimes [ $a = 0$ ;  $b$ ] (Fig. 4.9).

A constant time of closure upward in the stratigraphic column requires the erosion of a source block with a homogenous “b” million(s) years cooling age (Fig. 4.11). The erosion of sequences with constant time of closure are not numerous but may include (thick) piles of volcanic sequences rapidly extruded over short time periods (Fig. 4.11a); for example the Deccan Plateau basalts would have similar ages throughout.

Alternatively, extremely low denudation within a source region, such as a craton, that has had long-term stability might yield this pattern (Fig. 4.11b).

The lithology of the source region (heavy mineral analysis) and the thickness of the deposited sediments differentiate between these two possibilities (Fig. 4.11).

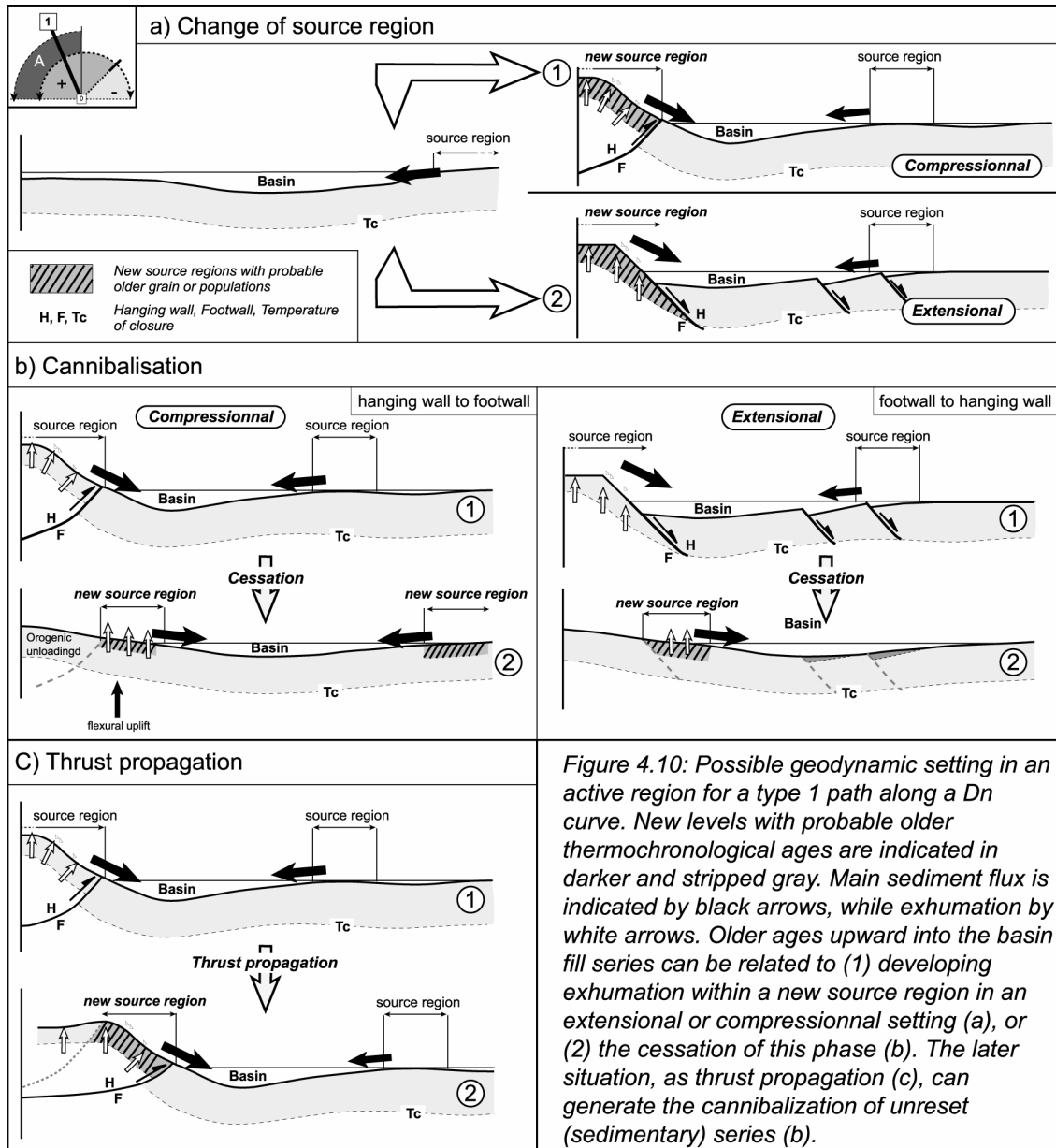


Figure 4.10: Possible geodynamic setting in an active region for a type 1 path along a  $D_n$  curve. New levels with probable older thermochronological ages are indicated in darker and striped gray. Main sediment flux is indicated by black arrows, while exhumation by white arrows. Older ages upward into the basin fill series can be related to (1) developing exhumation within a new source region in an extensional or compressional setting (a), or (2) the cessation of this phase (b). The later situation, as thrust propagation (c), can generate the cannibalization of unreset (sedimentary) series (b).

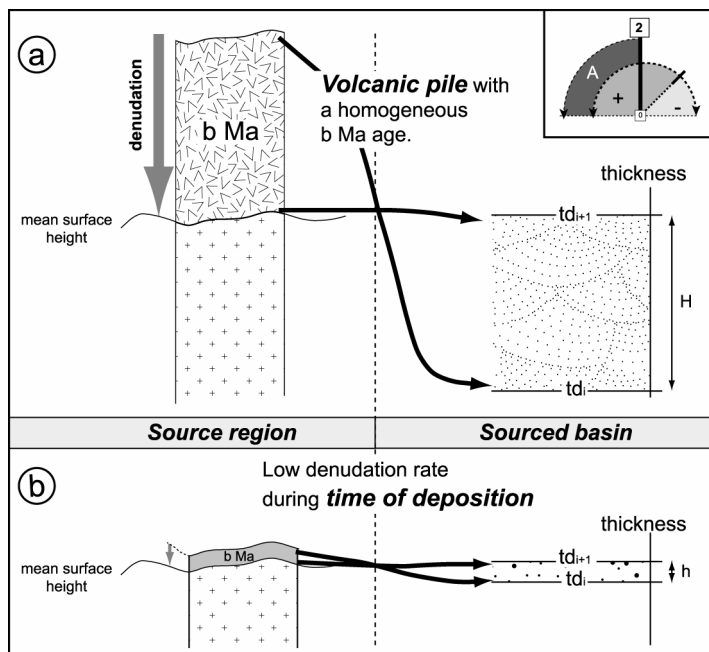


Figure 4.11: Possible source regions of a detrital type 2 path. Two scenarios are presented: (a) the continuous erosion of a volcanic pile with a homogeneous  $b$  Ma age, and (b) low denudation in the source region. Both situations would generate detrital populations with identical cooling ages upward in the basin fill series. However, the thickness of sediments representing this record would be much higher in the first case.

iii) **Type 3**, the path [0-3] is characterized by decreasing times of closure and increasing lagtimes [ $0 < a < 1$ ;  $b$ ] (Fig. 4.9).

The basis of such a path is seen in Fig. 4.6. However, in order that the lagtime increases a type 3 path implies a decrease of the source exhumation rate assuming (1) relatively constant surface and closure temperatures, (2) a constant geothermal gradient, and as a result (3) a constant depth of closure. Such a path may consequently reflect an abatement of the exhumation within the source region during time of deposition of the dated sedimentary series.

#### - Constant lagtime

**Type 4**, the path 0-4 is characterized by constant lagtime and decreasing time of closure ( $tc$ ) [ $a = 1$ ;  $b$ ] (Fig. 4.9).

The observation of a constant lagtime through the stratigraphic record is indicated by an alignment of the detrital grain age populations on an iso-lagtime line ( $Lg=b$ ) parallel to the 1/1 line ( $a=1$ , Fig. 4.9).

A constant lagtime upward in the stratigraphic column literally indicates that invariant and identical time was necessary to bring the appropriate markers to the surface where they were rapidly transported into the basin. It also probably indicates that cooling within the source region(s) was completed with a constant mean rate during a period of time equal to the lagtime for the duration of this record [ $tc_i$ ;  $tc_4$ ], considering  $T_c$  and  $T_s$  constant over time. Consequently, a constant lagtime or type 4

path characterizes a ‘*steady-state of cooling*’ within the source region but, does not necessarily imply that the source region has undergone a ‘*steady state exhumation*’ (Bernet et al., 2001), i.e. the absence of surface uplift during the sedimentary record. Rock uplift constantly balanced by denudational processes (England and Molnar, 1990) defines a ‘*steady state exhumation*’. Such a state of exhumation is believed to characterize mature orogens (Willet and Brandon, 2002), but would probably produce accelerating cooling within source regions, as denudation permits the isotherms to move closer to the surface (Moore and England, 2001). Hence, decreasing lagtimes will be recorded upward in the stratigraphic column of the sourced basin(s) (see type 5 path section).

As discussed in section 4.2.1.1c, long lagtimes are probably the record of more than one exhumational phase; this is further reinforced when they remain constant (section 4.2.1.2d). Thus, a type 4 path characterized by an important  $b$  value, e.g.  $\sim 30$  My (Fig. 4.8) is not yet perfectly understood and can be the result of many processes that cannot be any longer traced. In contrast, a type 4 path with a relatively small  $b$  value, e.g. 8 My (Bernet et al., 2001; Fig. 4.12) probably points to a single phase of exhumation within the source region(s), which was characterized at this time by thermal steady state (Willet and Brandon, 2002).

A specific form of constant lagtime, which is much easier to constrain is that of zero ( $\pm 1\sigma$ ; Fig. 4.8). Such a value is the result of persistent and extremely rapid cooling that can be directly interpreted as rapid exhumation within (a) source region(s).

By definition, the onset of the exhumational phase within the source region(s) that is responsible for this thermochronological record is slightly post-dated by the time of closure of the first population along this type 4 path ( $t_{c_i}$ , Fig. 4.9).

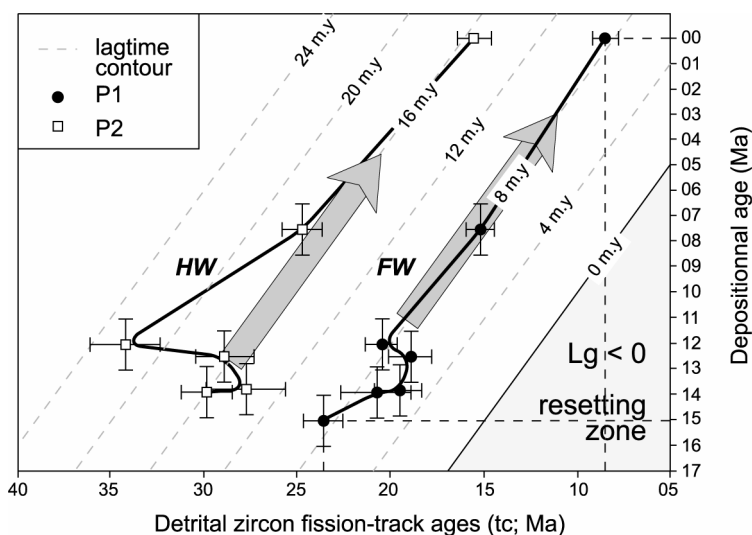


Figure 4.12: Plot showing the evolution with time of the  $P_1$  and  $P_2$  zircon fission-track populations, Ligurid-Apennines Basin (modified from Bernet et al., 2001). Contours show lines of constant lagtime. Error bars show  $\pm 1$  standard error for peak ages and  $\pm 1$  My uncertainty for depositional ages. HW: hanging wall and FW: footwall of the Simplon Fault (?).



- *Decreasing lagtime*

**Type 5**, the path 0-5 is characterized by decreasing lagtimes and times of closure (Figure 4.9) [ $a > 1$ ;  $b$ ].

A decreasing lagtime with time ( $a > 1$ ; Fig. 4.9) implies rapid exhumation in the source region(s) (Fig. 4.5; Garver et al., 1999), which is probably related to syn-orogenic development in the source regions of the studied basin.

However, a sudden increase of the exhumation involves a pre-orogenic thermal history (see type 1 section; Fig. 4.10). Hence, the calculation of exhumation rates using the associated lagtime values from these pre-orogenic ages would misinterpret the 'true' variation in the rate of exhumation. As a result, a type 5 path unambiguously characterizes developing exhumation within source region whose exhumation rate can only be constrained by a maximum value deduced from using the lagtime of the last population along the type 5 path.

Furthermore, a change toward high exhumation rates can eventually generate detrital grains or populations with almost no lagtime value ( $L_g=0$ ) using thermochronometers with low temperature of closure (e.g. zircon fission-track analysis, Fig. 4.8). Those with higher closure temperatures, e.g.  $^{40}\text{Ar}/^{39}\text{Ar}$  on hornblende (PRZ=463-544°C, Lister and Baldwin, 1996), may never allow the record of a zero lagtime as the rate of exhumation in the hinterland would be totally unrealistic even if it is associated with a noticeable increase of the geothermal gradient. If such a record is present within the basin fill series, a contemporaneous volcanic contamination should be then suspected. Najman et al. (2001) for example, provided a perfect example of such a misunderstanding from the oldest Himalayan Foredeep sediments with a supposed Early Eocene age (~55 Ma). Applying  $^{40}\text{Ar}/^{39}\text{Ar}$  methodology on detrital white micas, the authors obtained  $P_1$  populations with a range of 36-40 Ma. They thus concluded that these sediments were at least ~20 My younger than that previously estimated and most probably contemporaneous of rapid exhumation in the Himalayan Chain.

d) Common trends:

Noticeably, the commonality of the trends of the  $D_n$  curves is sometimes quite remarkable (Fig. 4.8). First, each  $D_n$  curve should be considered individually from the  $D_1$  to the  $D_n$ , before being compared with the other curves for the same time span. However, the commonality of trends may have important regional implications.

When  $n$  parallel (to sub parallel) detrital curves are observed (Fig. 4.13), this may imply that  $n$  different source areas had experienced common exhumation histories on the assumption that an identical regional geothermal gradient prevailed throughout (Fig. 4.13-A). If denudation of these different source blocks/terrane is such that it leads to

levels that passed through the temperature of closure at the same time, the  $D_n$  curves should merge into one where the thermochronological age ( $t_c$ ) indicates the time of onset of this common exhumational phase ( $t=20$  Ma in Fig. 4.13). The shapes of the  $D_n$  curves before they merge are related to a pre-orogenic exhumation thermal history (Fig. 4.13B).

If different detrital thermochronological curves merge along the 1/1 line in the resetting zone (Fig. 4.13C), this implies, as discussed above, that the onset of the common exhumational phase started by  $t_c$ . However, such a scenario is impossible (still considering unreset sediments) because it would imply that the onset of this common exhumational phase is younger than the stratigraphic ages of the sediments from which the record was obtained (Fig. 4.13C). Therefore, the special case of the merging of detrital curves along, or to the right of the 1/1 line, can only indicate that different source regions underwent strong phases of exhumation, since probably  $t_d$ , which possibly culminated by the time indicated by the merging point ( $t_c$ ) (Fig. 4.13C).

- Parallel to sub-parallel  $D_n$  curves with constant lagtimes upwards have already been observed, e.g. the Ligurid-Appennines basin, Italy (Fig. 4.12; Bernet et al., 2001) where the associated detrital zircon fission-track dataset is composed of two age populations, i.e.  $P_1$  and  $P_2$  that the authors respectively say exhibit relatively constant lagtimes of 8 and 15 My for the Middle Miocene to Recent deposits (15-0 Ma; Fig. 4.12). However, when did this "thermal steady state" start? As already mentioned in section 4.2.1.3C, a minimum age for this is indicated by the first detrital population along this path ( $t_c$ ), i.e. 23 Ma for the source region of the Ligurid-Appennines basin for this example (Fig. 4.12). The authors suggested that the two source regions for these two populations are possibly the hanging wall and footwall (Fig. 4.12) of the active normal Simplon Fault located in the Central Alps, whereas the offset of the detrital age populations (~7 Ma) is related to differential exhumation between both sides of the fault.

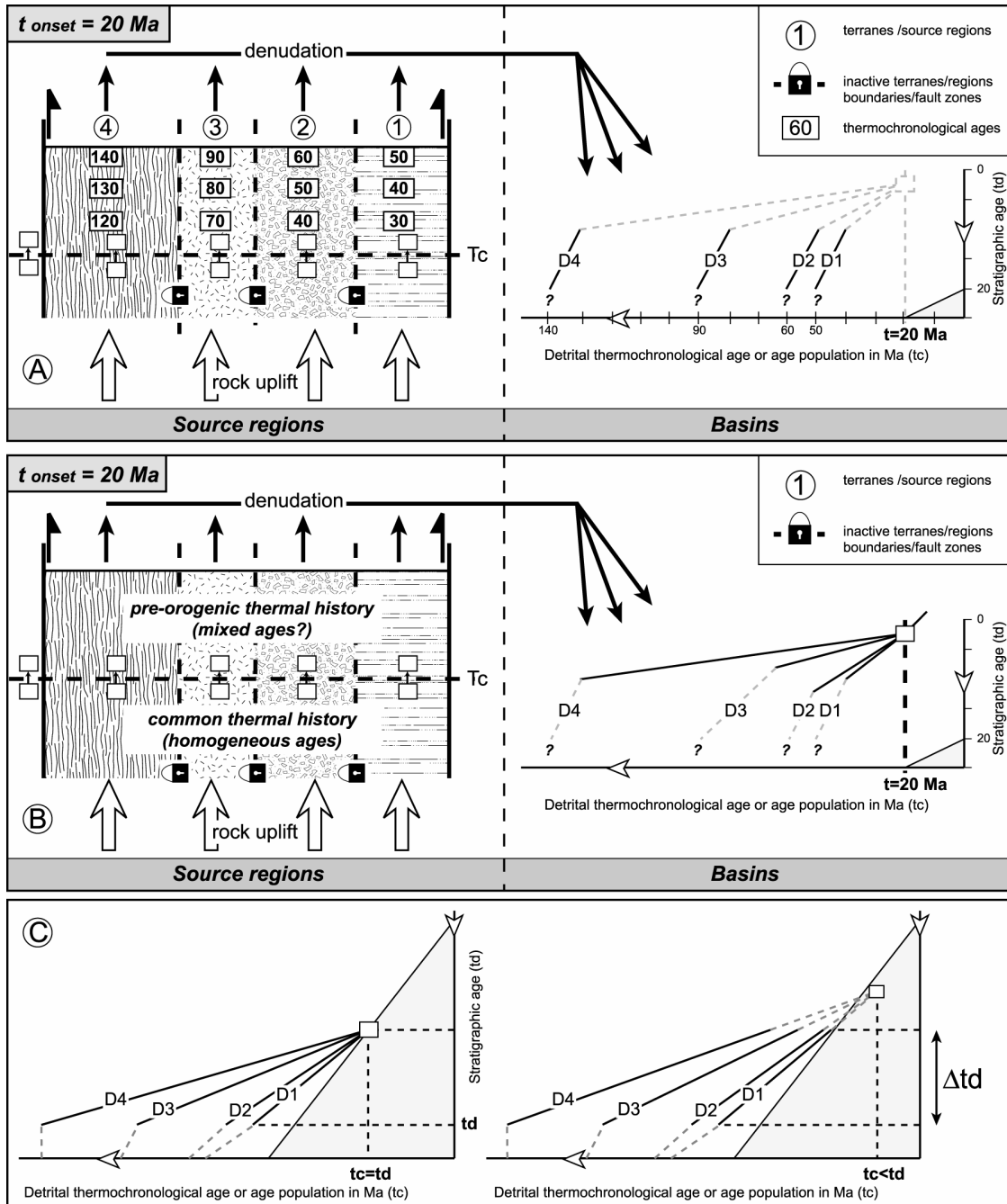


Figure 4.13: Common trends for the  $D_n$  curves. (a) Parallel to sub-parallel  $n$  detrital curves in the basin(s) are probably derived from  $n$  commonly exhuming source regions that previously underwent different cooling history with an identical regional geothermal gradient. (b) Heterogeneous pre-common exhumation thermal history. If an identical geothermal gradient is not envisaged, or if denudation exposed levels with mixed thermochronological ages, the detrital curves cannot be parallel. However, in both settings the  $D_n$  curves will further merge into a point that characterizes the common geothermal history of these different source regions if denudation permits the sourcing from levels that exhibit identical cooling ages. The associated  $t_c$  value along the x-axis proposes the time of onset (here 20 Ma) of this joined phase of exhumation. If this merging point is along the 1/1 line (c), or within the resetting zone ( $t_c < t_d$ ), it cannot indicate the onset of a common exhumational phase but rather characterizes common and important exhumation within source regions.

Another exhumational setting can also be envisaged, as mentioned above: the identical and common exhumation of two blocks that previously underwent different cooling history, e.g. Fig. 4.13A. If exhumation continued until the basin was sourced by levels that exhibit a common thermal history (Fig. 4.13A), the detrital curves derived from this previously heterogeneous source should merge into one (Fig. 4.13A & B). However, a simple calculation using the lagtime of the youngest population suggests an exhumation rate of  $\sim 0.85$  km/My (Fig. 4.5). Multiplying this value by the minimum duration of the associated exhumational phase, i.e.  $\sim 15$  My (Bernet et al., 2001), suggests that  $\sim 13$  kilometers of rocks have been denuded to generate such a record. The depth of closure of zircon fission-track is, as for any thermochronometer dependent of the geothermal gradient, but can be broadly approximated at  $\sim 8$ - $10$  km. Therefore, the denuded pile in the source region of the Ligurid-Appennines basin exceeds the depth of closure of zircon. Thus, a common exhumational phase of the different source region is rejected because sourcing from levels yielding homogeneous ages should have already occurred.

It is clearly very difficult to envisage source areas of dated sediments when these source regions have disappeared. If the thermochronology of potential source regions is known, extrapolations can be made (e.g. Wagner et al., 1979). With the addition of heavy mineral analysis of the sediments, reconstructions to the source are more reliable. For example increasing volumes of metamorphic minerals of increasing grade can be extrapolated back to even higher metamorphic zones that should be exposed today, if preserved. However, if it is established that this possible source region have undergone important and polyphased exhumation during time of deposition of the dated sediments, it most likely would have generated a mixture of type 1 and type 5 paths, which would be far from two parallel  $D_n$  curves with constant lagtimes upwards as for the example of the Ligurid-Appennines basin (Fig. 4.12). There are many variables and each region has its own problems that must be solved in an individual and specific basis.

### 4.2.2. Results

Up to 50 sediments from the entire stratigraphic sequence across the northern Ecuadorian SAZ, were separated following the procedure described in section 3.2. Lithologies vary from conglomerates to sandstones, quartz-arenites and a few siltstones. The geographical location of samples used for age determinations are indicated on a simplified geological map of the northern Sub-Andean Zone and Pastaza depression (Fig. 4.14).

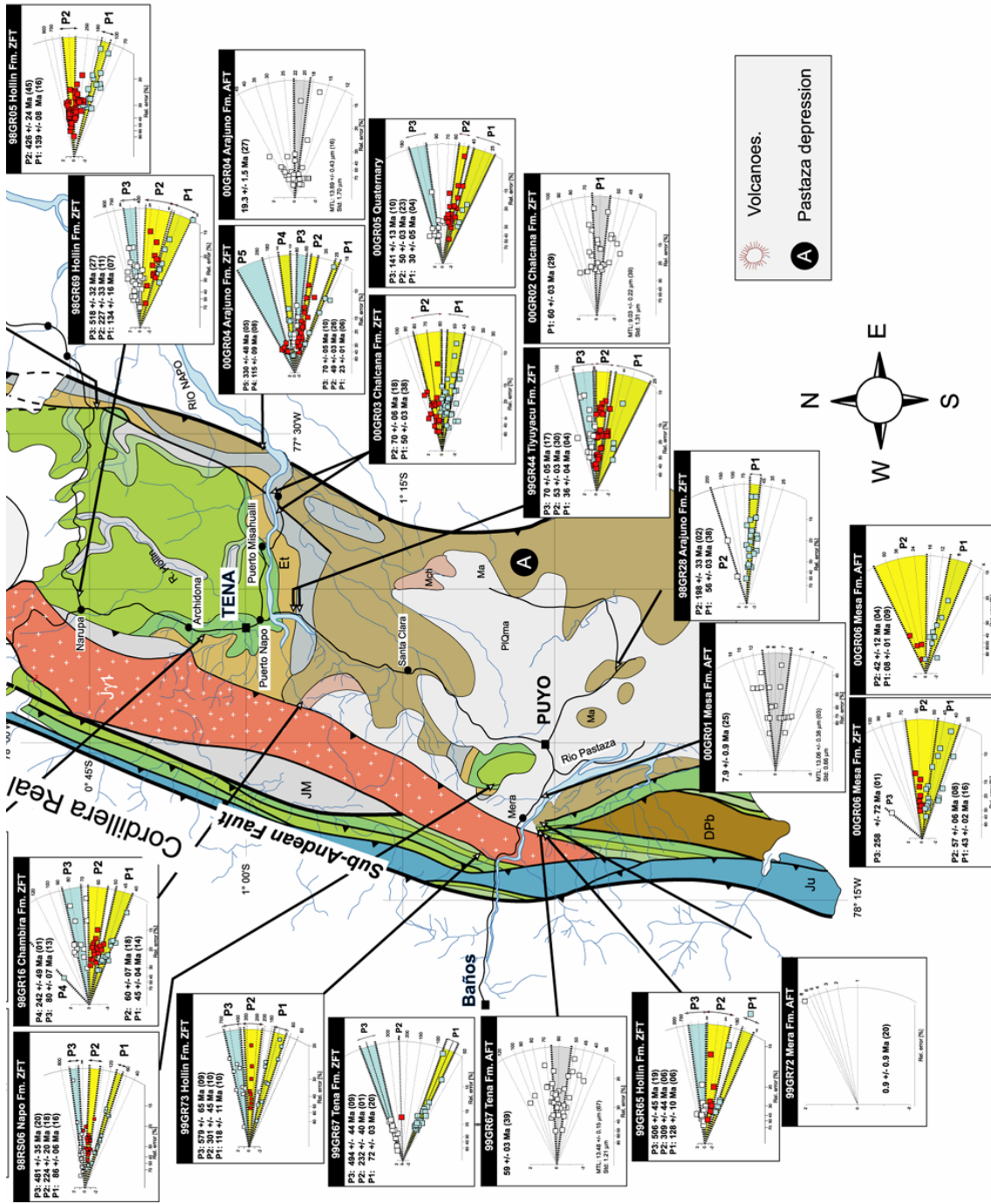
Unfortunately not all samples yielded apatites and/or zircons. Single crystals of zircon were finally extracted, mounted, counted and dated from approximately 30 samples, whereas only six samples yielded apatite (Fig. 4.14). This is not uncommon in sediments as zircon is a much more frequent mineral because of its greater resistance to abrasion and solution. Because of the possibility of different ages and the known fact that etching time of zircons is proportional to the age, up to eight zircon mounts were sometimes made for each sampling site and etched for different times. Fifty grains were dated per sample when it was possible, to obtain realistic and reliable detrital zircon fission-track age populations.

Many rounded, metamict and zoned zircons, mainly from the oldest sedimentary formations (Hollin and Napo formations) were undatable because they were (1) too old (track density too high to count), and (2) metamict.

Noticeably, only one sample exhibits a conspicuously younger apatite fission-track age than its assumed stratigraphic age, i.e. sample 99GR67 from the Tena Fm. (Maastrichtian, ~70 Ma; Fig. 4.14 and Table 4.1). It reinforces then the detrital character of the ZFT and probably AFT ages from the sedimentary formations of the Northern Ecuadorian SAZ, as already proven in the thermochronological study of the basement (see section 3.4).

Figure 4.14: Apatite and zircon fission-track ages from the sedimentary series of the northern Ecuadorian Sub-Andean Zone and Pastaza depression. Simplified geological map of the area (after Litherland et al., 1993). AFT: apatite fission-track ages; ZFT: zircon fission-track ages





1082 detrital grains of apatite and zircon were dated from ~30 samples, all with mean sample ages that had a  $P(\chi^2)$  value (Green, 1981) lower than 5%, thus indicating the presence of multiple populations (Table 4.1).

70 different detrital grain age populations were extracted from single grain ages (Fig. 4.15) using statistical techniques, i.e. BinomFit v.1.8 software (Brandon, 1992 and 1996), and labelled as  $P_1, P_2 \dots$  to  $P_n$  in increasing ages (Table 4.1 and Figure 4.14, see section 4.2.1.1-b). The detailed fission-track radial plots (Gailbraith, 1990) for all dated levels are presented in appendix 4.2.

The DZFT age populations show a significant variation from  $579 \pm 65$  Ma to  $22.9 \pm 1.2$  Ma ( $1\sigma$ ) whereas detrital apatite fission-track (DAFT) age populations lie between  $142 \pm 15$  Ma and  $0.9 \pm 0.9$  Ma ( $1\sigma$ ; Table 4.1).

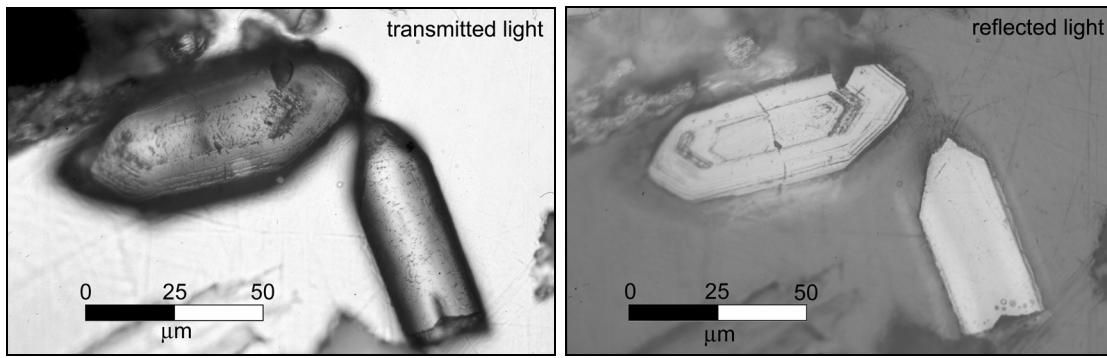


Figure 4.15: Zircon grains in transmitted and reflected light that yielded different fission-track ages (sample 99GR44, Tiyuyacu Fm.). The grains (left and right) are representative of ages of two populations of  $36 \pm 4$  Ma and  $53 \pm 3$  Ma ages, respectively (Table 4.1).



Sample number	Alt. m	N	$P\chi^2$ %	Central age $\pm 1\sigma$	$P_1$ (Ma)	$P_2$ (Ma)	$P_3$ (Ma)	$P_4$ (Ma)	$P_5$ (Ma)	Strat. age Ma	Lg <sub>1</sub> My	MTL1 $\mu\text{m}$ (N)	Std1 $\mu\text{m}$	MTL2 $\mu\text{m}$ (N)	Std2 $\mu\text{m}$
<b>Hollin Fm.</b>															
98GR65	1350	31	0.0	316 $\pm$ 40	128 $\pm$ 10 (6)	309 $\pm$ 44 (6)	506 $\pm$ 45 (19)	-	-	115	3-23	-	-	-	-
98GR05	1150	61	0.0	285 $\pm$ 26	139 $\pm$ 8 (16)	426 $\pm$ 24 (45)	-	-	-	113	18-34	-	-	-	-
98GR50	1400	33	0.0	258 $\pm$ 25	174 $\pm$ 11 (15)	359 $\pm$ 48 (11)	569 $\pm$ 85 (7)	-	-	112	51-62	-	-	-	-
98GR69	1150	45	0.0	298 $\pm$ 29	134 $\pm$ 16 (7)	227 $\pm$ 33 (11)	518 $\pm$ 32 (27)	-	-	110	8-40	-	-	-	-
99GR22	610	50	0.0	284 $\pm$ 22	150 $\pm$ 16 (10)	355 $\pm$ 23 (40)	-	-	-	107	27-59	-	-	-	-
99GR73	1280	29	0.0	227 $\pm$ 30	118 $\pm$ 11 (10)	301 $\pm$ 45 (10)	579 $\pm$ 65 (9)	-	-	105	2-24	-	-	-	-
<b>Napo Fm.</b>															
98GR02	1600	57	0.0	263 $\pm$ 24	101 $\pm$ 11 (6)	267 $\pm$ 22 (36)	516 $\pm$ 43 (15)	-	-	101	0-11	-	-	-	-
98GR57	1800	16	2.1	188 $\pm$ 26	139 $\pm$ 18 (9)	323 $\pm$ 69 (7)	-	-	-	99	22-58	-	-	-	-
98GR41	1100	49	0.4	247 $\pm$ 18	153 $\pm$ 13 (16)	335 $\pm$ 23 (33)	-	-	-	90	50-76	-	-	-	-
98RS06	1240	54	0.0	189 $\pm$ 20	86 $\pm$ 6 (16)	224 $\pm$ 20 (18)	481 $\pm$ 35 (20)	-	-	86	0-6	-	-	-	-
<b>Tena Fm.</b>															
99GR67*	1320	30	0.0	106 $\pm$ 13	72 $\pm$ 3 (20)	232 $\pm$ 40 (1)	494 $\pm$ 44 (9)	-	-	70	0-5	8.45 $\pm$ 0.28 (14)	0.95	-	-
98GR83	600	35	13.7	65 $\pm$ 07	63 $\pm$ 3 (34)	242 $\pm$ 72 (1)	-	-	-	59	1-7	-	-	-	-
99GR67*	1320	39	96.5	58.7 $\pm$ 3.0	58.7 $\pm$ 3.0	-	-	-	-	70	-	13.48 $\pm$ 0.15 (67)	1.21	-	-
98GR37	500	28	4.3	97 $\pm$ 16	78 $\pm$ 6 (19)	142 $\pm$ 15 (9)	-	-	-	68	4-16	9.50 $\pm$ 1.40 (7)	1.70	11.99 $\pm$ 0.49 (8)	1.38

Table 4.1: Apatite and zircon fission-track ages from the Aptian to recent basin fill series of the northern Ecuadorian Sub-Andean Zone and Pastaza depression. For sample localities see Figure 4.14. The different age populations have been separated using statistical techniques (Brandon, 1992 and 1996) and labelled as  $P_1, P_2, \dots$  to  $P_n$  with increasing age. Track length measurements for both apatites and zircons are also indicated when completed with their associated standard deviation (Std). MTL: Mean Track Length. The stratigraphic age of each dated level is indicated (age) as the lagtime associated with the  $P_n$  population ( $Lg_1$ ). Asterisks correspond to samples that yielded both AFT and ZFT ages. Numbers in parentheses indicate the number of counted grains for each population, or measured track lengths. Abbreviations for the formations are: Chambira (Ch), Mesa Fm. (Ms), Mera (Me) and Quaternary (Qt). Alt.: altitude in meters. All zircon and apatite separates were counted by G.M. Ruiz using zeta calibration of 121  $\pm$  3 (zircon analysis, CN1 standard glass) and 359  $\pm$  11 (apatite analysis, CN5 standard glass). Samples were irradiated at the ANSTO Facility Lucas Heights, Australia. ANSTO Facility Lucas Heights, Australia

Sample number	Alt. m	N	P $\chi^2$ %	Central age $\pm 1\sigma$	P <sub>1</sub> (Ma)	P <sub>2</sub> (Ma)	P <sub>3</sub> (Ma)	P <sub>4</sub> (Ma)	P <sub>5</sub> (Ma)	Stra. age Ma	Lg <sub>1</sub> My	MTL1 $\mu$ m (N)	Std1 $\mu$ m
<b>Tiyuyacu Fm.</b>													
99GR36	560	24	0.0	56.8 $\pm$ 6.9	50.7 $\pm$ 5.0 (4)	72.7 $\pm$ 6.0 (8)		-	-	52	0-4	8.57 $\pm$ 0.65 (9)	1.96
99GR52	840	10	57.0	234 $\pm$ 31	234 $\pm$ 31 (10)	-		-	-	50	150-210	-	-
98GR81	600	25	0.0	69 $\pm$ 5	67 $\pm$ 3 (24)	269 $\pm$ 46 (1)		-	-	44	20-26	-	-
99GR44	480	51	0.0	56.2 $\pm$ 5.4	36 $\pm$ 4 (4)	53 $\pm$ 3 (30)	70 $\pm$ 5 (17)	-	-	37	0-3	7.46 $\pm$ 0.19 (63)	1.55
<b>Orteguaza Fm.</b>													
99GR81	400	23	0.0	98 $\pm$ 07	77 $\pm$ 5 (12)	123 $\pm$ 8 (11)	<b>Zircon</b>	-	-	32	41-51	-	-
<b>Chalcana Fm.</b>													
00GR02	571	29	17.0	59.9 $\pm$ 2.6	59.9 $\pm$ 2.6 (29)	-	<b>Zircon</b>	-	-	27	30-36	9.03 $\pm$ 0.22 (39)	1.31
00GR03	374	56	0.3	54.9 $\pm$ 5.0	49.6 $\pm$ 2.6 (38)	70.3 $\pm$ 6.3 (18)		-	-	24	23-28	8.16 $\pm$ 0.20 (65)	1.60
<b>Arajuno Fm.</b>													
00GR04*	364	55	0.0	56.9 $\pm$ 4.9	23 $\pm$ 1 (6)	49 $\pm$ 3 (26)	<b>Zircon</b>	115 $\pm$ 9 (8)	330 $\pm$ 48 (5)	22	0	-	-
98GR28	-	40	0.0	62.5 $\pm$ 3.7	56 $\pm$ 3 (38)	198 $\pm$ 33 (2)		-	-	16	37-43	-	-
00GR04*	364	27	68.8	19.3 $\pm$ 1.5	19.3 $\pm$ 1.5	-	<b>Apatite</b>	-	-	22	0	13.69 $\pm$ 0.43 (16)	1.70
<b>Others</b>													
98GR16 (Ch)	590	46	0.0	60.7 $\pm$ 3.5	45 $\pm$ 4 (14)	60 $\pm$ 7 (18)	<b>Zircon</b>	242 $\pm$ 49 (1)	-	9	32-40	-	-
00GR06* (Ms)	1018	25	0.0	49.3 $\pm$ 6.8	42.7 $\pm$ 2.4 (16)	56.7 $\pm$ 6.0 (8)		-	-	4	36-41	7.58 $\pm$ 0.59 (7)	1.54
00GR05 (qt)	357	37	0.0	59.4 $\pm$ 5.6	30.2 $\pm$ 4.6 (4)	50 $\pm$ 2.6 (23)	141.5 $\pm$ 13.5 (10)	-	-	0	26-35	7.79 $\pm$ 0.23 (33)	1.32
00GR06* (Ms)	1018	13	0.0	16.3 $\pm$ 4.7	8 $\pm$ 1 (9)	42 $\pm$ 12 (4)	<b>Apatite</b>	-	-	4	3-5	-	-
00GR01 (Ms)	1084	25	99.7	7.9 $\pm$ 0.9	7.9 $\pm$ 0.9	-		-	-	3	4-6	13.06 $\pm$ 0.38 (3)	0.66
99GR72 (Me)	1160	20	99.0	0.9 $\pm$ 0.9	0.9 $\pm$ 0.9	-		-	-	1	0-1	-	-

Table 4.1 (continued)

#### 4.2.2.1. Detrital zircon fission-track ages

Most of the dated samples yielded several populations ( $2 < n < 5$ ) with the exception of samples 99GR52 and 00GR02. In the former case this was probably due to the low number of grains suitable for dating (10) (Table 4.1).

The DZFT grain age populations of the complete suite fall into three major groups defining three distinct source domains with probable different exhumation histories:

1) The oldest group (579-224 Ma) is mainly hosted in the shallow marine Aptian-Campanian Hollin and Napo formations where it represents the majority of the dated grains (Table 4.1; Fig. 4.16). It is almost absent, or rarely present in the younger deposits (Fig. 4.16), i.e. nine grains in sample 99GR67 from the Tena Fm. (Table 4.1), ten grains in sample 99GR52 (Tiyuyacu Fm., Table 4.1) and finally by one grain in samples 98GR81 (Tiyuyacu Fm., Table 4.1), and 98GR16 (Chambira Fm., Table 4.1). An important observation is that from 70Ma, an older subgroup (the oldest suite within the older population) clearly dies out (Fig. 4.16).

2) The second group of ages, i.e. 198-118 Ma (Fig. 4.16) is also mostly present within the DZFT age population record of the Hollin and Napo formations where it often represents the  $P_1$  populations (Table 4.1). This cluster of ages disappears during the deposition of the Tena and Tiyuyacu Fms. (Maastrichtian-Eocene, see section 2.1; Fig. 4.16) but is re-encountered in the Orteguzaza Fm., Arajuno Fm., and also in the recent Napo River sand (Fig. 4.16 and Table 4.1).

3) The third and youngest cluster (101-23 Ma; Fig. 4.16) is recorded from the deposition of the Napo Fm. (Albian) to Recent but is more dominant since the time of deposition of the Tena Fm. (Maastrichtian) with the exception of sample 99GR52 from the Tiyuyacu Fm. (Fig. 4.16).

#### 4.2.2.2. Detrital apatite fission-track ages

AFT ages are absent or almost absent, from the Hollin and Napo Fms. respectively. The oldest horizon yielding suitable AFT ages was within the Maastrichtian-Paleocene levels of the Tena Fm. (Table 4.1)

A basal Tena sandstone from the Rio Gringo area, southwest of the village of Mera (99GR67, Fig. 4.14) yielded an AFT age of  $59 \pm 3$  Ma (Table 4.1) that was partially reset, as it is younger than its assumed Maastrichtian stratigraphic age (see section 4.3.1). The detrital signature has been removed (see section 3.3.4). Two detrital apatite fission-track age populations, i.e.  $78 \pm 6$  Ma ( $P_1$ ) and  $142 \pm 15$  Ma ( $P_2$ ) were produced from a siltstone level of the Lower Tena Mb. (98GR37; Table 4.1), indicating the

erosion of two source regions with respectively Campanian and Late Jurassic-Early Cretaceous cooling ages. Some track length measurements were made on apatites that could be attributed to the two populations:  $9.5 \pm 1.4 \mu\text{m}$  (7) from the younger and  $12.0 \pm 0.5 \mu\text{m}$  (8) from the second population (Table 4.1).

A single and significantly younger population ( $P_1$ ), i.e.  $19.3 \pm 1.5 \text{ Ma}$  was produced from an Arajuno level where an almost identical age was obtained for the  $P_1$  zircon population, i.e.  $23 \pm 1 \text{ Ma}$  (00GR04; Table 4.1).

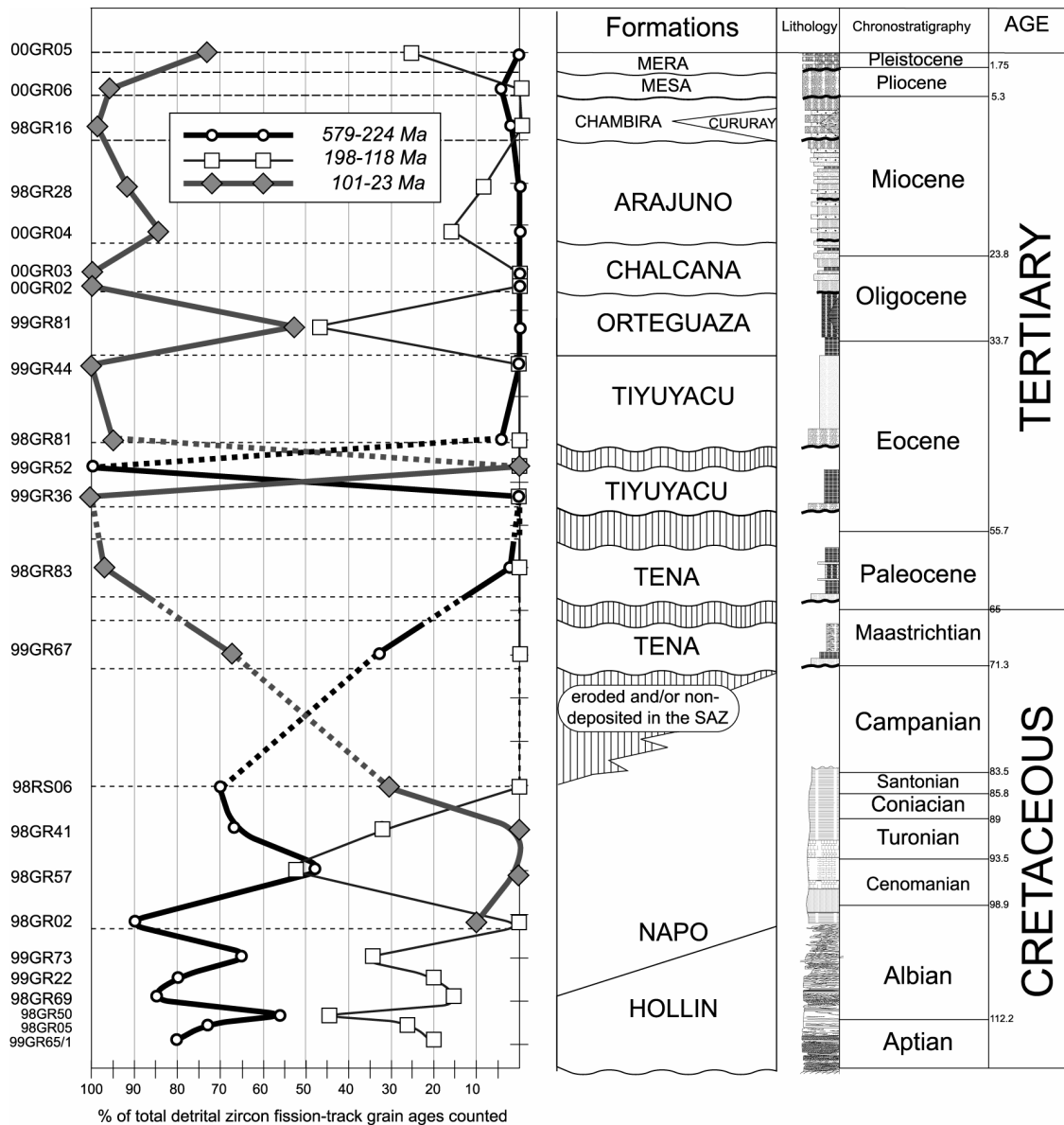


Figure 4.16: Variation of detrital zircon fission-track age populations upwards within the stratigraphic column of the northern Ecuadorian Sub-Andean. Three groups have been recognized and isolated, i.e. 579-224 Ma, 198-118 Ma and 101-23 Ma. The complete dataset is presented in Table 4.1.

Additional detrital apatites were dated from the Mesa and Mera formations encountered in the region of Puyo-Mera, i.e. samples 00GR01, 00GR06 and 99GR72 (Fig. 4.14). They yielded AFT ages range from  $8 \pm 1$  Ma to  $1 \pm 1$  Ma for the  $P_1$  populations while the older ( $P_2$ ) population gave a  $42 \pm 12$  Ma for sample 00GR06 from the Mesa Fm. (Table 4.1).

## 4.3. Interpretation

### 4.3.1. Stratigraphic ages:

Because radiometric dating (e.g.  $^{40}\text{Ar}/^{39}\text{Ar}$  on biotite from an intercalated ash layer) as well as biostratigraphic age correlations are rare in the sedimentary formations of the Ecuadorian AAB younger than the Cretaceous Napo Fm., the attribution of absolute stratigraphic ages to these continental sedimentary series remains problematic. However, the knowledge of the stratigraphic ages are crucial in the investigation of exhumation in the source regions of the AAB using the advanced methodology detailed in section 4.2. The present section will consequently attempt to assign a stratigraphic age to any dated level of the northern SAZ based on previous studies described in section 2.2.2, but also through detrital fission-track ages when better constraints do not exist. Using heavy mineral analysis, it has been recognized that some horizons reveal dominant volcanic contamination. Thus, in such sediments, the  $P_1$  population of zircons (and possibly apatite), together with a euhedral form, is assumed to represent the time of eruption that is further assumed to be within error the age of the hosting stratigraphic horizon. Because post-depositional heating toward temperatures higher than  $100^\circ\text{C}$  can be excluded for the Aptian to Recent sediments of the Ecuadorian AAB in the northern Ecuadorian SAZ (see section 3.5), a maximum stratigraphic age can be estimated by the youngest detrital zircon fission-track population ( $P_1$ ) for all dated horizons.

#### a) *Hollin Fm.:*

The dated levels from the Hollin Fm. were sampled from widespread locations in the northern SAZ and the Pastaza depression (see Fig. 4.14). These are (1) west of the Abitagua batholith in the Baños-Puyo region within the Sub-Andean Thrust Belt (99GR73, Fig. 4.14), (2) just east of the same batholith and south west of the village of Mera (99GR65; Fig. 4.14), (3) east of the northern SAZ and close to the Sub-Andean Front (99GR22; Fig. 4.14), (4) east of the Abitagua batholith along the Narupa-Loreto road (98GR05 and 98GR69; Fig. 4.14), and finally (5) east of the Reventador volcano in the northern part of the northern SAZ (98GR50; Fig. 4.14).

Only one of the dated quartz-rich sandstones (98GR50) from the Hollin Fm. directly overlay the Jurassic Misahualli, whereas sample 99GR73 is assumed to be in unconformable contact with the Abitagua batholith (Litherland et al., 1994). Sample 99GR65 corresponds to a quartzitic sliver encountered along the Rio Gringo section, i.e. southwest of Mera (Fig. 4.14). It was attributed to the Hollin Fm. because it is (1) adjacent to both the Abitagua batholith (99GR66; section 3.3.1) and the Misahualli Fm. (99GR64; see section 3.3.2), and (2) characterized by blue quartz grains as observed

within other Hollin levels. However, the Hollin Fm. is not reported in this location on the geological map of the area (1:100 000 scale Baños geological map of Ecuador, 1980) whereas it is reported outcropping further south along the eastern flank of the batholith. The assignment of these levels to the Hollin Fm. is therefore probably appropriate. The three other samples (98GR05, 98GR69 and 99GR22) were simply taken from sites where the Hollin Fm. is recorded on the geological map of Ecuador (Litherland et al., 1993).

Each Hollin sample contained a Middle Jurassic to Early Cretaceous age for the P<sub>1</sub> zircon population (Table 4.1 and Fig. 4.16). Hence, this implies that all the dated Hollin levels are at least younger than the Late Jurassic-Early Cretaceous. This is thus in agreement with the accepted Aptian-Albian depositional age for the Hollin Fm. (Fig. 4.17; see section 2.3.2.1). However, the precise stratigraphic relationships between all these regionally scattered Hollin samples are difficult to evaluate. As a result, these levels were placed in approximate position in the lithostratigraphic section of the Hollin Fm. (see section 2.2.2).

#### *b) Napo Fm.:*

Localities of the Napo samples are in the 'Mirador anticline' northeast of the town of Mera (98RS06; Fig. 4.14) and also in the region of Baeza and Lumbaqui further north (98GR02, 98GR57 and 98GR41; Fig. 4.14).

Sample 98GR02 is from a glauconitic sandstone level encountered above the Hollin Fm., in the vicinity of the village of El Chaco (Fig. 4.14). It possibly represents the sediment deposited during the maximum transgression attributed to the Albian that characterizes the transition between the Hollin and Napo formations (White et al., 1995; Villagomez et al., 1996; Jaillard, 1997b). The dated P<sub>1</sub> zircon population is very young, i.e.  $101 \pm 11$  Ma (Table 4.1) confirming that its stratigraphic age is probably as young as Middle to Late Albian (~105-100 Ma; Fig. 4.17 and Table 4.1).

Sample 98GR57 was extracted from a glauconitic level stratigraphically 200 m above sample 98GR02 that revealed a youngest population of  $\sim 101 \pm 11$  Ma. Hence, its stratigraphic age probably lies between  $\sim 100$ -90 Ma (Table 4.1; Fig. 4.18).

Sample 98GR41 is located 50 m below from the boundary with the Maastrichtian-Paleocene Tena Fm. in the Lumbaqui region (Fig. 4.14). Because the Napo Fm. was significantly truncated prior to the deposition of the Tena Fm. (see section 2.1.2), an approximate stratigraphic age of  $\sim 90$  Ma is thus assigned to sample 98GR41 (Table 4.1; Fig. 4.18).

Sample 98RS06 is from the 'Mirador anticline' location, north of the village of Mera (Fig. 4.14). Jaillard (1997b) ascribed a Coniacian-Santonian stratigraphic age (89-84 Ma) to the same level using biostratigraphic arguments (sample 94.32; Jaillard, 1997b,

Fig. 44). In assuming rapid exhumation in the source region, the  $P_1$  zircon population of  $86 \pm 6$  Ma (Fig. 4.17; Table 4.1) corroborates this biostratigraphic correlation.



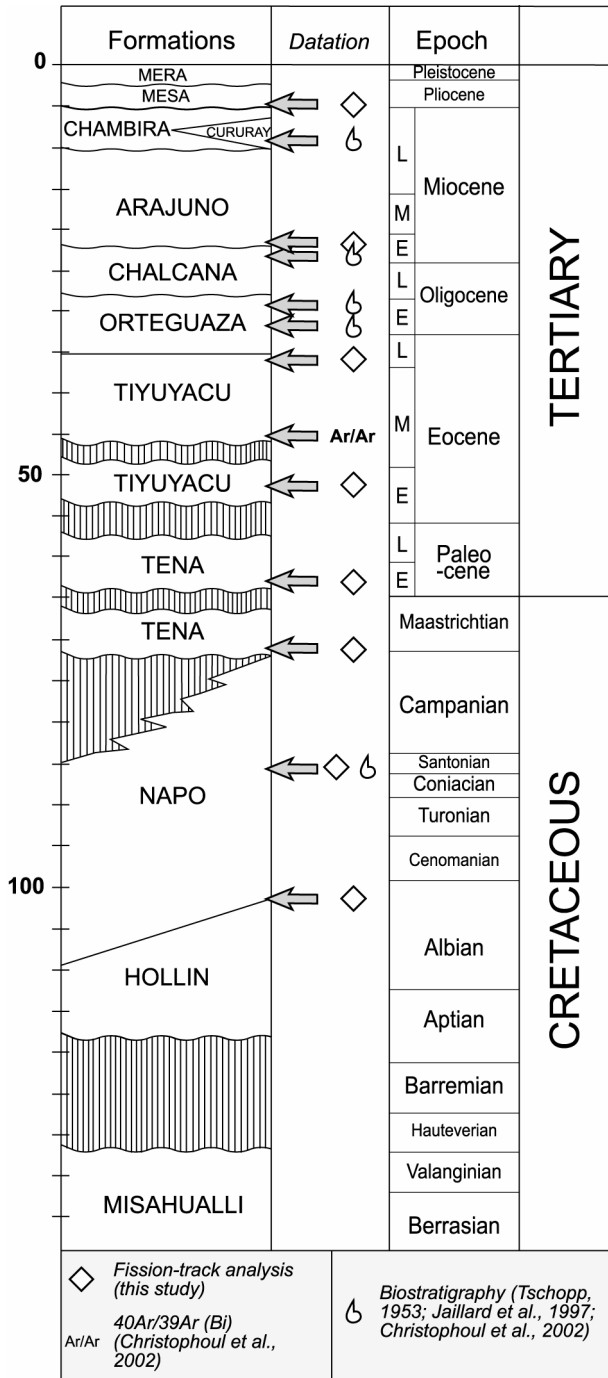


Figure 4.17: Stratigraphy of the Aptian to Recent interval in the Ecuadorian Amazon Basin. Two recent studies (Jaillard, 1997b; Christophoul et al., 2002) provided biostratigraphic ages that are combined with one <sup>40</sup>Ar/<sup>39</sup>Ar age on biotite from an intercalated ash layer (Christophoul et al., 2002) and some of the fission-track ages from this study to constrain the depositional ages of the basin fill series. Mesozoic and Cenozoic chronostratigraphy after Gradstein et al. (1995) and Berggren et al. (1995), respectively.

c) Tena Fm.:

The dated Tena levels are less abundant, because the apatite and zircon yields were low. The locations of the dated Tena Fm. samples are: (1) along the Rio Gringo River southwest of Mera (99GR67; Fig. 4.14), (2) west of Narupa where it is overlain by the Tiyuyacu Fm. (98GR83; Fig. 4.14), and (3) further north along the Baeza-Lumbaqui road (98GR37; Fig. 4.14).

Sample 99GR67 taken near to the boundary with the Napo Fm. hosts a P<sub>1</sub> DZFT population of 72 ± 3 Ma (Table 4.1). Using this population as a maximum stratigraphic age, a post-Late Campanian-Early Maastrichtian age is attributed to this basal Tena level (Fig. 4.17; Table 4.1).

Sample 98GR37 is also ascribed to the lower Tena Mb. due to its proximity with the Napo Fm. (Fig. 4.14). Furthermore, the apatite P<sub>1</sub> population yielded a 78 ± 6 Ma age (Table 4.1) that corroborates with a post-Campanian stratigraphic age.

Sample 98GR83 was encountered below the typical conglomeratic deposits of the upper Tiyuyacu Mb. (see section 2.2.2). Therefore, it is included in the upper Tena Mb., which is assumed to be Paleocene in age (~65-57 Ma; Table 4.1; see section 2.2.2). Moreover, sample 98GR83 yielded a P<sub>1</sub> zircon fission-track population of 63 ± 3 Ma, which confirms that the Tena Fm. in this locality at least extended until

the Paleocene as suggested by Jaillard (1997b; Fig. 4.17).

*d) Tiyuyacu Fm.:*

Sample 99GR36 was extracted from a basal Tiyuyacu Fm. level in the vicinity of Lumbaqui (Fig. 4.14) where it overlies red siltstones of the Tena Fm. A  $51 \pm 5$  Ma age was obtained for the P<sub>1</sub> DZFT population (Table 4.1) that was probably derived from contemporaneous (?) volcanic sourcing inferred by the presence of (1) devitrified volcanic glass in the matrix, and (2) a few idiomorphic zircon grains (see section 4.1). As a result, an Early Eocene depositional age (55-49 Ma) is attributed to sample 99GR36 (Table 4.1, Fig. 4.17) that correlates with the previous (Christophoul et al., 2001) but unconstrained age estimate (see section 2.2.2).

The stratigraphic age of sample 99GR52 is less well constrained, as it does not exhibit a young detrital zircon fission-track population (Table 4.1; Fig. 4.16). It is however also ascribed to the Early Eocene (55-49 Ma) as it is stratigraphically higher than the basal Tiyuyacu Fm. sample (99GR36).

Sample 98GR81 from the Tiyuyacu Fm. corresponds to characteristic conglomeratic levels of the basal upper Tiyuyacu Mb. in the region of Tena (Fig. 4.14). Christophoul et al. (2002), using <sup>40</sup>Ar/<sup>39</sup>Ar thermochronology on biotite from an intercalated ash layer (Fig. 4.17) dated the basal deposits of this member at 46 Ma. A stratigraphic age of 46 Ma is therefore assumed for sample 98GR81 (Table 4.1).

Sample 99GR44 was encountered in the Pastaza depression along the Tena-Puyo road where it corresponds to the uppermost levels of the Tiyuyacu Fm. (Fig. 4.14). Fission-track analysis on this level produced a P<sub>1</sub> DZFT population of  $36 \pm 4$  Ma (Table 4.1). It therefore implies that the deposition of Tiyuyacu Fm. lasted at least until the Late Eocene in the Ecuadorian AAB (Fig. 4.17).

*e) Orteguzaza and Chalcana Fms.:*

Faunal evidence allowed Zambrano (1999) to assign an Early Oligocene (~33-28 Ma) and Late Oligocene-Early Miocene (~28-20 Ma) stratigraphic ages to the Orteguzaza and Chalcana Fms., respectively (Fig. 4.17). These are however the only constraints for the depositional ages of samples (1) 99GR81 from the Orteguzaza Fm. (Fig. 4.14), and (2) 00GR02 and 00GR03 from the Chalcana Fm., because these levels did not yield detrital fission-track populations young enough to refine their stratigraphic ages (Table 4.1). However, sample 00GR03 is considered to have a younger depositional age than sample 00GR02 as indicated by younging direction of the stratigraphic column in the Pastaza depression (Fig. 4.14).

*f) Arajuno Fm.:*

Two Arajuno levels were sampled in the Pastaza depression; these are samples 00GR04 and 98GR28 (Fig. 4.14). Heavy mineral analysis revealed a contemporaneous volcanic contamination for sample 00GR04 (see section 4.1). Both prismatic apatites and zircons present in the detritus yielded almost identical ages of 21-22 Ma within  $2\sigma$  error (Table 4.1). A mid-Early Miocene stratigraphic age (~21-22 Ma) is then ascribed to sample 00GR04 that may represent the early stage of deposition of the Arajuno Fm. (Fig. 4.17).

No clear depositional age could be attributed to sample 98GR28 using detrital thermochronology; it is thus arbitrarily positioned in the Middle Miocene at approximately 16 Ma, because it lies stratigraphically above sample 00GR04 and below the overlying Late Miocene Chambira Fm.

*g) Chambira-Mesa-Mera Fms.:*

Very little information is available allowing stratigraphic constraints on the stratigraphic ages of the four dated levels from the Chambira, Mesa and Mera formations, i.e. samples 98GR16 (Chambira Fm.), 00GR06 and 00GR01 (Mesa Fm.), 99GR72 (Mera Fm.).

Sample 98GR16 from the Chambira Fm. was collected in the Talag syncline, southwest of Puerto Napo (see section 2.2.2; Fig. 4.14). It is ascribed to the Late Miocene (Fig. 4.17) according to palynological data from its lateral time equivalent, the Curaray Fm. (Tschopp, 1953; section 2.2.2.8). Furthermore, the Chambira Fm. in the Talag syncline location is reported to form a progressive unconformity with the Abitagua batholith (Christophoul, 1999, see section 2.2.2), which according to fission-track analysis has been exhuming since the Late Miocene (see section 3.5). Hence, sample 98GR16 is placed into the Late Miocene.

Two samples from the probable Mesa Fm. (00GR01 and 00GR06) produced identical 8 Ma age for their respective apatite  $P_1$  fission-track populations (Table 4.1). This thus proposes post 8 Ma depositional ages (Late Miocene-Pliocene) for these two levels from the Mesa Fm. considering that no post-depositional resetting occurred (Fig. 4.17).

Sample 99GR72 from the Mera Fm. yielded a  $0.9 \pm 1.8$  Ma ( $2\sigma$ ) AFT age. Because post-depositional resetting is also not envisaged, this therefore suggests a probable Late Pliocene to Pleistocene stratigraphic age for this level (Table 4.1).

### 4.3.2. Provenance

All provenance analyses, including (1) detrital fission-track ages, (2) paths along the zircon fission-track  $D_n$  curves, and (3) heavy mineral analysis of the Aptian to Recent basin series of the Ecuadorian AAB are combined and discussed in the present section to investigate changes in the source regions of the AAB (Fig. 4.18). This description constrains the identity of particular source regions (Yim et al., 1985) and reveals changes in provenance through time, which can be used to investigate tectonic rearrangements in the source regions of the Ecuadorian AAB.

#### *- Hollin-Upper Napo Formations (Aptian-Turonian)*

Abundant zircon, tourmaline and rutile, commonly referred to as a ZTR assemblage, (Fig. 4.2), in the clastic rocks of the Hollin and Napo Formations indicates that these formations were mainly derived from (1) crystalline basement rocks (e.g. granitoids and low-grade gneisses), and (2) their correlative sedimentary cover. Detrital fission-track analyses indicate that the majority of the source regions of the Hollin and Napo Fms. had relatively old zircon ages (>250 Ma; Fig.4.16) compared to the stratigraphic ages of the dated strata (110-90 Ma; see section 4.3.1). Furthermore, these zircons are characteristically dark, display complex crystallographic zoning, possess rounded faces and are commonly associated with monazite, suggesting that they have a long and complex history and that they are probably derived from the Guyana and Brazilian craton region to the east of the basin (Fig. 1.1). The zircons may have passed through more than one sedimentary cycle and their pre-existing host rocks may have been the Paleozoic Pumbuiza and Macuma Formations, which constitute part of the substratum of the Andean Amazon Basin and platform cover of the Guyana Shield (Tschopp, 1953; Bristow and Hoffstetter, 1977; Baldock, 1982, Rivadeneira and Baby, 1999). Minor muscovite, biotite and epidote are observed in the westernmost Hollin sample (99GR73), which suggests that there may have been a minor contribution from metamorphic rocks exposed to the west.

A second group mostly from  $P_1$  populations (Fig. 4.18) that lie between 120 and 170 Ma (Table 4.1; Fig. 4.16) indicate that the sediments of the Hollin and Napo Fms. were partly sourced from regions with Middle Jurassic to Early Cretaceous cooling and exhumation ages (in the ZFT system; Table 4.1; Fig. 4.16) which, combined with the presence of a minor component of diopside and cassiterite (Fig. 4.1.), probably identifies the Jurassic Misahualli suite as a source region (see section 3.5). A 50-70 My hiatus between the Hollin Fm. and the underlying tuffaceous and ignimbritic rocks of the Misahualli Fm. has been dated in the central part of the northern SAZ (see section 3.5); whereas, an Early Cretaceous age is assigned to the uppermost levels of continental volcanic arc deposits in the Ecuadorian Andes (see section 3.5) that is in

agreement with a coeval volcanic cessation in Colombia (Hall and Calle, 1982). Therefore, it is valid to suggest that a rock pile corresponding to 30 - 50 My of volcanic activity is locally missing in the northern SAZ and may have been eroded contributing a significant component of the detrital Jurassic-Upper Cretaceous zircon fission-track populations present in the overlying Hollin and Napo Fms. (see section 4.2.2).

The low precision of the stratigraphic ages of the sampled quartz arenites from the Hollin Napo Fms. (with the exception of samples 98GR02 and 98RS06 of the Napo Fm.; see section 4.3.1) precludes the construction of reliable paths along the  $D_n$  zircon fission-track curves for the Aptian to Cenomanian. Consequently, the lagtime of the  $P_1$  populations cannot be utilised to determine reliable estimates of the contemporaneous exhumation rate(s) of the source region(s) (see section 4.2.1.1-e).

Sample 98GR02 of the lower Napo Fm was deposited during an eastward transgression towards the Guyana and Brazilian cratons (Villagomez et al., 1996) where the source regions probably preserved relatively old zircon fission-track ages (Harman et al., 1998). This corroborates with the older  $P_2$  and  $P_3$  zircon fission-track populations in sample 98GR02, which have ages of  $267 \pm 22$  Ma and  $516 \pm 43$  Ma respectively (Table 4.1). However, sample 98GR02 also yields a  $P_1$  population, whose ZFT of  $101 \pm 11$  Ma (Table 4.1) is indistinguishable from its stratigraphic age (Fig. 4.18). A simple calculation, utilising the associated lagtime  $<11$  My ( $+1\sigma$ ; Table 4.1) yields a source exhumation rate  $>0.75$  mm/y (Fig. 4.5), which is unreasonably high for shield regions.

Several igneous bodies, which intruded the Napo Fm., yield K/Ar ages that range from the Albian to the Coniacian (106-84 Ma; Barragan, 1997), and are located above SSW-NNE oriented, pre-Cretaceous structures in the Oriente region and Sub-Andean Zone (see section 2.2.2). These Cretaceous igneous bodies may have contributed detritus to sample 98GR02 during a transgressive episode, resulting in the relatively young  $P_1$  age of  $101 \pm 11$  Ma. However, no volcanic signature was encountered in the heavy mineral from sample 98GR02. If a volcanic derivation cannot be envisaged for this population, the large error (11 My) leaves open the question if it is really on the correlation 1/1 line.

The heavy mineral assemblage in the Hollin and Napo Fms. during the Aptian to Turonian (?) is diagnostic of a shallow, sedimentary and crystalline continental crustal source region that was located to the east of the Ecuadorian AAB within cratonic South America although a minor component may have been derived from upper crustal levels of an exhuming source to the west.

The near-absence of typical volcanic minerals in the heavy minerals fraction of the sampled quartz arenites from the Hollin and Napo Fms. may reflect the paucity of heavy minerals in the eroding Misahualli Fm. (plagioclase and devitrified glass dominate the modal composition of a majority of the volcanic rocks; Wasson and Sinclair, 1927; Romeuf et al., 1995). Furthermore, any eroding zircons may have been trapped in the poorly studied back-arc sedimentary series of the continental arc, otherwise referred to as the Chapiza Fm. (Tschopp, 1953). The high-energy depositional environment as inferred in particular for the sampled Hollin strata

(Tschopp, 1953; Balkwill et al., 1995; Dashwood and Abbotts, 1990; Jaillard, 1997b; Christophoul, 1999), may have eliminated the unstable, heavy, volcanic ferromagnesian phases.

*- Upper Napo Fm.-Tena Fm. (Coniacian-Paleocene)*

A clear type 5 path toward a short lagtime value, i.e. 0-6 My (Table 4.1; Fig. 4.18) is observed along the  $D_1$  curve for the upper Napo Formation in the SAZ (98GR41 to 98RS06; Fig. 4.18). This is justified by the well-constrained Coniacian-Santonian (~86 Ma, see section 4.3.1), stratigraphic age of sample 98RS06 and the exclusion of possible contemporaneous volcanic contamination (see section 4.1). The type 5 path implies that an exhumational phase affected one or more source regions of the Ecuadorian AAB at ~90-85 Ma with a minimum rate of 1 mm/y (Fig. 4.5; Table 4.1). Such high exhumation rates are rarely documented in cratonic regions and hence it is unlikely this material was sourced from the east. This transition towards rapid exhumation in the source regions of the Ecuadorian AAB is associated with the clear appearance of low to medium grade metamorphic minerals in the heavy mineral detritus of the Upper Napo Fm. (Figs. 4.1 and 4.2, section 4.1). Such suites are only recognized to the west of the AAB; therefore one concludes that this time represents a period of rapid exhumation of the proto-Cordillera Real at 90-85 Ma.

The heavy mineral assemblages become progressively more heterogeneous and the proportion of medium-grade metamorphic mineral grains (Fig. 4.1) increases stratigraphically upwards from the basal Tena Fm. (~Maastrichtian; see section 4.3.1; Fig. 4.1). Consequently, several source lithologies were contributing to the infilling of the AAB since the beginning of the Maastrichtian. The detrital zircon fission-track record becomes less disperse from the upper Tena Mb. with the proportion of older zircon fission-track populations decreasing. No ages >260 Ma occur (Fig. 4.16 and 4.18) suggesting that supply from the shield regions was minor or even lacking. The  $D_1$  zircon fission-track curve is characterized by a type 4 path, with a zero lagtime value that persists until the deposition of the Early Eocene, basal Tiyuyacu Fm. indicating that the source region was exhuming at rates  $\geq 1$  mm/y during the Maastrichtian to Paleocene period (see section 4.3.1; Fig. 4.18). Therefore, a significant proportion of detrital material was being drained from metamorphic rocks located to the west of the present day SAZ, which in turn implies a period of rapid uplift and exhumation of the rocks that currently comprise the Cordillera Real during the Maastrichtian. The drop in contribution of detritus from the east revealed both by the loss of the older population, and the heavy mineral suites suggests that the shield regions had been progressively buried beneath the basin fill sequence of the AAB since at least the deposition of the Aptian-Albian Hollin Fm. (see section 4.3.1). Therefore, we can assume that the shield areas and basin cover to the east of the northern SAZ were not topographically prominent and consequently were not being uplifted or exhumed. In summary, a combination of the heterogeneous metamorphic character of the heavy mineral content

and the detrital zircon-fission track record of the Maastrichtian to Recent sedimentary rocks reflect the heterogeneous composition of source regions that were located to the west of the northern SAZ.

The ages of the  $P_2$  zircon fission-track populations from the Upper Napo Fm. through to the Tena Fm. are indistinguishable ( $224 \pm 20$  Ma to  $242 \pm 72$  Ma), and hence the  $D_2$  curve follows a type 2 path (Fig. 4.18). Both the Tena Fm. and the upper Napo Fm. may have been partly derived from rocks located to the west of the basin that hosted Triassic zircon fission-track ages. Potential source rocks with Triassic cooling ages are not commonly preserved today although various Triassic to Early Jurassic plutons are reported in the Cordillera Real to the west of the AAB, e.g. the Tres Lagunas granitoids (Litherland et al., 1994), which may have rapidly cooled through the zircon partial annealing zone ( $\sim 310$ - $230^\circ\text{C}$ ) in the Triassic-Early Jurassic when the Ecuadorian margin was undergoing extension during a phase of rifting (Aspden and Litherland, 1992). Exhumation of these granitoids during the Late Cretaceous-Maastrichtian, which was evidenced here by both type 5 and 4 paths along the  $D_1$  curve may have exhumed at least parts of these granitoids and subsequently they were eroded into the adjacent Ecuadorian AAB. Alternatively, these Triassic zircon fission-track ages from the Tena and Upper Napo Fms. may also confirm that the Tena Fm. was partly sourced by reworking of the Upper Napo Fm. that would corroborate with the truncation of the Napo Fm. prior to the deposition of the Tena Fm. to the west of the SAZ (see section 2.1.2).

Numerous prismatic and inclusion rich apatites yielded a fission track population with an age of  $142 \pm 15$  Ma from a single stratum in the Lower Tena Member (98GR37; see section 4.2.2). These apatites may have been derived from a late Jurassic (volcanic?) source rock during the Maastrichtian (see section 3.3.1). In turn, it is reasonable to suggest that part of the Jurassic continental arc was eroded in the Maastrichtian and was contributing sediment to the Tena Fm. The younger apatite population, with an age of  $78 \pm 7$  Ma yields a partially annealed, mean track length of  $9.5 \pm 1.4 \mu\text{m}$  (see section 4.2.2), which indicates that a source region of the basal Tena rocks experienced a protracted and potentially complex exhumational history prior to its erosion.

#### *- Tiyuyacu Fm. (Early-Late Eocene)-Orteguaza Fm. (Late Eocene-Early Oligocene)*

The tuffaceous cement, phosphatic matter and idiomorphic zircons from a basal conglomeratic level of the Tiyuyacu Fm. (sample 99GR36) evidence the derivation of part of the material from a volcanic source. The idiomorphic zircons yield a detrital zircon fission-track population with an age of  $51 \pm 5$  Ma ( $P_1$ ), which has been excluded from the  $D_1$  curve and replaced by the second youngest ( $P_2$ ) population, which yields

an age of  $72.7 \pm 6.0$  Ma (Fig. 4.18; Table 4.1). The type 1 path along the  $D_1$  curve from the Tena Fm. (99GR83) to the Tiyuyacu Fm. (99GR36) is evidence for a clear change in provenance in the Late Paleocene-Early Eocene (Fig. 4.18), which correlates with the disappearance of metamorphic minerals and the exclusive presence of a ZTR assemblage (Fig. 4.1). The source rocks of these conglomeratic deposits were noticeably composed of 10-12 cm sub-rounded clasts of radiolarian black cherts (see section 2.1.2). Hence, all this suggests that (1) pelagic sediments (of an oceanic domain), (2) shallow continental crustal levels, and (3) contemporaneous volcanic centers were supplying the AAB in the Early Eocene.

Several authors, e.g. Hughes and Pilatasig (2002), Kerr et al. (2002 in press) propose that volcanic activity resumed along the Ecuadorian margin in the Early Tertiary, probably after the accretion of the Pallatanga island-arc. However, Hungerbühler et al. (2002) produced a single zircon fission-track age from the volcanic Sacapalca Fm. of  $67 \pm 6$  Ma that was spatially linked with an intrusion that yields a K/Ar age of  $70 \pm 2$  Ma (Kennerley, 1973). This suggests that igneous activity might have resumed earlier, i.e. in the latest Cretaceous-early Maastrichtian along the southern segment of the Ecuadorian margin. Considering that volcanic activity probably extended further north along the Ecuadorian margin, i.e. to the west of the present-day location of the northern SAZ, the volcanic detritus encountered in the basal deposits of the Tiyuyacu Fm. were thus most probably derived from west of the Ecuadorian AAB.

The  $P_2$  DZFT population of  $73 \pm 6$  Ma from sample 99GR36 is indistinguishable from the  $P_1$  population obtained from the sample 99GR67 of the Tena Fm., i.e.  $72 \pm 3$  Ma (Fig. 4.18). Because an important erosive unconformity characterizes the contact between the Tena and Tiyuyacu Fms. (see section 2.1.2), it is possible that upper levels of the Tena Fm. were reworked and contributed to the basal strata of the Tiyuyacu Fm. Alternatively, another source of these zircons with Late Cretaceous fission-track ages from the Lower Tiyuyacu Mb. may be assumed to have been derived from the Yunguilla Fm. of the Pallatanga Terrane in the Cordillera Occidental (Hughes and Pilatasig, 2002). The Yunguilla Fm. represents a marine time-equivalent of the Tena Fm. with a syn-accretionary signature (71-65 Ma, Hughes and Pilatasig, 2002) to the west of the Ecuadorian AAB that was deposited while the Cordillera Real was uplifting. Preliminary analyses from the Yunguilla Fm. (Winkler and Vallejo, pers. com. 2002) indicate a partial sourcing in shallow continental levels from most likely the Cordillera Real to the east. Therefore, detrital zircon fission-track populations with almost zero lagtime values from the Cordillera Real may have been shed into the Yunguilla unit. Subsequently, the  $P_2$  population of  $73 \pm 6$  Ma present in the basal Tiyuyacu Fm. may be derived from the Yunguilla unit that was exhumed and eroded during in the Late Paleocene-Early Eocene, and subsequently deposited into the Ecuadorian AAB, i.e. in the basal Tiyuyacu Fm. Finally, these radiolarian black cherts may be correlative of the highly deformed Late Cretaceous black cherts present-today in the western succession of the Pallatanga unit (Jaillard et al., 2002b) but also from other locations of the Western Cordillera (BGS reports).

The Lower Tiyuyacu Mb. is characterized by a type 1 path along the  $D_1$  curve towards the oldest DZFT cluster at 224-579 Ma (99GR36-98GR52; Fig. 4.18), which is



associated with a prominent shift from a shallow continental source (ZTR, Fig. 4.1) to medium-grade metamorphic source rocks with a dominance of chloritoid (Fig. 4.1). This is a striking example for the reactivation of a new clastic source with an older exhumation history.

From the Lower (99GR52) to the Upper Tiyuyacu Mb. (98GR83 and 99GR44), there is a change to a type 5 path with lagtimes from the  $P_1$  zircon fission-track populations that decrease towards 0-3 My by the end of the Upper Tiyuyacu Member (Late Eocene; Fig. 4.18). The  $D_2$  curve follows the same trend (Fig. 4.18). Such patterns are diagnostic of accelerating rates of exhumation (see section 4.2.1.3) in the source regions of the Ecuadorian AAB by the mid-Middle to the Late Eocene, with rates exceeding 2 mm/y (Fig. 4.5). The presence of two sub-parallel  $D_1$  and  $D_2$  curves suggests that two different hinterland blocks, which hosted distinguishable zircon fission-track ages, were being eroded. Important exhumation in one or all sources of the Upper Tiyuyacu Mb. is corroborated by the abundance of high-grade mineral grains (Fig. 4.1). Additionally, Christophoul et al. (2002) proposed that the rounded quartz pebbles that characterise the conglomeratic deposits of the Upper Tiyuyacu Mb. (see section 2.1.2.) are probably derived from the reworking of sedimentary rocks while the distance of sediment transport had increased. Such characteristics clearly suggests that source region changed from the Lower Member to upper crustal levels that may also have been metamorphic quartz veins from the exhuming Cordillera Real. High grade metamorphic basement rocks occur over a vast area in the present day Cordillera Real and Amotape complex (Litherland et al., 1994), they include: (1) gneisses and kyanite schists of the Agoyan unit, (2) kyanite sillimanite orthogneisses of the Sabanilla migmatite, (3) andalusite and cordierite bearing meta-carbonates of the Cerro Hermoso unit, (4) contact metamorphic minerals in metasediments of the Agoyan unit proximal to the Azafrán granitoid, (5) andalusite, kyanite, sillimanite bearing Mormoro Granites (Amotape complex), and (6) kyanite and glaucophane in the Raspas Eclogite in the Amotape Complex (Litherland et al., 1994). This clearly implies that the Cordillera Real represented the main source of detrital material for the Ecuadorian AAB in the Late Eocene. However, it is not possible to identify in detail any unit. From the geographic position a main contribution from the Agoyan unit and Azafrán granite may be suggested.

The transition from the Tiyuyacu Fm. (99GR44) to the Orteguzaza Fm. (99GR81) is characterized by an increase in lagtime for the  $P_1$  population from 0 to 45 My whereas a similar trend is also observed along the  $D_2$  curve (Fig. 4.18). These type 1 paths suggest that source regions changed in the Late Eocene-Early Oligocene to low and medium grade metamorphic rocks (Fig. 4.1 and 4.2) with older  $P_1$  populations characterized by lagtimes greater than ~30 My (Fig. 4.18).

- *Chalcana Fm. (Late Oligocene-Early Miocene)*

The abundance of medium to high-grade metamorphic minerals in the heavy mineral assemblage increases stratigraphically upward within the Chalcana Fm. (see section 4.1) and the DZFT record is characterised by two, sub-parallel type 5 paths ( $D_1$  and  $D_2$ ; Fig. 4.18). Collectively, these observations suggest that two distinct source regions of the AAB were exhumed at approximately the same rate during the Late Oligocene to the Early Miocene, which exposed deeper, high-grade crustal levels. The geographic position of the high-grade metamorphic source rocks of the Chalcana Fm. cannot be accurately identified although they were probably similar to that which contributed to the Tiyuyacu Fm., i.e. the Agoyan and Cerro Hermoso units and the Azafrán pluton, currently exposed in the Cordillera Real to the west. Considering the similar (1) detrital zircon fission-track ages (Fig. 4.18) and (2) heavy mineral patterns of the Chalcana Fm. with those of both the Tiyuyacu and Orteguzaza Fms. (Fig. 4.1), it is plausible to envisage that the Chalcana Fm. may have been partly supplied from the erosion of both the Tiyuyacu and Orteguzaza Fms. The thermochronological study of the basement of the northern SAZ has shown that the northern SAZ was exhumed during the Late Oligocene-Early Miocene (section 3.5); this may account for the absence of the Orteguzaza Fm. in the proximal AAB and supports the reworking of the Orteguzaza Fm. into stratigraphically younger rocks.

- *Arajuno Fm. (Early Miocene-Late Miocene)*

Pseudo-hexagonal biotites, hornblende, diopside, euhedral, inclusion-rich apatites and idiomorphic zircons in the basal Arajuno strata, combined with indistinguishable ZFT and AFT ages of 22 Ma, suggest there was a contemporaneous volcanic supply into the Ecuadorian AAB during the Early Miocene. The volcanic source rocks were most likely located to the west of the basin, where voluminous volcanic arc activity prevailed, e.g. the volcanic Saraguro Group (Hughes and Pilatasig, 2002; Hungerbühler et al., 2002). Because of the volcanic contamination, the  $P_1$  ZFT age of sample 00GR04 was removed from the  $D_1$  curve (Fig. 4.18) and the resulting  $D_1$  and  $D_2$  curves, spanning time of the upper Chalcana and Arajuno Fms., depict two type 2 paths (Fig. 4.18). Such type 2 paths are either related to extremely low exhumation rates within the source region, or to the erosion of two volcanic piles with cooling ages of  $49 \pm 3$  Ma and  $70 \pm 5$  Ma (see section 4.2.1.3). However, in the absence of dominating volcanic mineral grains and the presence of medium to high-grade metamorphic mineral grains like in the underlying Chalcana Fm., it is preferred to interpret these paths to document slow exhumation in the source area combined with the reworking of strata of the upper Chalcana Fm. (e.g. 00GR03). This scenario is reinforced by: (1) the presence of almost identical heavy mineral assemblages in both formations (with the exception of chromite and volcanic detritus in the Arajuno Fm.; see section 4.1), (2) the unconformable

contact between the Chalcana and Arajuno Fms. (Christophoul et al., 2002). The occurrence of chromite and diopside in the Arajuno Fm. implies the presence of mafic and ultra-mafic rocks in the source region(s) of the AAB during the Early Miocene that were most likely related to a change in the drainage pattern in the source areas. The exposure of chromite bearing rocks during the Early Miocene probably occurred to the west of the Cordillera Real but are difficult to trace as several oceanic terranes (e.g. Pallatanga oceanic plateau, the Macuchi island arc and the Piñon Terrane) and hence sources of chromite, existed along the Ecuadorian forearc at that time.

#### *- Chambira, Mesa and Mera Fms. (Late Miocene-Pliocene)*

The sedimentary facies (see section 2.1.2) and the heavy mineral content (i.e. more ZTR representation on the expense of metamorphic minerals, Fig. 4.1) of the Chambira Fm. clearly document a change of provenance that occurred in the Late Miocene (?) between the Arajuno and the Chambira Fms, while this is not seen in the DZFT record. An unlikely explanation for this observation is that the source of the dated zircons was not the same as that which was contributing the bulk of the heavy mineral content.

A type 4 path, with a long and constant lagtime of ~35-40 My is observed along the D<sub>1</sub> curve during the deposition of all formations from the Arajuno Fm. until Recent (98GR28 to 00GR05, Fig. 4.18). Such a characteristic pattern is also seen along the parallel D<sub>2</sub> curve but is restricted to the Late Miocene to Recent (Fig. 4.18). A constant lagtime (within the limits of the sampling density) stratigraphically upward indicates that an effectively constant time of ~30-35 My was necessary to bring rocks from the partial annealing zone of zircon fission tracks (230-310°C; Tagami et al., 1998) to the surface where they were eroded and subsequently contributed to the infilling of the Ecuadorian AAB. It is very tempting to conclude that the source regions of the Early Miocene to recent deposits of the Ecuadorian AAB were in a thermal steady state (Willet and Brandon, 2002), regardless of the changes in the lithologies of the source rocks. However, the P<sub>1</sub> lagtimes are long (~25-40 My) and persisted for a long period (~20-15 My; Fig. 4.18). Hence, it is difficult to envisage that a single process along such a heterogeneous margin drove a single and stable phase of exhumation in the source regions probably located to the west of the basin (see section 4.2.1.3). Therefore, given that the accuracy of the DZFT curve is limited by the sampling density, this DZFT record simply indicates that the source regions did not experience any rapid exhumational phase from the Middle Miocene to Recent.

Another interesting observation is the heavy mineral content of the Late Miocene to (?) Pleistocene Mesa and Mera Fms. The sudden increase in the quantity of augite, hypersthene and olivine is diagnostic of the erosion of basic volcanic and oceanic rocks. Source rocks with such lithologies are currently exposed in the Cordillera Occidental and the Inter-Andean region, especially along the western flank of the valley in the Pallatanga Terrane. Consequently, various levels of these regions should have been exhuming since the Late

Miocene-Pliocene and contributed to the contemporaneous sedimentary sequences of the Ecuadorian AAB. Therefore, the drainage pattern must have been similar to that seen today in the region, as for example the Pastaza River that drains via the town of Baños part of the Cordillera Occidental and Inter-Andean region into the AAB. Looking more in detail towards the  $D_1$  curve, it is possible to distinguish a type 5 path from ~5 to 0 Ma that is characteristic of renewed exhumation in the source regions.

#### - Quaternary Napo River sand

Three distinguishable regions are captured within the present drainage system of the Napo River in the vicinity of Puerto Misahualli, these are: (1) green-schist and higher-grade bedrocks (e.g. the Salado Group) of the Cordillera Real between  $0^{\circ}45'S$  and  $1^{\circ}15'S$ , (2) the southern part of the northern Sub-Andean Zone, and (3) the northern part of the Pastaza depression (Fig. 4.14). The Chalcana, and Arajuno formations are currently exposed in the northern Pastaza depression and southern part of the northern SAZ (see section 4.1). Predictably, the heavy mineral content of sample 00GR05, taken from the bed of the present day Napo River (see section 4.1; Fig. 4.14) should be a combination of detritus derived from these rocks.

Sample 00GR05 yielded three DZFT populations of  $30 \pm 5$  Ma ( $P_1$ ),  $50 \pm 3$  Ma ( $P_2$ ) and  $141 \pm 13$  Ma ( $P_3$ ) (Fig. 4.18). It is likely that the  $P_1$  population was not derived from the northern SAZ as no bedrock outcropping today in that region yields a similar ZFT age, with the exception of  $P_1$  from strata in the upper Tiyuyacu Mb. (see sections 3.4 and 4.2.2). However, a ZFT age of ~30 Ma is yielded by metamorphic rocks from the surface of parts of the Cordillera Real (Azafrán batholith, Spikings et al., 2000 and 2001). As expected, this observation confirms that the Cordillera Real is supplying load to the Napo River to the site of sample 00GR05, i.e. the Puerto Misahualli (Fig. 4.14). The Early Eocene age of the  $P_2$  population is commonly encountered in both the sedimentary rocks of the northern SAZ and metamorphic rocks of the Cordillera Real (see sections 3.4 and 4.2.2) and it is likely that both regions contribute to this ZFT population. The Abitagua batholith and Misahualli Volcanics magmatic suite, which constitutes the basement of the northern SAZ, yields Late Jurassic to Early Cretaceous ZFT ages that are probably similar to their crystallisation and extrusion ages (see section 3.4). Similar detrital ages are also encountered in the dated Napo and Hollin strata (Table 4.1, Fig. 4.18). Therefore, this group of zircons, which yield the older ZFT ages, are probably derived from the southern flank of the northern SAZ where the Abitagua batholith, the Misahualli, Hollin and Napo Fms. are all outcropping (Fig. 4.14).

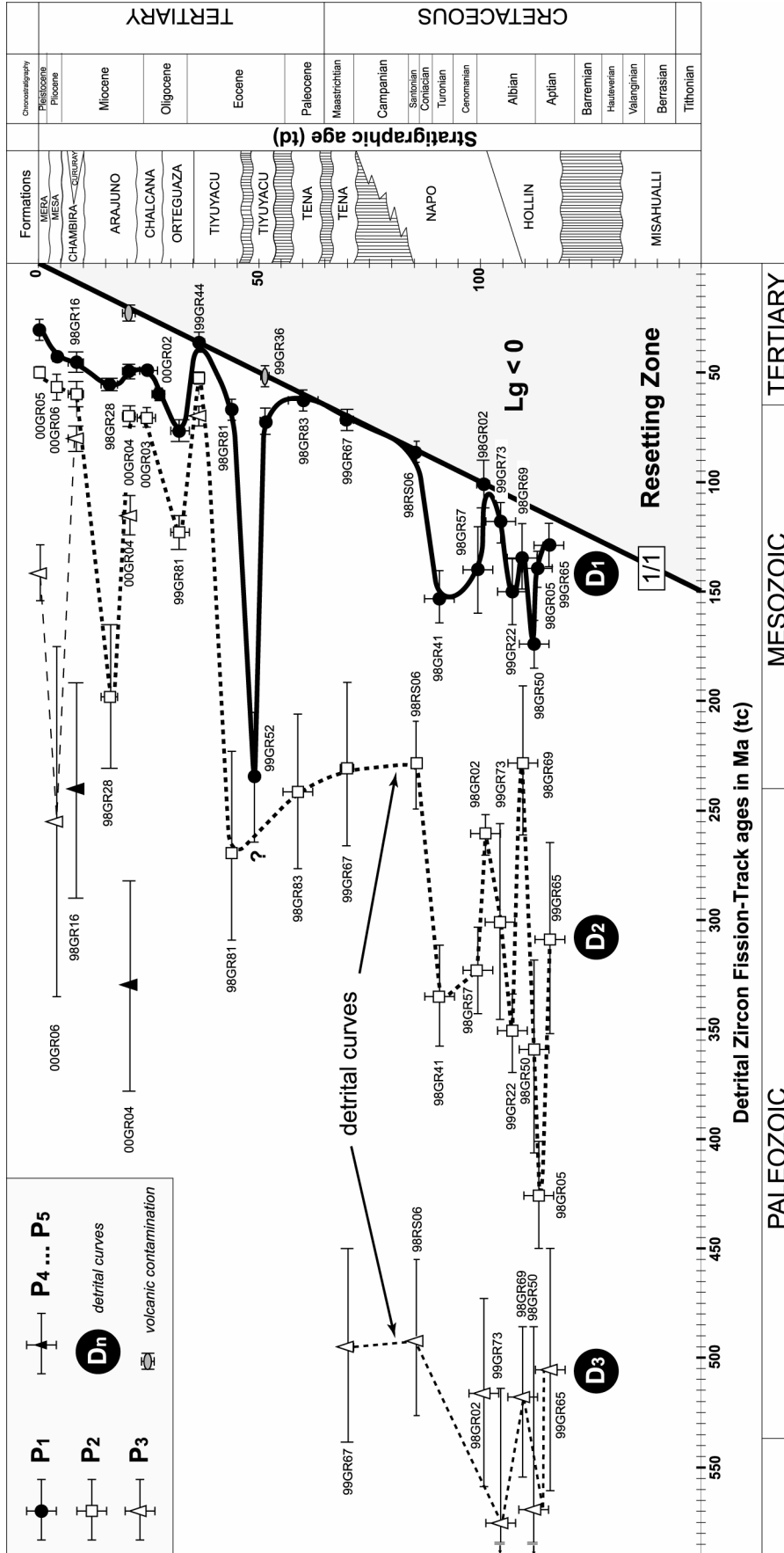


Figure 4.18: detrital zircon fission-track populations of the Cretaceous to recent basin fill series of the Ecuadorian Amazon Basin following the representation that is fully described in Figure 4.8. The attribution of stratigraphic ages to the dated levels is discussed in section 4.3.1.  $P_1$  populations (see Table 4.1) that are assumed to be derived from contemporaneous volcanic activity are excluded from the  $D_1$  curve.

Figure 4.18 : detrital zircon fission-track populations of the Cretaceous to Recent basin fill series of the Ecuadorian Amazon Basin following the representation that is fully described in Figure 4.8. The attribution of stratigraphic ages to the dated levels is discussed in section 4.3.1.  $P_1$  population (see Table 4.1) that are assumed to be derived from contemporaneous volcanic activity are excluded from the  $D_1$  curve.



## 5. Geological evolution of the northern Ecuadorian Sub-Andean Zone and its source regions

### *Middle Jurassic-Early Cretaceous: Peltetec event and pre-structuration of the SOAM plate*

Along the northern margin of South America an extensional regime prevailed during the Triassic-Early Jurassic that was associated with the deposition of the marine Santiago and Sacha Fms. in the Ecuadorian AAB (Baldock, 1982; Litherland et al., 1994; Christophoul, 1999). From the Middle Jurassic the paleo-Pacific oceanic plate was subducting beneath South America generating the NNE trending Misahualli volcanic arc along the Ecuadorian margin and its associated back-arc sediments, i.e. the Chapiza Fm. further east toward the Brazilian and Guyana shields in the Oriente region (Tschopp, 1953; Aspden et al., 1987; Jaillard et al., 1995; Litherland et al., 1994; Jaillard et al., 2000). Contemporaneous deposition to the west toward the trench in the fore-arc regions is very poorly understood and might be represented by the meta-sedimentary rocks of the Cordillera Real and SAZ, e.g. the Upano (Litherland et al., 1994) and Paradalarga units (Buitron and Vallejo, 1999) but also possibly by the metasedimentary and meta-volcanic Rio Blanco Fm. identified further west in the Cordillera Real (Pratt et al., 2002). The present fission-track study on both volcanic rocks of the Misahualli Fm. and its associated plutonic phase (i.e. the Abitagua batholith) is here combined with K/Ar ages from the genetically related Zamora batholith further south in the SAZ (Litherland et al., 1994) to confirm the development of magmatism along the Ecuadorian margin at ~190-180 Ma (see also Jaillard et al., 2000). Zircon and apatite fission-track ages from volcanic series taken in the northern SAZ suggest that volcanism and hence subduction probably ceased by the Late Jurassic-Early Cretaceous (140-130 Ma, Fig. 5.1) that would be in agreement with coeval volcanic cessation in Colombia (Hall and Calle, 1982).

During the last decade researchers of the British Geological Survey have developed a model of accretion of small continental terranes in the Late Jurassic-Early Cretaceous along the northern segment of the South American Plate with intervening oceanic domain (e.g. Chaucha, Loja Terranes, Litherland et al., 1994; Fig. 5.1). Some continental blocks between North and South America were envisaged as a possible site of derivation of these terranes. This phase, which is recognized in Ecuador as the Peltetec tectono-metamorphic event, would have been responsible for the cessation in the Early Cretaceous of subduction-related volcanism (Fig. 5.1). However, the rocks that constitute this Late Jurassic-Early Cretaceous suture, referred to as the oceanic Peltetec suture (Litherland et al., 1994) were never precisely dated, because this model did not satisfy all requirements (pers. comm. Aspden, 1996), in particular the additional oceanic suture inferred along the Cosanga Fault in the SAZ that does not appear to be

evident at all in the field. Furthermore, oceanic basement and metamorphic rocks in sparse outcrops in the Inter-Andean Valley (IAV), which have not been dated yet and remain almost inaccessible because thick Tertiary and Quaternary deposits today overlie it, may have affinities with parts of the Pallatanga and Guamote Terranes, and hence do not completely support the presence of an individual terrane (i.e. Chaucha Terrane) as suggested by Litherland et al. (1994) below the IAV (pers. comm. W. Winkler, R. Spikings). The Peltetec event is ascribed to the Late Jurassic-Early Cretaceous using the stratigraphic age of the youngest involved series (Jurassic) of the Cordillera Real and the Aptian-Albian age for the post-accretionary Hollin Fm. in the Ecuadorian Andean Amazon Basin (Litherland et al., 1994). Spikings et al. (2000) applied fission-track methodology on Paleozoic to Jurassic (Cretaceous?) formations of the Cordillera Real. Tertiary fission-track cooling ages were obtained that are unfortunately much too young to refine the Jurassic-Early Cretaceous development of the Ecuadorian Andes. In this respect, the correlation of Jurassic and Cretaceous volcanic and sedimentary series in the SAZ with those present in the Cordillera Real is crucial and will be undertaken in detail soon (Pratt et al., 2002). In the following discussion, we shall retain the useful division of the units in the Cordillera Real of Litherland et al. (1994) without entering into the debate on their derivation.

Nevertheless, in the Sub-Andean Zone and further east into the back-arc regions, the Peltetec event is seen through a phase of exhumation that started at ~140 Ma and affected part of the basement of the region (Fig. 5.1). This exhumational period was most likely responsible for the hiatus of 40-60 My between the Jurassic Misahualli volcanics and the unconformably overlying deposits of the Hollin Fm. in the center of the northern SAZ. This phase can be in turn correlated with the peneplanation of the entire AAB at a time between 140 and 110 Ma already evidenced by Tschopp in 1953. Associated unroofing within a rising proto-Cordillera located to the west of the AAB in the Early Cretaceous probably generated detritus that can be traced through the occurrence of blue quartz grains in the westernmost Hollin samples, and hence would suggest a derivation from the exhuming Tres Laguna Granite in the Cordillera Real's region. Heavy mineral analyses did not yield strong evidence of sourcing from metamorphic rocks but one can say that volcanic mineral grains derived from the underlying Misahualli volcanics are also almost absent in the Hollin and Napo samples. All this is most likely explained by the high energy depositional environment of the Hollin Fm. Further positive evidence for the creation of an early relief in the Cretaceous to the west may come from detrital zircon fission-track populations in the Hollin and Napo Fms: many zoned, metamict 'old' zircons (i.e. >250 Ma) most likely document a main derivation from the shield areas to the east of the basin, whereas the rocks providing the youngest populations (198-118 Ma) with lagtimes of ~20 to 60 My must be derived from sources that have exhumed at much faster rates, unusual for shield complexes (Harman et al., 1998). These heterogeneous populations could have been supplied from (1) shallow continental crust rocks located in the incipient Cordillera Real to the west of the basin, and/or (2) the overlain Jurassic Misahualli volcanic arc (Fig. 5.1) through transient deposition into the back-arc region.



A major change of convergence direction from SE to NE occurred in the Late Jurassic-Early Cretaceous between the paleo-Pacific oceanic plate and the northern margin of the South American plate that was contemporaneous with the opening of the South Atlantic Ocean (Aspden et al., 1987; Jaillard et al., 2000; Fig. 5.1). Because the Ecuadorian segment was NNE oriented, this (1) generated the cessation of the subduction of the oceanic plate beneath the northern segment of the South American Plate (Aspden et al., 1987; Jaillard et al., 2000), and (2) may have permitted the accretion of allochthonous terranes along the northern Andean segment (Litherland et al., 1994; Fig. 5.1). This switch of convergence established a right-lateral transpressive tectonic regime in the continental margin in Middle-Cretaceous (Baby et al., 1999) with uplift to the west of the AAB (Fig. 5.1). Additionally, if it can be proven that the Jurassic and Early Cretaceous rocks of the Cordillera Real were formed in situ, i.e. along the northern South American margin, the terrane concept of Litherland et al. (1994) may become obsolete.

### *Aptian-Cenomanian*

The sedimentary Aptian to Cenomanian horizons of the Hollin and Lower Napo Formations in the northern SAZ are characterized by heavy mineral and detrital zircon fission-track populations that indicate a main provenance from the east, i.e. in the shield regions (White, 1995; Jaillard, 1997b; Dashwood and Abbotts, 1990; Balkwill et al., 1995; Canfield et al., 1982; Fig. 5.1). The youngest detrital zircon populations reveal an additional supply that was most likely from the underlying Jurassic arc in the region of the AAB but could have also been from the upper levels of an exhuming source region to the west of the AAB. Cretaceous igneous bodies (dated at 106-84 Ma) are reported intercalated with the Napo Fm. above SSW-NNE oriented pre-Cretaceous structures in the flat lying AAB (Oriente region) (Barragan et al., 1997) that were reactivated in a dextral transpressive regime in the Cretaceous as suggested by Baby et al. (1999) (Fig. 5.1). Because igneous bodies are also reported in the SAZ and not restricted to the flat lying AAB (Oriente), this suggests that both the (1) pre-structuration of the basin, and (2) later Cretaceous re-activation most probably extended westward at least to the present-day location of the northern SAZ. This transpressive regime along the Ecuadorian margin possibly facilitated the emergence of a shallow paleo-relief to the west of the AAB (Jaillard, 1997b; Jaillard et al., 2000) that was possibly a relic of the Peltetec event but most probably an equivalent of both the (1) Olmos arch in northern Peru (Baldock, 1982), and (2) emergent Central Cordillera in Colombia (Rangel et al., 2000; Ramón et al., 2001; Fig. 5.1). Additional evidence for the presence of a topographic barrier in the Cretaceous to the west of the Ecuadorian Andean Amazon Basin are the accumulation of marine derived particulate organic matter with high TOC (Total Organic Carbon) values, indicating dysoxic-anoxic bottom water and restricted oceanographic conditions (Vallejo et al., 2002). Further to the southwest toward Peru, i.e. where the South American margin was probably NW-SE

oriented, the NE-oriented displacement of the oceanic Farallon plate generated the NW-SE oriented offshore (?) subduction that prevailed in the Celica-Lancones region during the Middle to Late Cretaceous (Jaillard et al., 1999).

### *Turonian-Paleocene : accretion of the Pallatanga Terrane*

Detrital zircon fission-track thermochronology from the Upper Napo Fm. suggests very rapid exhumation (> 2mm/y) in the sources to the west of the basin since at least 90-85 Ma (Fig. 5.1). From ~85 to 60-55 Ma rapid and continued exhumation is implied by detrital thermochronology spanning the time of the Upper Napo and Tena Fms. deposition. The coeval and disrupted history of the SAZ and proximal Oriente Basin is recorded by (1) a major transgression and establishment of a predominantly marine environment during the deposition of the Upper Napo Fm. (Jaillard, 1997b; Vallejo et al., 2002), (2) the absence of Campanian deposits of the Napo Fm. in the proximal SAZ (erosion or non-deposition; Tschopp, 1953; Balkwill et al., 1995; Jaillard, 1997b; Fig. 5.1), (3) the unconformable deposition of the continental red beds of the Tena Fm. above the shallow marine Napo Fm. (Fig. 5.1), (4) syn-sedimentary faulting during deposition of the Lower Tena Mb. (Rivadeneira and Baby, 1999; Fig. 5.1), (5) a net increase of tectonic subsidence during deposition of the Maastrichtian Lower Tena Mb. (Fig. 5.1), and (6) the appearance of detrital medium-grade metamorphic grains in the Upper Tena Mb.

The above characteristics of the Late Cretaceous tectono-sedimentary development of the (SAZ and proximal Oriente) AAB correlates in time with the supposed accretion of the Pallatanga Terrane along the western forearc of Ecuador (Hughes and Pilatasig, 2002; Fig. 5.1). The Pallatanga Terrane represents an accreted part of an oceanic plateau complex (Cosma et al., 1998; Lapierre et al., 2000; Hughes and Pilatasig, 2002). It is bounded by the Pallatanga-Pujili-Calacali Fault to the east with the Cordillera Real (Fig. 1.3), and to the west by the Chimbo-Toachi-shear-zone with the later accreted Macuchi arc Terrane (Hughes and Pilatasig, 2002; Fig. 1.3). The end of the accretion of the Pallatanga Terrane is stratigraphically constrained by the post-accretionary turbiditic Yunguilla Fm. The Maastrichtian to (?) Paleocene age of the Yunguilla Fm. implies that the accretion occurred before the Maastrichtian, e.g. the Campanian as suggested by Hughes and Pilatasig (2002). A cluster of reset K/Ar ages of 85-65 Ma from rocks in the Cordillera Real (Litherland et al., 1994) would corroborate a Santonian-Campanian peak of exhumation in the uplifting Cordillera Real due to compression driven by accretion of the buoyant Pallatanga Terrane along the western margin of the SOAM plate. This is in perfect agreement with both the present young detrital zircon fission-track ages in the Upper Napo and Tena Fm. and the observed increase in tectonic subsidence in the entire AAB (Fig. 5.1).

Further, Hungerbühler et al. (2002) assigned a Maastrichtian age to the 2000m thick volcanic rocks of the Sacapalca Fm. of southwest Ecuador that can be correlated with the calc-alkaline rocks of the Rio Calas Fm. further north. Both formations are

located above the newly formed Ecuadorian margin, i.e. the Sacapalca Fm., above metamorphosed rocks of the Cordillera Real while the Rio Calas lavas are reported above the Pallatanga Terrane (Kerr et al., 2002 in press). This implies that the deposition of the Tena Fm., which characterizes the first continental series in the AAB in a retro-foreland position (Jaillard, 1997b), was contemporaneous with resuming arc activity along the Ecuadorian margin further west after the accretion of the Pallatanga Terrane (Fig. 5.1).

### *Eocene: Macuchi and Piñon Terranes accretions*

The transition from the Paleocene to the Early Eocene is another major turning point in the evolution of the AAB that can be recognized through the unconformable deposition of the continental Eocene Tiyuyacu Fm. above the Maastrichtian-Paleocene Tena Fm. (Tschopp, 1953; Campbell, 1970; Fig. 5.1). The present clasts, heavy mineral analyses and detrital zircon fission-track populations all indicate a clear change of provenance toward source rocks with volcanic to pelagic sedimentary signatures to the west of the basin. Furthermore, apatite fission-track modelling from the basement rocks of the northern SAZ suggests that the region underwent an exhumational period in the Early to Middle Eocene (Fig. 5.1) that probably also drove the pre-Eocene truncation of the Tena Fm. to the west of the AAB as depicted by Jaillard (1997b) and Rivadeneira and Baby (1999). The limit between the two members of the Tiyuyacu Fm. is also characterized by an erosive unconformity (Fig. 5.1) that is associated with the partial or total erosion of the Lower Tiyuyacu Mb. that occurred prior to 46 Ma because that is the minimum age obtained by Christophoul et al. (2002) for the base of the Upper Member. Noticeably, the Tiyuyacu Fm. does not occur imbricate with the pre-Eocene series, i.e. the Hollin, Napo and Tena Fms. to the west of the northern SAZ in the Subandean Thrust Belt (Fig. 5.1). This therefore indicates that faulting occurred along the western edge of the northern SAZ in the Early Eocene and was thus synchronous with the reactivation of pre-Cretaceous cortical faults in the flat lying AAB in a transpressive regime as suggested by Rivadeneira and Baby (1999) (Fig. 5.1).

With regard to the evolution of the source terranes during deposition of the Tiyuyacu Fm., two events are recognized: (1) the Lower Tiyuyacu Mb. is characterized by a change of source terrane that experienced earlier exhumation, and (2) the Upper Tiyuyacu Mb. records exhumation of high-grade metamorphic terranes during the Middle and Late Eocene. The first may be interpreted as representing a radical tectonic rearrangement of the source region for the Tiyuyacu Fm., whereas the latter indicates a substantial exhumation that reached rates  $>2$  mm/y (Fig. 5.1). This Middle to Late Eocene rapid exhumation period correlates with increased exhumation observed in the Cordillera Real and Amotape complex since  $\sim 43$  Ma, which lasted until  $\sim 30$  Ma (Spikings et al., 2000 and 2001; Spiking et al., 2002 submitted; Fig. 5.1). The above arguments prove that the Eocene epoch was characterized by significant tectonic activity involving the entire northern Andes of Ecuador. Notably, the presence of pelagic radiolarian chert clasts in the Lower Tiyuyacu Mb. (Early Eocene) indicates that

sedimentary series associated with the Pallatanga Terrane (?) may have contributed to the flux of clastic material. Furthermore, Pecora et al. (1999) suggested that in the Late Paleocene accretion a buoyant basaltic plateau, referred to as the Piñon block (Jaillard et al., 1995 and 1997a; Fig. 5.1), accreted against the northernmost margin of Peru from where, it later migrated north-eastward along dextral wrench faults to its present day location, north of Guayaquil where it defines the basement of the coastal region. According to Aspden and McCourt (2002) this was probably synchronous with the accretion of the Naranjal arc present today to the north of the Cordillera Occidental. Developing thrusting and exhumation in the Early Eocene related to the accretion of these terranes are in agreement with reported synchronous cooling ages from the southern part of the Cordillera Real (Spiking et al., 2001; Fig. 5.1). The exhumation of the westernmost region of the Ecuadorian margin probably permitted the denudation of levels with low-grade paragenetic heavy mineral associations as well as sourcing from the already accreted Pallatanga Terrane into the AAB. This tectonic phase can be traced further east into the Oriente region where tectonic subsidence probably increased due to the probable flex of the South American Plate as during the deposition of the Lower Tena Mb. (Fig. 5.1). It is not yet clear if the accretion of the Macuchi island-arc was involved in the same event; however, from stratigraphic relationships (Egüez, 1986) as well as radiometric dating (Hughes and Pilatasig, 2002), this event is attributed to the Middle Eocene (~48 Ma; Fig. 5.1). Fission-track data suggest that the peak of exhumation in the Cordillera Real occurred with the deposition of the Upper Tiyuyacu Mb. during the Middle to Late Eocene (Fig. 5.1). Combining rapid exhumation in the Cordillera Real in the Middle to Late Eocene and the modification of the sedimentary source in the basin, Christophoul et al. (2002) proposed that the erosive base of the Upper Tiyuyacu Mb. could be considered to be the expression of the beginning of an isostatic readjustment due to the progressive erosion of orogenic load (Heller et al., 1988), i.e. the Cordillera Real. This is corroborated by the (1) appearance of higher metamorphic grade minerals upward into the Tiyuyacu Fm. that is characteristic of sourcing from lower crustal levels, (2) the absence of tectonic subsidence in the basin, (3) the homogeneous thickness of the Upper Tiyuyacu Mb. across the basin (Rivadeneira, pers. com, 2002), and (4) finally rapid exhumation in the source regions. Many authors, e.g. Pilger (1984), Pardo-Casas and Molnar (1987), Daly (1989) reported an increase of the convergence rate of the Farallon plate relatively to the Ecuadorian margin from 48 Ma to 37 Ma that was most likely accommodated by the Chimbo-Toachi Fault separating the Macuchi from the Pallatanga Terranes to the west of the Cordillera Real (Hughes and Pilatasig, 2002). As a result, this probably permitted the unloading of the Cordillera Real-AAB system in the Middle to Late Eocene.

### *Oligocene-Early Miocene*

The Eocene-Oligocene transition in the AAB is characterized by the change from continental (Upper Tiyuyacu Mb.) to brackish deposition of the Orteguzza Fm. (Baldock, 1982; Rivadeneira and Baby, 1999; Christophoul et al., 2002). The fine-grained fluvial sediments of the Chalcana Fm. in turn unconformably overlie the Orteguzza Fm. (Baldock, 1982; Christophoul, 1999). The occurrence of a brackish depositional environment in the Orteguzza Fm. possibly implies that tectonic loading onto of the SOAM plate, probably increased by the Early Oligocene with the final docking of the Macuchi island-arc onto the Ecuadorian margin (Hughes and Pilatasig, 2002; Fig. 5.1), allowing a marginal marine ingression in the AAB. This event probably also generated a deformation event represented by a hiatus in the continental-arc volcanism of the Saraguro Fm. to the west (Hughes and Pilatasig, 2002).

According to the present results, the Orteguzza and Chalcana depositional systems depict first a change to a mixed low and medium-grade source rock followed by increased exhumation of medium to high-grade metamorphic source (Fig. 5.1). Therefore, the break-up of the Farallon plate into the Cocos and Nazca plates at ~26-25 Ma (Hey, 1977; Lonsdale and Klitgord, 1978; Fig. 5.1) during the deposition of the Chalcana Fm. and the subsequent nearly orthogonal subduction of the Nazca plate beneath the Ecuadorian margin (Fig. 5.1) most probably has driven uplift and denudation of high-grade metamorphic source rocks. These observations would indicate continued exhumation of lower crustal levels in the source terranes most likely located in the early Cordillera Real.

### *Early-Middle Miocene to Recent*

From the Early-Middle to Late Miocene was deposited the Arajuno Fm. in the AAB. The basal Arajuno Fm. is again characterized by a change of source rocks; in particular and according to heavy mineral analyses a new source in mafic rocks is indicated. The mafic source (including blue amphiboles from high pressure/low temperature rocks) may have been derived from lithologies in the Cordillera Occidental (e.g. the Pallatanga Terrane? Macuchi? Piñon?). Metamorphic mineral grains, which are also present, derived from the Cordillera Real where a pulse of enhanced exhumation in the northern segment from 22-15 Ma was evidenced (Spikings et al., 2000; 2001; Fig. 5.1). Both the acceleration of the relative convergence of the Nazca and South American Plate as well as accelerating spreading rates at the South Atlantic Ridge (Brozena, 1986; Daly, 1989), most likely maintained a general compressive state of stress along the entire Ecuadorian margin in the Early to Middle Miocene (Daly, 1989) that permitted exhumation along the Ecuadorian margin. This is corroborated in the northern SAZ by apatite fission-track modelling from the basement of the region as well as the imbrication of Pre-Arajuno Fms. along the Sub-Andean Front to the east of the SAZ

(Fig. 5.1). The volcanic contamination encountered within the oldest sampled strata of the Arajuno Fm. may be derived from the growth of a contemporaneous continental volcanic arc to the west (Saraguro Fm.; Steinmann et al., 1999; Hungerbühler et al., 2002), and as a result can be used to infer a minimum Lower Miocene stratigraphic age for the Arajuno Fm.

Along strike variations in cooling ages in the Cordillera Real combined with reconstructions of the Nazca and SOAM plates led Spikings et al., (2001) to propose that the Carnegie Ridge has been subducting beneath the north-western SOAM margin since ~ 15 Ma (Fig. 5.1). The segment of oceanic crust that supports the buoyant Carnegie Ridge causes it to subduct with a flat configuration (Gutscher et al., 1999). Coupling of the slab with the upper plate reactivated pre-existing weaknesses in the upper plate and dextrally displaced the oceanic domain towards the northeast, causing extension and subsidence in the south and in the coastal forearc with related opening of the Progreso basin and marine incursion into the Southern Ecuadorian forearc (Steinmann et al., 1999; Deniaud, 2000; Spikings et al., 2001; Hungerbühler et al., 2002). Little is known for this time period in the AAB that it is characterized by large lagtimes for the youngest detrital zircon fission-track population (25-40 My). This implies that the source regions of the deposits of the AAB in the Early Miocene were probably denudated slowly (Fig. 5.1), and as a result suggests that tectonic activity was probably displaced westward in the fore-arc region. Such relative quiescence in the Cordillera Real is then in agreement with the development of seaways in the Middle Miocene to the south of the Ecuador across the Cordillera Real (Hungerbühler et al., 2002), a region of low topography at this time. Hence, the authors correlated this marine incursion with the marine to brackish deposits of the Curaray Fm. reported in the AAB (Tschopp, 1953). However, Christophoul (1999) brought a contradictory argument proposing that the Curaray Fm. may represent the distal and lateral time equivalent of the proximal Chambira Fm. This hypothesis is equivocal because the continental Chambira formation may represent the contemporaneous deposits of an exhumational phase that can be seen in Ecuador through (1) increasing exhumation rates in the adjacent Cordillera Real (Spikings et al., 2000; Fig. 5.1), (2) syn-sedimentary compression in the southern Inter-Andean depression (Noblet et al., 1988; Steinmann et al., 1999; Hungerbühler et al.; 2002), (3) the progressive unconformity of the Chambira Fm. with the Abitagua batholith in the northern SAZ (Christophoul, 1999), and (4) the imbrication of the Arajuno Fm. along the Cosanga Fault to the south of the Pastaza depression (Fig. 5.1). Because the Miocene stratigraphy of the AAB requires detailed investigation, it is rather believed that the marine incursion observed in both the region of the Cordillera Real and AAB were coeval in the Middle Miocene and ceased by the Late Miocene (Hoorn et al., 1995; Hungerbühler et al., 2002) when a major phase of exhumation affected the complete Andes.

Numerous studies (see compilation in Jaillard et al., 2000) have shown that the entire Andean Chain was involved in a compressive deformation and uplift during the Late Miocene. In the southern Ecuadorian forearc at ~10-9 Ma the marine incursion ended by the establishment of intermontane basins associated with coeval uplift of the southern Cordillera Occidental (Steinmann et al., 1999; Hungerbühler et al., 2002). The

northern Cordillera Real and in particular the far north experienced accelerated exhumation since ~10 Ma (Spikings et al., 2000; Fig. 5.1). In contrast, the southern Cordillera Real, south of the Baños-Puyo transect remained rather inactive corroborating that in the coupling of the subducting Carnegie Ridge may have driven uplift of the northern segment (Spikings et al., 2001). With regards to the SAZ and the AAB: the apatite fission-track data suggest uplift and exhumation of the Abitagua batholith since the Late Miocene (~10 Ma; Fig. 5.1) that generated the progressive unconformity of the Chambira Fm. onto the Abitagua batholith (Christophoul et al., 1999). This exhumational stage did not affect only the Abitagua batholith in the northern SAZ but also the westernmost part further north, i.e. in the vicinity of the Colombian border. However, because this phase is not restricted to the Ecuadorian margin (Jaillard et al., 2000), the probable increase in coupling between the subducting Carnegie Ridge and the overriding coastal block in Ecuador (Spikings et al., 2001) cannot be the sole driving force. Rather, increasing spreading rates in the South Atlantic (Brozena, 1986; Fig. 5.1), which caused additional acceleration of Nazca plate convergence, most probably played a major role in the Late Miocene compressive phase that was experienced across the entire Ecuadorian margin (Steinmann et al., 1999; Deniaud, 2000; Jaillard et al., 2000; Spikings et al., 2001; Hungerbühler et al., 2002).

In this study apatite fission-track ages from the northern SAZ suggest that significant exhumation occurred from ~10-6 Ma in the Sub-Andean Thrust Belt between the Sub-Andean and Cosanga Faults. Paleo-stress measurements (Pasquarè et al., 1990) indicate that this belt accommodates a significant proportion of transcurrent stress since the Late Miocene-Pliocene. New apatite and zircon fission-track data from the Cordillera Occidental reveal a further significant pulse of exhumation at ~5 Ma in the vicinity of the Chimbo-Toachi Shear Zone that separates the Macuchi Terrane from the Pallatanga Terrane (Spikings et al., 2002 submitted). This pulse was earlier recognized in the Cordillera Real (La Sofia Fault system; Spikings et al., 2001) that is also identified by the detrital zircon fission-track record from the Pliocene to Recent sediments of the AAB (Fig. 5.1). Furthermore, the oldest sediments in the northern Inter-Andean Valley are not older than 6-5 Ma (Tobler, 2001; Abegglen, 2001; Fig. 5.1). All these data are then used to formulate a model, which proposed that the Chimbo-Toachi Shear Zone formed part of a large-scale, complex transtensive system that was responsible for the (1) opening of the Inter-Andean Valley (Winkler et al., 2002; Fig. 5.1), and (2) uplift of both the Cordillera Occidental (Spikings, 2002, pers. comm.) and the Neogene basins of Southern Ecuador (Hungerbühler et al., 2002). A similar system probably developed on the other side of the Cordillera Real and was responsible for the exhumation of the northern SAZ. Notably, the Late Miocene (?)-Pliocene

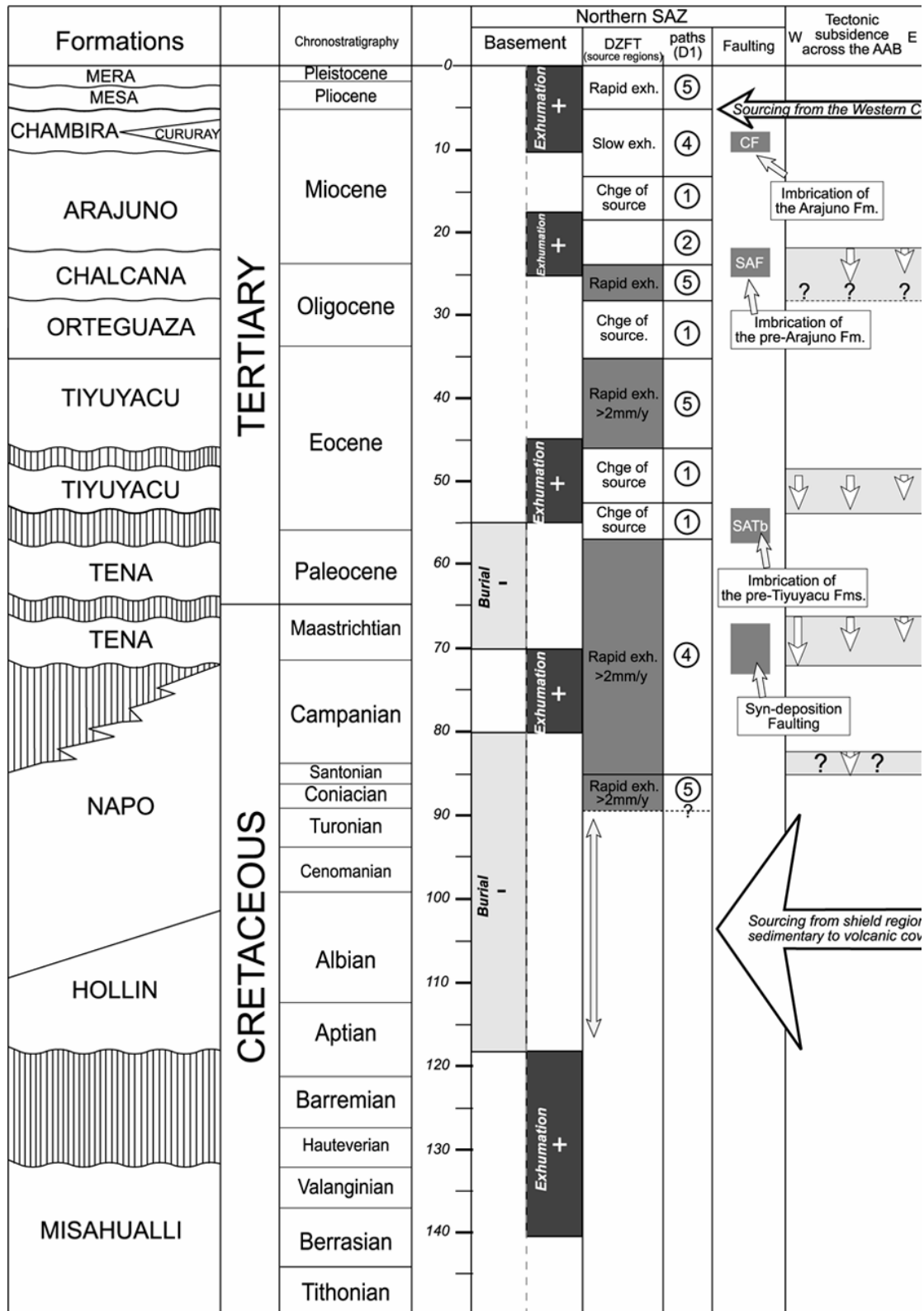
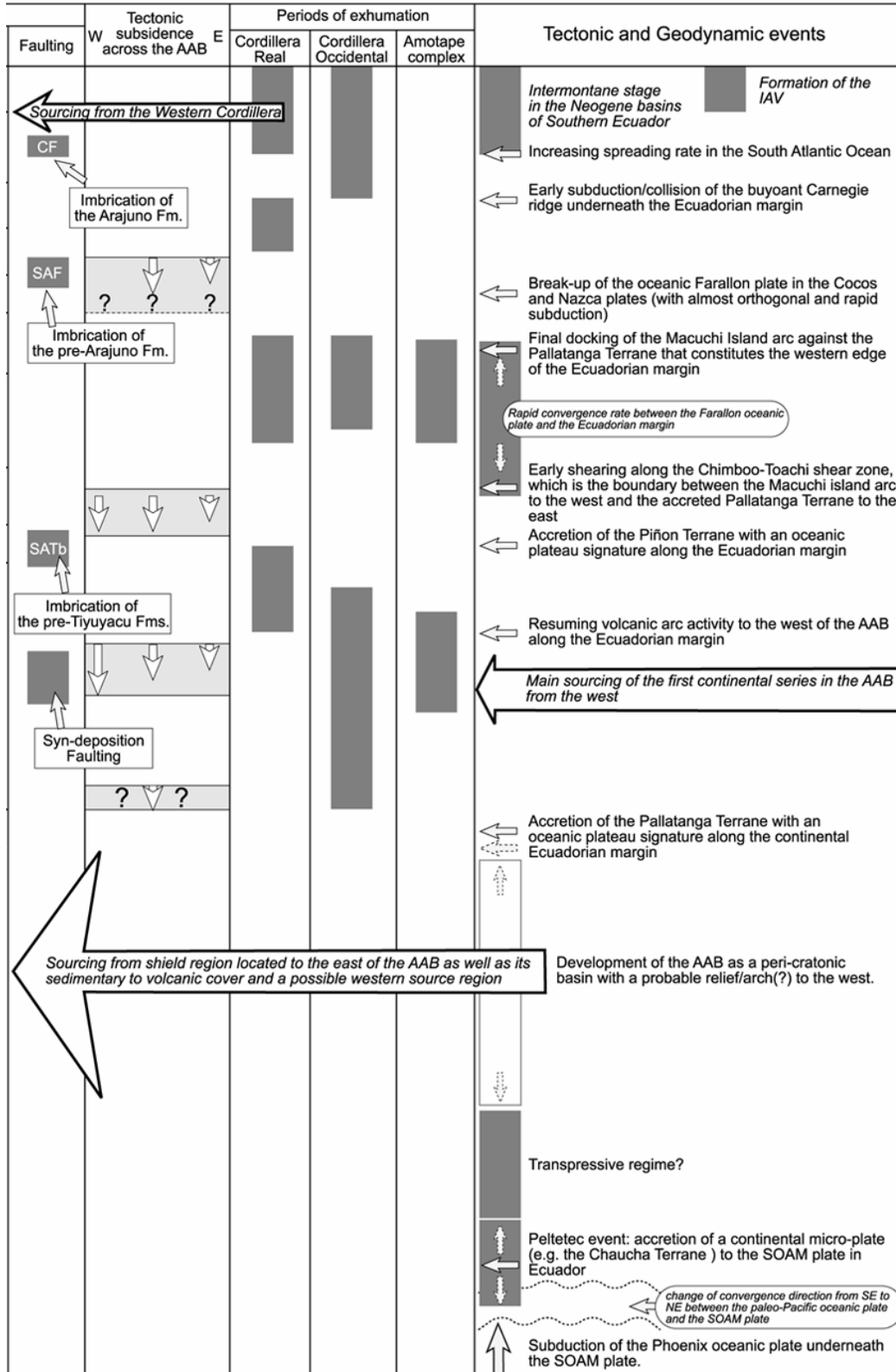


Figure 5.1: Geological evolution of the Ecuadorian margin from the Late Jurassic to Recent with special are taken from Spikings et al. (2000, 2001, and submitted.), and the intermontane stage of the Neogene SAF (Sub- Andean Front), CF (Cosanga Fault), SAZ (Sub-Andean Zone), AAB (Andean Amazon Basin),





reference to the northern Sub-Andean Ecuadorian Zone. Periods of exhumation in the Ecuadorian Cordillera basins of Southern Ecuador in Hungerbühler et al. (2002). Abbreviations: SATB (Sub-Andean Thrust Belt), SOAM (South American plate), IAV (Inter-Andean Valley).

Mesa/Mera Fms. In the AAB are characterized in their heavy mineral associations by the predominant occurrence of grains derived from basic and ultra basic source rocks. This observation implies and confirms that the Cordillera Occidental and the Inter-Andean Valley were sufficiently exhumed during the Pliocene to source deposits to the west into the AAB (Fig. 5.1).

## 6. Future work

(a) Additional work is still required in the Napo region and Pastaza depression such as detailed mapping, especially along the faulted contact of the SAZ with the Cordillera Real to the west. This may help to refine the different Andean phases of deformation in the Sub-Andean Thrust Belt that were recognised in the Cordillera Real by the British Geological Survey.

(b) Absolute stratigraphic ages of the Tertiary to Recent sedimentary series remain scarce, and consequently the absence of reliable sedimentation rates. An accurate way to resolve this problem of quantification in the AAB would be to determine ages on intercalated volcanic beds (when present) using a thermochronometer with a high temperature of closure (e.g. FT or U-Pb dating on zircons or  $^{40}\text{Ar}/^{39}\text{Ar}$  on muscovite, biotite or hornblende).

(c) The current study has provided a frame for exhumation and provenance analyses of the series in the northern SAZ and Pastaza depression of ~110 to 0 Ma age. Such series are also present to the south, in the Cutucú region. In the southern SAZ, the exposure of rocks defining the basement of the region, which are traced with difficulty, or are absent further north (e.g. Chapiza Fm., Santiago Fm., Macuma Fm.; Baldock, 1982), are better exposed. Thus, a similar approach, combining (1) fission-track analyses on both the basement and the overlying sediments of the southern SAZ but also (2) heavy mineral analyses, would further enhance and refine the understanding of exhumation in the source regions of the AAB.

(d) Some rocks of the volcanic Misahualli Fm. yielded zircon fission-track ages between 140-120 Ma that were considered as eruption ages. Investigating the thermochronology from within the same rocks with a higher temperature of closure may help to develop a time stratigraphy of the Misahualli Fm to better understand the development of the arc system at that time.



## 7. Conclusions

(a) Burial never generated temperatures greater than 100°C in the northern SAZ since the Early Cretaceous, and thus, in the main body of the basin the cumulative thickness of sedimentary rocks did not exceed ~3-4km, assuming a 30°C/km geothermal gradient

(b) A major rearrangement of the geodynamic system occurred during the Early Cretaceous that possibly led to the accretion of micro-plates along the northern Andean margin. This event, referred to as the Pelletec event caused the peneplanation of the former Misahualli arc as indicated by a 50-60 My hiatus with the overlying transgressive deposits of the Hollin Fm. Source regions of these early deposits in the northern SAZ were located to the east of the basin towards the shield regions but a small percentage of material may also have been shed from the west where a rising relief was being initiated.

(c) Detrital grain ages of all sedimentary suites yield information that has led to the identification of clear orogenic phases in the Andean chain in the Late Cretaceous to Paleocene and the Middle to Late Eocene, each characterized by exhumation rates greater than 2mm/yr.

(d) Changes in source regions were identified from,

*i) large scale:-* continental sedimentation in the AAB is thought to have begun by the Maastrichtian with the deposition of the Tena Fm., when the main detrital supply switched from the east (Guyana Shield region) to the west (Cordilleras) coevally with the appearance of metamorphic detritus. However detrital thermochronology points to rapid exhumation earlier in the source regions, i.e. at the latest during the Coniacian-Santonian, which was probably caused by the collision of the oceanic Pallatanga plateau along the Ecuadorian margin that later generated the deposition of the continental Tena Fm.

*ii) small scale:-* within the Cordilleras in the Eocene. FT data sets are in general in agreement with the changes in the heavy mineral suites. A short-term cycle from ZTR (zircon-tourmaline-rutile) to metamorphic mineral grain dominance is observed stratigraphically upward within the upper member of the Tiyuyacu Fm. of Middle to Late Eocene age. This cycle indicates the exhumation and erosion of lower crustal levels with a high rate that finished with the accretion of the Macuchi island-arc along the Ecuadorian margin in the Late Eocene-Early Oligocene.

(e) Reset apatite fission-track ages of 12 to 1 Ma are restricted to the narrow Sub-Andean Thrust Belt located to the vicinity of the Cordillera Real, indicating that significant exhumation has been restricted to the western edge of the northern SAZ since at least the Middle-Late Miocene.

(f) Both the Inter-Andean region and Cordillera Occidental have been exhumed since the Pliocene, as mafic minerals derived from these regions are present in the contemporaneous series of the northern SAZ and Pastaza depression.

---

## References:

Abegglen, P., 2001. Geologie des intermontanen Beckens von Chota (Pliozän, Nordecuador)-Ostteil (MSc. thesis): Zürich, Eidgenössische Technische Hochschule, 88 p.

Allen, P.A., and Allen, J.R., 1990. Basin Analysis: principles and applications. Blackwell science, 451 p.

Aspden, J.A., McCourt, W.J., and Brook, M., 1987. Geometrical control of subduction-related magmatism: the Mesozoic and Cenozoic plutonic history of Western Colombia. J. Geol. Soc. Lond., 144, p. 893-905.

Aspden, J.A., and Litherland, M., 1992. The geology and Mesozoic collisional history of the Cordillera Real, Ecuador. Tectonophysics, 205, p. 187-204.

Aspden, J., McCourt W., 2002. Late Cretaceous to Tertiary events in the western Cordillera of Ecuador. 5<sup>th</sup> Symposium on Andean Geodynamics (ISAG), Toulouse, IRD ed., Paris, p. 45-48.

Baby, P., Rivadeneira, M., Christophoul, C., and Barragan, R., 1999. Style and timing of deformation in the Oriente Basin of Ecuador. 4<sup>th</sup> Symposium on Andean Geodynamics (ISAG), Göttingen, IRD ed., Paris, p. 68-72.

Baldock, J.W., 1982. Geología del Ecuador, Boletín de Explicación del Mapa geológico de la República del Ecuador. Dirección General de Geología y Minas, Quito, 70 p.

Balkwill, H.R., Rodrigue, G., Paredes, F.I., Almeida, J.P., 1995. Northern part of the Oriente basin, Ecuador: reflexion seismic expression of structures. AAPG Memoir 62, p. 559-571.

Barragan, R., Ramirez, F., and Rodas, J. 1997. Evidence of an Intra Plate "Hot Spot" under the Ecuadorian Oriente Basin during the Cretaceous tectonic evolution. VI Simposio Bolivariano "Exploración Petrolera en las cuencas Subandinas", Cartagena de Indias, Colombia, p. 99-104.

Berggren, W.A., Kent, D.V., Swicher, C.C., and Aubry, M.P., 1995. A revised Cenozoic geochronology and chronostratigraphy. In Berggren, W.A., Kent, D.V., Aubry, M.P., and Hardenbol, J. (eds): Geochronology, time scales and global stratigraphic correlations, Sp. Publ. for Sedimentary Geology, 54, p. 129-212.

Bernet, M., Zattin, M., Garver, J.I., Brandon, M.T., and Vance, J.A., 2001. Steady-state exhumation of the European Alps. Geology, v. 29, p. 35-38.

---

Berrones, G., 1992. Estudio de la subsidencia de la cuenca Oriental Ecuatoriana entre el Jurásico superior y el reciente. CONUEP y Petroecuador ed., tomo II, pp. 937-968. Simposium Nacional, Investigación y Desarrollo Tecnológico en el área de los hidrocarburos, Marzo 11-13/1992, Quito.

Berrones, G., and Cotrina, J., 1996. Estudios de subsidencia y decompactación en el Noreste de la cuenca oriental, implicaciones tectónicas. VII Congreso Ecuatoriano de Geología, Minas, Petróleos y Medio Ambiente, Quito, Octubre de 1996, p. 247-258.

Bes De Berc, S., Baby, P., Soula, J.C., Souris, M., and Rosero, J., 2002. Uplift and active deformation of the Pastaza alluvial fan (Subandean Zone of Ecuador). 5<sup>th</sup> Symposium on Andean Geodynamics (ISAG), Toulouse, IRD ed., Paris, p.85-88.

Bourgeois, J., Egüez, A., Butterlin, J., and De Wever, P., 1990. Evolution Géodynamique de la Cordillère Occidentale des Andes d'Equateur: la découverte de la formation éocène d'Apagua. *Compte Rendus de l'Académie des sciences, Paris*, 311 (II), p. 173-180.

Brandon, M.T., and Vance, J.A., 1992. Fission-track ages of detrital zircon grains: implications for the tectonic evolution of the Cenozoic Olympic subduction complex. *American Journal of Science*, v. 292, p. 565-636.

Brandon, M.T., 1992. Decomposition of fission-track grain age distributions. *American Journal of Science*, v. 292, p. 535-564.

Brandon, M.T., 1996. Probability density plot for fission-track grain-age samples. *Radiation Measurements*, v. 26, p. 663-676.

Brandon, M.T., Roden-Tice, M.K., and Garver, J.I., 1998. Late Cenozoic exhumation of the Cascadia accretionary wedge in the Olympic Mountains, NW Washington State. *Geological Society of America Bulletin*, v. 110, p. 985-1009.

Bristow, C.R., Hoffstetter, R., 1977. Ecuador. *Lexique stratigraphique international*. 2<sup>ème</sup> éd., vol. V, 5a2, CNRS (ed.), Paris, 410 p.

Brozena, J.M., 1986. Temporal and spatial variability of seafloor spreading processes in the Northern South Atlantic. *J. Geophys. Res.*, 91, B1, p. 497-510.

Buitron A., and Vallejo C., 1999. Estudio Estratigráfico Estructural de la Zona Subandina Norte entre 0°25' y 0°40' Sur. Tesis previa a la obtención del título de Ingeniero Geólogo, Escuela Politécnica Nacional, Quito, 154 p.

Burbank, D.W., and Anderson, R.S., 2001. *Tectonic geomorphology*. Blackwell, Oxford, 274 p.



---

Campbell, C.J., 1970. Guide to the Puerto Napo area, Eastern Ecuador. Ecuadorian Geological and Geophysical Society, 39 p. (November).

Canfield, R.W., Bonilla, G., Robbins, R.K., 1982. Sacha oil field of Ecuadorian Oriente. AAPG Bull. v. 66, no. 8, p. 1076-1090.

Carter, A., 1999. Present status and future avenues of source region discrimination and characterization using fission track analysis. *Sedimentary Geology*, 124, p. 31-45.

Carter, A., and Moss, S.J., 1999. Combined detrital-zircon fission-track and U-Pb dating: a new approach to understanding hinterland evolution. *Geology*, v. 27, no. 3, p. 235-238.

Cervený, P.F., Naeser, N.D., Zeitler, P.K., Naeser, C.W., and Johnson, N.M., 1988. History of uplift and relief of the Himalaya during the past 18 million years: evidence from fission-track ages of detrital zircons from sandstones from the Siwalik Group. In Kleinspehn, K.L., and Paola, C., eds., *New perspectives in basin analysis*: New York, Springer-verlag, p. 43-61.

Christophoul, F., 1999. Discrimination des influences tectoniques et eustatiques dans les bassins liés à des zones de convergence: exemples du bassin Subandin d'Équateur. Thèse de doctorat, Université de Toulouse III.

Christophoul, F., Baby, P., Dávila, C., 2002. Stratigraphic response to a major tectonic event in a foreland basin: the Ecuadorian Oriente basin from Eocene to Oligocene times. *Tectonophysics*, 345, p. 281-298.

Colony, R.J., and Sinclair, J.H., 1932. Igneous and metamorphic rocks of Eastern Ecuador. *Annals New York Acad. Sci.*, vol. 34 (August).

Cosma, L., Lapiere, H., Jaillard, E., Laubacher, G., Bosch, D., Desmet, A., Mamberti, M., Gabriele, P., 1998. Pétrographie et géochimie des unités magmatiques de la Cordillere occidentale d'Equateur (0°30'S): implications tectoniques. *Bulletin Société Géologique de France* 169, p. 739– 751.

Daly, M.C., 1989. Correlations between Nazca/Farallon plate kinematics and forearc basin evolution in Ecuador. *Tectonics*, vol. 8, p. 769-790.

Dashwood, M.F., Abbotts, I.L., 1990. Aspects of the petroleum geology of the Oriente Basin, Ecuador. In Brooks, J. (ed), *Classic Petroleum Provinces*, Geological Society Special Publication, no. 50, p. 89-117.

---

Deniaud, Y., 2000. Enregistrement sédimentaire et structural de l'évolution géodynamique des Andes Équatoriennes au cours du Néogène : étude des bassins d'avant-arc et bilans de masse. *Géologie Alpine*, Mémoire H.S n°32.

Dodson, M.H., 1973. Closure temperature in cooling geochronological and petrological systems. *Cont. Min. Pet.* 40, p. 259 - 274.

DeCelles, P.G., and Giles, K.A., 1996. Foreland Basin Systems. *Basin Research*. 8, p. 105-123.

Dumitru, T.A., 1993. A new computer-automated microscope stage system for fission-track analysis. *Nuclear Tracks and Radiation Measurements*, v. 21, p. 575-580.

Ego, F., Sebrier, M., Lavenu, A., Yepes, H., and Equez, 1996. Quaternary state of stress in the northern Andes and the restraining bend model of the Ecuadorian Andes. *Tectonophysics*, 259, p. 101-116.

Egüez, A., 1986. Evolution Cénozoïque de la Cordillère Septentrionale d'Equateur : les minéralisations associées. Unpublished Ph.D thesis, Université Pierre et Marie Curie, Paris.

England, P., Molnar, P., 1990. Surface uplift, uplift of rocks, and exhumation of rocks. *Geology*, v. 19, p. 1173-1177.

Faucher, B., Savoyat, E., 1973. Esquisse géologique des Andes de l'Equateur. *Revue de géographie physique et de géologie dynamique* (2), Vol. XV, fasc. 1-2, p. 115-142, Paris.

Feininger, T., 1975. Origin of petroleum in the Oriente of Ecuador. *Bulletin of the American Association of Petroleum Geologists*, Vol. 57, No. 7, p. 1166-1175.

Feininger, T., Bristow, C.R., 1980. Cretaceous and Paleogene geologic history of coastal Ecuador. *Geologische Rundschau*, vol. 69, Part. 3, p. 849-874.

Feininger, T., Silberman, M.L., 1982. K-AR geochronology of basement rocks on the Northern Flank of the Huancabamba deflection, Ecuador. U.S Geological Survey, open-file report, 21 p, Menlo Park, p. 82-206.

Fleischer, R.L., Price, P.B., and Walker, R.M., 1975. Nuclear tracks in solids – principles and applications. Berkeley, University of California Press, 605 p.

Galbraith, R.F., 1981. On statistical models for fission track counts. *Math. Geol.*, 13, p. 471-478; Reply 485-488.

---

Galbraith, R.F., and Green, P.F., 1990, Estimating the component ages in a finite mixture: Nuclear Tracks and Radiation Measurements, v. 17, p. 197-206.

Galbraith, R.F., 1990. The radial plots: graphical assessment of spread in ages. Nuclear tracks and Radiation Measurements, 17, p. 207-214.

Galbraith, R.F., and Laslett, G.M., 1993. Statistical models for mixed fission track ages. Nucl. Tracks Radiat. Meas., 21, p. 459-470.

Gallagher, K., 1995. Evolving thermal histories from fission-track data. Earth Plan. Sci. Lett., v. 136, p. 421-435.

Gansser, A., 1973. Fact and theories on the Andes. J. Geol. Soc. Lond., 129, p. 93-131.

Garver, J.I., Brandon, M.T., Roden-Tice, M., and Kamp, P.J.J., 1999. Erosional denudation determined by fission-track ages of detrital apatite and zircon. In Ring, U., Brandon, M.T., Willett, S., and Lister, G., eds, Exhumation Processes: Normal Faulting, Ductile Flow, and Erosion, Geological Society of London Special Publication, v. 154, p. 283-304.

Gleadow, A.J.W., Hurford, A.J., and Quaife, R.D., 1976. Fission-track dating of zircon: Improved etching techniques. Earth Planet. Sci. Lett., 33, p. 273-276.

Gradstein, F.M., Agterberg, F.P., Ogg, J.G., Hardenbol, J., Van Veen, P., Thierry, J., and Huang Zehui, 1995. A Triassic, Jurassic and Cretaceous time scale. In Berggren, W.A., Kent, D.V., Aubrey, M.-P., and Hardenbol, J., eds., Geochronology, Time Scales and Global Stratigraphic Correlation: SEPM (Society for Sedimentary Geology) Special Publication No. 54, p. 95-126.

Green, P.F., 1981. A new look at statistics in fission-track dating. Nuclear Tracks and Radiation Measures, v. 5, p. 77-86.

Green, P.F., Duddy, I.R., Gleadow, A.J.W., Tingate, P.R., and Laslett, G.M., 1986. Thermal annealing of fission tracks in apatite: A qualitative description. Chemical Geology, v. 59, p. 237 - 253.

Green, P.F., Duddy, I.R., Laslett, G.M., Hegarty, K.A., Gleadow, A.J.W., Lovering, J.F., 1989. Thermal annealing of fission tracks in apatite - Qualitative modelling techniques and extensions to geological timescales. Chem. Geol. 79, 155-182.

Gutscher, M-A., Malavielle, J., Lallemand, S., and Collot, J-Y., 1999. Tectonic segmentation of the North Andean margin: impact of the Carnegie Ridge collision. Earth and Planetary Science Letters, v. 168, p. 255-270.

---

Hall, M.L., and Calle, J., 1982. Geochronological control for the main tectonic-magmatic events of Ecuador. *Earth Science Review*, 18, p. 215-239.

Harman, R., Gallagher, K., Brown, R., and Raza, A., 1998. Accelerated denudation and tectonic/geomorphic reactivation of the cratons of northeastern Brazil in the Late Cretaceous. *Journal of geophysical Research*, vol. 103, No. B11, pp. 27091-27105.

Hasebe N., Tagami T. and Nishimura S., 1994. Towards zircon fission-track thermochronology: Reference framework for confined track length measurements. *Chemical Geology, Isotope Geoscience Section*, 112, p. 169-178.

Heller, P.L., Angevine, C.L., Winslow, N.S., and Paola, C., 1988. Two-phase stratigraphic model of foreland basin development. *Geology*, v. 16, p. 501-504.

Herbert, H., 1977. Petrochimie und Ausgangmaterial von Grünschiefern aus der E-cordillere Ecuadors [Petrochemistry and origin of the greenschist from the Eastern Cordillera of Ecuador]. *Fortschritte der Mineralogie*, vol. 55, No. 1.

Herbert, H., and Pichler, H., 1983. K-Ar ages of rocks from the Eastern Cordillera of Ecuador. *Zeitschrift der deutschen Geologischen Forschungen*, vol. 134, p. 483-493.

Hey, R.N., 1977. Tectonic evolution of the Cocos-Nazca spreading center. *Geol. Soc. Am. Bull.*, 88, p. 1414-1420.

Higley, D., 2000. The Putumayo-Oriente-Marañon Province of Colombia, Ecuador, and Peru\Mesozoic-Cenozoic and Paleozoic Petroleum Systems. U.S.G.S Digital Data Series 63, 40 p.

Hughes, R.A., and Pilatasig, L.F., 2002. Cretaceous and Tertiary terrane accretion in the Cordillera Occidental of the Andes of Ecuador. *Tectonophysics*, 35 (1-4), p. 29-48.

Hungerbühler; D., Steinmann, M., Winkler, W., Seward, D., Egüez, A., Peterson, D.E., and Hammer, C., 2002. Neogene stratigraphy and Andean geodynamics of southern Ecuador. *Earth-Science Reviews*, 57 (1-2), p. 75-124.

Hurford, A.J, Fitch, M., and Jäger, E., 1984. Resolution of the age structure of the detrital zircon populations of two Lower Cretaceous sandstones from the Weald of England by fission track dating. *Geol. Mag.*, 121, pp. 269-277.

Hungerbühler, D., Steinman, M., Winkler, W., Seward, D., Egüez, A., Peterson, D.E., Helg, U., and Hammer, C., 2002. Neogene stratigraphy and Andean geodynamics of Southern Ecuador. *Earth Science Reviews*, 46p.

---

Hurford, A.J., and Green, P.F., 1983. The zeta calibration of fission-track dating. *Isotope Geoscience*, v. 1, p. 285-317.

Hurford, A.J., and Carter, A., 1991. The role of fission track dating in discrimination of provenance. In Morton, A.C., Todd, S.P., and Haughton, P.D.W. (eds.), *Developments in Sedimentary Provenance Studies*. Geological Society Special Publication, No. 57, p. 67-78.

Jaillard, E., Soler, P., Carlier, G., and Mourier, T., 1990. Geodynamic evolution of the northern and Central Andes during early to middle Mesozoic times: a Tethyan model. *J. Geol. Soc. Lond.*, vol. 147, Part 6, p. 1009-1022.

Jaillard, E., Soler, P., 1995. Cretaceous to Early Paleogene tectonic evolution of the northern Central Andes (0-18°S) and its relation to geodynamics. *Tectonophysics*, 259, p. 41-51.

Jaillard, E., Benitez, S., Mascle, G., 1997 (a). Les deformations paléogènes de la zone d'avant-arc sud-équatorienne en relation avec l'évolution géodynamique. *Bull. Soc. France*, t. 168, n°4, p. 403-412.

Jaillard, E., 1997 (b). Síntesis estratigráfica del cretáceo y paleógeno de la cuenca oriental del Ecuador. *Convenio ORSTOM-Petroproducción*, Quito, 164 p.

Jaillard, E., Laubacher, G., Bengston, P., Dhondt, A., and Bulot, L., 1999. Stratigraphy and evolution of the Cretaceous forearc "Celica-Lancones Basin" of Southwestern Ecuador. *Journal of South American Earth Sciences*, 12, p. 51-68.

Jaillard, E., Hérail, G., Monfret, T., Diaz-Martinez, E., Baby, P., Lavenu, A., and Dumont, J.F., 2000. Tectonic evolution of the Andes of Ecuador, Peru, Bolivian and northernmost Chile, in Cordani, U.G., Milani, E.J., Thomaz-Filo, A., Campos, D.A., eds., *Tectonic evolution of South America*, p. 481-559, Rio de Janeiro.

Jaillard, E., Lapierre, H., Lamberti, M., 2001. Oceanic terranes of western Ecuador: accretion dates and possible origin. In the workshop held in Leicester (UK): *The Geochemistry of the Caribbean plateau and Cretaceous island arc terranes, and their implications for the geodynamics of the Caribbean*, 23-24 April 2001.

Jaillard, E., Hérail, G., Monfret, T., and Wörner, G., 2002 (a). Andean geodynamics: main issues and contributions from the 4th ISAG, Göttingen. *Tectonophysics* 345, p. 1-15.

---

Jaillard, É., Ordoñez, M., Jiménez, N., Suárez, J. & Toro, J., 2002 (b). Litho- and biostratigraphy of the Late Cretaceous-Paleogene detrital units of the Western Cordillera of Ecuador (0-4°S). 3rd Europ. Meet. Paleont. Stratigr. Latin Amer.-EMPSLA, Toulouse 2002, Ext. Abstracts Vol., p. 63-66.

Johnsson, M.J., 1993. The system controlling the composition of clastic sediments. In Johnsson, M.J., and Basu, A. (editors), Processes controlling the composition of clastic sediments, Geological Society of America (GSA), Special Paper, 283, pp. 1-19.

Jordan, T., 1995. Retroarc foreland and related basins, in Busby, C.J., and Ingersoll, R.V., eds., Tectonics of sedimentary basins, Blackwell Science (579 pp), p. 331-362.

Kennerley, J.B., 1971. Geology of the Llanganates area, Ecuador. Institute of Geological Sciences (Overseas division), London, Unpublished report 21.

Kennerley, J.B., 1973. Geology of the Loja Province, Southern Ecuador. Institute of Geological Sciences (Overseas division), London, Unpublished report 23, 17 pp.

Kennerley, J.B., 1980. Outline of the Geology of Ecuador. Overseas Geol., Miner. Resour., vol. 55, 17 p, H.M.S.O., London.

Kerr, A.C., Aspden, J.A., Tarney, J., and Pilatasig, L., 2002 in press. The nature and provenance of accreted oceanic terranes in western Ecuador: geochemical and tectonic constraints. J. Geol. Soc. Lond.

Lapierre, H., Bosch, D., Dupuis, V., Polvé, M., Maury, R.C., Hernandez, J., Monié, P., Yeghicheyan, D., Jaillard, E., Tardy, M., Mercier de Lépinay, B., Mamberti, M., Desmet, A., Keller, F., Sénebier, F., 2000. Multiple plume events in the genesis of the peri-Caribbean Cretaceous oceanic plateau province. Journal of Geophysical Research 105, p. 8403–8421.

Laslett, G., Green, P.F., Duddy, I.R., and Gleadow, A.J.W., 1987. Thermal annealing of fission tracks in apatite. Chem. Geol., v. 65, no.1, p. 1-13.

Lister, G.S., Baldwin, S., 1996. Modelling the effect of arbitrary P-T-t histories on argon diffusion in minerals using the Mac Argon program for the Apple Macintosh. Tectonophysics, 253, p. 83 - 109.

Litherland, M., Aspden, J.A., and Jemielita, R.A., 1994. The metamorphic belts of Ecuador. British Geological Survey, Overseas Memoir, 11, 147 pp.

Litherland, M., Egüez, A., and Zamora, A., 1993. Mapa geológico del Ecuador, escala 1: 1 000 000. Cogidem, BGS, Quito.

---

Lonsdale, P., Klitgord, P.D., 1978. Structure and tectonic history of the eastern Panama Basin. *Geol. Soc. Am. Bull.*, 89, p. 981-999.

McDougall, I., Harrison, T.M., 1999. *Geochronology and thermochronology by the  $^{40}\text{Ar}/^{39}\text{Ar}$  method*. Oxford monographs on Geology and Geophysics, Oxford University Press, 282 pp.

Mange, M.A., Maurer, H.F.W., 1992. *Heavy minerals in colour*. London, Chapman and Hall, 147 p..

Marksteiner, R., and Aleman, A.M., 1996. Petroleum systems along the foldbelt associated to the Marañon-Oriente-Putumayo foreland basins. *American Association of Petroleum Geologists Bulletin*, v. 80, no. 8, p. 1311.

Moore, M.A, and England, P.C, 2001. On the inference of denudation rates from cooling ages of minerals. *Earth and Planetary Science Letters*, 185, p. 265-284.

Morton, A.C., 1984. Stability of detrital heavy minerals in tertiary sandstones of the North Sea Basin. *Clay Minerals*, v. 19, p. 287-308.

Morton, A.C., Johnsson, M.J., 1993. Factors influencing the composition of detrital heavy mineral suites in Holocene sands of the Apure River drainage basin, Venezuela. In Johnsson, M.J., and Basu, A. (editors), *Processes controlling the composition of clastic sediments*, Special Paper, Geological Society of America (GSA), 284, p. 171-185.

Naeser, C.W., 1979. Thermal history of sedimentary basins: fission-track dating of subsurface rocks. In P.A. Scholle and P.R. Schluger, eds., *Aspect of diagenesis: SEPM Special Publication*, 26, p. 109-112.

Naeser, C.W., Crochet, J-Y., Jaillard, E., Laubacher, G., Mourier, T., and Sigé, B., 1991. tertiary fission-track ages from the Bagua syncline (Northern Peru): Stratigraphic and tectonic implications. *Journal of South American Earth Sciences*, 4, p. 61-71.

Najman, Y.M.R., Pringle, M.S., Johnson, M.R.W., Robertson, A.H.F., and Wijbrans, J.R., 1997. Laser  $^{40}\text{Ar}/^{39}\text{Ar}$  dating of single detrital muscovite grains from early foreland-basin sedimentary deposits in India; implications for early Himalayan evolution. *Geology*, v.25, p. 535-538.

Najman, Y.M.R., Pringle, M.S., Godin, L., Grahame, O., 2001. Dating of the oldest continental sediments from the Himalayan foreland basin. *Nature*, v. 410, p. 194-197.

---

Noblet, C., Lavenu, A., and Schneider, F., 1988. Etude géodynamique d'un bassin intramontagneux tertiaire sur décrochements dans les Andes du sud de l'Equateur: L'exemple du bassin de Cuenca, *Géodynamique*, v. 3, p. 117-138.

Norabuena, E.O., Dixon, T.H., Stein, S., Harrison, C.G.A., 1999. Decelerating Nazca-South America and Nazca-Pacific plate motions. *Geophys. Res. Lett.*, 26, p. 3405-3408.

Pardo-Casas, F., Molnar, P., 1987. Relative motion of the Nazca (Farallon) and South America plate since late Cretaceous time. *Tectonics*, 6, p. 233-248.

Pasquarè, G., Tibaldi, A., and Ferrari, L., 1990. Relationships between plate convergence and tectonic evolution in the Ecuadorian active thrust belt. In *Critical Aspects of the Plate Tectonics Theory*, vol. 1, edited by V. Belousov, et al., Theophrastus, Athens, p. 356-387

Pecora, L., Jaillard, E., Lapierre, H., 1999. Paleogene accretion and dextral displacement of an oceanic terrane in northern Peru. *Comptes Rendus de l'Académie des Sciences, Paris, série IIa* 329 (6), p. 389– 396.

Pichler, H., and Aly, S., 1983. Neue K/Ar-Alter plutonischer Gesteine in Ecuador [New K/Ar dates of plutonic rocks in Ecuador.]. *Zeitschrift der Deutschen Geologischen Gesellschaft*, Vol. 134, p. 495-506.

Pilger, R.H., 1984. Cenozoic plate kinematics subduction and magmatism: South American Andes. *J. Geol. Soc. Lond.*, 141, p. 793-802.

Pindell, J.L., Tabbutt, K., 1995. Mesozoic-Cenozoic Andean paleogeography and regional Controls on hydrocarbons systems. In Tankard, A.J., Suárez S, R., Welsink, H.J., *Petroleum basins of South America*, AAPG Memoir, 62, p. 101-128.

Pratt, W., Duquez, P., Poncet, M., 2002. Orthogonal deformation in the eastern Andes of Ecuador. 5<sup>th</sup> Symposium on Andean Geodynamics (ISAG), Toulouse, IRD ed., Paris, p. 485-488.

Price, P.B. and Walker, R.L., 1962a. Observation of charged particle tracks in solids. *J. Appl. Phys.*, Vol. 33, p. 3400 - 3406.

Price, P.B. and Walker, R.L., 1962b. Observation of fossil particle tracks in natural micas. *Nature*, Vol. 196, p. 732 - 734.

Rangel, A., Parra, P., and Nino, C., 2000. The La Luna Formation; chemostratigraphy and organic facies in the Middle Magdalena Basin. In: *Advances in organic*



geochemistry 1999; proceedings of the 19th international meeting on Organic geochemistry. *Organic Geochemistry*. 31, 12, p. 1267-1284.

Reiners, P.W., 2002. (U-Th)/He chronometry experiences a renaissance. *Eos, Transactions, American Geophysical Union*. 83; 3, Pages 21, p. 26-27.

Rivadeneira, M., Baby, P., 1999. La Cuenca Oriente: estilo tectónico, etapas de deformación y características geológicas de los principales campos de Petroproducción. Convenio ORSTOM-Petroproducción, Quito, 89 p.

Romeuf, N., Aguirre, L., Soler, P., Féraud, G., Jaillard, E., and Ruffet, G., 1995. Middle Jurassic volcanism in the Northern and Central Andes. *Revista geológica de Chile, Santiago*, 22, p. 245-259.

Romeuf, N., Münch, P., Soler, P., Jaillard, E., Pik, R., Aguirre, L., 1997. Mise en évidence de deux lignées magmatiques dans le volcanisme du Jurassique inférieur de la Zone subandine équatorienne. *C.R. Acad. Sci. Paris*, t. 324, série II a, p. 361-368.

Rosero-Castillo, J.E., 1997. Estructuras y etapas de deformación de la zona subandina en el nor Oriente Ecuatoriano (entre 0°10 'S y 0°50'S). Tesis previa a la obtención del título de Ingeniero Geólogo, Escuela Politecnica Nacional, Quito, 87 p.

Rosero-Revelo, M.R., 1999. Análisis tectono-sedimentaria y interpretación geodinámica de las secuencias Oligocenas y Neogenas de la Cuenca Oriente Ecuatoriana. Tesis de grado, Universidad Central del Ecuador, 103 pp.

Sambridge, M.S., and Compston, W., 1994. Mixture modelling of multi-components data sets with application to ion-probe zircon ages. *Earth Planet. Sci. Lett.*, 128, p. 373-390.

Sauer, W., 1965. *Geología del Ecuador [Geology of Ecuador]*. Quito, Ministerio de Educación.

Shanmugam, G., Poffenberger, M., and Toro Alava, J., 2000. Tide-dominated estuarine facies in the Hollin and Napo ("T" and "U") formations (Cretaceous), Sacha Field, Oriente basin, Ecuador. *AAPG Bulletin*, v. 84, No. 5, p. 652-682.

Silk, E.C.H. and Barns, R.S., 1959. Examination of fission fragment tracks in an electron microscope. *Phil. Mag.*, Vol. 4, p. 970 - 971.

Spiegel, C., Kuhlmann, J., Dunkl, I., Frisch, W., Von Eynatten, H., and Balogh, K., 2001. The erosion history of the Central Alps: evidence from zircon fission track data of the foreland basin sediments. *Terra Nova*, vol. 12, p. 163-170.

Spikings, R., Seward, D., Winkler, W., Ruiz, G., 2000. Low-temperature thermochronology of the northern Cordillera Real, Ecuador: tectonic insights for zircon and apatite fission track analysis. *Tectonics*, 19 (4), p. 649– 668.

Spikings, R.A., Winkler, W., Seward, D., and Handler, R., 2001. Along-strike variations in the thermal and tectonic response of the continental Ecuadorian Andes to the collision with heterogeneous oceanic crust. *Earth and Planetary Science Letters*, v. 186, p. 57–73.

Spikings, R.A., W. Winkler, Hughes, R.A., and R. Handler (2002, submitted). Thermochronology of the Cordillera Occidental and the Amotape Complex, Ecuador: unravelling the accretionary and post-accretionary history of the Northern Andes.

Stam, B., Gradstein, F.M., Lloyd, P., and Gillis, D., 1987. Algorithms for porosity and subsidence history.: *Computers and Geosci.*, 13, p.317-349.

Steinmann, M., Hungerbühler, D., Seward, D., and Winkler, W., 1999. Neogene tectonic evolution and exhumation of the southern Ecuadorian Andes: a combined stratigraphy and fission-track approach. *Tectonophysics*, v. 307, p. 255-276.

Steckler, M.S., and Watts, A.B., 1978. Subsidence of the Atlantic-type continental margin off New York. *Earth. plat. Sci. Letters*, 41, p. 1-13.

Tagami, T., Galbraith, R.F., Yamada, R. and Laslett, G.M., 1998. Revised annealing kinetics of fission tracks in zircon and geological implications. In *Advances in Fission-Track Geochronology*, edited by P. Van den Haute and F. de Corte, Solid Earth Sciences Library, Dordrecht, Kluwer Academic Publishers, 10, p. 99 -112.

Thomas, G., Lavenu, A., and Berrones, G., 1995. Évolution de la subsidence dans le Nord du bassin de l'Oriente équatorien (Crétacé supérieur à actuel). *C.R. Acad. Sci. Paris*, t. 320, série II a, p. 617 à 624.

Tobler, S., 2001, *Geologie des intermontanen Beckens von Chota (Pliozän, Nordecuador)-Westteil.* (MSc. Thesis). Zürich, Eidgenössische Technische Hochschule, 102 p.

Tschopp, H.J., 1948. Geologische Skizze von Ekuador. *Bull. Ass. Suisse Géol. et Ing. du Pétrole*, Vol. 15, No. 48, p. 14-45.

Tschopp, H.J., 1953. Oil exploration in the Oriente of Ecuador. *AAPG Bull.* 37, p. 2303-2347.

---

Valdez-Pardo, A.M., 1997. Reinterpretación sedimentológica, estratigráfica de la Formación Tiyuyacu y su relación con la tectónica del Terciario inferior. Tesis de grado, Universidad Central del Ecuador, 141, 5 annexes.

Vallejo, C., Hochuli, Winkler, W., 2002. Particulate organic matter analyses and oil potential of the Napo group, Subandean Zone, Ecuador. 5<sup>th</sup> Symposium on Andean Geodynamics (ISAG), Toulouse, IRD ed., Paris, p. 661-664.

Vallejo C., Hochuli P.A., Winkler, W. von Salis K., 2002 (submitted). Palynological and sequence stratigraphic analysis of the Napo Group, Subandean Zone, Ecuador.

Villagómez, R. Jaillard, E., Bulot, L., Rivadeneira, M., and Vera, R., 1996. The Aptian-Late Albian marine transgression in the Oriente basin of Ecuador. 3<sup>rd</sup> International Symposium on Andean Geodynamics-ISAG, Saint-Malo, Orstom ed., Paris, p. 521-524.

Wagner, G.A., Miller, D.S., Jäger, E., 1979. Fission track ages on apatite of Bergell rocks from the central Alps and Bergell boulders in Oligocene sediments. Earth Planet. Sci. Lett., 45, p. 355-360.

Wasson, T., and Sinclair, J.H., 1927. Geological Explorations East of the Andes in Ecuador. Bull. Amer. Assoc. Petrol. Geol., vol. 11, No. 12, p. 1253-1281.

White, H.J., Skopec, R.A., Ramirez, F.A., Rodas, J.A., Bonilla, G., 1995. Reservoir characterization of the Hollin and Napo Formations, Western Oriente Basin, Ecuador. In Tankard, A.J., Suárez S, R., Welsink, H.J., Petroleum basins of South America. AAPG Memoir, 62, p. 573-596.

Willett, S.D., Brandon, M.T., 2002. On steady states in mountain belts. Geology, v. 30, no. 2, p. 175-178.

Winkler, W., 1988. Mid-to early Late Cretaceous flysch and melange formations in the western part of the Eastern Alps; palaeotectonic implications. Jahrbuch der Geologischen Bundesanstalt Wien, 131; 2, p. 341-389.

Winkler, W., Spikings, R.A., Villagomez, D., Egeuz, A., Abegglen, P., and Tobler, S., 2002. The Chota basin and its significance for the formation of the Inter-Andean valley in Ecuador. 5<sup>th</sup> Symposium on Andean Geodynamics (ISAG), Toulouse, IRD ed., Paris, p. 705-708.

Wolf, T., 1892. Geografía y Geología del Ecuador [Geography and geology of Ecuador]. Leipzig: Brockhaus.

Yim, W.W.-S., Gleadow, A.J.W., and Moort, J.C., 1985. Fission track dating of alluvial zircons and heavy mineral provenance in Northeast Tasmania. *J. Geol. Soc. Lond.*, 142, p. 351-356.

Zambrano, I., Ordoñez, M., Jiménez, N., 1999. Micropaleontología de 63 muestras de afloramientos de la Cuenca Oriental Ecuatoriana. Informe técnico No. 016-PPG-99, LABOGEO, Petroproducción, distrito de Guayaquil.

Zeitler, P.K., Johnson, N.M., Briggs, N.D., and Naeser, C.W., 1986. Uplift history of the NW Himalaya as recorded by fission-track ages on detrital Siwalik zircons. In Huang Jiqing ed., *Proceedings of the symposium on Mesozoic and Cenozoic geology in connection of the 60th anniversary of the Geological Society of China*, Geol. Publ. House, Beijing, China, p. 481-496.

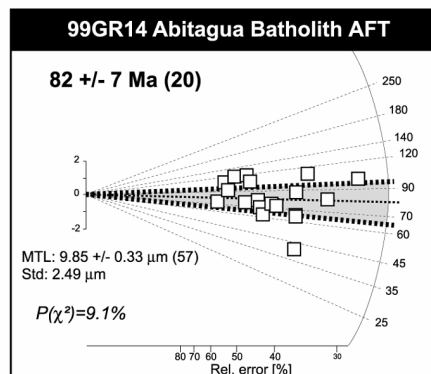
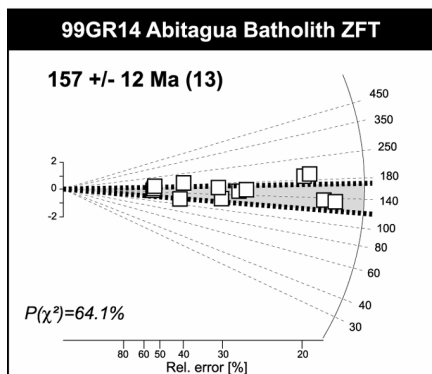
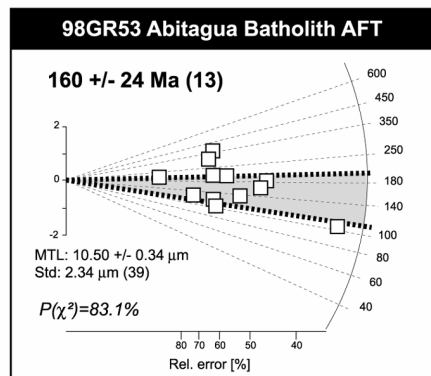
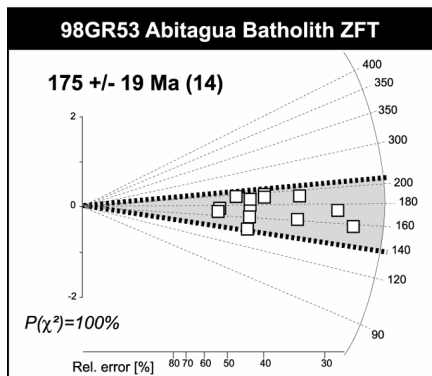
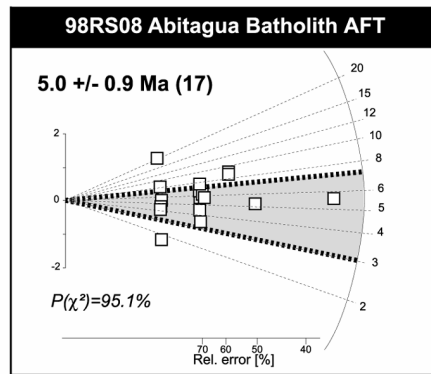
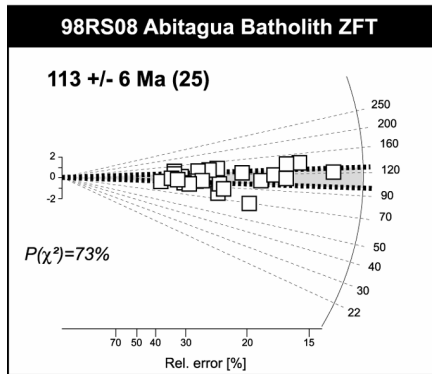
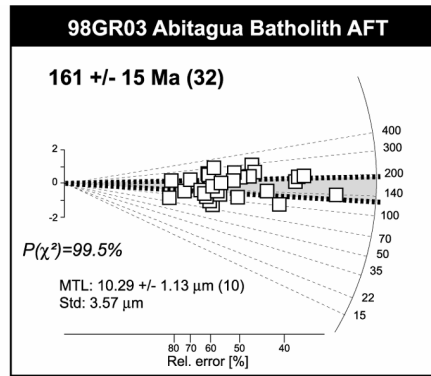
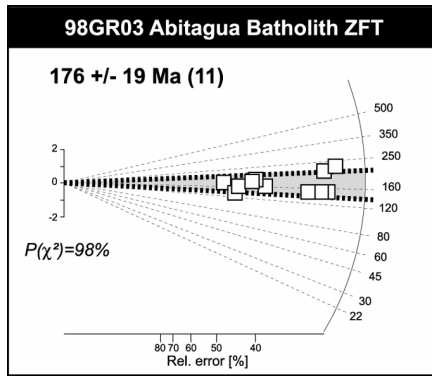
## **Appendices**

Sample no.	UTM	UTM	Map sheet	Formation	Location	Rock type	Altitude
1998							
98RS01	184110	9965750	Santa Rosa de Quijos	Paradalarga	Rio Oyocachi	Rhyolite	1650
98GR02	191210	9968100	Santa Rosa de Quijos	Napo	El Chaco	Immature glauconitic SS	1600
98GR03	185490	9931363	Cosanga	Abitagua	Huacamayos	Feldspar phyrlic granite	2150
98GR05	187585	9921730	Sardinas	Hollin	Cosanga-Tena	Quartz-arenite	1150
98RS06	160050	9842950	Mera	Napo	Mirador Anticline	Micro-conglomerate	1240
98RS08	171533	9880887	Puerto Napo	Abitagua	Tena - Latacunga	Medium granite	530
98RS10	199500	9979125	Las Palmas	MISAHUALLI	Rio Salado-Rio Coca	Ep-K feldspar rhyolite	1350
98GR16	176850	9883480	Puerto Napo	Chambira	Talag	Conglomerate with Qtz pebbles	590
98GR19	196723	9977438	Las Palmas	Misahualli	Rio Salado-Rio Coca	Andesite	1550
98GR28	183856	9822555	Vera Cruz	Arajuno	Puyo-Macas	Coarse SS	700
98GR29	195117	9921137	Pavayacu	Misahualli	Rio Hollin	Ash	1225
98GR31	195117	9921137	Pavayacu	Misahualli	Rio Hollin	Volcanic breccias	1225
98GR33	195117	9921137	Pavayacu	Misahualli	Rio Hollin	Massive pumice tuff	1225
98GR34	196300	9922900	Pavayacu	Misahualli?	Rio Hollin-Chico	Rhyolite	990
98GR37	232689	9999867	Atenas	Tena	La Delicia	Red siltstone	500
98GR41	224435	9998965	Atenas	Napo	San Francisco-La Delicia	Qtz-feldspar arenite	1100
98RS41	145400	9843910	Mera	Abitagua	Rio Zuñag	Kspar phyrlic granite	1270
98RS44	151200	9840200	Mera	Abitagua	Cumanda-La Delicia	Granite	1200
98GR50	212376	9989981	Volcan El Reventador	Hollin	Baeza-Lumbaqui	Quartz arenite	1400
98GR51	212376	9989981	Volcan El Reventador	Misahualli	Baeza-Lumbaqui	Diorite	1400
98GR52	202162	9981039	Volcan El Reventador	Misahualli	Baeza-Lumbaqui	Kfeld-plag-hbl-rhyolite	1375
98GR53	201500	9978500	Volcan El Reventador	Abitagua	Rio Coca	Diorite (Pyr-Chl-Ep)	1350
98GR57	196101	9973320	Las Palmas	Napo	Baeza-Lumbaqui	Glauconitic sandstone	1800
98GR69	193292	9919767	Sardinas	Hollin	Narupa	Coarse SS with blue Qtz	1150
98GR81	185967	9896510	Tena	Tiyuyacu	Tena	Conglomerate with Qtz pebbles	600
98GR83	185967	9896510	Tena	Tena	Tena	Red-green biopert-SS	600

Appendix 3.1: Location and description of samples

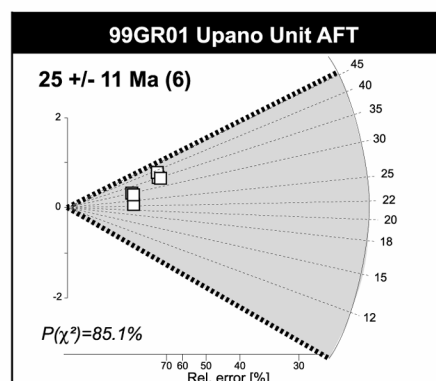
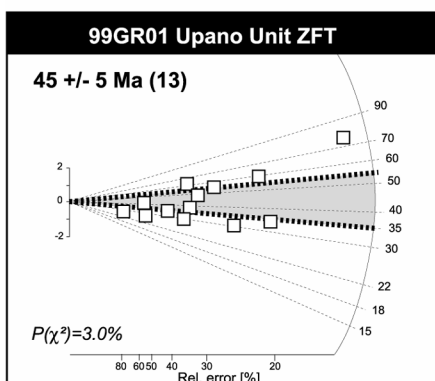
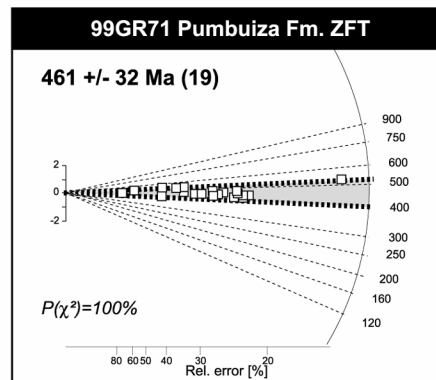
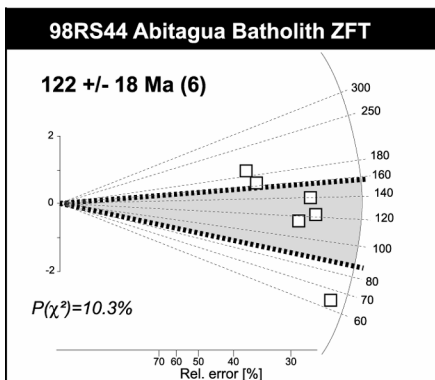
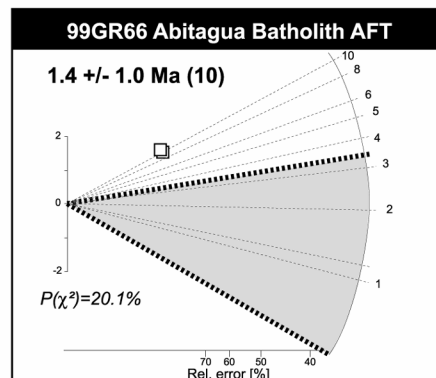
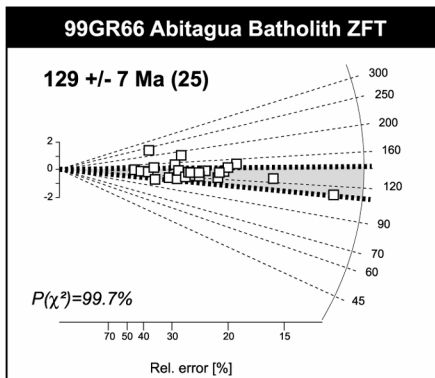
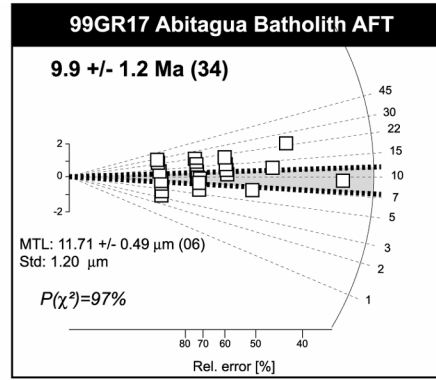
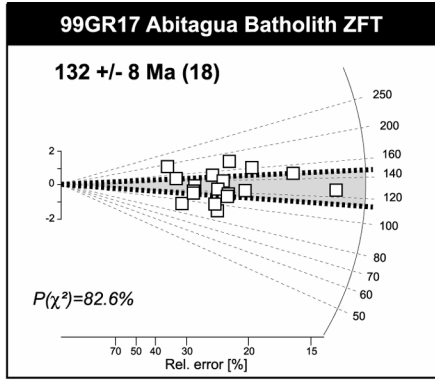
Sample no.	UTM	UTM	Map sheet	Formation	Location	Rock type	Altitude
1999							
99GR01	172910	9950200	Baeza	Upano	St Fermin	Augengneiss	2040
99GR04	173743	9949289	Baeza	Paradalarga	Rio Quijos	Meta-volcaniclastics (green-schist)	2015
99GR08	175694	9948458	Baeza	Paradalarga	Baeza	Meta-volcaniclastics (green-schist)	1880
99GR09	179650	9953800	Baeza	Paradalarga	Rio Sardinas Chico	Meta-volcaniclastics (green-schist)	2120
99GR14	182703	9899563	Tena	Abitagua	Rio Inchiagua	Monzogranite	700
99GR16	184650	9909050	Sardinas	Misahualli	Estera sardina	Rhyolite	1020
99GR17	186192	9923329	Sardinas	Abitagua	E-foothills Huacamoyos	Mica-rich granite (Py)	1330
99GR22	223150	9918125	Loreto	Hollin	Rio Tucsi	Sandstone	610
99GR36	244995	N0003650	Lumbaqui	Tiyuyacu	Cerro lumbaqui	Conglomerate	560
99GR44	189343	9880298	Puerto Napo	Tiyuyacu	Road Tena-Puyo	Fine sandstone	500
99GR47	225183	N0349551	Puerto Libre	Misahualli	Rio Chingual	Volcaniclastic	800
99GR52	242139	N0004314	Lumbaqui	Tiyuyacu	Cerro Lumbaqui	SS with white mica	840
99GR64	149490	9936204	Mera	Misahualli	Rio Gringo	feldspar-pyr volcanic	1350
99GR65	149450	9936250	Mera	Hollin	Rio Gringo	Ind. Qtz arenite with blue Qtz	1370
99GR66	149310	9836286	Mera	Abitagua	Rio Gringo	Granodiorite-Hb	1400
99GR67	150510	9936429	Mera	Tena	Rio Gringo	Cryst fine green SS	1320
99GR71	150700	9937050	Mera	Pumbuiza	Rio Gringo	Muscovite rich-SS	1220
99GR72	151530	9938102	Mera	Mera	Rio Gringo	Conglomerate	1160
99GR73	144450	9844850	Mera	Hollin	Rio Topo	Blue Qtz arenite	1280
99GR81	246500	N0009350	Lumbaqui	Orteguaza	Rio Aguarico	Conglomerate	400
99GR84	196290	9923500	Pavayacu	Misahualli	Rio Hollin Chico	Ignimbrite	1040
2000							
00GR01	154600	9837582	Mera	Mesa	Mera	Immature sandy matrix	1084
00GR02	189475	9879828	Puerto Napo	Chalcana	Road Tena-Puyo	Arkosic siltstone	571
00GR03	212561	9886172	Puerto Misahualli	Chalcana	P. Misahualli, Rio Napo	Sandstone	374
00GR04	216517	9882580	Puerto Misahualli	Arajuno	P. Misahualli, Rio Napo	Arkosic arenite (Bt, Hb, VMM)	364
00GR05	-	-	Puerto Misahualli	Quaternary	Rio Napo	River gravel	357
00GR06	184083	9820200	Vera Cruz	Mesa	Puyo-Macas	Lithic arenite	1018

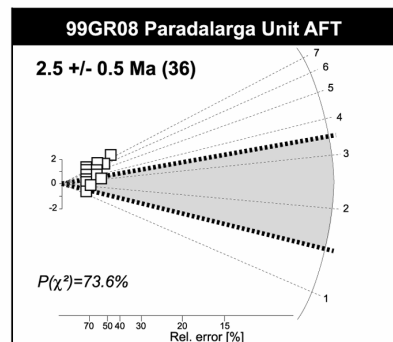
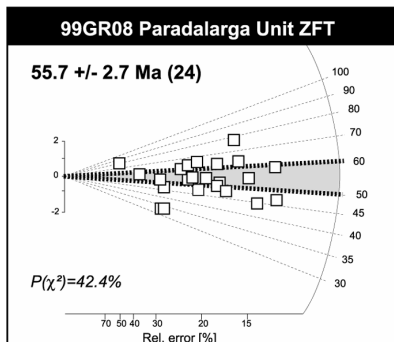
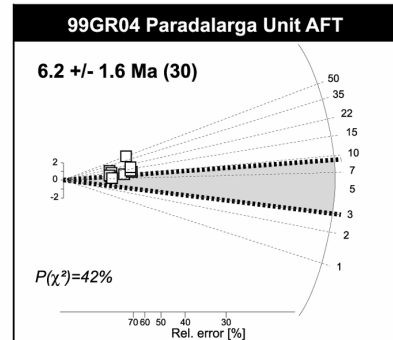
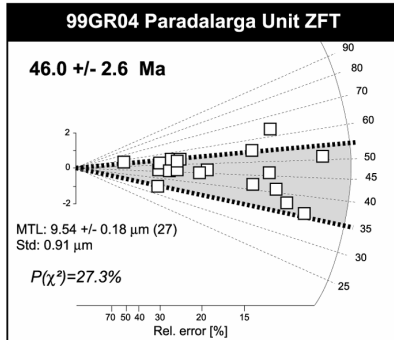
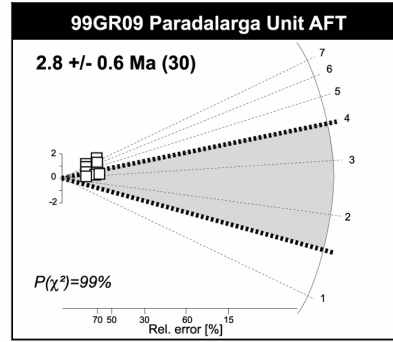
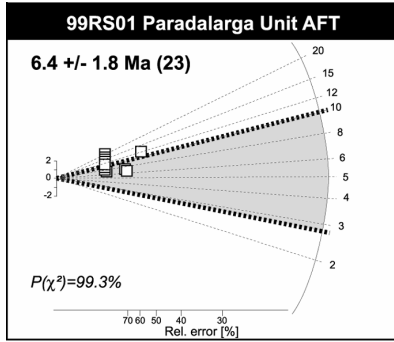
Appendix 3.1 Continued



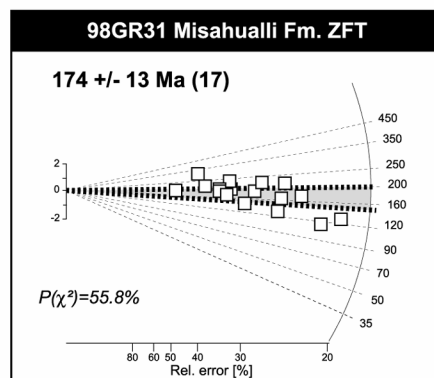
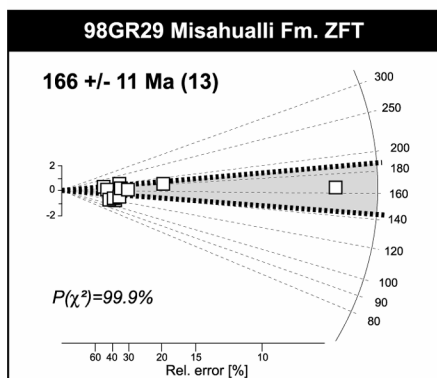
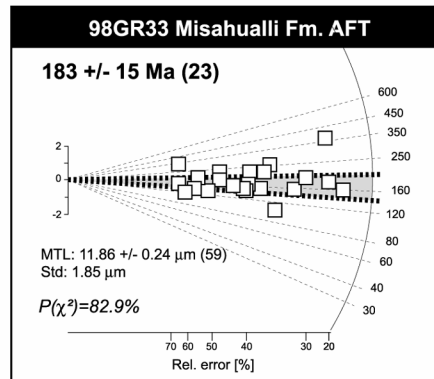
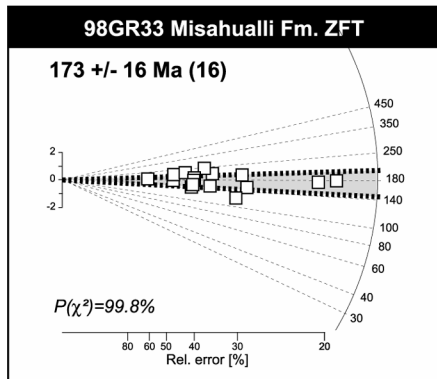
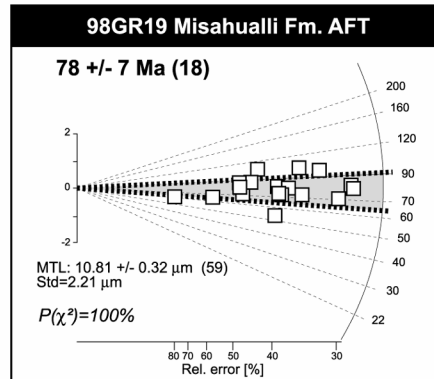
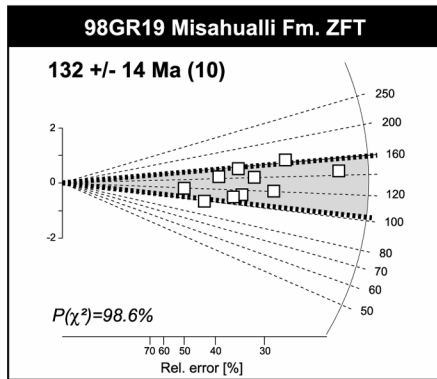
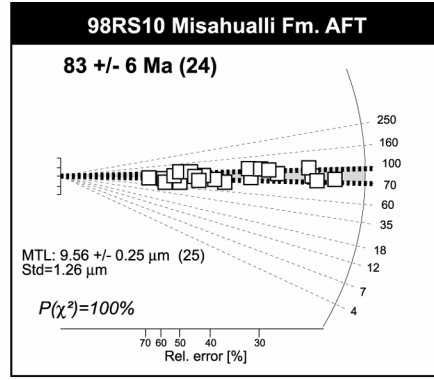
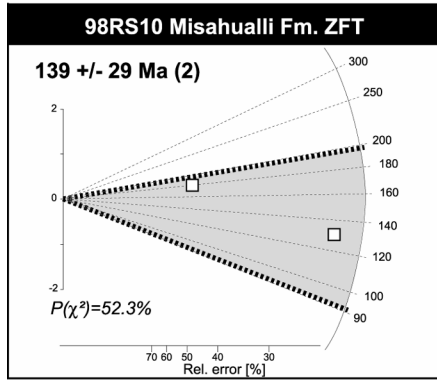
Appendix 3.2: Radial plots (Gailbraith, 1990) for fission-track age determinations of the basement (and assimilated) of the northern SAZ and Pastaza depression. In brackets is the number of counted grains or track lengths. ZFT: Zircon Fission-Track; AFT: Apatite Fission-Track. MTL: Mean Track length; Std: Standard deviation.  $P(\chi^2)$  (see section 4.2.1.1).

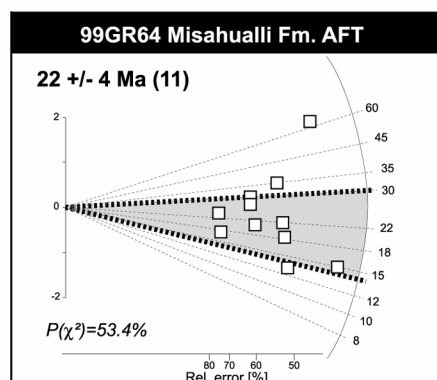
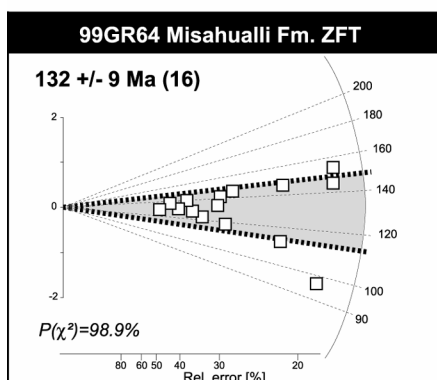
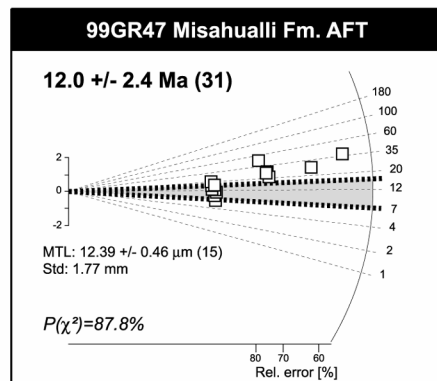
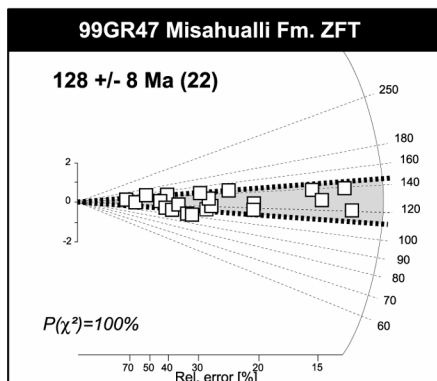
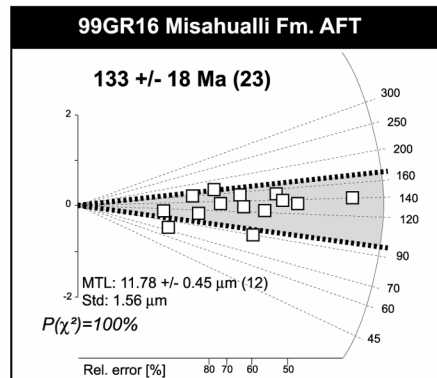
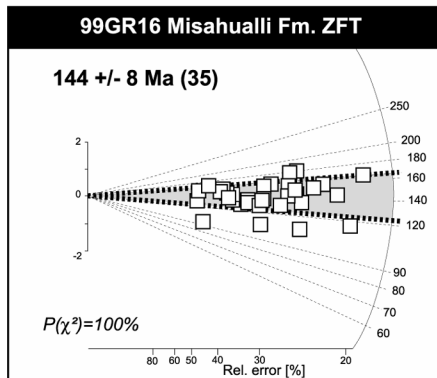
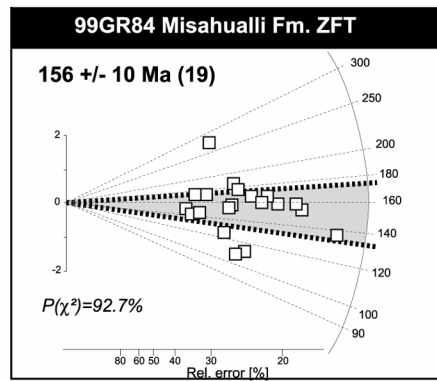
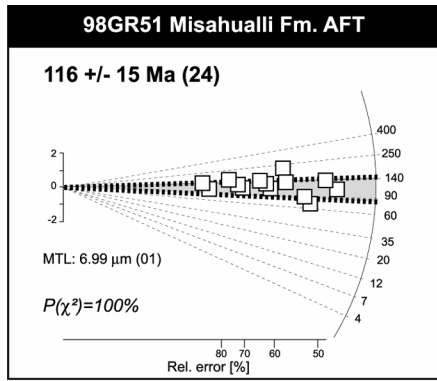






Appendix 3.2 (Continued)





	00GR05	00GR01	00GR06	98GR16	98GR28	00GR04
Fm.	Qt	Ms	Ms	Chambira	Arajuno	Arajuno
Zircon Id.	1	0	0	3	0	4
Zircon Id. Znd.	0	0	0	0	0	1
Zircon rd.	2	2	0	46	4	15
Zircon rd. Znd.	0	0	0	2	0	2
Total Zr.	3	2	0	51	4	22
Tourmaline	6	5	0	116	9	5
Rutile	1	0	1	28	2	10
Brookite	0	1	0	7	0	0
Anastase	0	0	0	6	0	4
Titanite	4	3	0	4	0	8
Apatite	15	11	0	0	0	64
AT-index	71,4	68,8	-	0,0	0,0	92,8
Spinel	0	0	0	0	0	8
Garnet	6	0	0	1	2	1
Epidote	5	0	0	0	7	10
Chloritoid	4	0	0	3	40	10
Staurolith	0	0	0	0	0	0
Alkaline Hornblende	0	0	0	0	0	4
Brown Hb	1	11	4	0	0	5
Green Hb	15	7	0	0	7	6
Augite	7	94	215	0	0	1
Diopside	0	0	0	0	0	11
Hypersthen	0	65	15	0	0	0
Olivine	0	31	5	0	0	0
Chromite	0	0	0	0	0	0
Monazite	1	0	0	5	0	2
Pumpellite	0	1	0	0	9	1
Baryte	0	0	0	0	9	0
Sillimanite	0	0	0	2	3	0
Kyanite	0	0	0	14	29	13
Corindon	0	0	0	1	0	0
Clinozoite	161	0	0	3	101	9
Andalousite	1	0	0	0	0	0
Zoisite	0	0	0	0	5	7
Tremolite	0	0	0	0	0	5
kaersulit	0	0	0	0	0	2
Cassiterite	0	0	0	0	0	0
Diallag	0	0	0	0	0	0
Xenotine	0	0	0	0	0	0
Muscovite	rare	frequent	abs.	frequent	6	present
Biotite	present	rare	abs.	abs.	0	rare (hexagonal)
Chlorite	present	present	abs.	abs.	3	abs.
Phosphate	nc	nc	nc	nc	nc	nc
Glauconite	0	0	0	0	0	0
remarks						
total	230	231	240	241	236	208

Appendix 4.1. heavy mineral analyses; number of grain counted (Id: idiomorphic; Zr: zircon; znd: zoned; abs: absent; nc: non-counted; Hb: hornblende).

	00GR03	00GR02	99GR81	99GR44	98GR81	99GR52
Fm.	Chalcana	Chalcana	Orteguaza	Tiyuyacu	Tiyuyacu	Tiyuyacu
Zircon Id.	0	1	0	2	0	0
Zircon Id. Znd.	0	0	0	1	0	0
Zircon rd.	13	22	47	48	26	8
Zircon rd. Znd.	1	5	2	1	6	1
Total Zr.	14	28	49	52	32	9
Tourmaline	31	83	16	105	52	8
Rutile	5	8	7	17	16	5
Brookite	1	4	0	8	4	0
Anastase	3	1	1	4	2	0
Titanite	2	0	1	5	3	0
Apatite	3	2	14	1	0	11
AT-index	8,8	2,4	46,7	0,9	0,0	57,9
Spinel	0	0	0	0	0	0
Garnet	12	61	5	0	1	1
Epidote	20	0	5	0	3	0
Chloritoid	9	29	7	0	0	105
Staurolith	5	0	0	0	0	0
Alkaline Hornblende	0	0	0	0	0	0
Brown Hb	0	2	0	0	0	0
Green Hb	0	2	0	0	0	0
Augite	0	0	0	0	0	0
Diopside	0	0	0	0	0	0
Hypersthen	0	0	0	0	0	0
Olivine	0	0	0	0	0	0
Chromite	0	0	0	0	0	0
Monazite	0	0	2	0	0	0
Pumpellite	1	1	0	0	0	0
Baryte	0	0	0	0	0	0
Sillimanite	6	3	0	30	0	0
Kyanite	24	15	0	28	0	0
Corindon	0	0	0	0	0	0
Clinozoite	41	5	0	0	0	0
Andalousite	0	0	0	0	0	0
Zoisite	8	2	0	0	0	0
Tremolite	0	0	0	0	0	0
kaersulit	0	0	0	0	0	0
Cassiterite	0	0	0	0	0	0
Diallag	0	0	0	0	0	0
Xenotime	0	0	0	0	0	0
Muscovite	frequent	present	frequent	very ab.	frequent	very ab.
Biotite	abs.	present	nc.	rare	nc	very ab.
Chlorite	present	rare	present	nc.	nc	present
Phosphate	present	present	nc.	nc.	nc	nc.
Glauconite	0	2	nc.	nc.	nc	nc.
remarks						small Zr
total	185	248	107	250	113	139

Appendix 4.1 (Continued)

	99GR36	98GR83	98GR37	99GR67	98RS06
Fm.	Tiyuyacu	Tena	Tena	Tena	Napo
Zircon Id.	6	0	0	1	0
Zircon Id. Znd.	2	0	0	0	0
Zircon rd.	67	12	16	22	99
Zircon rd. Znd.	8	0	4	6	39
Total Zr.	83	12	20	29	138
Tourmaline	0	54	45	8	80
Rutile	6	11	5	3	18
Brookite	5	2	0	1	3
Anastase	1	1	2	3	7
Titanite	2	0	0	0	1
Apatite	4	1	218	55	64
AT-index	100,0	1,8	82,9	87,3	44,4
Spinel	0	0	0	0	0
Garnet	0	12	0	0	3
Epidote	0	0	0	0	0
Chloritoid	0	2	1	0	0
Staurolith	0	0	0	0	0
Alkaline Hornblende	0	0	0	0	0
Brown Hb	0	0	0	0	0
Green Hb	0	0	1	0	0
Augite	0	0	0	0	0
Diopside	0	0	0	0	0
Hypersthen	0	0	0	0	0
Olivine	0	0	0	0	0
Chromite	0	0	0	0	0
Monazite	4	0	0	1	0
Pumpellite	0	0	0	0	0
Baryte	0	0	0	present	0
Sillimanite	0	0	0	0	0
Kyanite	2	0	0	0	0
Corindon	0	0	0	0	0
Clinozoite	0	0	5	0	0
Andalousite	0	0	0	0	0
Zoisite	0	0	1	0	0
Tremolite	0	0	0	0	0
kaersulit	0	0	0	0	0
Cassiterite	0	0	0	0	0
Diallag	0	0	0	0	0
Xenotime	0	0	0	0	0
Muscovite	rare	rare	nc.	nc.	frequent
Biotite	nc.	nc.	nc.	nc.	present
Chlorite	nc.	rare	nc.	nc.	present
Phosphate	very ab.	nc.	present	very ab.	nc.
Glauconite	nc.	nc.	nc.	nc.	21
remarks	many lithic frgts	red opaques	Op.	very ab. Op.	all
total	107	95	318	100	335

Appendix 4.1 (Continued)

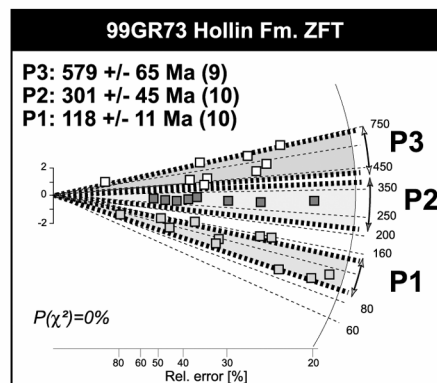
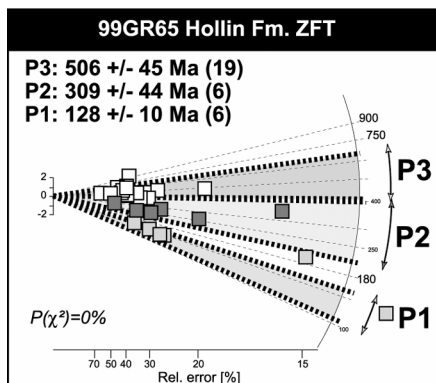
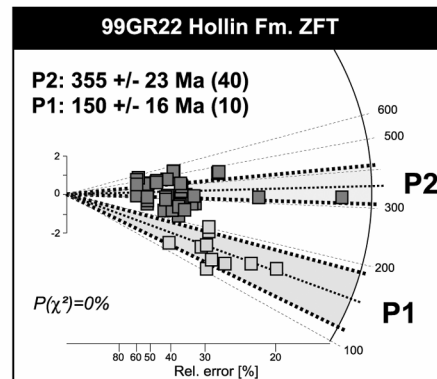
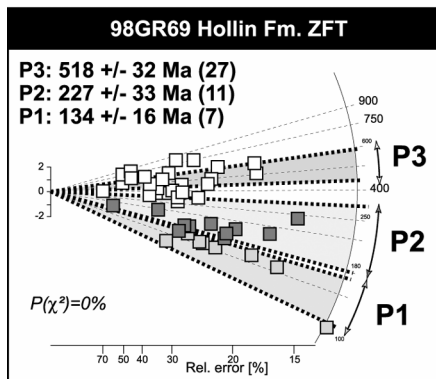
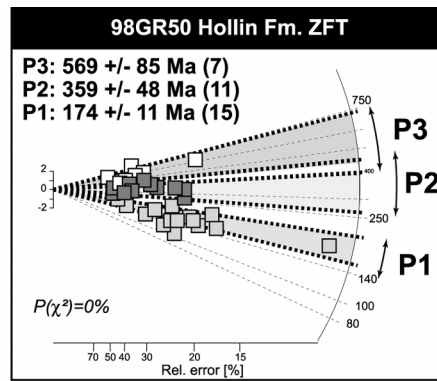
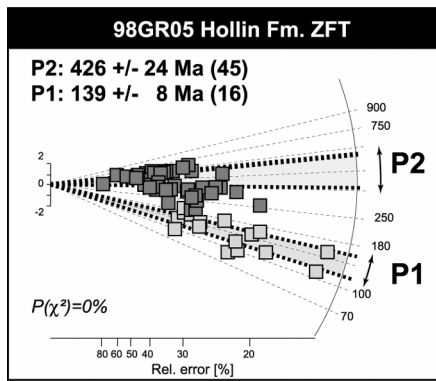
	98GR41	98GR57	98GR02	99GR22	99GR73	98GR69	98GR09
Fm.	Napo	Napo	Napo	Hollin	Hollin	Hollin	Hollin
Zircon Id.	0	2	2	0	1	4	10
Zircon Id. Znd.	0	2	1	1	2	1	4
Zircon rd.	106	79	85	79	74	135	185
Zircon rd. Znd.	22	19	56	35	17	113	58
Total Zr.	128	102	144	115	94	253	257
Tourmaline	10	25	48	51	59	5	34
Rutile	56	6	20	20	11	15	24
Brookite	1	1	4	4	5	1	0
Anastase	1	3	9	28	4	5	4
Titanite	5	0	2	8	28	1	2
Apatite	0	0	0	0	0	3	0
AT-index	0,0	0,0	0,0	0,0	0,0	37,5	0,0
Spinel	0	0	0	0	0	0	0
Garnet	1	0	0	2	0	0	0
Epidote	0	0	0	1	2	0	0
Chloritoid	0	0	0	0	0	0	0
Staurolith	0	0	0	0	0	0	0
Alkaline Hornblende	0	0	0	0	0	0	0
Brown Hb	1	0	0	0	0	0	0
Green Hb	0	0	1	0	0	0	0
Augite	5	0	1	0	0	0	4
Diopside	0	0	0	0	0	0	0
Hypersthen	0	0	0	0	0	0	0
Olivine	0	0	0	0	0	0	0
Chromite	0	0	0	0	0	0	0
Monazite	6	0	2	2	0	3	13
Pumpellite	0	0	0	0	0	0	0
Baryte	1	0	0	0	0	0	0
Sillimanite	0	0	0	0	0	0	0
Kyanite	0	0	1	0	1	0	0
Corindon	0	0	0	0	0	0	0
Clinozoite	0	0	0	0	0	0	0
Andalousite	0	0	0	0	0	0	0
Zoisite	0	0	0	0	0	0	0
Tremolite	0	0	0	0	0	0	0
kaersulit	0	0	0	0	0	0	0
Cassiterite	0	0	0	2	0	0	0
Diallag	0	0	0	1	0	0	0
Xenotime	5	0	0	0	0	0	0
Muscovite	nc.	present	nc.	frequent	present	present	rare
Biotite	nc.	nc.	nc.	nc.	present	nc.	nc.
Chlorite	nc.	present	nc.	nc.	nc.	nc.	nc.
Phosphate	present	very ab.	nc. very	frequent	nc.	nc.	nc.
Glauconite	nc.	frequent	frequent	frequent	nc.	nc.	nc.
remarks				opaques			
total	220	137	232	234	204	286	338

Appendix 4.1 (Continued)

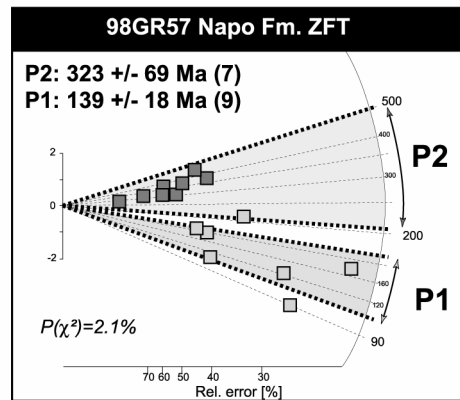
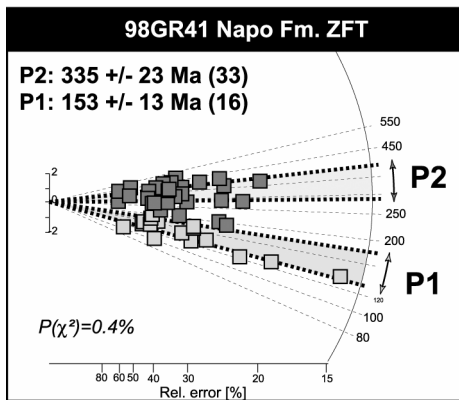
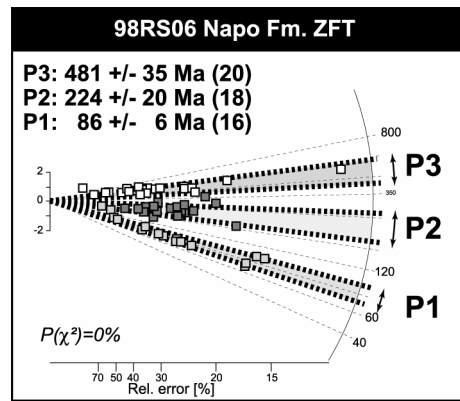
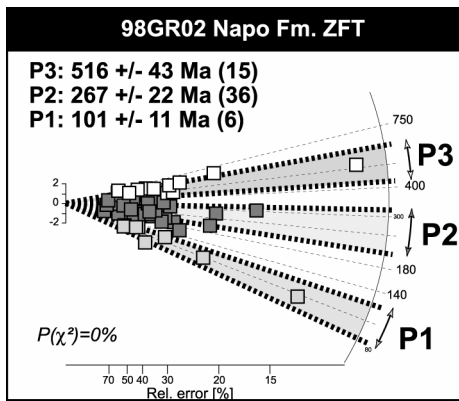


	98GR50	98GR05	98GR65/2	99GR65/1	99GR71	99GR77
Fm.	Hollin	Hollin	Hollin	Hollin	Pumbuiza	Hollin
Zircon Id.	0	3	1	0	2	0
Zircon Id. Znd.	2	1	1	1	3	15
Zircon rd.	59	191	66	90	87	4
Zircon rd. Znd.	29	67	20	33	33	19
Total Zr.	90	262	88	124	125	31
Tourmaline	79	18	31	34	62	32
Rutile	12	14	7	13	21	4
Brookite	1	0	0	0	1	0
Anastase	4	7	27	29	3	2
Titanite	1	2	1	12	7	0
Apatite	1	5	0	0	0	160
AT-index	1,3	21,7	0,0	0,0	0,0	83,3
Spinel	0	0	0	0	0	0
Garnet	0	0	0	1	0	0
Epidote	0	0	0	0	1	0
Chloritoid	0	0	0	0	0	1
Staurolith	0	0	0	0	0	0
Alkaline Hornblende	0	0	0	0	0	0
Brown Hb	1	0	0	0	0	0
Green Hb	0	0	0	0	0	0
Augite	6	0	0	0	0	0
Diopside	0	0	0	0	0	0
Hypersthen	1	0	0	0	0	0
Olivine	0	0	0	0	0	0
Chromite	0	0	0	0	0	0
Monazite	3	10	6	2	3	0
Pumpellite	0	0	0	0	0	0
Baryte	0	0	15	0	0	0
Sillimanite	0	0	0	0	0	0
Kyanite	0	0	0	0	0	0
Corindon	0	0	0	0	0	0
Clinozoite	0	0	0	0	0	20
Andalousite	0	0	0	0	0	0
Zoisite	0	0	0	0	0	0
Tremolite	0	0	0	0	0	0
kaersulit	0	0	0	0	0	0
Cassiterite	0	0	5	8	2	0
Diallag	0	0	0	0	0	0
Xenotime	0	0	0	0	0	0
Muscovite	present	nc.	present	present	frequent	nc.
Biotite	nc.	nc.	nc.	nc.	nc.	nc.
Chlorite	nc.	nc.	nc.	nc.	rare	nc.
Phosphate	nc.	nc.	nc.	nc.	nc.	very ab.
Glauconite	nc.	nc.	1	nc.	nc.	nc.
remarks	brown znd Zrs				pink Zrs	
total	199	318	181	223	225	250

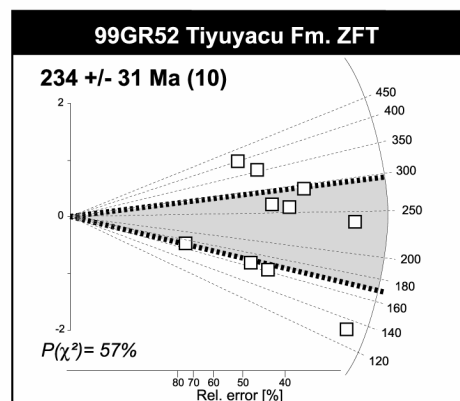
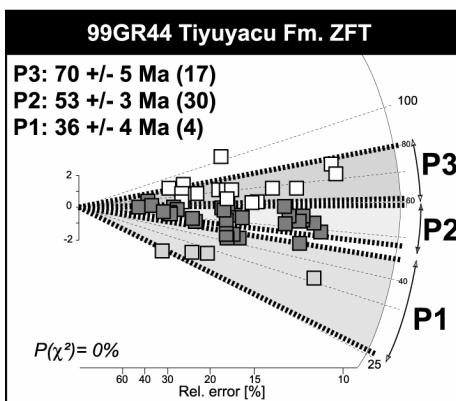
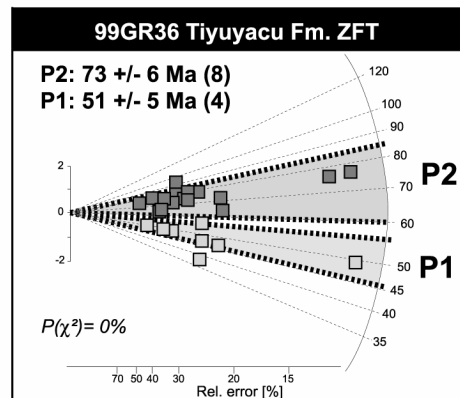
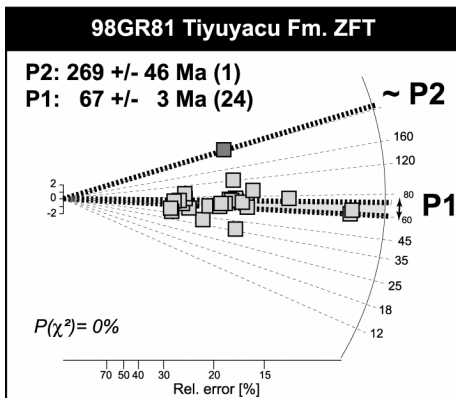
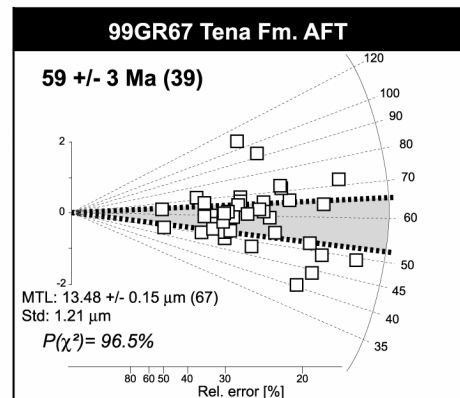
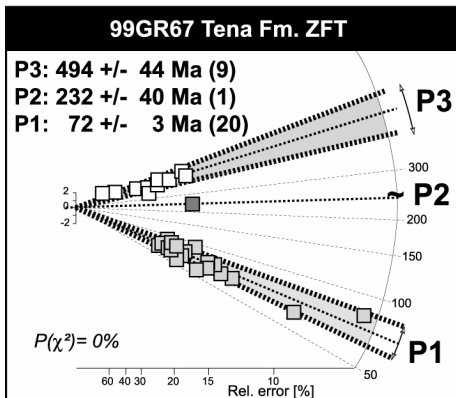
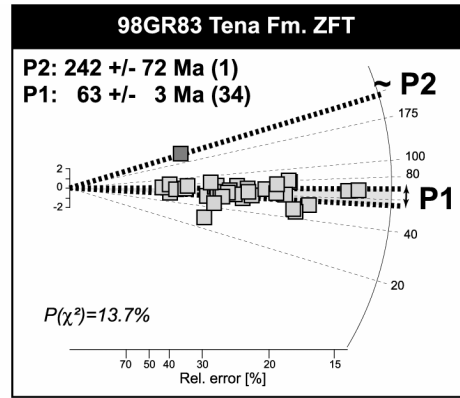
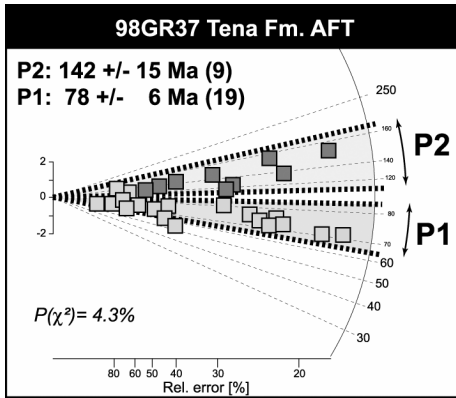
Appendix 4.1 (Continued)

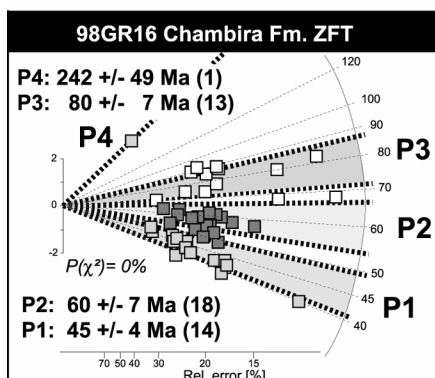
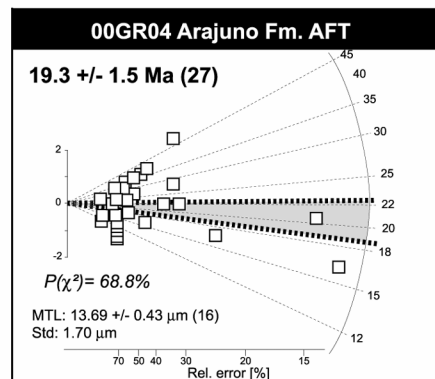
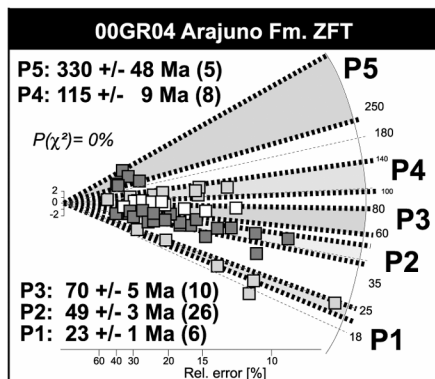
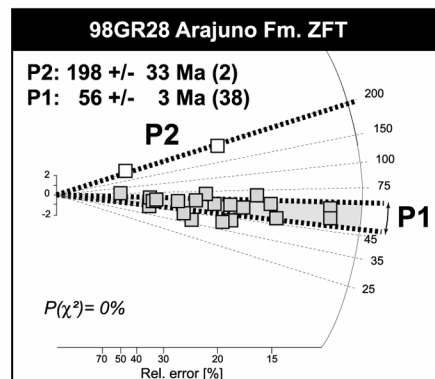
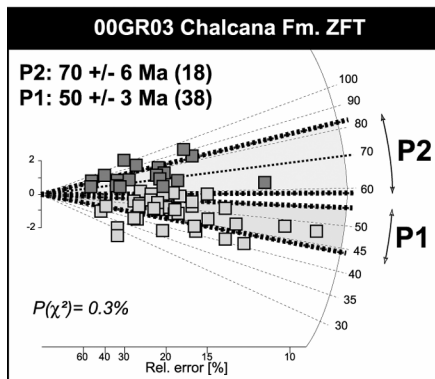
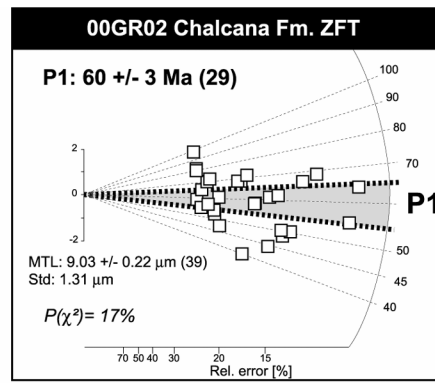
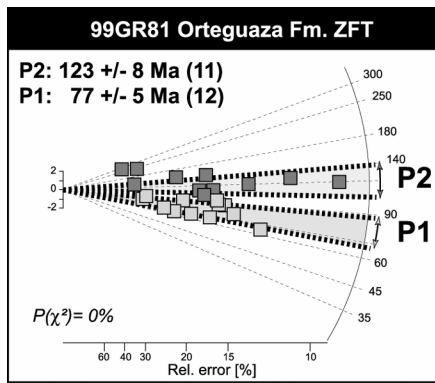


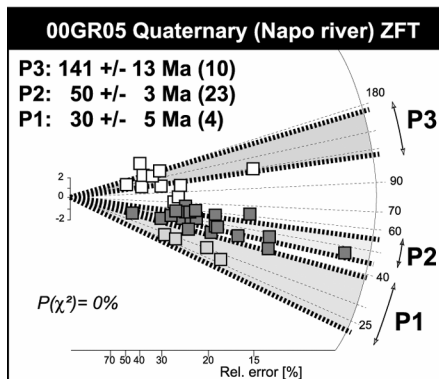
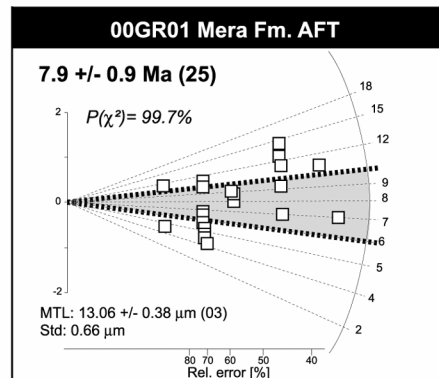
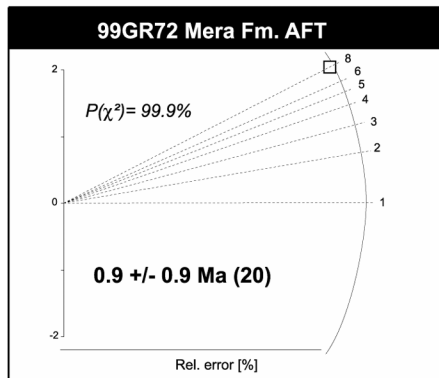
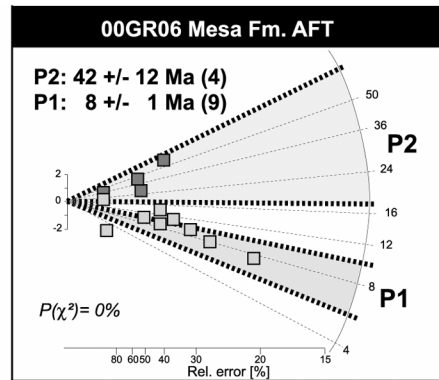
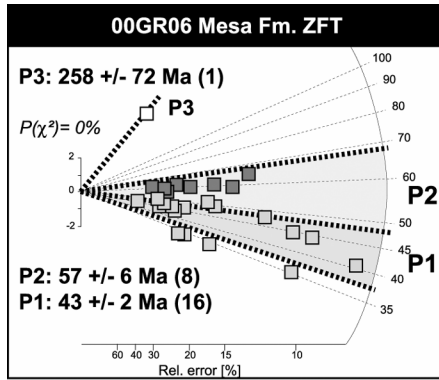
Appendix 4.2: Radial plots (Gailbraith, 1990) for fission-track age determinations of samples from the Aptian to recent basin fill series of the northern Ecuadorian Sub-Andean Zone and Pastaza depression. In brackets is the number of counted grains or track lengths. ZFT: Zircon Fission-Track; AFT: Apatite Fission-Track. MTL: Mean Track length; Std: Standard deviation.  $P(\chi^2)$  (section 4.2.1.1).



Appendix 4.2 (Continued)







Appendix 4.2 (Continued)

Appendix 4.3: Individual fission-track grain-age analysis, combined (sediments) with parameters and results for best-fit peaks from Binomfit's software (Brandon, 1992 & 1996).

## Abitagua batholith

## 98GR03 Apatite

n (cryst.)	Ns	Ni	Sum Ns	Sum Ni	Grain age	± 1s	Chi-sq.	Sum age	± 1s
17	2	5	2	5	82.1	68.8	---	82.1	68.8
7	4	10	6	15	82.1	48.7	---	82.1	39.8
23	4	9	10	24	91.2	54.9	99.1	85.5	32.3
24	9	18	19	42	102.5	42	98.9	92.8	25.8
19	9	18	28	60	102.5	42	99.7	95.7	22.1
27	4	7.83	32	67	104.7	64.4	99.9	97.9	21.3
9	6	11	38	78	111.7	56.8	100	99.9	20
29	5	8.81	43	86	116.2	65.2	100	102.5	19.5
31	3	4.89	46	90	125.5	92.1	100	104.7	19.3
32	5	7.83	51	97	130.6	74.9	100	107.7	19
13	16	24	67	121	136.3	44.2	100	113.4	17.7
4	4	6	71	127	136.3	88.1	100	114.5	17.4
10	9	13	80	140	141.5	61.5	100	117	16.9
25	5	6.85	85	146	149.1	87.8	100	119.2	16.8
6	3	4	88	150	153.1	117.1	100	120.1	16.6
11	7	9	95	159	158.7	80.2	100	122.3	16.4
3	6	7	101	166	174.7	97.4	100	124.5	16.3
18	13	15	114	181	176.6	67.2	100	128.8	16
14	7	8	121	189	178.3	92.5	100	130.9	15.9
28	14	14.7	135	203	194.1	72.8	99.9	135.9	15.8
22	8	8	143	211	203.3	101.9	99.9	138.5	15.7
21	9	9	152	220	203.3	96.1	99.9	141.2	15.6
8	15	15	167	235	203.3	74.6	99.8	145.2	15.5
5	4	4	171	239	203.3	144	99.9	146.1	15.5
1	8	8	179	247	203.3	101.9	99.9	148	15.4
20	10	9	189	256	225.5	103.9	99.8	150.7	15.3
16	8	7	197	263	231.9	120.3	99.8	152.9	15.3
12	6	5	203	268	243.3	147.5	99.8	154.6	15.3
2	6	5	209	273	243.3	147.5	99.8	156.2	15.3
30	6	4.89	215	277	248.6	151.7	99.8	158.4	15.4
15	7	5	222	282	282.9	165.9	99.7	160.6	15.4
26	11	7.83	233	289	283.9	133.1	99.5	164.4	15.5

## 98GR03 Zircon

n (cryst.)	Ns	Ni	Sum Ns	Sum Ni	Grain age	± 1s	Chi-sq.	Sum age	± 1s
9	33	6	33	6	133.1	59.2	---	133.1	59.2
5	72	12	105	18	145.1	45.5	87.3	141.1	36.3
6	87	14	192	32	150.2	43.5	97.4	145.1	28.1
8	82	13	274	45	152.4	45.8	99.5	147.2	24.1

1	41	6	315	51	165	72.3	99.8	149.3	23
10	55	8	370	59	166	63	99.9	151.6	21.8
11	36	5	406	64	173.7	83.1	100	153.3	21.2
2	52	7	458	71	179.2	72.3	100	155.9	20.5
4	55	7	513	78	189.3	76.2	100	158.9	19.9
7	118	13	631	91	218.2	64.1	99.5	167.4	19.5
3	136	14	767	105	233.3	65.9	98	176.2	19.2

## 98RS8 Apatite

n (cryst.)	Ns	Ni	Sum Ns	Sum Ni	Grain age	$\pm 1s$	Chi-sq.	Sum age	$\pm 1s$
15	0	32.4	0	32	0	0	---		
13	0	42.3	0	74	0	0	---		
7	0	15	0	89	0	0	---		
5	1	122	1	211	1.7	1.7	86.6	1	1
9	1	119	2	330	1.7	1.8	94.6	1.3	0.9
17	1	50	3	380	4.2	4.2	89.8	1.6	1
12	2	93.4	5	473	4.5	3.2	86.9	2.2	1
11	1	45.4	6	518	4.6	4.6	90.8	2.4	1
6	4	157	10	675	5.3	2.7	88.3	3.1	1
14	1	38.3	11	713	5.4	5.5	92.1	3.2	1
8	8	297	19	1010	5.6	2	91.4	3.9	0.9
10	2	70.5	21	1080	5.9	4.2	94.1	4	0.9
4	2	62	23	1142	6.7	4.8	95.5	4.2	0.9
16	2	54	25	1196	7.7	5.6	95.9	4.3	0.9
3	1	25	26	1221	8.3	8.5	96.9	4.4	0.9
1	4	71	30	1292	11.7	6	88.7	4.8	0.9
2	1	10	31	1302	20.8	21.8	81.9	5	0.9

## 98RS8 Zircon

n (cryst.)	Ns	Ni	Sum Ns	Sum Ni	Grain age	$\pm 1s$	Chi-sq.	Sum age	$\pm 1s$
13	90	36	90	36	67.3	13.4	---	67.3	13.4
10	67	24	157	60	75.1	18	72.1	70.4	10.9
25	80	24.8	237	84	86.8	20.1	69.5	75.9	9.9
2	52	15	289	99	93.1	27.4	75.4	78.5	9.5
11	32	9	321	108	95.5	36.1	83.1	79.9	9.2
16	50	13.9	371	121	96.8	29.5	86.3	82.4	9
15	83	22.8	454	143	97.8	23.3	87.2	85.3	8.6
24	64	16.8	518	159	102	28.1	88.6	87.5	8.4
14	143	36.7	661	195	104.7	19.7	85.5	91	8
7	71	18	732	213	105.8	28.1	88	92.3	7.7
12	48	12	780	225	107.3	34.8	90.9	93.1	7.6
22	192	46.6	972	271	110.6	18.4	87.6	96.3	7.3
4	46	11	1018	282	112.1	37.8	90.4	96.9	7.2
19	175	40.6	1193	322	115.5	20.4	88	99.4	7
20	179	40.6	1372	362	118.1	20.9	85.8	101.7	6.8
1	58	13	1430	375	119.6	36.9	88.1	102.3	6.8



17	302	67.4	1732	442	120.2	16.6	83.7	105.1	6.5
8	133	29	1865	471	122.9	25.5	84.3	106.2	6.4
5	52	11	1917	482	126.6	42.2	86.7	106.7	6.4
9	80	16	1997	498	133.8	36.9	86.7	107.6	6.4
6	55	11	2052	509	133.8	44.4	87.9	108.1	6.3
3	98	19	2150	528	138	34.9	86.7	109.2	6.3
18	230	44.6	2380	572	138.1	23	79.6	111.6	6.3
23	257	49.5	2637	621	138.8	22	71.9	113.8	6.2
21	109	20.8	2746	641	140.2	33.8	71.7	114.8	6.2

98GR53 Apatite

n (cryst.)	Ns	Ni	Sum Ns	Sum Ni	Grain age	± 1s	Chi-sq.	Sum age	± 1s
9	4	8	4	8	103.6	63.5	---	103.6	63.5
5	13	26	17	34	103.6	35.4	---	103.6	31.0
10	4	7	21	41	118.3	74.2	98.2	106.1	28.7
11	3	5	24	46	124.1	90.8	99.4	108.1	27.4
13	6	9	30	55	137.8	72.8	99.3	113	25.9
12	8	10	38	65	165	78.5	97.8	121	25
8	9	10	47	75	185.3	85.4	95.9	129.6	24.5
4	9	10	56	85	185.3	85.4	95.8	136.2	23.9
3	6	6	62	91	205.6	118.9	96.1	140.8	23.6
2	2	2	64	93	205.6	205.7	97.7	142.2	23.6
1	5	5	69	98	205.6	130.2	98.2	145.4	23.3
6	6	4	75	102	306	197.8	96.1	151.8	23.6
7	7	4	82	106	355.6	223.2	90.7	159.6	24

98GR53 Zircon

n (cryst.)	Ns	Ni	Sum Ns	Sum Ni	Grain age	± 1s	Chi-sq.	Sum age	± 1s
13	38	6	38	6	141.9	62.5	---	141.9	62.5
5	113	16	151	22	158.1	42.5	83.2	153.7	35.4
9	43	6	194	28	160.4	70.1	97.4	155.1	31.7
2	72	10	266	38	161.1	54.6	99.6	156.7	27.6
11	30	4	296	42	167.7	89.4	99.9	157.8	26.5
10	31	4	327	46	173.3	92.2	100	159.1	25.6
4	109	14	436	60	174.1	49.7	100	162.6	23
3	48	6	484	66	178.8	77.6	100	164.1	22.1
8	51	6	535	72	189.8	82.1	100	166.2	21.5
1	85	10	620	82	189.8	63.7	100	169.1	20.6
6	61	7	681	89	194.5	77.9	100	171.1	20
14	44	5	725	94	196.4	92.9	100	172.4	19.7
12	44	5	769	99	196.4	92.9	100	173.7	19.3
7	62	7	831	106	197.6	79.1	100	175.2	18.9

## 99GR14 Apatite

n (cryst.)	Ns	Ni	Sum Ns	Sum Ni	Grain age	± 1s	Chi-sq.	Sum age	± 1s
3	9	50	9	50	40.5	14.7	---	40.5	14.7
16	7	25	16	75	62.9	27	42.8	48	13.3
9	7	25	23	100	62.9	27	64.2	51.8	12.1
14	10	35	33	135	64.2	23.1	77.4	55	10.8
8	7	22	40	157	71.5	31.1	84.5	57.3	10.3
18	8	25	48	182	71.9	29.3	89.8	59.3	9.8
19	8	24	56	206	74.9	30.7	93	61.1	9.4
7	6	18	62	224	74.9	35.4	95.8	62.2	9.1
2	4	12	66	236	74.9	43.3	97.7	62.9	9
17	7	20	73	256	78.6	34.6	98.5	64.1	8.7
6	14	39	87	295	80.6	25.2	98.7	66.3	8.4
15	11	28	98	323	88.1	31.5	98.6	68.2	8.2
12	5	12	103	335	93.5	49.8	98.9	69.1	8.1
13	19	42	122	377	101.4	28.2	97	72.7	7.9
11	7	15	129	392	104.6	48	97.2	73.9	7.9
4	5	10	134	402	112	61.4	97.4	74.9	7.8
1	13	26	147	428	112	38.2	96.1	77.1	7.8
5	7	13	154	441	120.5	56.6	95.8	78.4	7.8
10	6	11	160	452	122.1	62.1	95.8	79.5	7.7
20	16	28.6	176	480	125.2	39.3	92.5	82.3	7.7

## 99GR14 Zircon

n (cryst.)	Ns	Ni	Sum Ns	Sum Ni	Grain age	± 1s	Chi-sq.	Sum age	± 1s
9	33	7.15	33	7	118.1	48.9	---	118.1	49.3
1	66	13	99	20	129.8	39.6	85	126.6	31.3
10	205	38.8	304	58	135	24.1	94.7	133.9	19.7
8	197	36	501	94	139.8	25.8	98.2	136.2	16
5	24	4	525	98	153.1	82.8	99.4	136.9	15.7
13	97	16	622	114	154.7	42.1	99.4	139.4	14.9
6	106	17	728	131	159	41.9	99.4	141.9	14.3
7	78	12	806	143	165.7	51.7	99.5	143.9	13.9
2	26	4	832	147	165.7	89.2	99.8	144.5	13.8
11	30	4.04	862	151	188.9	100.3	99.8	145.7	13.7
4	52	7	914	158	189	76.4	99.8	147.7	13.6
3	223	29	1137	187	195.6	39.1	97.9	155.1	13.3
12	238	30	1375	217	201.7	39.6	94	161.6	13

n (cryst.)	Ns	Ni	Sum Ns	Sum Ni	Grain age	± 1s	Chi-sq.	Sum age	± 1s
18	0	36	0	36	0	0	---		
9	0	23	0	59	0	0	---		
32	0	21.6	0	80	0	0	---		
28	1	71.6	1	151	3.4	3.4	77.5	1.6	1.6
23	1	56.9	2	207	4.2	4.3	86.5	2.3	1.6

27	2	82.4	4	289	5.8	4.2	87.6	3.3	1.7
20	2	80	6	369	6	4.3	91.8	3.9	1.6
19	2	80	8	449	6	4.3	95.2	4.3	1.5
4	4	140	12	589	6.9	3.5	96.3	4.9	1.4
25	2	59.8	14	648	8	5.8	97.3	5.2	1.4
31	2	59.8	16	707	8	5.8	98.2	5.4	1.4
2	1	29	17	736	8.3	8.4	99	5.5	1.4
13	2	55	19	791	8.7	6.3	99.3	5.8	1.4
30	9	234	28	1025	9.2	3.1	98.7	6.6	1.3
10	1	25	29	1050	9.6	9.8	99.3	6.6	1.3
12	2	49	31	1099	9.8	7.1	99.5	6.8	1.3
7	2	49	33	1148	9.8	7.1	99.7	6.9	1.2
14	3	66	36	1214	10.9	6.4	99.7	7.1	1.2
16	2	42	38	1256	11.4	8.3	99.8	7.3	1.2
3	3	63	41	1319	11.4	6.8	99.8	7.5	1.2
8	2	39	43	1358	12.3	8.9	99.8	7.6	1.2
34	3	56.9	46	1414	12.6	7.5	99.8	7.8	1.2
29	5	94.2	51	1508	12.7	5.9	99.8	8.1	1.2
15	2	36	53	1544	13.3	9.7	99.8	8.2	1.2
33	3	54	56	1597	13.3	7.9	99.8	8.4	1.2
24	1	16.7	57	1613	14.4	14.8	99.9	8.5	1.2
22	1	16.6	58	1629	14.4	14.9	99.9	8.5	1.2
11	3	46	61	1675	15.6	9.3	99.9	8.7	1.2
21	2	26.5	63	1701	18.1	13.3	99.9	8.9	1.2
17	3	36	66	1737	20	12	99.7	9.1	1.2
1	2	22	68	1759	21.8	16.1	99.6	9.3	1.2
6	6	61	74	1820	23.6	10.1	97.4	9.7	1.2
26	1	9.81	75	1829	24.4	25.6	97.5	9.8	1.2
5	1	8	76	1837	29.9	31.8	97.1	9.9	1.2

## 99GR17 Zircon

n (cryst.)	Ns	Ni	Sum Ns	Sum Ni	Grain age	± 1s	Chi-sq.	Sum age	± 1s
2	87	22	87	22	94.1	22.7	---	94.1	22.7
17	53	13	140	35	97	30.2	93.8	95.1	18.3
1	91	21	231	56	103	25.2	96.4	98.1	15
18	118	24	349	80	116.8	26.4	91.8	103.7	13.3
12	74	15	423	95	117.1	33.4	95.5	105.8	12.5
9	76	15	499	110	120.3	34.2	97.3	107.8	11.9
6	123	24	622	134	121.7	27.4	98.1	110.3	11.1
15	155	29	777	163	126.8	26	98.1	113.2	10.5
3	113	21	890	184	127.7	30.6	98.7	114.9	10.1
11	356	65	1246	249	129.9	18.1	98.2	118.8	9.1
8	85	15	1331	264	134.4	37.9	98.9	119.7	9
13	132	22	1463	286	142.2	33.1	98.8	121.4	8.8
14	288	45	1751	331	151.6	24.8	96	125.5	8.6
4	71	11	1822	342	152.8	49.8	96.7	126.4	8.6
16	124	19	1946	361	154.5	38.4	96.6	127.9	8.5
7	210	30	2156	391	165.6	32.8	93.2	130.8	8.4
10	180	23	2336	414	184.9	41.4	85.1	133.8	8.4

5	75	9	2411	423	196.7	69.7	82.6	135.2	8.4
---	----	---	------	-----	-------	------	------	-------	-----

## 99GR66 Apatite

n (cryst.)	Ns	Ni	Sum Ns	Sum Ni	Grain age	± 1s	Chi-sq.	Sum age	± 1s
9	0	18	0	18	0	0	---		
8	0	18	0	36	0	0	---		
7	0	25	0	61	0	0	---		
6	0	50	0	111	0	0	---		
5	0	48	0	159	0	0	---		
4	0	31	0	190	0	0	---		
3	0	18	0	208	0	0	---		
2	0	53	0	261	0	0	---		
1	1	21	1	282	10.3	10.6	15.5	0.8	0.8
10	1	20	2	302	10.8	11.1	20.1	1.4	1

## 99GR66 Zircon

n (cryst.)	Ns	Ni	Sum Ns	Sum Ni	Grain age	± 1s	Chi-sq.	Sum age	± 1s
1	41	10	41	10	109.3	38.7	---	109.3	38.7
16	350	85	391	95	109.7	13.8	99.1	109.7	13.1
24	66	15.2	457	110	116.1	33.3	98.3	110.7	12.3
12	57	13	514	123	116.8	36.1	99.6	111.4	11.8
18	77	17.2	591	140	119.5	32.1	99.8	112.5	11.2
25	124	27.3	715	167	121.1	25.9	99.9	114.1	10.5
21	99	21.2	814	188	124.3	30	99.9	115.3	10.1
5	235	50	1049	238	125.1	19.9	99.9	117.4	9.3
13	87	18	1136	256	128.6	33.6	99.9	118.2	9.1
20	93	19.2	1229	275	129	32.6	100	119	8.9
23	40	8.08	1269	283	131.7	51	100	119.4	8.8
22	35	7.07	1304	290	131.7	54.5	100	119.7	8.7
19	75	15.2	1379	305	131.7	37.4	100	120.4	8.6
8	136	27	1515	332	134	28.6	100	121.5	8.4
11	76	15	1591	347	134.8	38.3	100	122.1	8.3
15	74	14	1665	361	140.5	41.2	100	122.8	8.2
4	32	6	1697	367	141.8	63.3	100	123.1	8.2
14	163	30	1860	397	144.4	29.1	100	124.7	8
9	50	9	1910	406	147.6	53.7	100	125.2	8
6	50	9	1960	415	147.6	53.7	100	125.7	8
17	85	15.2	2045	430	149.1	41.9	100	126.6	7.9
7	186	33	2231	463	149.8	28.7	100	128.2	7.8
10	83	14	2314	477	157.4	45.8	100	129.1	7.8
3	106	15	2420	492	187.2	52	100	130.9	7.8
2	72	8	2492	500	237.5	88.9	99.7	132.6	7.9

## Misahualli Fm.

## 98RS10 Apatite

n (cryst.)	Ns	Ni	Sum Ns	Sum Ni	Grain age	± 1s	Chi-sq.	Sum age	± 1s
4	5	18	5	18	56.5	28.6	---	56.5	28.6
3	4	14	9	32	58.1	33	97	57.2	21.7
2	4	13	13	45	62.6	35.8	99.1	58.8	18.6
1	10	31	23	76	65.6	24	99.5	61.6	14.8
8	9	26	32	102	70.4	27.3	99.7	63.8	13.1
16	7	20	39	122	71.2	31.3	99.9	65	12.1
23	25	71	64	193	71.6	16.8	99.9	67.4	10
22	4	11	68	204	73.9	43.2	100	67.8	9.7
12	4	11	72	215	73.9	43.2	100	68.1	9.5
6	3	8	75	223	76.2	51.7	100	68.4	9.4
9	29	77	104	300	76.5	16.9	100	70.5	8.3
17	7	18	111	318	79	35.3	100	71	8.2
7	14	36	125	354	79	25	100	71.8	7.8
5	25	62	150	416	81.9	19.6	100	73.3	7.4
21	5	12	155	428	84.6	45.1	100	73.6	7.3
13	5	12	160	440	84.6	45.1	100	73.9	7.2
19	8	19	168	459	85.5	36.1	100	74.4	7.1
15	19	43	187	502	89.7	24.9	100	75.7	6.9
24	18	37	205	539	98.7	28.5	100	77.3	6.8
20	17	34	222	573	101.4	30.3	100	78.7	6.7
18	7	14	229	587	101.4	47.1	100	79.3	6.7
14	6	12	235	599	101.4	50.8	100	79.7	6.7
11	26	51	261	650	103.4	25.1	100	81.6	6.5
10	15	29	276	679	104.9	33.5	100	82.6	6.5

## 98RS10 Zircon

n (cryst.)	Ns	Ni	Sum Ns	Sum Ni	Grain age	± 1s	Chi-sq.	Sum age	± 1s
1	125	23	125	23	130.2	29.8	---	130.2	29.8
2	38	5	163	28	181.3	86.4	52.3	139.3	28.8

## 98GR19 Apatite

n (cryst.)	Ns	Ni	Sum Ns	Sum Ni	Grain age	± 1s	Chi-sq.	Sum age	± 1s
11	8	32	8	32	53.7	21.3	---	53.7	21.3
9	2	7	10	39	61.3	49.2	88.1	55.1	19.6
1	4	13	14	52	66	37.8	95.3	57.8	17.5
16	15	46	29	98	70	20.9	96.1	63.5	13.6
7	9	27	38	125	71.5	27.6	98.5	65.3	12.3
5	11	33	49	158	71.5	25	99.5	66.6	11.1

4	6	18	55	176	71.5	33.8	99.9	67.1	10.6
3	9	26	64	202	74.3	28.8	99.9	68	10
8	17	47	81	249	77.6	22.1	100	69.8	9.2
6	10	27	91	276	79.4	29.5	100	70.7	8.9
18	9	24	100	300	80.4	31.5	100	71.5	8.6
17	6	16	106	316	80.4	38.6	100	72	8.4
14	17	45	123	361	81	23.2	100	73.1	8
12	6	15	129	376	85.7	41.5	100	73.6	7.9
10	7	17	136	393	88.2	39.7	100	74.2	7.8
2	14	31	150	424	96.7	31.3	100	75.9	7.6
15	12	25	162	449	102.7	36.2	100	77.4	7.5
13	8	16	170	465	107	46.5	100	78.4	7.5

## 98GR19 Zircon

n (cryst.)	Ns	Ni	Sum Ns	Sum Ni	Grain age	± 1s	Chi-sq.	Sum age	± 1s
10	25	7	25	7	100	42.9	---	100.0	42.9
4	39	10	64	17	109.1	38.8	87.4	105.3	29
9	45	11	109	28	114.4	38.7	96.9	108.9	23.4
6	21	5	130	33	117.4	58.6	99.4	110.2	21.8
2	65	15	195	48	121.1	34.9	99.7	113.6	18.7
1	60	12	255	60	139.5	44.4	99.2	118.8	17.5
5	41	8	296	68	143	55.5	99.4	121.6	16.9
8	129	25	425	93	143.9	31.8	99.1	127.6	15.2
3	56	10	481	103	156.1	53.8	99.2	130.4	14.8
7	96	16	577	119	167.1	45.5	98.6	135.3	14.4

## 98GR29 Zircon

n (cryst.)	Ns	Ni	Sum Ns	Sum Ni	Grain age	± 1s	Chi-sq.	Sum age	± 1s
7	31	7	31	7	125.7	52.8	---	125.7	52.8
9	37	8	68	15	131.2	51.3	94	128.6	36.9
2	47	9	115	24	147.9	54.1	95.1	135.9	30.8
4	42	8	157	32	148.7	57.6	98.6	139.1	27.4
6	45	8	202	40	159.2	61.3	99.3	143.1	25.2
10	40	7	242	47	161.7	66.5	99.7	145.9	23.8
13	1416	236	1658	283	169.7	13.2	98	165.7	12
8	54	9	1712	292	169.7	61.4	99.2	165.9	11.9
3	36	6	1748	298	169.7	75	99.7	165.9	11.8
1	194	29	1942	327	188.9	38.1	99.7	168	11.5
5	34	5	1976	332	192	92.2	99.8	168.3	11.4
12	35	5	2011	337	197.5	94.7	99.9	168.8	11.4
11	64	9	2075	346	200.6	71.7	99.9	169.6	11.4

## 98GR31 Zircon

n (cryst.)	Ns	Ni	Sum Ns	Sum Ni	Grain age	± 1s	Chi-sq.	Sum age	± 1s
6	122	30	122	30	116.9	24.1	---	116.9	24.1
7	157	34	279	64	132.6	25.5	64.8	125.3	17.9
14	94	20	373	84	135	33.5	86.8	127.6	16
15	72	14	445	98	147.5	43.4	91.8	130.4	15.2
16	120	20	565	118	171.8	41.9	80.5	137.5	14.6
2	147	24	712	142	175.3	39	74.5	143.9	14.1
10	68	11	780	153	176.9	57.8	79.3	146.3	13.8
12	67	10	847	163	191.5	65.2	80.5	149	13.7
3	101	15	948	178	192.5	53.6	79.5	152.7	13.5
17	35	5	983	183	200	95.8	83.5	154	13.4
9	35	5	1018	188	200	95.8	86.9	155.2	13.4
13	71	10	1089	198	202.8	68.8	87.4	157.7	13.3
4	62	8	1151	206	221.1	83.4	86.7	160.1	13.2
1	157	20	1308	226	223.9	53.7	78	165.8	13.2
8	128	16	1436	242	228.1	60.9	72.7	169.9	13.1
11	95	11	1531	253	245.9	78.7	68.2	173.2	13.1
5	78	7	1609	260	315.5	124.9	55.8	177.1	13.2

## 98GR33 Apatite

n (cryst.)	Ns	Ni	Sum Ns	Sum Ni	Grain age	± 1s	Chi-sq.	Sum age	± 1s
1	12	28	12	28	97.6	33.8	---	97.6	33.8
19	4	8	16	36	113.7	69.7	82.6	101.1	30.6
10	6	10	22	46	136.2	70.5	86.1	108.8	28.4
18	10	16	32	62	141.8	57.3	89.5	117.3	25.8
9	5	8	37	70	141.8	81	95.1	120.1	24.7
23	10	15	47	85	151.1	61.9	96.7	125.6	23.2
22	4	6	51	91	151.1	97.7	98.5	127.3	22.6
20	12	18	63	109	151.1	56.5	99.1	131.2	21.2
21	9	13	72	122	156.9	68.2	99.5	134	20.4
5	25	36	97	158	157.4	41.3	99.6	139.3	18.5
2	17	24	114	182	160.5	51.1	99.8	142.1	17.6
8	11	15	125	197	166.1	66.1	99.9	143.9	17.1
12	8	10	133	207	180.9	86	99.9	145.7	16.9
6	24	30	157	237	180.9	49.9	99.9	150.2	16.2
15	6	7	163	244	193.7	107.9	99.9	151.4	16.1
11	21	24	184	268	197.6	59.4	99.9	155.6	15.7
7	21	24	205	292	197.6	59.4	99.9	159.1	15.4
14	9	9	214	301	225.4	106.5	99.8	161.1	15.3
13	15	15	229	316	225.4	82.6	99.8	164.1	15.2
3	13	13	242	329	225.4	88.7	99.7	166.6	15.1
17	17	15	259	344	254.9	90.7	99.4	170.4	15.1
4	6	4	265	348	335.2	216.6	99.1	172.3	15.1
16	34	21	299	369	361.1	100.9	82.9	183.2	15.4

## 98GR33 Zircon

n (cryst.)	Ns	Ni	Sum Ns	Sum Ni	Grain age	± 1s	Chi-sq.	Sum age	± 1s
16	71	13	71	13	119.8	36.4	---	119.8	36.4
7	48	7	119	20	150	60.9	65.2	130.4	31.8
15	63	9	182	29	153.1	54.8	83.8	137.4	27.9
13	50	7	232	36	156.2	63.2	93.1	141.1	25.7
6	100	14	332	50	156.2	44.9	96.9	145.3	22.6
4	215	27	547	77	173.9	36	95.5	155.4	19.6
12	40	5	587	82	174.7	83.1	97.9	156.5	19.2
5	253	31	840	113	178.2	34.4	98.1	162.5	17.2
9	58	7	898	120	180.8	72.6	99.1	163.5	16.8
14	26	3	924	123	189	115.4	99.6	164.2	16.7
8	62	7	986	130	193.1	77.3	99.7	165.7	16.4
1	118	13	1104	143	197.8	58.2	99.8	168.7	16
10	48	5	1152	148	209.1	98.5	99.8	170	15.9
3	88	9	1240	157	212.9	74.8	99.8	172.5	15.7
2	60	6	1300	163	217.6	93.5	99.9	174.2	15.6
11	89	8	1389	171	241.7	89.6	99.8	177.3	15.5

## 98GR51 Apatite

n (cryst.)	Ns	Ni	Sum Ns	Sum Ni	Grain age	± 1s	Chi-sq.	Sum age	± 1s
13	5	16	5	16	67	34.4	---	67.0	34.4
23	5	13	10	29	82.4	43.4	77.7	73.9	27.2
24	4	8	14	37	106.9	65.6	84	81.1	25.6
22	2	4	16	41	106.9	92.6	93.3	83.6	24.8
20	3	6	19	47	106.9	75.7	97	86.6	23.7
18	4	8	23	55	106.9	65.6	98.7	89.5	22.4
15	3	6	26	61	106.9	75.7	99.5	91.2	21.6
14	3	6	29	67	106.9	75.7	99.8	92.6	20.8
12	3	6	32	73	106.9	75.7	99.9	93.8	20.1
10	2	4	34	77	106.9	92.6	100	94.5	19.7
8	4	8	38	85	106.9	65.6	100	95.7	18.9
5	7	14	45	99	106.9	49.6	100	97.2	17.8
19	4	7	49	106	122	76.6	100	98.9	17.4
11	4	7	53	113	122	76.6	100	100.3	17
9	3	5	56	118	128.1	93.6	100	101.5	16.8
1	3	5	59	123	128.1	93.6	100	102.6	16.6
6	5	8	64	131	133.3	76.1	100	104.5	16.3
21	7	11	71	142	135.7	65.8	100	106.9	16
16	4	6	75	148	142.1	91.9	100	108.3	15.8
4	2	3	77	151	142.1	129.8	100	109	15.7
3	2	3	79	154	142.1	129.8	100	109.6	15.6
2	4	6	83	160	142.1	91.9	100	110.9	15.5
17	3	4	86	164	159.7	122.1	100	112.1	15.4
7	6	6	92	170	212	122.6	100	115.6	15.5



## 98GR52 Apatite

n (cryst.)	Ns	Ni	Sum Ns	Sum Ni	Grain age	± 1s	Chi-sq.	Sum age	± 1s
10	0	12	0	12	0	0	---		
7	0	9	0	21	0	0	---		
24	0	7	0	28	0	0	---		
17	0	7	0	35	0	0	---		
2	0	6	0	41	0	0	---		
22	0	5	0	46	0	0	---		
19	0	5	0	51	0	0	---		
28	0	4	0	55	0	0	---		
27	0	2	0	57	0	0	---		
18	0	2	0	59	0	0	---		
5	1	20	1	79	11.4	11.7	98.5	2.9	2.9
25	1	17	2	96	13.4	13.8	98.9	4.8	3.4
11	1	11	3	107	20.8	21.7	98.4	6.4	3.8
15	1	10	4	117	22.8	24	98.4	7.8	4
20	1	8	5	125	28.5	30.3	98.1	9.1	4.2
14	1	8	6	133	28.5	30.3	98.3	10.3	4.3
23	1	7	7	140	32.6	34.9	98.3	11.4	4.4
8	2	12	9	152	38	29.1	97.2	13.5	4.7
1	1	6	10	158	38	41.1	97.6	14.5	4.7
16	1	5	11	163	45.6	50	97.6	15.4	4.8
6	1	5	12	168	45.6	50	97.7	16.3	4.9
3	2	10	14	178	45.6	35.4	97.4	18	5
26	1	4	15	182	57	63.7	97.4	18.8	5.1
21	2	8	17	190	57	45.1	96.6	20.4	5.2
13	2	8	19	198	57	45.1	96.2	21.9	5.3
12	1	3	20	201	75.8	87.6	96	22.7	5.4
9	7	10	27	211	158.2	78.2	37.2	29.2	6.1
4	3	4	30	215	169.4	129.5	22.3	31.9	6.3

## 99GR16 Apatite

n (cryst.)	Ns	Ni	Sum Ns	Sum Ni	Grain age	± 1s	Chi-sq.	Sum age	± 1s
20	1	3	1	3	76.4	88.3	---	76.4	88.3
19	4	10	5	13	91.6	54.3	88.8	88.1	46.4
22	2	4	7	17	114.3	99	95.8	94.3	42.4
21	2	4	9	21	114.3	99	98.9	98.1	39.2
18	1	2	10	23	114.3	140	99.8	99.5	37.8
15	2	4	12	27	114.3	99	99.9	101.7	35.4
12	2	4	14	31	114.3	99	100	103.3	33.4
7	5	9	19	40	126.9	70.9	100	108.6	30.5
16	4	7	23	47	130.4	81.9	100	111.9	28.7
4	4	7	27	54	130.4	81.9	100	114.3	27.2
14	7	12	34	66	133.1	63.5	100	117.7	25.1
11	3	5	37	71	136.9	100.1	100	119.1	24.4
10	3	5	40	76	136.9	100.1	100	120.2	23.8
9	6	10	46	86	136.9	70.8	100	122.2	22.7

8	3	5	49	91	136.9	100.1	100	123	22.1
1	11	18	60	109	139.4	53.5	100	125.7	20.6
23	4	6	64	115	151.9	98.2	100	127.1	20.2
17	4	6	68	121	151.9	98.2	100	128.3	19.9
13	4	6	72	127	151.9	98.2	100	129.4	19.5
6	4	6	76	133	151.9	98.2	100	130.4	19.2
5	2	3	78	136	151.9	138.8	100	130.9	19.1
3	6	9	84	145	151.9	80.2	100	132.2	18.6
2	3	4	87	149	170.7	130.5	100	133.3	18.5

## 99GR16 Zircon

n (cryst.)	Ns	Ni	Sum Ns	Sum Ni	Grain age	± 1s	Chi-sq.	Sum age	± 1s
3	29	6	29	6	94	42.3	---	94.0	42.3
34	72	13.3	101	19	105.2	31.6	82.5	103.3	26
6	110	20	211	39	106.9	26.2	96.7	105.2	18.6
2	182	31	393	70	114	22.4	98	109.1	14.6
21	66	10	459	80	128	43.6	98.3	111.5	14
7	67	10	526	90	130	44.2	98.8	113.5	13.4
8	88	13	614	103	131.3	39.2	99.1	115.8	12.9
18	61	9	675	112	131.5	47.1	99.5	117	12.5
22	34	5	709	117	131.9	63.3	99.8	117.7	12.3
26	111	16.1	820	133	133.8	35.9	99.9	119.7	11.8
11	76	11	896	144	134	43.4	99.9	120.8	11.5
1	140	20	1036	164	135.7	32.7	99.9	122.6	11
9	78	11	1114	175	137.5	44.5	100	123.5	10.8
13	93	13	1207	188	138.7	41.3	100	124.6	10.5
30	95	13.2	1302	201	139.9	41.4	100	125.7	10.3
17	95	13	1397	214	141.6	42.1	100	126.7	10.1
14	95	13	1492	227	141.6	42.1	100	127.5	9.9
12	201	27	1693	254	144.2	29.9	100	129.3	9.6
10	128	17	1821	271	145.9	37.9	100	130.3	9.4
16	69	9	1890	280	148.5	52.8	100	130.9	9.3
31	145	18.8	2035	298	149.2	36.9	100	132.4	9.2
29	62	8.05	2097	306	149.3	56.1	100	132.9	9.1
35	58	7.39	2155	313	152	59.6	100	133.5	9.1
32	175	21.9	2330	334	154.4	35.3	100	135.3	9
19	64	8	2394	342	154.9	58.3	100	135.7	8.9
23	139	17	2533	359	158.3	41	100	136.8	8.8
25	192	23.4	2725	382	158.8	35.1	100	138.3	8.7
27	42	5.12	2767	387	158.8	74.5	100	138.6	8.7
24	107	13	2874	400	159.3	47.1	100	139.3	8.6
33	62	7.39	2936	407	162.4	63.4	100	139.8	8.6
4	118	14	3054	421	163.1	46.4	100	140.6	8.5
20	276	32	3330	453	166.8	31.6	100	142.5	8.4
15	54	6	3384	459	174	75.1	100	142.9	8.4
5	158	17	3542	476	179.6	46.2	100	144.2	8.4
28	171	18.3	3713	494	180.7	44.8	100	145.6	8.3

## 99GR47 Apatite

n (cryst.)	Ns	Ni	Sum Ns	Sum Ni	Grain age	± 1s	Chi-sq.	Sum age	± 1s
29	0	24.6	0	24	0	0	---		
11	0	19	0	43	0	0	---		
20	0	13	0	56	0	0	---		
23	0	11.3	0	67	0	0	---		
7	0	11	0	78	0	0	---		
28	0	10.3	0	88	0	0	---		
13	0	10	0	98	0	0	---		
18	0	9	0	107	0	0	---		
27	0	8.2	0	115	0	0	---		
8	0	7	0	122	0	0	---		
31	0	6.15	0	128	0	0	---		
17	0	4	0	132	0	0	---		
5	1	26	1	158	7.2	7.4	96	1.2	1.2
24	1	19.5	2	177	9.7	9.9	95.4	2.1	1.5
19	1	18	3	195	10.5	10.8	95.9	2.9	1.7
12	1	16	4	211	11.8	12.1	96.4	3.6	1.8
3	1	16	5	227	11.8	12.1	97.2	4.1	1.9
25	1	15.4	6	242	12.2	12.6	97.9	4.7	1.9
21	1	15.4	7	257	12.2	12.6	98.5	5.1	2
9	1	15	8	272	12.6	13	98.9	5.5	2
16	1	13	9	285	14.5	15	99.1	5.9	2
6	1	12	10	297	15.7	16.3	99.3	6.3	2
14	1	11	11	308	17.1	17.9	99.4	6.7	2.1
10	1	11	12	319	17.1	17.9	99.5	7.1	2.1
26	1	10.3	13	329	18.4	19.2	99.6	7.4	2.1
15	1	10	14	339	18.8	19.7	99.6	7.8	2.1
2	2	17	16	356	22.1	16.6	99.5	8.5	2.2
22	2	14.4	18	370	26.2	19.8	99.1	9.2	2.2
1	3	21	21	391	26.9	16.6	98.3	10.1	2.3
4	4	20	25	411	37.6	20.6	92.9	11.5	2.4
30	2	8.2	27	419	45.8	36.2	88.3	12.1	2.4

## 99GR47 Zircon

n (cryst.)	Ns	Ni	Sum Ns	Sum Ni	Grain age	± 1s	Chi-sq.	Sum age	± 1s
20	63	12	63	12	103.1	32.7	---	103.1	32.7
17	58	11	121	23	103.6	34.2	99.2	103.3	23.7
19	44	8	165	31	108	41.7	99.5	104.5	20.7
1	40	7	205	38	112.2	46.1	99.8	105.9	19
7	87	15	292	53	113.8	32	99.9	108.2	16.5
9	167	28	459	81	117	24.2	99.9	111.2	13.9
22	97	16	556	97	118.9	32.3	100	112.5	12.9
6	419	69	975	166	119.1	16	100	115.3	10.4
13	55	9	1030	175	119.9	43.3	100	115.5	10.2
16	19	3	1049	178	124.2	77.3	100	115.6	10.1

12	178	28	1227	206	124.7	25.7	100	116.9	9.6
4	45	7	1272	213	126.1	51.4	100	117.2	9.5
3	39	6	1311	219	127.4	56	100	117.5	9.4
21	353	54	1664	273	128.2	19.2	100	119.6	8.7
5	103	15	1767	288	134.6	37.4	100	120.4	8.6
2	14	2	1781	290	137.1	103.8	100	120.5	8.6
8	347	49	2128	339	138.7	21.6	100	123.1	8.2
14	455	64	2583	403	139.3	19.1	100	125.7	7.9
10	96	13	2679	416	144.6	43	100	126.3	7.8
18	148	20	2827	436	144.9	34.8	100	127.1	7.7
15	52	7	2879	443	145.4	58.7	100	127.4	7.7
11	31	4	2910	447	151.7	80.7	100	127.6	7.7

## 99GR64 Apatite

n (cryst.)	Ns	Ni	Sum Ns	Sum Ni	Grain age	± 1s	Chi-sq.	Sum age	± 1s
9	4	62	4	62	13.1	6.7	---	13.1	6.7
7	6	81	10	143	15	6.4	83.6	14.1	4.6
11	2	23	12	166	17.6	13	94.4	14.6	4.4
4	4	44	16	210	18.4	9.6	96.8	15.4	4
1	3	29	19	239	20.9	12.7	97.7	16.1	3.9
5	4	37	23	276	21.9	11.5	98.1	16.9	3.7
2	2	17	25	293	23.8	17.8	98.9	17.3	3.6
10	3	22	28	315	27.6	17	98.5	18	3.6
8	3	20	31	335	30.3	18.8	98	18.7	3.6
3	4	23	35	358	35.1	19.1	95.6	19.8	3.6
6	6	19	41	377	63.6	29.9	53.5	22	3.7

## 99GR64 Zircon

n (cryst.)	Ns	Ni	Sum Ns	Sum Ni	Grain age	± 1s	Chi-sq.	Sum age	± 1s
7	83	14	83	14	118.9	34.6	---	118.9	34.6
3	32	5	115	19	128.2	61.8	89.1	121.3	30.3
9	58	9	173	28	129.1	46.4	98	123.8	25.5
2	58	9	231	37	129.1	46.4	99.7	125.1	22.5
10	46	7	277	44	131.6	53.6	99.9	126.2	20.9
6	41	6	318	50	136.8	60	100	127.4	19.8
1	56	8	374	58	140.1	53.1	100	129.2	18.7
5	92	13	466	71	141.7	42.2	100	131.5	17.3
4	109	15	575	86	145.4	40.3	100	133.9	16
11	183	25	758	111	146.5	31.6	100	136.7	14.5
8	293	38	1051	149	154.2	27	100	141.2	13.1

## 99GR84 Zircon

n (cryst.)	Ns	Ni	Sum Ns	Sum Ni	Grain age	± 1s	Chi-sq.	Sum age	± 1s
2	82	19	82	19	111.6	28.7	---	111.6	28.7
3	94	21	176	40	115.7	28.2	91.7	113.8	20.3
15	80	16	256	56	129.1	35.6	92	118.2	17.9
1	255	47	511	103	140	22.7	84.9	128.1	14.5
10	57	10	568	113	147	50.6	91.6	129.8	14.1
5	64	11	632	124	150	49.2	95	131.6	13.6
11	54	9	686	133	154.7	55.9	96.9	133.2	13.4
12	103	17	789	150	156.2	41.2	97.4	135.8	12.9
7	214	35	1003	185	157.6	29.2	97.1	139.9	12.1
9	207	33	1210	218	161.6	30.8	97	143.2	11.6
16	107	17	1317	235	162.1	42.7	98	144.6	11.3
13	177	28	1494	263	162.8	33.6	98.4	146.5	10.9
6	166	25	1660	288	170.9	37.1	98.5	148.6	10.7
19	140	21	1800	309	171.6	40.6	98.7	150.2	10.5
17	82	12	1882	321	175.8	54.7	99.1	151.2	10.4
18	69	10	1951	331	177.5	60.4	99.3	152	10.4
14	126	18	2077	349	180.1	45.8	99.4	153.4	10.2
8	126	17	2203	366	190.5	49.6	99.3	155.1	10.2
4	132	12	2335	378	280.8	85.2	92.7	159.2	10.3

## Paradalarga unit

## 98RS01 Apatite

n (cryst.)	Ns	Ni	Sum Ns	Sum Ni	Grain age	± 1s	Chi-sq.	Sum age	± 1s
22	0	9.13	0	9	0	0	---		
21	0	8.12	0	17	0	0	---		
18	0	9.13	0	26	0	0	---		
13	0	13	0	39	0	0	---		
12	0	13	0	52	0	0	---		
11	0	14	0	66	0	0	---		
9	0	12	0	78	0	0	---		
8	0	22	0	100	0	0	---		
7	0	18	0	118	0	0	---		
5	0	10	0	128	0	0	---		
4	0	22	0	150	0	0	---		
3	0	18	0	168	0	0	---		
2	0	9	0	177	0	0	---		
19	2	69	2	246	7	5	97.5	2	1.4
17	1	30.5	3	276	7.9	8	98.2	2.6	1.5
10	1	28	4	304	8.6	8.7	98.7	3.2	1.6
16	1	27.4	5	331	8.8	8.9	99.1	3.6	1.6
14	1	26	6	357	9.2	9.4	99.4	4	1.7
23	3	60.9	9	417	11.8	7	98.9	5.2	1.8
15	1	20	10	437	12	12.3	99.2	5.5	1.8

20	1	17.3	11	454	13.9	14.3	99.3	5.8	1.8
1	1	17	12	471	14.1	14.5	99.5	6.1	1.8
6	1	12	13	483	20	20.8	99.3	6.5	1.8

## 99GR04 Apatite

n (cryst.)	Ns	Ni	Sum Ns	Sum Ni	Grain age	± 1s	Chi-sq.	Sum age	± 1s
30	0	8.38	0	8	0	0	---		
29	0	7.3	0	15	0	0	---		
28	0	13.6	0	28	0	0	---		
27	0	15.7	0	43	0	0	---		
25	0	14.2	0	57	0	0	---		
23	0	26.4	0	83	0	0	---		
22	0	26.4	0	109	0	0	---		
20	0	18.3	0	127	0	0	---		
18	0	10.6	0	137	0	0	---		
15	0	8	0	145	0	0	---		
14	0	22	0	167	0	0	---		
12	0	17	0	184	0	0	---		
10	0	30	0	214	0	0	---		
9	0	8	0	222	0	0	---		
8	0	12	0	234	0	0	---		
6	0	8	0	242	0	0	---		
5	0	47	0	289	0	0	---		
4	0	20	0	309	0	0	---		
3	0	12	0	321	0	0	---		
1	0	19	0	340	0	0	---		
24	1	24.4	1	364	9.6	9.8	85.8	0.6	0.6
19	1	20.3	2	384	11.5	11.8	83.4	1.2	0.9
11	1	20	3	404	11.7	12	84.8	1.7	1
13	1	19	4	423	12.3	12.6	86.2	2.2	1.1
16	2	36.6	6	459	12.8	9.3	86.6	3.1	1.3
17	2	28.4	8	487	16.4	12	82.8	3.8	1.4
21	2	27.4	10	514	17	12.5	81.1	4.5	1.5
26	2	26.2	12	540	17.8	13.1	80.3	5.2	1.5
2	1	12	13	552	19.4	20.2	81.4	5.5	1.6
7	2	18	15	570	25.9	19.3	74.1	6.1	1.6

## 99GR04 Zircon

n (cryst.)	Ns	Ni	Sum Ns	Sum Ni	Grain age	± 1s	Chi-sq.	Sum age	± 1s
7	27	17	27	17	34.6	10.8	---	34.6	10.8
17	223	137	250	153	35.6	4	92.7	35.6	3.8
19	197	114	447	267	37.5	4.6	93.1	36.4	3.1
13	188	100	635	367	40.9	5.2	85	37.6	2.8
3	147	77	782	444	41.5	6	87.5	38.3	2.6
15	42	20.2	824	464	45.2	12.3	90.3	38.6	2.6
9	75	36	899	500	45.3	9.3	90.2	39.1	2.5

4	187	89	1086	589	45.7	6.1	83.8	40.1	2.4
11	34	16	1120	605	46.2	14.1	88.4	40.3	2.4
1	51	24	1171	629	46.2	11.5	91.1	40.5	2.4
8	86	40	1257	669	46.7	9.1	91.8	40.9	2.4
16	333	143	1590	811	50.8	5.3	66.4	42.6	2.3
6	55	23	1645	834	52	13	68.6	42.9	2.3
12	38	15.7	1683	849	52.6	15.9	72	43.1	2.3
5	60	24	1743	873	54.3	13.2	71.5	43.4	2.3
2	50	20	1793	893	54.3	14.5	72.6	43.7	2.3
14	175	69.8	1968	962	54.5	7.9	61.5	44.5	2.3
10	13	5	1981	967	56.5	29.8	66.7	44.6	2.3
18	238	81.9	2219	1048	63.1	8.3	27.1	46	2.3

99GR08 Apatite

n (cryst.)	Ns	Ni	Sum Ns	Sum Ni	Grain age	± 1s	Chi-sq.	Sum age	± 1s
36	0	16.4	0	16	0	0	---		
33	0	130	0	146	0	0	---		
29	0	88.3	0	234	0	0	---		
27	0	86.3	0	320	0	0	---		
25	0	34.9	0	354	0	0	---		
24	0	30.8	0	384	0	0	---		
22	0	20.5	0	404	0	0	---		
17	0	30	0	434	0	0	---		
16	0	23	0	457	0	0	---		
15	0	74	0	531	0	0	---		
12	0	64	0	595	0	0	---		
11	0	20	0	615	0	0	---		
9	0	43	0	658	0	0	---		
7	0	49	0	707	0	0	---		
4	0	27	0	734	0	0	---		
2	0	33	0	767	0	0	---		
20	1	124	1	891	1.4	1.4	98.6	0.2	0.2
19	1	85	2	976	2	2	97.4	0.3	0.2
30	1	84.2	3	1060	2	2	97.6	0.5	0.3
6	1	77	4	1137	2.2	2.2	97.9	0.6	0.3
5	1	72	5	1209	2.4	2.4	98.2	0.7	0.3
23	1	58.6	6	1267	2.9	2.9	98	0.8	0.3
18	1	58	7	1325	2.9	3	98.1	0.9	0.3
35	1	54.4	8	1379	3.1	3.2	98.2	1	0.4
34	1	48.3	9	1427	3.5	3.6	98.2	1.1	0.4
3	1	46	10	1473	3.7	3.7	98.2	1.2	0.4
31	1	44.2	11	1517	3.9	3.9	98.2	1.2	0.4
21	1	41.1	12	1558	4.1	4.2	98.2	1.3	0.4
32	2	82.2	14	1640	4.1	3	97.8	1.5	0.4
28	2	82.2	16	1722	4.1	3	97.6	1.6	0.4
1	2	67	18	1789	5.1	3.7	96.8	1.7	0.4
26	1	28.8	19	1817	5.9	6	96.5	1.8	0.4
14	3	81	22	1898	6.3	3.7	92.8	2	0.4
8	4	87	26	1985	7.8	4	80.2	2.2	0.4

10	2	42	28	2027	8.1	5.9	75.3	2.4	0.5
13	1	19	29	2046	9	9.2	74	2.5	0.5

99GR08 Zircon

n (cryst.)	Ns	Ni	Sum Ns	Sum Ni	Grain age	± 1s	Chi-sq.	Sum age	± 1s
17	33	20	33	20	33.3	9.5	---	33.3	9.5
16	35	21	68	41	33.6	9.3	98	33.4	6.7
21	162	73	230	114	44.7	6.5	48.6	40.7	4.8
19	44	19	274	133	46.6	12.9	64.4	41.5	4.6
22	205	88	479	221	46.9	6.2	69	43.7	3.8
9	80	34	559	255	47.4	9.8	79.2	44.2	3.6
20	120	50	679	305	48.3	8.3	85.1	44.8	3.4
7	111	44	790	349	50.8	9.2	87.6	45.6	3.3
2	116	45	906	394	51.9	9.3	89.1	46.3	3.2
3	45	17	951	411	53.3	15.3	92.1	46.6	3.1
10	75	28	1026	439	53.9	12.1	93.4	47.1	3.1
13	101	37	1127	476	54.9	10.7	93.6	47.7	3
6	172	63	1299	539	55	8.3	92.8	48.5	2.9
14	82	30	1381	569	55	11.9	94.3	48.9	2.9
11	29	10	1410	579	58.4	21.5	95.7	49	2.9
24	241	81	1651	660	59.9	7.9	90.1	50.4	2.8
12	73	24	1724	684	61.2	14.5	90.4	50.7	2.8
18	129	41	1853	725	63.3	11.5	87	51.5	2.8
5	86	27	1939	752	64.1	14.3	86.1	51.9	2.8
4	172	54	2111	806	64.1	10.2	81.1	52.7	2.8
23	360	110	2471	916	65.8	7.5	62.9	54.3	2.7
15	102	31	2573	947	66.2	13.7	62.7	54.7	2.7
1	189	49	2762	996	77.5	12.7	39.7	55.8	2.7
8	20	5	2782	1001	80.4	40.3	42.4	55.9	2.7

99GR09 Apatite

n (cryst.)	Ns	Ni	Sum Ns	Sum Ni	Grain age	± 1s	Chi-sq.	Sum age	± 1s
24	0	36.1	0	36	0	0	---		
23	0	50.7	0	86	0	0	---		
18	0	20	0	106	0	0	---		
17	0	27	0	133	0	0	---		
16	0	31	0	164	0	0	---		
15	0	46	0	210	0	0	---		
14	0	30	0	240	0	0	---		
11	0	60	0	300	0	0	---		
9	0	27	0	327	0	0	---		
7	0	35	0	362	0	0	---		
6	0	46	0	408	0	0	---		
3	0	34	0	442	0	0	---		
2	0	15	0	457	0	0	---		



12	1	56	1	513	3.2	3.2	84.1	0.4	0.4
27	1	54.6	2	567	3.3	3.3	88.2	0.6	0.4
5	1	54	3	621	3.3	3.4	91.5	0.9	0.5
30	1	52.7	4	673	3.4	3.4	93.9	1.1	0.5
1	1	52	5	725	3.5	3.5	95.8	1.2	0.6
10	2	100	7	825	3.6	2.6	96.8	1.5	0.6
29	1	48.8	8	873	3.7	3.7	97.8	1.6	0.6
22	1	48.8	9	921	3.7	3.7	98.6	1.8	0.6
13	1	48	10	969	3.7	3.8	99	1.9	0.6
8	2	86	12	1055	4.2	3	99.2	2	0.6
4	1	40	13	1095	4.5	4.5	99.4	2.1	0.6
26	1	40	14	1134	4.5	4.6	99.6	2.2	0.6
28	1	39	15	1173	4.6	4.7	99.7	2.3	0.6
25	2	61.4	17	1234	5.8	4.2	99.6	2.5	0.6
20	1	27	18	1261	6.7	6.8	99.7	2.6	0.6
21	2	42.9	20	1303	8.4	6.1	99.2	2.8	0.6
19	1	20	21	1323	9	9.2	99	2.8	0.6

Upano unit

99GR01 Apatite

n (cryst.)	Ns	Ni	Sum Ns	Sum Ni	Grain age	± 1s	Chi-sq.	Sum age	± 1s
5	0	6	0	6	0	0	---		
2	0	6	0	12	0	0	---		
6	1	9	1	21	23.5	24.8	53.3	10.1	10.3
3	1	7	2	28	30.2	32.3	68.8	15.1	11.1
1	2	12	4	40	35.3	27	77.6	21.2	11.1
4	2	11	6	51	38.5	29.6	85.1	24.9	10.8

99GR01 Zircon

n (cryst.)	Ns	Ni	Sum Ns	Sum Ni	Grain age	± 1s	Chi-sq.	Sum age	± 1s
12	8	6	8	6	27.4	14.8	---	27.4	14.8
10	4	3	12	9	27.4	21	---	27.4	12.1
9	19	13	31	22	30.1	10.9	98.7	29	8.1
1	40	27	71	49	30.5	7.7	99.8	29.8	5.6
13	64	39	135	88	33.8	6.9	99.3	31.6	4.4
2	15	9	150	97	34.3	14.5	99.8	31.8	4.3
8	24	13	174	110	38	13.1	99.8	32.5	4.1
6	10	5	184	115	41.1	22.6	99.8	32.9	4.1
7	33	14	217	129	48.4	15.5	98.1	34.6	4
3	45	17	262	146	54.4	15.6	89.3	36.9	4
5	84	29	346	175	59.5	13	58.4	40.7	4
11	33	11	379	186	61.6	21.5	53.9	41.9	4
4	215	58	594	244	76	11.5	3	50	4.1

## Pumbuiza Fm.

## 99GR71 Zircon

n (cryst.)	Ns	Ni	Sum Ns	Sum Ni	Grain age	± 1s	Chi-sq.	Sum age	± 1s
15	116	6	116	6	415.1	174.4	---	415.1	174.4
7	414	21	530	27	423	95.8	96.7	421.2	84.4
14	283	14	813	41	433.3	119.6	99.5	425.4	69.7
18	422	20.7	1235	61	436.1	99.3	99.9	434	58.9
9	453	22	1688	83	441.1	97.6	100	435.9	51.4
17	226	10.9	1914	93	445.5	139.3	100	440.9	49.3
4	316	15	2230	108	451	120.2	100	442.3	46.3
16	252	11.9	2482	119	455.1	136.2	100	446.7	44.8
3	412	19	2894	138	463.7	110	100	449	42.2
19	44	2.03	2938	140	464.7	334.4	100	449.3	42
2	348	16	3286	156	465.1	120	100	450.9	40.2
13	197	9	3483	165	468	160.4	100	451.9	39.4
5	311	14	3794	179	474.7	130.8	100	453.7	38.2
6	428	19	4222	198	481.1	114.1	100	456.3	36.9
8	71	3	4293	201	504.5	297.9	100	457	36.7
11	196	8	4489	209	521.6	189	100	459.5	36.3
10	221	9	4710	218	522.7	178.7	100	462.1	35.9
1	1233	50	5943	268	524.9	77.9	100	473.9	34
12	151	6	6094	274	535.2	223.6	100	475.2	33.8

## Sediments

## 98GR2 Zircon

n (cryst.)	Ns	Ni	Sum Ns	Sum Ni	Grain age	± 1s	Chi-sq.	Sum age	± 1s
7	21	10	21	10	73.2	28.2	---	73.2	28.2
16	220	80	241	90	95.7	12.8	50.5	93.2	11.9
39	14	4.96	255	94	98.2	51.4	79.3	94.4	11.8
56	79	27.8	334	121	99	22.1	91.2	96	10.6
18	23	7	357	128	114.2	49.4	95	97	10.4
46	47	13.9	404	141	117.6	36.1	94.9	99.7	10.2
45	24	5.95	428	146	139.9	64.2	93.7	101.9	10.3
51	80	16.9	508	162	164.3	44.3	64.1	109	10.4
12	38	8	546	170	164.4	64.2	59.4	111.6	10.4
54	34	6.94	580	176	169.5	70.8	56	114.5	10.5
40	10	1.98	590	177	174.6	136	61	115.8	10.6
36	64	12	654	189	184.3	58.3	45.6	120.2	10.6
28	32	6	686	195	184.3	82.2	44.3	122.1	10.6
55	43	7.93	729	202	187.3	72.6	39.6	125.3	10.7
47	22	3.97	751	205	191.4	104.5	40.6	127.2	10.8
48	84	14.9	835	219	195	55.2	27.9	132.3	10.9
38	17	2.97	852	221	197.6	124.4	30.1	133.7	10.9
14	42	7	894	228	207	84.7	27.4	136	10.9
31	159	26	1053	254	210.9	45.1	11	143.7	11
27	80	13	1133	267	212.2	63.8	8.3	147.1	11

42	75	11.9	1208	278	217.4	68.2	6.4	150.5	11.1
50	33	4.96	1241	282	229.1	110.6	6.4	152.4	11.1
25	20	3	1261	285	229.5	142.3	7.3	153.3	11.1
52	71	9.91	1332	294	246.4	83.9	4.9	156.9	11.2
29	217	27	1549	321	275.7	56.9	0.5	175.3	12.1
26	73	9	1622	330	278.2	98.7	0.3	179.3	12.2
24	85	10	1707	340	291.3	97.8	0.2	183.5	12.3
11	17	2	1724	342	291.3	217.9	0.2	187.4	12.5
32	114	13	1838	355	300.3	88.4	0.1	191.3	12.6
35	393	44	2231	399	305.7	49.5	0	195.2	12.2
15	38	4	2269	403	324.7	171	0	199.4	12.4
9	72	7	2341	410	350.8	139.3	0	204.2	12.7
49	42	3.97	2383	413	360.6	189.7	0	209.0	12.9
20	43	4	2426	417	366.2	191.8	0	213.6	13.1
57	87	7.93	2513	424	373.5	139	0	218.3	13.3
21	45	4	2558	428	382.8	200.1	0	222.9	13.6
44	104	8.92	2662	436	396.3	138.8	0	227.6	13.7
33	82	7	2744	443	398.1	157.2	0	232.2	13.9
8	24	2	2768	445	407.5	300.2	0	236.7	14.2
53	66	4.96	2834	449	450.3	210.1	0	242.2	14.4
30	168	12	3002	461	473	142.1	0	247.9	14.6
37	28	1.98	3030	462	477.6	351.5	0	253.5	14.9
34	58	4	3088	466	489.2	253.4	0	259.0	15.2
10	44	3	3132	469	494.6	295.6	0	264.5	15.5
3	74	5	3206	474	499	231.1	0	269.8	15.7
23	30	2	3236	476	505.4	369.5	0	275.0	16
43	1542	100	4778	576	518.3	55.9	0	280.3	15.1
1	31	2	4809	578	521.6	380.9	0	285.4	15.4
2	32	2	4841	580	537.8	392.3	0	290.7	15.7
6	51	3	4892	583	569.9	339.1	0	296.4	15.9
5	35	2	4927	585	586	426.4	0	302.2	16.2
17	107	6	5034	591	596.6	251	0	308.0	16.5
4	489	25	5523	616	651.6	135.1	0	314.6	16.6
19	59	3	5582	619	654.9	388.2	0	321.1	16.9
13	43	2	5625	621	712.7	516	0	328.4	17.3
22	44	2	5669	623	728.4	527.1	0	335.8	17.6
41	46	1.98	5715	624	766.9	557.1	0	343.6	18

====BinomFit Program v. 1.8=====

DATE\TIME: 03-09-2001\14:45:26 FILENAME:

C:\PROGRA~1\TRACKKEY\FTPEAKS\98GR2.FTZ

FILE HEADER:"98GR2"

FIT OPTION: Best-fit peaks using the binomial model of Galbraith and Green

-----INITIAL GUESS FOR MODEL PARAMETERS-----

NUMBER OF PEAKS TO FIT = 3

PEAK #)	PEAK AGE	THETA	FRACTION(%)	COUNT
1)	100.00	0.742	10.1	5.75
2)	260.00	0.883	21.3	12.15
3)	500.00	0.937	19.0	10.81

TOTAL RANGE FOR GRAIN AGES = 71.4 to 640.0 Ma

NUMBER OF GRAINS = 57  
 DEGREES OF FREEDOM FOR FIT = 52  
 AVERAGE OF THE SE(Z)'S FOR THE GRAINS = 0.46  
 ESTIMATED WIDTH OF PEAKS IN PD PLOT IN Z UNITS = 0.54

-----PARAMETERS FOR BEST-FIT PEAKS-----  
 {Standard error for peak age includes group error}  
 {Peak width is for PD plot assuming a kernel factor = 0.60}

PEAK NUMBER	MEAN	63% CI	95% CI	W(Z)	FRAC(%)	SE(%)	COUNT	
1)	101.1	( -11.2 +12.5)	( -20.7 +26.0)	0.27	10.1	5.2	5.7	
2)	266.5	( -22.6 +24.6)	( -42.5 +50.4)	0.42	62.7	12.7	35.8	
3)	515.5	( -43.5 +47.3)	( -81.8 +96.6)	0.35	27.2	12.2	15.5	
TOTAL:							100.0	57.0

LOG-LIKELIHOOD FOR BEST FIT = -1.5116E+02  
 CHI-SQUARED VALUE FOR BEST FIT = 5.1110E+01  
 REDUCED CHI-SQUARED VALUE = 9.8288E-01  
 DEGREES OF FREEDOM FOR FIT = 52  
 CONDITION NUMBER FOR COVAR MATRIX = 11.02  
 NUMBER OF ITERATIONS = 13  
 =====BinomFit Program v. 1.8=====

98GR5 Zircon

n (cryst.)	Ns	Ni	Sum Ns	Sum Ni	Grain age	± 1s	Chi-sq.	Sum age	± 1s
45	83	26.6	83	26	94.2	21.2	---	94.2	21.4
25	43	12.5	126	38	103.8	33.5	76.7	100.1	18.8
11	101	29	227	67	105.1	22.4	92.5	102.2	14.6
54	215	57.6	442	124	112.5	17.1	92.4	107.5	11.5
42	145	37.1	587	161	117.8	22	94.7	110	10.4
52	111	27.3	698	188	122.5	26.5	96.1	112	9.9
24	78	17.3	776	205	135.7	36.3	95.4	114.1	9.7
36	60	12.4	836	217	145.5	45.7	94.4	116.1	9.6
53	159	31.3	995	248	152.7	30.3	83.5	120.9	9.5
49	88	17.1	1083	265	154.7	41.2	81.6	123.1	9.4
40	306	59	1389	324	155.9	22.8	63.8	129.1	9
33	182	33.3	1571	357	164.1	31.4	56	132.5	8.9
47	80	13.3	1651	370	180.4	53.8	53.5	134.3	8.9
55	145	22.2	1796	392	195.7	45.1	37.9	137.9	8.9
1	88	13	1884	405	202.7	60.6	32.2	140	9
58	97	14.1	1981	419	205.9	59.1	26.4	142.2	9
2	72	10	2053	429	215.4	73	23.2	143.9	9
43	283	31.4	2336	460	268.5	51.3	1.6	152.6	9.3
8	131	14	2467	474	278.5	78.9	0.5	164	9.9
50	92	8.6	2559	482	317.4	113.7	0.2	171.7	10.2
17	193	18	2752	500	318.2	79.1	0	178.8	10.5
46	84	7.6	2836	507	327.7	124.6	0	185.6	10.9
5	144	13	2980	520	328.4	95.7	0	191.9	11.1
60	101	9.1	3081	529	329.1	114.4	0	197.7	11.4
9	113	10	3194	539	334.9	111	0	203.2	11.6
59	149	13.1	3343	552	337	97.8	0	208.4	11.8
15	275	24	3618	576	339.4	73.1	0	213.3	11.9

37	79	6.7	3697	582	349	140.9	0	218.2	12.1
28	94	7.7	3791	589	361	135.9	0	223.2	12.3
13	246	20	4037	609	363.7	85.4	0	227.9	12.5
10	197	16	4234	625	364	95.4	0	232.4	12.6
32	235	19	4469	644	365.6	88	0	236.6	12.7
38	131	10.5	4600	654	368.7	118.9	0	240.6	12.8
61	79	6.1	4679	660	382.4	161.2	0	244.8	13
4	92	7	4771	667	387.9	152.6	0	249	13.2
21	26	1.9	4797	668	403.4	303.4	0	253.3	13.4
35	109	7.6	4906	675	422.1	159	0	257.9	13.6
12	96	6	5002	681	469.2	198	0	263.6	13.9
14	336	20	5338	701	491.8	114.4	0	269.5	14
56	177	10.1	5515	711	512.2	166.6	0	275.7	14.3
31	85	4.8	5600	715	517.3	243.3	0	281.7	14.6
51	155	8.1	5755	723	557.3	201.7	0	288.4	14.9
48	257	13.3	6012	736	562.5	159.3	0	294.9	15.1
44	169	8.6	6181	744	571.6	200.7	0	301.3	15.4
23	75	3.8	6256	747	574	302.4	0	307.5	15.7
18	181	9	6437	756	584.4	200.5	0	313.7	15.9
3	141	7	6578	763	585.3	227.5	0	319.6	16.2
7	202	10	6780	773	586.9	191.1	0	325.3	16.4
6	122	6	6902	779	590.6	247.7	0	330.8	16.6
16	163	8	7065	787	591.7	215.2	0	336.1	16.8
39	98	4.8	7163	791	592.9	277.9	0	341.2	17.1
19	144	7	7307	798	597.2	232	0	346.3	17.3
57	126	6.1	7433	804	599.5	249.3	0	351.1	17.5
22	163	7.7	7596	811	613.7	227.2	0	356.1	17.7
20	106	5	7702	816	614.6	282	0	360.9	17.9
29	143	6.7	7845	822	618.6	245.4	0	365.6	18.1
26	184	8.6	8029	830	620	217.3	0	370.1	18.2
27	249	11.5	8278	841	627.1	190.3	0	374.6	18.4
41	149	6.7	8427	847	643.3	254.9	0	379.3	18.6
30	286	12.5	8713	859	660.9	192.2	0	384.1	18.7
34	69	2.9	8782	861	685.9	411.8	0	389.2	18.9

====BinomFit Program v. 1.8====  
 DATE\TIME: 12-15-2002\12:52:37 FILENAME: D:\TRACKK~1\FTPEAKS\98GR5.FTZ  
 FILE HEADER:"98GR5"

FIT OPTION: Best-fit peaks using the binomial model of Galbraith and Green

-----INITIAL GUESS FOR MODEL PARAMETERS-----

NUMBER OF PEAKS TO FIT = 2

PEAK #)	PEAK AGE	THETA	FRACTION(%)	COUNT
1)	140.00	0.826	12.3	7.51
2)	450.00	0.940	24.0	14.64

TOTAL RANGE FOR GRAIN AGES = 90.9 to 623.9 Ma

NUMBER OF GRAINS = 61

DEGREES OF FREEDOM FOR FIT = 58

AVERAGE OF THE SE(Z)'S FOR THE GRAINS = 0.33

ESTIMATED WIDTH OF PEAKS IN PD PLOT IN Z UNITS = 0.39

-----PARAMETERS FOR BEST-FIT PEAKS-----

{Standard error for peak age includes group error}

{Peak width is for PD plot assuming a kernel factor = 0.60}

PEAK NUMBER	MEAN	63% CI	95% CI	W(Z)	FRAC (%)	SE (%)	COUNT	
1)	138.9	( -8.7 +9.3)	( -16.6 +18.8)	0.25	26.6	6.0	16.2	
2)	426.1	( -23.8 +25.2)	( -45.5 +50.7)	0.38	73.4	6.0	44.8	
TOTAL:							100.0	61.0

LOG-LIKELIHOOD FOR BEST FIT = -1.9109E+02  
 CHI-SQUARED VALUE FOR BEST FIT = 6.0862E+01  
 REDUCED CHI-SQUARED VALUE = 1.0493E+00  
 DEGREES OF FREEDOM FOR FIT = 58  
 CONDITION NUMBER FOR COVAR MATRIX = 1.58  
 NUMBER OF ITERATIONS = 6

====BinomFit Program v. 1.8=====

98RS6 Zircon

n (cryst.)	Ns	Ni	Sum Ns	Sum Ni	Grain age	± 1s	Chi-sq.	Sum age	± 1s
31	118	49.2	118	49	69.1	11.9	---	69.1	12
44	27	10.4	145	59	74.5	27.3	84	70.7	11.2
34	65	25.1	210	84	74.6	17.7	95.5	71.9	9.6
5	52	20	262	104	74.8	19.8	99	72.5	8.7
35	53	20.3	315	124	75.3	19.8	99.8	73.1	8.1
37	56	21.2	371	145	76	19.5	99.9	73.6	7.6
47	57	20.8	428	165	78.7	20.3	100	74.6	7.3
9	44	16	472	181	79.1	23.2	100	75	7
3	31	10	503	191	89.1	32.5	100	75.7	6.9
53	24	7.58	527	198	91	38	100	76.5	6.9
29	164	51	691	249	92.4	15.1	99.6	79.8	6.5
49	181	54.9	872	303	94.6	14.9	98.7	82.7	6.2
23	23	6.9	895	309	95.7	41.7	99.2	83.3	6.2
32	17	4.82	912	313	101.2	52.4	99.5	83.7	6.2
10	25	7	937	320	102.5	44	99.6	84.2	6.1
4	77	18	1014	338	122.6	32.4	97.8	86.2	6.1
13	20	4	1034	342	143.1	78.5	97.2	86.9	6.1
46	61	11.4	1095	353	153.5	49.9	88.3	89.1	6.2
43	65	11.4	1160	364	163.4	52.8	70	91.5	6.3
14	220	37	1380	401	169.8	30.7	10.2	98.8	6.5
8	58	9	1438	410	183.8	66.1	6	100.7	6.6
2	112	17	1550	427	187.8	49.3	1.5	104.2	6.7
6	64	9	1614	436	202.5	72.4	0.7	113	7.2
16	88	12	1702	448	208.7	64.6	0.2	117	7.3
22	44	5.9	1746	453	212.2	93.3	0.1	120.8	7.5
24	63	7.8	1809	460	229.5	87.5	0	125	7.7
50	172	20.8	1981	480	234.6	55	0	129.1	7.8
7	127	15	2108	495	240.4	66.1	0	133.1	8
1	78	9	2186	504	246	87	0	137.1	8.2
11	140	16	2326	520	248.3	66	0	140.8	8.3
15	97	11	2423	531	250.2	80	0	144.4	8.4
45	113	11.4	2536	542	281.5	88.1	0	148.7	8.6
12	183	18	2719	560	287.6	71.7	0	152.9	8.7
18	298	27.5	3017	587	306.1	61.8	0	157.5	8.8
21	34	2.9	3051	589	330.6	202.5	0	162.5	9.1

19	306	23.5	3357	612	366.1	79.3	0	168.3	9.3
41	158	11.6	3515	623	383.8	117.6	0	174.2	9.5
33	305	20.3	3820	643	421.7	97.8	0	180.8	9.8
28	123	7.8	3943	650	440.8	163.4	0	187.6	10.1
20	141	8.8	4084	658	447.6	156.2	0	194.2	10.4
27	115	6.9	4199	664	465	182.9	0	201	10.7
30	340	19.6	4539	683	483.3	113.4	0	207.8	11
36	306	17.3	4845	700	491.3	122.4	0	214.6	11.2
17	1585	83.4	6430	783	527.6	61.8	0	221.9	11.2
38	225	11.6	6655	794	539.8	163.8	0	229.1	11.5
42	599	30.3	7254	824	548	103.6	0	236.2	11.7
25	121	5.9	7375	829	567.6	240	0	243.4	12
26	106	4.9	7481	833	597.3	276.7	0	251	12.4
39	173	7.71	7654	840	618.5	228.6	0	258.7	12.7
51	43	1.9	7697	841	623.6	462.7	0	266.2	13.1
52	174	7.58	7871	848	632.1	235.5	0	273.6	13.4
54	67	2.84	7938	850	648.8	393.6	0	281	13.8
48	134	5.68	8072	855	648.8	278.8	0	288.2	14.1
40	76	0.96	8148	855	1959.8	2014	0	323.4	15.8

====BinomFit Program v. 1.8=====

DATE\TIME: 03-09-2001\15:25:43 FILENAME:  
 C:\PROGRA~1\TRACKKEY\FTPEAKS\98RS6-A.FTZ  
 FILE HEADER:"eth-175/15 98RS6"

FIT OPTION: Best-fit peaks using the binomial model of Galbraith and Green

-----INITIAL GUESS FOR MODEL PARAMETERS-----

NUMBER OF PEAKS TO FIT = 3  
 PEAK #) PEAK AGE THETA FRACTION(%) COUNT  
 1) 85.00 0.752 18.5 9.98  
 2) 230.00 0.892 16.8 9.05  
 3) 500.00 0.948 21.2 11.46

TOTAL RANGE FOR GRAIN AGES = 67.1 to 1333.4 Ma  
 NUMBER OF GRAINS = 54  
 DEGREES OF FREEDOM FOR FIT = 49  
 AVERAGE OF THE SE(Z)'S FOR THE GRAINS = 0.35  
 ESTIMATED WIDTH OF PEAKS IN PD PLOT IN Z UNITS = 0.41

-----PARAMETERS FOR BEST-FIT PEAKS-----

{Standard error for peak age includes group error}  
 {Peak width is for PD plot assuming a kernel factor = 0.60}

PEAK NUMBER	PEAK AGE & CONF. INTERVAL (MA)	PEAK WIDTH W(Z)	GRAINS IN PEAK
	MEAN (---63% CI---) (---95% CI---)		FRAC(%) SE(%) COUNT
1)	83.8 ( -6.0 +6.5) ( -11.3 +13.1)	0.29	29.2 6.8 15.7
2)	224.5 ( -21.6 +23.8) ( -40.3 +49.0)	0.33	34.2 8.3 18.5
3)	480.9 ( -34.8 +37.4) ( -65.9 +75.9)	0.31	36.7 8.1 19.8
			TOTAL: 100.0 54.0

LOG-LIKELIHOOD FOR BEST FIT = -1.7961E+02  
 CHI-SQUARED VALUE FOR BEST FIT = 4.8877E+01  
 REDUCED CHI-SQUARED VALUE = 9.9749E-01  
 DEGREES OF FREEDOM FOR FIT = 49  
 CONDITION NUMBER FOR COVAR MATRIX = 4.52  
 NUMBER OF ITERATIONS = 6

====BinomFit Program v. 1.8=====

## 98GR16 Zircon

n (cryst.)	Ns	Ni	Sum Ns	Sum Ni	Grain age	± 1s	Chi-sq.	Sum age	± 1s
3	43	25	43	25	38.7	9.8	---	38.7	9.8
5	85	49	128	74	39	7.1	97.8	38.9	5.8
23	196	110	324	184	40	4.9	98.9	39.6	3.9
27	93	50.5	417	234	41.4	7.3	99.5	40.1	3.5
1	80	43	497	277	41.8	8	99.8	40.3	3.3
2	58	31	555	308	42	9.5	99.9	40.5	3.2
18	95	50	650	358	42.7	7.6	100	40.8	3
17	54	28	704	386	43.3	10.2	100	41	2.9
22	45	23	749	409	44	11.4	100	41.2	2.9
4	49	24	798	433	45.9	11.5	100	41.4	2.8
45	58	28.3	856	461	46	10.7	100	41.7	2.8
19	31	15	887	476	46.4	14.7	100	41.9	2.7
10	46	22	933	498	47	12.3	100	42.1	2.7
11	77	36	1010	534	48	9.8	100	42.5	2.7
12	30	14	1040	548	48.1	15.7	100	42.6	2.6
26	95	43.5	1135	591	49.1	9.1	100	43.2	2.6
15	78	35	1213	626	50.1	10.3	100	43.5	2.6
7	93	40	1306	666	52.2	10	100	44.1	2.5
30	71	30.3	1377	696	52.6	11.5	100	44.5	2.5
9	48	20	1425	716	53.9	14.4	100	44.7	2.5
41	93	37.4	1518	753	55.8	11	99.9	45.3	2.5
6	163	64	1681	817	57.2	8.6	99.2	46.2	2.5
16	126	49	1807	866	57.7	9.9	98.3	46.9	2.5
24	76	29.3	1883	895	58.2	12.8	97.9	47.3	2.5
29	83	31.3	1966	926	59.4	12.6	97.2	47.7	2.4
40	113	42.5	2079	968	59.7	10.9	95.8	48.2	2.4
46	60	22.2	2139	990	60.5	15.2	95.6	48.5	2.4
38	107	39.4	2246	1029	60.9	11.5	94	49	2.4
13	64	23	2310	1052	62.4	15.3	93.4	49.3	2.4
21	48	17	2358	1069	63.4	18	93.3	49.5	2.4
14	364	126	2722	1195	64.8	7	72.5	51.2	2.4
25	230	76.8	2952	1271	67.2	9.1	55.1	52.2	2.4
31	44	14.2	2996	1285	69.7	21.4	55.1	52.4	2.4
44	109	33.4	3105	1318	73.3	14.7	44.9	52.9	2.4
20	80	24	3185	1342	74.7	17.6	38.7	53.3	2.4
39	130	37.4	3315	1379	77.9	14.7	25.2	54	2.5
32	264	73.8	3579	1452	80.2	10.9	6.6	55.3	2.5
33	379	103	3958	1555	82.4	9.5	0.5	55.2	2.4
36	122	32.4	4080	1587	84.5	16.9	0.3	56	2.5
35	146	37.4	4226	1624	87.4	16.3	0.1	56.8	2.5
42	144	36.4	4370	1660	88.6	16.7	0	57.5	2.5
43	102	25.3	4472	1685	90.4	20.3	0	58.3	2.5
34	113	27.3	4585	1712	92.7	20	0	59.1	2.5
37	164	37.4	4749	1749	98.1	18.1	0	60	2.6
8	71	12	4820	1761	132	41.4	0	61.6	2.6
28	230	21.2	5050	1782	239.8	54.9	0	65.5	2.8



```

=====BinomFit Program v. 1.8=====
DATE\TIME: 12-15-2002\18:31:04 FILENAME:
D:\TRACKK~1\FTPEAKS\98GR16.FTZ
FILE HEADER:"98GR16"
    
```

FIT OPTION: Best-fit peaks using the binomial model of Galbraith and Green

-----INITIAL GUESS FOR MODEL PARAMETERS-----

```

NUMBER OF PEAKS TO FIT = 4
PEAK #)  PEAK AGE      THETA      FRACTION(%)  COUNT
  1)      45.00        0.667        40.1        18.46
  2)      60.00        0.728        41.8        19.22
  3)      80.00        0.781        29.7        13.65
  4)     240.00        0.916         2.4         1.10
    
```

```

TOTAL RANGE FOR GRAIN AGES = 38.3 to 234.8 Ma
NUMBER OF GRAINS = 46
DEGREES OF FREEDOM FOR FIT = 39
AVERAGE OF THE SE(Z)'S FOR THE GRAINS = 0.21
ESTIMATED WIDTH OF PEAKS IN PD PLOT IN Z UNITS = 0.25
    
```

-----PARAMETERS FOR BEST-FIT PEAKS-----

```

{Standard error for peak age includes group error}
{Peak width is for PD plot assuming a kernel factor = 0.60}
    
```

PEAK NUMBER	MEAN	----63% CI----		----95% CI----		W(Z)	FRAC (%)	SE (%)	COUNT
1)	46.1	( -4.2	+4.7)	( -8.0	+9.6)	0.23	35.2	23.9	16.2
2)	60.4	( -7.4	+8.4)	( -13.7	+17.7)	0.22	35.1	24.8	16.1
3)	81.1	( -6.7	+7.3)	( -12.6	+15.0)	0.21	27.4	12.9	12.6
4)	238.9	( -49.3	+61.9)	( -87.2	+135.9)	0.27	2.3	2.3	1.1
TOTAL: 100.0									46.0

```

LOG-LIKELIHOOD FOR BEST FIT = -1.5812E+02
CHI-SQUARED VALUE FOR BEST FIT = 4.2898E+01
REDUCED CHI-SQUARED VALUE = 1.1000E+00
DEGREES OF FREEDOM FOR FIT = 39
CONDITION NUMBER FOR COVAR MATRIX = 708.02
NUMBER OF ITERATIONS = 6
    
```

=====BinomFit Program v. 1.8=====

98GR28 Zircon

n (cryst.)	Ns	Ni	Sum Ns	Sum Ni	Grain age	± 1s	Chi-sq.	Sum age	± 1s
14	50	27	50	27	38.8	9.4	---	38.8	9.4
12	78	40	128	67	40.9	8.1	86.7	40.1	6.2
8	91	44	219	111	43.4	8.1	93.2	41.4	5
13	48	23	267	134	43.8	11.2	98.1	41.8	4.6
18	26	12	293	146	45.4	15.9	99.4	42.1	4.5
40	90	40.4	383	186	46.7	9	99.3	43.2	4.1
11	160	68	543	254	49.3	7.3	98.1	44.8	3.7
17	261	104	804	358	52.6	6.3	92.7	47.1	3.4
31	32	12.1	836	370	55.3	18.7	95	47.4	3.3
28	43	16.2	879	386	55.7	16.4	96.2	47.7	3.3
1	124	46	1003	432	56.5	9.9	95	48.7	3.2
27	30	11.1	1033	443	56.6	20	96.6	48.9	3.2

4	33	12	1066	455	57.6	19.5	97.6	49.1	3.2
6	92	33	1158	488	58.4	12	97.3	49.7	3.1
3	112	40	1270	528	58.6	11	96.9	50.4	3.1
33	60	21.2	1330	549	59.2	15.1	97.4	50.8	3.1
19	286	100	1616	649	59.9	7.2	94.5	52.2	3
23	87	30.3	1703	679	60.1	12.8	95.2	52.6	2.9
16	55	19	1758	698	60.6	16.3	96.2	52.8	2.9
26	41	14.1	1799	712	60.7	18.8	97.1	52.9	2.9
10	174	60	1973	772	60.7	9.3	96.8	53.6	2.9
20	74	25	2047	797	62	14.5	97.3	53.8	2.8
34	42	14.1	2089	811	62.2	19.2	97.9	54	2.8
5	36	12	2125	823	62.8	21	98.4	54.1	2.8
36	64	21.2	2189	844	63.2	16	98.7	54.3	2.8
24	52	17.2	2241	861	63.4	17.8	98.9	54.5	2.8
32	78	25.3	2319	886	64.7	15	99	54.8	2.8
15	34	11	2353	897	64.7	22.5	99.2	55	2.8
38	63	20.2	2416	917	65.3	16.8	99.3	55.2	2.8
37	218	66.7	2634	983	68.5	9.8	98.2	56.1	2.8
2	170	51	2804	1034	69.8	11.4	97	56.8	2.8
30	61	18.2	2865	1052	70.2	18.9	97.1	57	2.8
9	96	28	2961	1080	71.7	15.6	96.5	57.4	2.8
7	18	5	2979	1085	75.3	38.1	97.1	57.5	2.8
25	79	20.2	3058	1105	81.8	20.6	95.2	58	2.8
29	65	16.2	3123	1121	84.1	23.5	93.2	58.4	2.8
35	96	23.2	3219	1144	86.4	20.2	87.7	58.9	2.8
39	84	19.2	3303	1163	91.4	23.3	79.8	59.5	2.8
21	263	28	3566	1191	194.7	39.2	0.1	64.7	3
22	52	5	3618	1196	215.2	101	0	68.5	3.2

```

=====BinomFit Program v. 1.8=====
DATE\TIME: 12-15-2002\18:06:29 FILENAME:
D:\TRACKK~1\FTPEAKS\98GR28.FTZ
FILE HEADER: "Puyo-Macas 98GR28"

```

FIT OPTION: Best-fit peaks using the binomial model of Galbraith and Green

-----INITIAL GUESS FOR MODEL PARAMETERS-----

```

NUMBER OF PEAKS TO FIT = 2
PEAK #)  PEAK AGE      THETA      FRACTION(%)  COUNT
  1)      55.00         0.724         56.5         22.59
  2)     200.00         0.906          4.4          1.74

```

```

TOTAL RANGE FOR GRAIN AGES = 38.5 to 197.8 Ma
NUMBER OF GRAINS = 40
DEGREES OF FREEDOM FOR FIT = 37
AVERAGE OF THE SE(Z)'S FOR THE GRAINS = 0.26
ESTIMATED WIDTH OF PEAKS IN PD PLOT IN Z UNITS = 0.30

```

-----PARAMETERS FOR BEST-FIT PEAKS-----

```

{Standard error for peak age includes group error}
{Peak width is for PD plot assuming a kernel factor = 0.60}

```

```

PEAK  ----PEAK AGE & CONF. INTERVAL (MA)----  PEAK WIDTH  --GRAINS IN PEAK----
NUMBER  MEAN (----63% CI---) (----95% CI---)  W(Z)  FRAC(%) SE(%)  COUNT
  1)    59.5 ( -2.7  +2.9) ( -5.2  +5.7)  0.25   95.1  3.5  38.1
  2)   196.8 ( -33.5 +40.2) ( -60.3 +86.3)  0.30    4.9  3.5   1.9

```

TOTAL: 100.0 40.0

LOG-LIKELIHOOD FOR BEST FIT = -1.1723E+02  
 CHI-SQUARED VALUE FOR BEST FIT = 3.6670E+01  
 REDUCED CHI-SQUARED VALUE = 9.9108E-01  
 DEGREES OF FREEDOM FOR FIT = 37  
 CONDITION NUMBER FOR COVAR MATRIX = 29.83  
 NUMBER OF ITERATIONS = 5

====BinomFit Program v. 1.8=====

98GR37 Apatite

n (cryst.)	Ns	Ni	Sum Ns	Sum Ni	Grain age	± 1s	Chi-sq.	Sum age	± 1s
21	8	27	8	26	56.1	22.7	---	56.1	22.7
8	7	21	15	47	63	27.6	83.6	60.3	18
5	1	3	16	50	63	72.8	97.8	60.5	17.5
22	41	112	57	161	69.3	12.9	96.8	66.9	10.5
4	3	8	60	169	70.8	48	99.2	67.1	10.3
15	48	127	108	296	71.3	12.3	99.6	68.9	8.1
14	27	71.3	135	367	71.6	16.3	99.9	69.5	7.4
13	30	77	165	444	73.5	16	100	70.2	6.8
2	6	15	171	459	75.5	36.6	100	70.4	6.7
16	25	61.6	196	520	76.6	18.3	100	71.2	6.4
18	29	70.3	225	590	77.9	17.4	100	72	6.1
23	2	4.82	227	594	78.3	65.9	100	72.2	6.1
7	23	53	250	647	81.9	20.6	100	73	5.9
9	8	18	258	665	83.9	35.7	100	73.3	5.9
6	18	37	276	702	91.7	26.5	100	74.2	5.8
3	3	6	279	708	94.3	66.7	100	74.4	5.8
19	20	32.7	299	740	115	32.8	99.9	76.3	5.8
27	22	33.4	321	773	124	34.3	98	78.4	5.8
26	4	5.89	325	778	127.7	82.8	98.1	78.8	5.8
20	6	8.67	331	786	130.1	69.2	97.8	79.5	5.8
17	6	8.67	337	794	130.1	69.2	97.5	80.1	5.8
24	38	53	375	846	134.8	29	80.7	83.6	5.9
25	8	10.6	383	856	141.9	66.6	78.4	84.4	5.9
28	3	3.93	386	859	143.4	110	80.4	84.8	5.9
11	11	14	397	873	147.5	59.6	75.1	85.8	5.9
10	19	23	416	896	155	48.3	59.7	87.6	5.9
12	59	68	475	964	162.7	29.4	13.6	92.9	6
1	37	41	512	1005	169.1	38.7	4.4	96	6.1

====BinomFit Program v. 1.8=====

DATE\TIME: 12-15-2002\17:18:53 FILENAME:  
 D:\TRACKK~1\FTPEAKS\98GR37.APA  
 FILE HEADER:"98GR37"

FIT OPTION: Best-fit peaks using the binomial model of Galbraith and Green

-----INITIAL GUESS FOR MODEL PARAMETERS-----

NUMBER OF PEAKS TO FIT = 2  
 PEAK #) PEAK AGE THETA FRACTION(%) COUNT  
 1) 70.00 0.270 38.1 10.68

2) 140.00 0.427 27.7 7.75

TOTAL RANGE FOR GRAIN AGES = 58.5 to 169.3 Ma  
 NUMBER OF GRAINS = 28  
 DEGREES OF FREEDOM FOR FIT = 25  
 AVERAGE OF THE SE(Z)'S FOR THE GRAINS = 0.45  
 ESTIMATED WIDTH OF PEAKS IN PD PLOT IN Z UNITS = 0.52

-----PARAMETERS FOR BEST-FIT PEAKS-----

{Standard error for peak age includes group error}  
 {Peak width is for PD plot assuming a kernel factor = 0.60}  
 PEAK ----PEAK AGE & CONF. INTERVAL (MA)---- PEAK WIDTH --GRAINS IN PEAK----  
 NUMBER MEAN (----63% CI---) (----95% CI---) W(Z) FRAC(%) SE(%) COUNT  
 1) 78.5 ( -6.4 +6.9) ( -12.0 +14.2) 0.34 66.6 15.2 18.6  
 2) 142.2 ( -15.6 +17.5) ( -28.9 +36.2) 0.34 33.4 15.2 9.4  
 TOTAL: 100.0 28.0

LOG-LIKELIHOOD FOR BEST FIT = -6.8440E+01  
 CHI-SQUARED VALUE FOR BEST FIT = 1.6429E+01  
 REDUCED CHI-SQUARED VALUE = 6.5716E-01  
 DEGREES OF FREEDOM FOR FIT = 25  
 CONDITION NUMBER FOR COVAR MATRIX = 5.13  
 NUMBER OF ITERATIONS = 10

====BinomFit Program v. 1.8=====

98GR41 Zircon

n (cryst.)	Ns	Ni	Sum Ns	Sum Ni	Grain age	± 1s	Chi-sq.	Sum age	± 1s
39	31	8	31	8	108.2	43.1	---	108.2	43.1
18	16	4	47	12	111.7	62.5	96.3	109.3	35.6
17	118	26	165	38	126.5	27.7	93	121.1	22.2
23	67	14	232	52	133.4	39.4	97.3	124.4	19.5
6	168	35	400	87	133.8	25.2	98.8	128.2	15.7
2	297	60	697	147	137.9	20	99.2	132.1	12.8
45	89	17	786	164	145.7	38.9	99.6	133.6	12.3
21	32	6	818	170	148.4	66.2	99.9	134.1	12.1
8	64	12	882	182	148.4	47	99.9	135	11.9
49	39	7	921	189	155	63.8	100	135.8	11.7
4	34	6	955	195	157.6	70	100	136.4	11.6
31	49	8	1004	203	170.2	65.1	100	137.8	11.5
30	87	14	1091	217	172.6	50	99.9	140	11.4
44	91	14	1182	231	180.5	52.2	99.9	142.5	11.3
26	46	7	1228	238	182.4	74.3	99.9	143.7	11.2
29	50	7	1278	245	198	80.2	99.8	145.2	11.2
5	152	21	1430	266	200.6	47.2	99.1	149.6	11.1
7	141	19	1571	285	205.6	50.7	97.8	153.4	11.1
9	86	11	1657	296	216.5	69.7	96.7	155.7	11.1
20	68	8	1725	304	235	88.2	95.4	157.8	11.1
34	70	7	1795	311	275.6	109.6	91.2	160.5	11.2
13	91	9	1886	320	278.6	97.8	82.9	163.8	11.3
10	94	9	1980	329	287.6	100.8	71.9	167.3	11.4
32	105	10	2085	339	289.1	96.1	59	170.9	11.5
36	255	24	2340	363	292.4	63.2	26.8	179	11.7
14	202	19	2542	382	292.6	70.9	13.9	184.7	11.8
42	128	12	2670	394	293.5	89.2	10.1	188	11.9

41	32	3	2702	397	293.5	177.5	11.1	188.8	11.9
38	92	8	2794	405	315.9	116.9	8.7	191.4	12
25	118	10	2912	415	324	107.2	5.9	194.6	12.1
24	71	6	2983	421	324.9	138.5	5.2	196.5	12.1
43	98	8	3081	429	336	124	3.8	199.1	12.2
27	139	11	3220	440	346.3	109.1	2.1	202.8	12.3
46	53	4	3273	444	362.7	188.4	2	204.3	12.3
37	263	19	3536	463	378.4	90.8	0.4	227.9	13.6
12	392	28	3928	491	382.6	75.9	0	232.3	13.5
15	87	6	4015	497	395.9	167.6	0	236.7	13.7
22	131	9	4146	506	397.3	137.5	0	241	13.9
28	118	8	4264	514	402.5	147.6	0	245.2	14
33	163	11	4427	525	404.3	126.6	0	249.2	14.2
3	150	10	4577	535	409.1	134.3	0	253.2	14.3
16	108	7	4685	542	420.4	164.6	0	257.2	14.4
1	279	18	4964	560	422.3	103.6	0	261.1	14.5
11	219	14	5183	574	426.1	118.3	0	264.9	14.6
40	50	3	5233	577	453	269.7	0	269.1	14.8
19	136	8	5369	585	461.7	168.7	0	273.4	15
48	154	9	5523	594	464.6	160.1	0	277.5	15.1
47	71	4	5594	598	481.3	247.9	0	281.8	15.3
35	180	10	5774	608	487.9	159.3	0	286.1	15.4

====BinomFit Program v. 1.8=====

DATE\TIME: 12-15-2002\16:38:56 FILENAME:

D:\TRACKK~1\FTPEAKS\98GR41.FTZ

FILE HEADER:"ETH-160/28 98GR41"

FIT OPTION: Best-fit peaks using the binomial model of Galbraith and Green

-----INITIAL GUESS FOR MODEL PARAMETERS-----

NUMBER OF PEAKS TO FIT = 2

PEAK #)	PEAK AGE	THETA	FRACTION(%)	COUNT
1)	140.00	0.837	22.1	10.85
2)	300.00	0.918	28.8	14.09

TOTAL RANGE FOR GRAIN AGES = 100.1 to 456.5 Ma

NUMBER OF GRAINS = 49

DEGREES OF FREEDOM FOR FIT = 46

AVERAGE OF THE SE(Z)'S FOR THE GRAINS = 0.35

ESTIMATED WIDTH OF PEAKS IN PD PLOT IN Z UNITS = 0.41

-----PARAMETERS FOR BEST-FIT PEAKS-----

{Standard error for peak age includes group error}

{Peak width is for PD plot assuming a kernel factor = 0.60}

PEAK NUMBER	PEAK AGE & CONF. INTERVAL (MA)	PEAK WIDTH W(Z)	GRAINS IN PEAK
	MEAN (----63% CI---) (----95% CI---)		FRAC(%) SE(%) COUNT
1)	152.2 ( -12.9 +14.1) ( -24.3 +28.9)	0.31	32.5 9.4 15.9
2)	334.0 ( -23.5 +25.2) ( -44.5 +51.1)	0.38	67.5 9.4 33.1
		TOTAL:	100.0 49.0

LOG-LIKELIHOOD FOR BEST FIT = -1.3622E+02

CHI-SQUARED VALUE FOR BEST FIT = 3.9274E+01

REDUCED CHI-SQUARED VALUE = 8.5378E-01

DEGREES OF FREEDOM FOR FIT = 46

CONDITION NUMBER FOR COVAR MATRIX = 3.33  
 NUMBER OF ITERATIONS = 8

====BinomFit Program v. 1.8=====

98GR50 Zircon

n (cryst.)	Ns	Ni	Sum Ns	Sum Ni	Grain age	± 1s	Chi-sq.	Sum age	± 1s
2	83	24	83	24	111.9	26.2	---	111.9	26.2
29	79	19.2	162	43	133	34.1	61.2	121.8	21.3
32	99	21.2	261	64	150.7	36.4	66.1	131.8	18.9
14	61	13	322	77	151.4	46.5	79.3	135.1	17.7
12	119	24	441	101	159.9	36.2	82.2	141	16.2
23	162	32.3	603	133	161.7	31.6	85.2	146.3	14.8
8	209	41	812	174	164.3	28.6	87.8	150.6	13.5
3	159	29	971	203	176.6	36.1	88.3	154.3	13
6	674	119	1645	322	182.3	19.1	75.3	164.7	11.4
26	86	15.1	1731	337	183.3	51.5	81.5	165.6	11.3
30	163	28.3	1894	365	185.4	38.2	85.1	167.2	11
19	244	37.4	2138	402	209.6	37.4	78	171.3	10.9
16	41	6	2179	408	219.3	96.1	81.6	172	10.9
22	153	21.2	2332	429	231.4	54.2	74.6	175.1	10.9
21	45	5.05	2377	434	284.5	133.9	72.2	176.4	10.9
9	223	25	2600	459	284.8	60.8	38.1	182.3	11
5	67	7	2667	466	305.1	121.6	32.9	184.2	11.1
13	92	9	2759	475	325.4	114.2	23	186.9	11.2
15	257	24	3016	499	340.5	73.5	4.1	194.4	11.4
11	238	21	3254	520	359.8	82.8	0.6	216.4	12.5
31	58	5	3312	525	368	172	0.5	223.7	12.9
4	174	15	3486	540	368	99.8	0.1	230.4	13.1
20	62	5.05	3548	545	388.9	180.4	0.1	237.3	13.5
18	162	13	3710	558	394.5	114.5	0	244	13.7
24	107	8.1	3817	566	417.5	152.8	0	251	14
17	164	11	3981	577	469.2	147	0	259.5	14.4
7	90	6	4071	583	472	199.6	0	267.5	14.8
1	117	7	4188	590	523.8	204.6	0	276.9	15.2
33	173	9.1	4361	599	592.6	202.5	0	288	15.8
28	553	27.3	4914	626	629.6	125.2	0	299.7	16.1
10	223	11	5137	637	630	195.7	0	310.6	16.6
25	88	4.04	5225	641	674.6	344	0	322.3	17.2
27	223	8.1	5448	649	841.4	302.3	0	338.7	18

====BinomFit Program v. 1.8=====

DATE\TIME: 12-15-2002\12:56:59 FILENAME:

D:\TRACKK~1\FTPEAKS\98GR50.FTZ

FILE HEADER:"eth-160/14-15 98GR50"

FIT OPTION: Best-fit peaks using the binomial model of Galbraith and Green

-----INITIAL GUESS FOR MODEL PARAMETERS-----

NUMBER OF PEAKS TO FIT = 3

PEAK #)	PEAK AGE	THETA	FRACTION(%)	COUNT
1)	150.00	0.826	24.9	8.21

2) 350.00 0.919 24.9 8.22  
 3) 500.00 0.942 14.5 4.78

TOTAL RANGE FOR GRAIN AGES = 107.8 to 780.0 Ma  
 NUMBER OF GRAINS = 33  
 DEGREES OF FREEDOM FOR FIT = 28  
 AVERAGE OF THE SE(Z)'S FOR THE GRAINS = 0.31  
 ESTIMATED WIDTH OF PEAKS IN PD PLOT IN Z UNITS = 0.36

-----PARAMETERS FOR BEST-FIT PEAKS-----  
 {Standard error for peak age includes group error}  
 {Peak width is for PD plot assuming a kernel factor = 0.60}

PEAK NUMBER	MEAN	63% CI	95% CI	W(Z)	FRAC (%)	SE (%)	COUNT	
1)	174.0	(-11.0 +11.8)	(-21.0 +23.8)	0.23	44.6	9.9	14.7	
2)	356.4	(-47.6 +54.7)	(-87.4 +114.8)	0.34	32.6	16.3	10.8	
3)	564.1	(-84.6 +98.7)	(-154.2 +208.8)	0.36	22.8	15.4	7.5	
TOTAL:							100.0	33.0

LOG-LIKELIHOOD FOR BEST FIT = -1.0722E+02  
 CHI-SQUARED VALUE FOR BEST FIT = 3.2176E+01  
 REDUCED CHI-SQUARED VALUE = 1.1491E+00  
 DEGREES OF FREEDOM FOR FIT = 28  
 CONDITION NUMBER FOR COVAR MATRIX = 14.44  
 NUMBER OF ITERATIONS = 8

====BinomFit Program v. 1.8=====

98GR57 Zircon

n (cryst.)	Ns	Ni	Sum Ns	Sum Ni	Grain age	± 1s	Chi-sq.	Sum age	± 1s
9	56	19.9	56	19	86	22.6	---	86	23
14	29	7.82	85	26	113	45.7	51.6	99.7	22.6
2	70	17	155	43	125.3	34.1	56.5	109.8	19.3
7	38	8.37	193	51	138	52.9	65.7	115.2	18.5
12	142	28.2	335	79	152.7	31.9	50.5	129	16.7
16	38	6.93	373	85	166.3	68.9	56.5	133.4	16.6
15	33	5.94	406	90	168.5	75.3	62.6	137.1	16.6
10	76	10.5	482	100	219.5	72.7	43.6	146.4	16.8
5	10	1	492	101	300.2	315	47.8	148	16.9
3	10	1	502	102	300.2	315	51.7	149.5	17
1	42	4	544	106	314.8	165.1	37	155.8	17.3
8	34	3.14	578	109	324.4	191.6	29.6	160.9	17.6
4	23	2	601	111	344	253.9	27.3	164.3	17.8
11	40	3.14	641	114	380	223.1	18.5	170.5	18.2
13	82	6.28	723	120	389.2	161.7	6.2	182.5	19
6	81	5.23	804	125	459.1	207.7	1.6	194.7	19.8

====BinomFit Program v. 1.8=====

DATE\TIME: 12-15-2002\13:24:01 FILENAME:  
 D:\TRACKK~1\FTPEAKS\98GR57.FTZ  
 FILE HEADER:"98GR57"

FIT OPTION: Best-fit peaks using the binomial model of Galbraith and Green

```

-----INITIAL GUESS FOR MODEL PARAMETERS-----
NUMBER OF PEAKS TO FIT = 2
PEAK #)  PEAK AGE      THETA      FRACTION(%)  COUNT
  1)      140.00       0.825      27.9         4.47
  2)      350.00       0.923      18.3         2.93

          TOTAL RANGE FOR GRAIN AGES = 82.8 to 413.5 Ma
          NUMBER OF GRAINS = 16
          DEGREES OF FREEDOM FOR FIT = 13
          AVERAGE OF THE SE(Z)'S FOR THE GRAINS = 0.51
ESTIMATED WIDTH OF PEAKS IN PD PLOT IN Z UNITS = 0.59
    
```

```

-----PARAMETERS FOR BEST-FIT PEAKS-----
{Standard error for peak age includes group error}
{Peak width is for PD plot assuming a kernel factor = 0.60}
    
```

```

PEAK  ----PEAK AGE & CONF. INTERVAL (MA)---- PEAK WIDTH --GRAINS IN PEAK----
NUMBER  MEAN (----63% CI---) (----95% CI---)  W(Z)  FRAC(%) SE(%)  COUNT
  1)    138.6 ( -18.7 +21.6) ( -34.4 +45.5)  0.38   53.7  20.9   8.6
  2)    322.7 ( -69.1 +87.3) (-121.7 +192.4)  0.59   46.3  20.9   7.4
                                     TOTAL: 100.0 16.0
    
```

```

          LOG-LIKELIHOOD FOR BEST FIT = -3.8822E+01
          CHI-SQUARED VALUE FOR BEST FIT = 1.3402E+01
          REDUCED CHI-SQUARED VALUE = 1.0309E+00
          DEGREES OF FREEDOM FOR FIT = 13
          CONDITION NUMBER FOR COVAR MATRIX = 5.66
          NUMBER OF ITERATIONS = 9
    
```

====BinomFit Program v. 1.8=====

98GR69 Zircon

n (cryst.)	Ns	Ni	Sum Ns	Sum Ni	Grain age	± 1s	Chi-sq.	Sum age	± 1s
28	221	80	221	80	95.6	12.9	---	95.6	12.9
7	45	13	266	93	119.6	37.9	50.7	99	12.4
34	92	21	358	114	151	36.9	22.6	108.6	12.2
43	88	20	446	134	151.7	37.9	20	115.1	12
29	110	25	556	159	151.7	34	19.2	120.8	11.6
22	213	48	769	207	152.9	25	15.6	128.3	10.9
4	173	37	942	244	161	29.7	14.5	133.3	10.5
27	82	17	1024	261	166.1	44.6	17.3	135.4	10.4
6	146	27	1170	288	185.9	39.4	12.5	140.2	10.3
13	95	17	1265	305	192	51	11.6	143.1	10.3
19	159	27	1424	332	202.2	42.6	7.2	147.9	10.3
45	21	3.3	1445	335	218.2	129.4	9.1	148.7	10.3
16	194	30	1639	365	221.7	44.1	3.7	154.7	10.3
23	144	22	1783	387	224.3	51.9	2.3	158.7	10.3
36	278	42	2061	429	226.8	38.3	0.8	174.8	10.9
14	73	10	2134	439	249.7	84.6	0.7	179.5	11.1
31	448	52	2582	491	293.7	44.1	0	186.3	11.1
40	131	13.4	2713	504	332.3	95.9	0	194.5	11.4
11	134	13	2847	517	349.8	102.3	0	202.8	11.8
21	85	8	2932	525	360.3	133.8	0	210.7	12.2
32	192	18	3124	543	361.7	90	0	218	12.4



33	128	11	3252	554	393.6	124.3	0	226.1	12.8
37	107	9	3359	563	401.9	140.1	0	233.8	13.2
18	167	14	3526	577	403.2	113	0	241	13.4
3	168	14	3694	591	405.5	113.6	0	247.6	13.7
8	146	12	3840	603	411	124.2	0	254	13.9
41	28	2.2	3868	605	429.3	300.9	0	260.6	14.3
9	120	9	3988	614	449	155.9	0	267.4	14.6
38	193	14	4181	628	463.7	129.3	0	274.3	14.8
42	277	20	4458	648	465.8	109	0	280.8	15
25	111	8	4569	656	466.6	171.5	0	286.8	15.3
44	319	21.1	4888	677	506.8	115.2	0	293.8	15.5
35	123	8	5011	685	515.1	188.7	0	300.6	15.8
10	540	34	5551	719	531.4	95.6	0	307.6	15.9
20	172	10	5723	729	573.6	187.6	0	315.3	16.2
26	73	4	5796	733	607	312.4	0	323.6	16.6
17	612	33	6408	766	616.4	112	0	331.7	16.8
5	416	22	6824	788	627.9	138.9	0	339.7	17
12	134	7	6958	795	635.3	247.2	0	347.4	17.4
1	214	11	7172	806	645.1	200.6	0	355	17.7
30	103	5	7275	811	681.2	312.8	0	363.2	18
15	376	16	7651	827	771.6	198.6	0	373.2	18.4
2	97	4	7748	831	794.7	406.3	0	383.3	18.9
24	126	5	7874	836	823.9	376.7	0	393.7	19.4
39	315	12.2	8189	848	842.9	247.5	0	404	19.8

====BinomFit Program v. 1.8====  
 DATE\TIME: 12-15-2002\13:02:07 FILENAME:  
 D:\TRACKK~1\FTPEAKS\98GR69.FTZ  
 FILE HEADER: "ETH-160/7-18 98GR69 "

FIT OPTION: Best-fit peaks using the binomial model of Galbraith and Green

-----INITIAL GUESS FOR MODEL PARAMETERS-----

NUMBER OF PEAKS TO FIT = 3  
 PEAK #) PEAK AGE THETA FRACTION(%) COUNT  
 1) 140.00 0.806 15.7 7.09  
 2) 250.00 0.882 11.3 5.10  
 3) 500.00 0.938 24.5 11.01

TOTAL RANGE FOR GRAIN AGES = 93.1 to 795.6 Ma  
 NUMBER OF GRAINS = 45  
 DEGREES OF FREEDOM FOR FIT = 40  
 AVERAGE OF THE SE(Z)'S FOR THE GRAINS = 0.31  
 ESTIMATED WIDTH OF PEAKS IN PD PLOT IN Z UNITS = 0.36

-----PARAMETERS FOR BEST-FIT PEAKS-----

{Standard error for peak age includes group error}  
 {Peak width is for PD plot assuming a kernel factor = 0.60}

PEAK NUMBER	MEAN	63% CI	95% CI	W(Z)	FRAC(%)	SE(%)	COUNT	
1)	134.0	(-16.8 +19.2)	(-31.0 +40.2)	0.23	16.2	11.5	7.3	
2)	227.4	(-33.2 +38.7)	(-60.5 +81.9)	0.25	23.7	11.3	10.7	
3)	518.4	(-32.3 +34.3)	(-61.4 +69.3)	0.34	60.1	8.5	27.1	
TOTAL:							100.0	45.0

LOG-LIKELIHOOD FOR BEST FIT = -1.5406E+02

CHI-SQUARED VALUE FOR BEST FIT = 4.0985E+01  
 REDUCED CHI-SQUARED VALUE = 1.0246E+00  
 DEGREES OF FREEDOM FOR FIT = 40  
 CONDITION NUMBER FOR COVAR MATRIX = 18.59  
 NUMBER OF ITERATIONS = 19

====BinomFit Program v. 1.8=====

98GR81 Zircon

n (cryst.)	Ns	Ni	Sum Ns	Sum Ni	Grain age	± 1s	Chi-sq.	Sum age	± 1s
21	77	59.2	77	59	33	5.8	---	33	5.8
5	55	35	132	94	39.8	8.7	49.4	35.6	4.9
14	35	20	167	114	44.3	12.5	61.2	37.1	4.7
12	40	19	207	133	53.3	14.9	48.6	39.5	4.6
11	57	25	264	158	57.7	14	33.1	42.3	4.5
17	319	133	583	291	60.7	6.6	4.7	50.7	4
15	81	33	664	324	62.1	13	5.8	51.9	3.9
18	96	39	760	363	62.3	12	7	53	3.8
10	133	53	893	416	63.5	10.5	7.4	54.4	3.7
7	338	134	1231	550	63.8	6.8	5.9	56.7	3.4
6	100	39	1331	589	64.9	12.4	7.5	57.2	3.4
1	57	22	1388	611	65.5	16.6	10	57.5	3.3
3	107	40	1495	651	67.7	12.7	11.3	58.1	3.3
19	105	39	1600	690	68.1	12.9	12.8	58.7	3.2
16	56	20	1656	710	70.8	18.6	15.1	59	3.2
9	129	45	1785	755	72.5	12.8	14.2	59.8	3.2
20	123	42.4	1908	797	73.3	13.3	13.7	60.6	3.2
23	232	76.9	2140	873	76.3	10.3	8.9	62	3.2
4	124	41	2264	914	76.4	14	8.5	62.7	3.2
8	67	22	2331	936	77	19.1	9.5	63	3.1
2	136	43	2467	979	79.9	14.2	8	63.8	3.1
13	180	51	2647	1030	89.1	14.4	3.6	65	3.1
22	75	20.7	2722	1050	91.5	22.9	3	65.6	3.2
24	182	39.4	2904	1089	116.4	20.8	0.2	67.9	3.2
25	335	31	3239	1120	269.1	51.2	0	76.1	3.6

====BinomFit Program v. 1.8=====

DATE\TIME: 03-09-2001\15:05:56 FILENAME:  
 C:\PROGRA~1\TRACKKEY\FTPEAKS\98GR81.FTZ  
 FILE HEADER:"98GR81"

FIT OPTION: Best-fit peaks using the binomial model of Galbraith and Green

-----INITIAL GUESS FOR MODEL PARAMETERS-----

NUMBER OF PEAKS TO FIT = 2  
 PEAK #) PEAK AGE THETA FRACTION(%) COUNT  
 1) 65.00 0.720 70.5 17.62  
 2) 270.00 0.916 5.3 1.32

TOTAL RANGE FOR GRAIN AGES = 32.9 to 265.3 Ma  
 NUMBER OF GRAINS = 25  
 DEGREES OF FREEDOM FOR FIT = 22

AVERAGE OF THE SE(Z)'S FOR THE GRAINS = 0.20  
 ESTIMATED WIDTH OF PEAKS IN PD PLOT IN Z UNITS = 0.23

-----PARAMETERS FOR BEST-FIT PEAKS-----  
 {Standard error for peak age includes group error}  
 {Peak width is for PD plot assuming a kernel factor = 0.60}

PEAK NUMBER	MEAN	----PEAK AGE & CONF. INTERVAL (MA)----		PEAK WIDTH	--GRAINS IN PEAK----				
		(----63% CI--)	(----95% CI--)	W(Z)	FRAC(%)	SE(%)	COUNT		
1)	67.3	( -3.1	+3.3)	( -6.0	+6.5)	0.20	96.0	3.9	24.0
2)	269.1	( -45.9	+55.1)	( -82.6	+118.2)	0.22	4.0	3.9	1.0
TOTAL:							100.0		25.0

LOG-LIKELIHOOD FOR BEST FIT = -9.2348E+01  
 CHI-SQUARED VALUE FOR BEST FIT = 4.1962E+01  
 REDUCED CHI-SQUARED VALUE = 1.9074E+00  
 DEGREES OF FREEDOM FOR FIT = 22  
 CONDITION NUMBER FOR COVAR MATRIX = 27.98  
 NUMBER OF ITERATIONS = 5  
 =====BinomFit Program v. 1.8=====

98GR83 Zircon

n (cryst.)	Ns	Ni	Sum Ns	Sum Ni	Grain age	± 1s	Chi-sq.	Sum age	± 1s
7	21	26	21	26	28.7	8.5	---	28.7	8.5
9	75	57	96	83	46.6	8.3	15.2	41	6.3
21	31	23	127	106	47.8	13.2	31.7	42.5	5.8
3	75	55	202	161	48.3	8.7	44.9	44.5	4.9
14	92	61	294	222	53.4	9	47	46.9	4.5
19	50	31	344	253	57.1	13.2	51.9	48.2	4.3
26	39	24	383	277	57.5	15	58.9	49	4.2
13	31	19	414	296	57.8	16.9	66.4	49.5	4.1
33	38	23	452	319	58.5	15.6	72	50.2	4
5	17	10	469	329	60.2	24.1	78.4	50.5	4
31	57	33	526	362	61.1	13.5	79.2	51.5	3.9
17	47	27	573	389	61.6	15	81.5	52.2	3.8
35	82	46	655	435	63.1	11.8	80.2	53.3	3.7
24	45	25	700	460	63.7	16	82.5	53.9	3.7
29	77	42	777	502	64.9	12.6	82	54.8	3.6
12	39	21	816	523	65.7	17.9	84.3	55.2	3.6
16	59	31	875	554	67.3	15.1	84.4	55.9	3.6
6	21	11	896	565	67.5	25.2	87.3	56.1	3.5
11	48	25	944	590	67.9	16.9	88.3	56.6	3.5
25	148	76	1092	666	68.9	10	83.6	58	3.4
28	160	82	1252	748	69	9.7	80.1	59.2	3.4
22	73	37	1325	785	69.8	14.3	81.1	59.7	3.3
2	26	13	1351	798	70.7	24.1	84.1	59.9	3.3
15	61	30	1412	828	71.9	16.2	84.8	60.4	3.3
27	42	20	1454	848	74.2	20.3	85.9	60.7	3.3
10	17	8	1471	856	75.1	32.3	88.1	60.8	3.3
30	56	26	1527	882	76.1	18.2	87.8	61.3	3.3
8	28	13	1555	895	76.1	25.7	89.2	61.5	3.3
34	87	40	1642	935	76.9	14.9	87.4	62.1	3.3
20	44	20	1686	955	77.8	21.1	87.8	62.5	3.3

18	101	44	1787	999	81.1	14.9	83.3	63.3	3.3
23	102	44	1889	1043	81.9	15	78.5	64.1	3.3
1	21	9	1910	1052	82.4	33	80.4	64.2	3.3
32	44	18	1954	1070	86.3	24.3	79.4	64.6	3.3
4	64	9	2018	1079	248	88.7	13.7	66.2	3.3

=====  
 =====BinomFit Program v. 1.8=====

DATE\TIME: 03-09-2001\14:55:20 FILENAME:  
 C:\PROGRA~1\TRACKKEY\FTPEAKS\98GR83.FTZ  
 FILE HEADER:"98GR83"

FIT OPTION: Best-fit peaks using the binomial model of Galbraith and Green

-----INITIAL GUESS FOR MODEL PARAMETERS-----

NUMBER OF PEAKS TO FIT = 2  
 PEAK #) PEAK AGE THETA FRACTION(%) COUNT  
 1) 65.00 0.653 67.4 23.58  
 2) 240.00 0.876 2.0 0.71

TOTAL RANGE FOR GRAIN AGES = 28.1 to 231.7 Ma  
 NUMBER OF GRAINS = 35  
 DEGREES OF FREEDOM FOR FIT = 32  
 AVERAGE OF THE SE(Z)'S FOR THE GRAINS = 0.26  
 ESTIMATED WIDTH OF PEAKS IN PD PLOT IN Z UNITS = 0.30

-----PARAMETERS FOR BEST-FIT PEAKS-----

{Standard error for peak age includes group error}  
 {Peak width is for PD plot assuming a kernel factor = 0.60}

PEAK NUMBER	MEAN	63% CI	95% CI	W(Z)	FRAC (%)	SE (%)	COUNT	
1)	63.2	( -3.0 +3.2)	( -5.8 +6.4)	0.26	97.1	2.8	34.0	
2)	241.9	( -72.1 +102.0)	(-121.3 +238.6)	0.42	2.9	2.8	1.0	
TOTAL:							100.0	35.0

LOG-LIKELIHOOD FOR BEST FIT = -9.9186E+01  
 CHI-SQUARED VALUE FOR BEST FIT = 2.8491E+01  
 REDUCED CHI-SQUARED VALUE = 8.9034E-01  
 DEGREES OF FREEDOM FOR FIT = 32  
 CONDITION NUMBER FOR COVAR MATRIX = 160.84  
 NUMBER OF ITERATIONS = 5

=====  
 =====BinomFit Program v. 1.8=====

99GR22 Zircon

n (cryst.)	Ns	Ni	Sum Ns	Sum Ni	Grain age	± 1s	Chi-sq.	Sum age	± 1s
45	65	13.8	65	13	103.6	30.9	---	103.6	31.6
32	37	7.1	102	20	114.5	47.1	78.4	112.1	27.6
34	81	14.2	183	34	125.2	36.2	88.3	118.3	22.4
5	99	17	282	51	127.9	33.8	94.7	121.5	18.9
2	77	12	359	63	140.7	43.9	96.1	125.1	17.5
42	151	22.7	510	85	146	33.2	95.4	131.7	16
14	89	13	599	98	150.1	44.8	97	134.1	15.2
43	210	29.6	809	127	155.6	31	96.2	139.7	14
7	115	13	924	140	193.2	56.9	91.4	144.7	13.9

3	123	13	1047	153	206.5	60.6	83.9	150	13.8
18	81	8	1128	161	220.7	82.1	79.8	153.5	13.8
16	64	6	1192	167	232.3	99.5	77.3	156.4	13.8
4	77	7	1269	174	239.4	94.8	72.9	159.7	13.9
25	100	8.75	1369	182	248.6	88	64.4	164.7	14
39	48	4.06	1417	186	257	133.1	64.3	166.8	14
29	96	7.78	1513	193	268	100.3	55.6	171.5	14.2
15	103	8	1616	201	279.4	102.9	46.5	175.9	14.3
24	126	9.72	1742	210	281.2	94	36.1	181.4	14.4
11	52	4	1794	214	282	146.6	36.5	183.3	14.5
33	135	10.2	1929	224	288.4	94.3	28.3	188.2	14.5
30	55	3.89	1984	227	306.2	160.9	27.3	191	14.7
17	87	6	2071	233	313.8	132.8	23.7	194.2	14.7
8	116	8	2187	241	313.8	115.1	18.8	198.2	14.8
9	340	23	2527	264	319.8	69.6	6.3	208.8	15
44	44	2.96	2571	266	321.5	193.3	6.7	210.9	15.1
48	715	47.3	3286	313	326.7	50.1	0.6	229.7	15.4
50	149	9.86	3435	322	326.7	107.9	0.5	233.3	15.5
37	124	8.12	3559	330	330.1	120	0.5	236.8	15.5
10	110	6	3669	336	394.3	165.7	0.4	242.3	15.8
38	149	8.12	3818	344	394.6	142.7	0.2	247.4	16
41	152	7.89	3970	351	413.7	151.6	0.1	252.9	16.2
31	96	4.86	4066	355	423.8	197.5	0.1	258.3	16.4
12	80	4	4146	359	428.9	220.2	0.1	263.5	16.7
35	82	4.06	4228	363	433	220.6	0.1	268.6	17
49	80	3.94	4308	366	435.2	225	0.1	273.4	17.2
27	81	3.89	4389	369	446	231.9	0.1	278.3	17.4
28	102	4.86	4491	373	449.4	209.1	0	282.9	17.7
13	84	4	4575	377	449.6	230.5	0	287.4	17.9
23	62	2.92	4637	379	454.5	272.5	0	291.7	18.1
20	62	2.92	4699	381	454.5	272.5	0	295.8	18.3
46	297	13.8	4996	394	460.4	127.6	0	299.9	18.3
6	302	14	5298	408	461.4	127	0	303.8	18.3
1	151	7	5449	415	461.4	179	0	307.5	18.4
19	131	6	5580	421	466.9	195.5	0	311.2	18.5
22	151	6.8	5731	427	474.5	186.6	0	314.8	18.6
26	109	4.86	5840	431	479.1	222.6	0	318.5	18.8
40	156	6.9	5996	437	482.8	188.4	0	322	18.9
21	169	6.8	6165	443	528.8	207.5	0	326.4	19.1
47	74	2.96	6239	445	531.8	315.7	0	330.6	19.3
36	80	3.04	6319	448	558.7	326.9	0	335.3	19.5

```

=====BinomFit Program v. 1.8=====
DATE\TIME: 01-16-2001\20:35:16 FILENAME:
C:\PROGRA~1\FISSON~1\FTPEAKS\99GR22.FTZ
FILE HEADER:"99GR22"

```

FIT OPTION: Best-fit peaks using the binomial model of Galbraith and Green

```

-----INITIAL GUESS FOR MODEL PARAMETERS-----
NUMBER OF PEAKS TO FIT = 2
PEAK #)  PEAK AGE      THETA      FRACTION(%)  COUNT
1)        150.00      0.873      13.5         6.74

```

2) 350.00 0.942 32.2 16.12

TOTAL RANGE FOR GRAIN AGES = 100.8 to 495.4 Ma  
 NUMBER OF GRAINS = 50  
 DEGREES OF FREEDOM FOR FIT = 47  
 AVERAGE OF THE SE(Z)'S FOR THE GRAINS = 0.39  
 ESTIMATED WIDTH OF PEAKS IN PD PLOT IN Z UNITS = 0.46

-----PARAMETERS FOR BEST-FIT PEAKS-----  
 {Standard error for peak age includes group error}  
 {Peak width is for PD plot assuming a kernel factor = 0.60}

PEAK NUMBER	PEAK AGE & CONF. INTERVAL (MA)	PEAK WIDTH W(Z)	GRAINS IN PEAK
	MEAN (---63% CI---) (---95% CI---)		FRAC(%) SE(%) COUNT
1)	150.1 ( -16.4 +18.4) ( -30.5 +38.2)	0.33	20.0 7.1 10.0
2)	355.0 ( -23.3 +24.9) ( -44.2 +50.3)	0.42	80.0 7.1 40.0
TOTAL:			100.0 50.0

LOG-LIKELIHOOD FOR BEST FIT = -1.2794E+02  
 CHI-SQUARED VALUE FOR BEST FIT = 4.2487E+01  
 REDUCED CHI-SQUARED VALUE = 9.0399E-01  
 DEGREES OF FREEDOM FOR FIT = 47  
 CONDITION NUMBER FOR COVAR MATRIX = 4.09  
 NUMBER OF ITERATIONS = 8

=====BinomFit Program v. 1.8=====

99GR36 Zircon

n (cryst.)	Ns	Ni	Sum Ns	Sum Ni	Grain age	± 1s	Chi-sq.	Sum age	± 1s
12	42	25	42	25	38.2	9.7	---	38.2	9.7
4	249	115	291	140	49.2	5.8	35.8	47.2	5.1
8	18	8	309	148	51.1	21.8	64.5	47.4	5
5	57	23	366	171	56.2	14	72.9	48.6	4.8
9	28	10	394	181	63.5	23.5	77	49.4	4.7
1	85	30	479	211	64.2	13.8	67.6	51.5	4.6
2	29	10	508	221	65.8	24.2	73.1	52.2	4.5
11	42	13	550	234	73.2	23.4	69.5	53.3	4.5
6	333	99	883	333	76.2	9.1	16.5	60.1	4.3
3	69	20	952	353	78.1	20	17.2	61.2	4.3
7	29	8	981	361	82.1	32.9	20.3	61.6	4.3
10	53	13	1034	374	92.2	28.7	17.5	62.7	4.3

=====BinomFit Program v. 1.8=====

DATE\TIME: 12-15-2002\17:30:15 FILENAME:  
 D:\TRACKK~1\FTPEAKS\99GR36.FTZ  
 FILE HEADER:"99GR36"

FIT OPTION: Best-fit peaks using the binomial model of Galbraith and Green

-----INITIAL GUESS FOR MODEL PARAMETERS-----  
 NUMBER OF PEAKS TO FIT = 2

PEAK #)	PEAK AGE	THETA	FRACTION(%)	COUNT
1)	50.00	0.688	41.2	4.95
2)	70.00	0.755	51.6	6.19

TOTAL RANGE FOR GRAIN AGES = 37.9 to 89.7 Ma

NUMBER OF GRAINS = 12  
 DEGREES OF FREEDOM FOR FIT = 9  
 AVERAGE OF THE SE(Z)'S FOR THE GRAINS = 0.29  
 ESTIMATED WIDTH OF PEAKS IN PD PLOT IN Z UNITS = 0.34

-----PARAMETERS FOR BEST-FIT PEAKS-----  
 {Standard error for peak age includes group error}  
 {Peak width is for PD plot assuming a kernel factor = 0.60}

PEAK NUMBER	MEAN	63% CI		95% CI		W(Z)	FRAC (%)	SE (%)	COUNT
1)	50.9	-5.8	+6.5	-10.7	+13.5	0.22	35.8	26.7	4.3
2)	72.8	-6.6	+7.3	-12.4	+14.9	0.26	64.2	26.7	7.7
TOTAL: 100.0									12.0

LOG-LIKELIHOOD FOR BEST FIT = -3.2905E+01  
 CHI-SQUARED VALUE FOR BEST FIT = 7.7982E+00  
 REDUCED CHI-SQUARED VALUE = 8.6647E-01  
 DEGREES OF FREEDOM FOR FIT = 9  
 CONDITION NUMBER FOR COVAR MATRIX = 10.25  
 NUMBER OF ITERATIONS = 8

====BinomFit Program v. 1.8=====

99GR44 Zircon

n (cryst.)	Ns	Ni	Sum Ns	Sum Ni	Grain age	± 1s	Chi-sq.	Sum age	± 1s
48	20	18.7	20	18	24.1	7.8	---	24.1	7.9
32	44	32.7	64	50	30.2	7	55.3	28.7	5.5
44	212	135	276	184	35.3	4.1	46.7	33.6	3.4
15	79	44	355	228	40.2	7.7	50.3	34.9	3.2
33	74	40.6	429	268	40.8	8.1	56.3	35.9	3
51	90	48.2	519	316	41.9	7.6	59.3	36.8	2.9
50	96	51.1	615	367	42.1	7.4	63.5	37.6	2.8
34	109	57.5	724	424	42.5	7.1	67.3	38.3	2.7
41	102	52	826	476	43.9	7.6	69.6	38.9	2.6
4	214	107	1040	583	44.8	5.5	64.9	40	2.4
26	61	29	1101	612	47.1	10.7	68.3	40.3	2.4
22	100	46	1201	658	48.7	8.8	66	40.9	2.4
25	61	28	1262	686	48.8	11.3	68.5	41.2	2.4
37	280	127	1542	812	49.5	5.5	53.9	42.6	2.3
24	105	46	1647	858	51.1	9.2	52.8	43	2.3
28	206	90	1853	948	51.3	6.7	45.8	43.8	2.3
13	276	118	2129	1066	52.4	6	35.5	44.8	2.2
19	132	56	2261	1122	52.8	8.6	35.1	45.2	2.2
12	249	105	2510	1227	53.1	6.4	30.1	45.8	2.2
31	40	16.9	2550	1243	53.2	15.5	34.4	46	2.2
8	430	179	2980	1422	53.8	5.1	24.6	47	2.1
35	41	16.9	3021	1438	54.5	15.9	28.3	47.1	2.1
36	50	19.8	3071	1457	56.5	15.1	31	47.2	2.1
43	110	43.2	3181	1500	57	10.4	30.4	47.5	2.1
39	109	42.6	3290	1542	57.3	10.5	30	47.8	2.1
18	108	42	3398	1584	57.6	10.6	29.8	48.1	2.1
14	18	7	3416	1591	57.6	25.7	33.9	48.1	2.1
40	46	17.8	3462	1608	57.7	16.2	36.6	48.2	2.1

45	208	80.5	3670	1688	57.8	7.8	32	48.7	2.1
5	228	86	3898	1774	59.3	7.8	25.7	49.2	2.1
2	117	44	4015	1818	59.5	10.7	25	49.5	2.1
6	167	62	4182	1880	60.3	9.2	22.2	49.8	2.1
38	169	62.4	4351	1942	60.6	9.2	19.6	50.2	2.1
49	58	20.6	4409	1962	62.9	16.3	20.4	50.3	2.1
27	30	10	4439	1972	67.1	24.6	21.7	50.4	2.1
23	27	9	4466	1981	67.1	25.9	23.3	50.5	2.1
30	284	94.1	4750	2075	67.5	8.3	10.5	51.3	2.1
29	118	39	4868	2114	67.7	12.7	8.4	51.6	2.1
17	220	72	5088	2186	68.3	9.5	4.5	52.1	2.2
16	189	61	5277	2247	69.3	10.4	2.6	52.6	2.2
42	143	45.2	5420	2292	70.8	12.3	1.7	53	2.2
10	67	21	5487	2313	71.3	18	1.6	53.1	2.2
11	83	26	5570	2339	71.4	16.2	1.4	53.3	2.2
46	135	42.2	5705	2381	71.5	12.8	1	54.5	2.2
9	120	37	5825	2418	72.5	13.8	0.7	54.9	2.2
1	422	130	6247	2548	72.6	7.7	0.1	55.3	2.2
21	62	19	6309	2567	73	19.3	0.1	55.7	2.2
47	423	123	6732	2689	77	8.3	0	56.1	2.2
20	55	15	6787	2704	81.9	24	0	56.7	2.2
7	76	20	6863	2724	84.9	21.5	0	57.2	2.3
3	166	35	7029	2759	105.8	20	0	58.2	2.3

====BinomFit Program v. 1.8====  
 DATE\TIME: 12-15-2002\17:43:10 FILENAME:  
 D:\TRACKK~1\FTPEAKS\99GR44.FTZ  
 FILE HEADER:"99GR44"

FIT OPTION: Best-fit peaks using the binomial model of Galbraith and Green

-----INITIAL GUESS FOR MODEL PARAMETERS-----

NUMBER OF PEAKS TO FIT = 3  
 PEAK #) PEAK AGE THETA FRACTION(%) COUNT  
 1) 35.00 0.609 11.1 5.67  
 2) 55.00 0.711 58.5 29.86  
 3) 70.00 0.758 46.0 23.47

TOTAL RANGE FOR GRAIN AGES = 24.0 to 104.6 Ma  
 NUMBER OF GRAINS = 51  
 DEGREES OF FREEDOM FOR FIT = 46  
 AVERAGE OF THE SE(Z)'S FOR THE GRAINS = 0.21  
 ESTIMATED WIDTH OF PEAKS IN PD PLOT IN Z UNITS = 0.24

-----PARAMETERS FOR BEST-FIT PEAKS-----

{Standard error for peak age includes group error}  
 {Peak width is for PD plot assuming a kernel factor = 0.60}

PEAK NUMBER	MEAN	63% CI	95% CI	W(Z)	FRAC(%)	SE(%)	COUNT	
1)	36.6	(-4.5 +5.1)	(-8.3 +10.7)	0.18	6.7	6.1	3.4	
2)	52.8	(-2.9 +3.0)	(-5.5 +6.1)	0.19	60.5	15.2	30.9	
3)	70.0	(-4.5 +4.8)	(-8.5 +9.7)	0.19	32.8	14.6	16.7	
TOTAL:							100.0	51.0

LOG-LIKELIHOOD FOR BEST FIT = -1.7526E+02  
 CHI-SQUARED VALUE FOR BEST FIT = 4.9353E+01



REDUCED CHI-SQUARED VALUE = 1.0729E+00  
 DEGREES OF FREEDOM FOR FIT = 46  
 CONDITION NUMBER FOR COVAR MATRIX = 25.13  
 NUMBER OF ITERATIONS = 9

====BinomFit Program v. 1.8=====

99GR52 Zircon

n (cryst.)	Ns	Ni	Sum Ns	Sum Ni	Grain age	± 1s	Chi-sq.	Sum age	± 1s
2	74	12	74	12	131.4	41.1	---	131.4	41.1
5	46	6	120	18	163	70.9	68.3	142	36.2
3	39	5	159	23	165.8	78.9	88	147.1	33.2
7	16	2	175	25	170	127.6	96.1	149	32.2
6	134	12	309	37	236	71.5	74.4	177.3	31.4
1	87	7	396	44	262.2	103.3	70.9	190.9	30.9
8	76	6	472	50	267.1	113.6	72.7	200.1	30.4
10	111	8	583	58	292	107.3	68.7	212.9	30.1
9	84	5	667	63	351.9	162.4	63	224	30.4
4	76	4	743	67	396.6	203.8	57	234.4	30.8

99GR65 Zircon

n (cryst.)	Ns	Ni	Sum Ns	Sum Ni	Grain age	± 1s	Chi-sq.	Sum age	± 1s
1	531	118	531	118	112.5	12.1	---	112.5	12.1
20	84	16.2	615	134	129.7	35.5	62.1	114.8	11.7
21	93	17.2	708	151	135.1	35.8	74	117.2	11.3
4	77	13	785	164	147.7	44.6	75.7	119.6	11.1
22	56	9.1	841	173	153.4	55.1	79.6	121.5	11
14	355	54.6	1196	227	162	24.2	43.3	131.6	10.6
28	294	27.7	1490	254	262.3	53	1	146.3	11.2
18	97	9.1	1587	263	263.4	91.8	0.5	171	12.9
24	172	15.2	1759	278	279.9	75.6	0.1	183.2	13.5
27	60	4.89	1819	282	302.3	142.6	0.1	195.2	14.3
11	507	39	2326	321	319.9	54.3	0	206.6	14.3
25	163	9.78	2489	330	407.3	134.9	0	223.6	15.3
31	202	11.9	2691	341	415.6	125	0	238.6	16.1
19	133	7.08	2824	348	457.3	177.1	0	254.4	17
16	78	4.04	2902	352	469.5	240.1	0	269	17.9
15	80	4.04	2982	356	481.1	245.9	0	282.5	18.7
10	181	9	3163	365	488.4	167.7	0	294.8	19.3
3	123	6	3286	371	497.4	208.7	0	306.2	19.9
17	605	29.3	3891	400	500.6	96.3	0	316.6	20
29	62	2.97	3953	402	506.2	301.2	0	326.2	20.6
13	296	14	4249	416	512.4	141.3	0	335.2	20.9
5	90	4	4339	420	544	278.6	0	344.8	21.4
26	135	5.87	4474	425	555.5	235	0	354.1	21.9
7	138	6	4612	431	555.6	232.5	0	362.6	22.3
8	139	6	4751	437	559.4	234.1	0	370.6	22.7
2	71	3	4822	440	571	337.1	0	378.5	23.1
9	168	7	4990	447	578.7	224.2	0	386	23.4

6	75	3	5065	450	601.7	354.9	0	393.8	23.8
30	188	6.92	5253	456	651.3	253.1	0	402.9	24.3
23	138	5.06	5391	461	653.7	296.8	0	411.4	24.7
12	293	7	5684	468	977.9	375.6	0	430.5	25.7

=====  
 BinomFit Program v. 1.8  
 DATE\TIME: 12-15-2002\12:45:18 FILENAME: D:\TRACKK~1\FTPEAKS\99GR65-1.FTZ  
 FILE HEADER:"99GR65"

FIT OPTION: Best-fit peaks using the binomial model of Galbraith and Green

-----INITIAL GUESS FOR MODEL PARAMETERS-----

NUMBER OF PEAKS TO FIT = 3  
 PEAK #) PEAK AGE THETA FRACTION(%) COUNT  
 1) 128.00 0.840 11.1 3.44  
 2) 309.00 0.928 19.7 6.10  
 3) 506.00 0.955 33.7 10.45

TOTAL RANGE FOR GRAIN AGES = 109.6 to 899.0 Ma  
 NUMBER OF GRAINS = 31  
 DEGREES OF FREEDOM FOR FIT = 26  
 AVERAGE OF THE SE(Z)'S FOR THE GRAINS = 0.37  
 ESTIMATED WIDTH OF PEAKS IN PD PLOT IN Z UNITS = 0.43

-----PARAMETERS FOR BEST-FIT PEAKS-----

{Standard error for peak age includes group error}  
 {Peak width is for PD plot assuming a kernel factor = 0.60}

PEAK NUMBER	MEAN	63% CI	95% CI	W(Z)	FRAC(%)	SE(%)	COUNT	
1)	128.4	(-10.0 +10.8)	(-18.8 +22.0)	0.20	18.8	7.3	5.8	
2)	309.4	(-44.4 +51.7)	(-81.2 +109.1)	0.30	19.9	13.6	6.2	
3)	506.1	(-49.4 +54.5)	(-92.4 +112.1)	0.42	61.3	14.3	19.0	
TOTAL:							100.0	31.0

LOG-LIKELIHOOD FOR BEST FIT = -9.1787E+01  
 CHI-SQUARED VALUE FOR BEST FIT = 2.4687E+01  
 REDUCED CHI-SQUARED VALUE = 9.4951E-01  
 DEGREES OF FREEDOM FOR FIT = 26  
 CONDITION NUMBER FOR COVAR MATRIX = 6.85  
 NUMBER OF ITERATIONS = 10

=====  
 BinomFit Program v. 1.8

99GR67 Apatite

n (cryst.)	Ns	Ni	Sum Ns	Sum Ni	Grain age	± 1s	Chi-sq.	Sum age	± 1s
16	29	143	29	143	40.3	8.3	---	40.3	8.3
23	33	148	62	291	44.2	8.6	74.3	42.4	6.1
32	19	78.6	81	369	48.1	12.4	86.2	43.7	5.5
30	37	150	118	518	49.2	9.2	89.7	45.3	4.8
34	48	194	166	711	49.3	8.1	93.8	46.4	4.3
17	14	56	180	767	49.7	14.9	97.4	46.7	4.1
2	5	20	185	787	49.7	24.9	99	46.7	4.1
24	10	39.8	195	826	49.9	17.7	99.6	46.9	4
7	14	54	209	880	51.5	15.5	99.8	47.2	3.9

18	34	130	243	1010	52	10.2	99.9	47.8	3.7
11	12	45	255	1055	53	17.3	99.9	48.1	3.7
12	15	56	270	1111	53.2	15.6	100	48.3	3.6
39	25	91.5	295	1202	54.3	12.4	100	48.8	3.5
29	12	42.8	307	1244	55.8	18.3	100	49.1	3.5
21	14	48.6	321	1292	57.3	17.5	100	49.4	3.5
37	16	54.1	337	1346	58.8	16.8	100	49.8	3.4
20	11	37	348	1382	59.1	20.4	100	50.1	3.4
31	24	80.6	372	1462	59.2	13.9	100	50.6	3.4
19	20	67	392	1529	59.3	15.2	100	51	3.3
22	12	40.1	404	1569	59.4	19.6	100	51.2	3.3
10	19	62	423	1631	60.9	16.1	100	51.6	3.3
9	16	52	439	1683	61.1	17.6	100	51.9	3.2
25	15	48.4	454	1731	61.5	18.3	100	52.1	3.2
4	23	74	477	1805	61.7	14.9	100	52.5	3.2
26	22	69.2	499	1874	63.1	15.6	100	52.9	3.2
8	40	124	539	1998	64.1	11.8	100	53.6	3.1
27	5	15.3	544	2013	65	33.6	100	53.7	3.1
1	23	70	567	2083	65.2	15.8	100	54.1	3.1
35	15	45.2	582	2128	65.9	19.7	100	54.4	3.1
15	18	54	600	2182	66.2	18.1	100	54.6	3.1
14	30	90	630	2272	66.2	14.1	100	55.1	3
5	15	45	645	2317	66.2	19.8	100	55.3	3
38	11	32.4	656	2349	67.3	23.6	100	55.5	3
33	18	52.1	674	2401	68.6	18.9	100	55.8	3
3	28	78	702	2479	71.2	15.9	100	56.3	3
28	28	77.4	730	2556	71.8	16	100	56.8	3
36	10	27.5	740	2583	72.1	26.7	100	56.9	3
6	56	127	796	2710	87.4	14.3	98.8	58.4	3
13	24	51	820	2761	93.2	23.3	96.5	59	3

99GR67 Zircon

n (cryst.)	Ns	Ni	Sum Ns	Sum Ni	Grain age	± 1s	Chi-sq.	Sum age	± 1s
7	86	37	86	37	56.1	11.2	---	56.1	11.2
3	126	54	212	91	56.3	9.3	98.8	56.2	7.3
6	464	179	676	270	62.5	5.9	78.4	60.4	4.8
4	65	24	741	294	65.3	15.7	89.9	60.8	4.6
5	205	75	946	369	65.9	9.1	92.8	61.8	4.3
9	170	62	1116	431	66.1	10	95.8	62.5	4.1
10	241	87	1357	518	66.8	8.6	97.1	63.2	3.8
29	110	39.4	1467	557	67.3	12.7	98.5	63.5	3.8
19	91	32.3	1558	589	67.9	14.1	99.2	63.8	3.7
18	86	30	1644	619	69.1	14.8	99.6	64.1	3.7
12	94	31	1738	650	73.1	15.3	99.6	64.5	3.6
13	76	25	1814	675	73.3	17.1	99.7	64.8	3.6
30	83	27.3	1897	702	73.4	16.4	99.7	65.2	3.6
11	203	66	2100	768	74.1	10.8	99.6	65.9	3.5
25	87	28.3	2187	796	74.1	16.2	99.7	66.3	3.5
16	185	60	2372	856	74.3	11.3	99.6	66.8	3.4
26	131	40.4	2503	896	78.1	14.3	99.5	67.4	3.4

---

27	1043	303	3546	1199	82.9	6	73.7	71.3	3.3
8	104	28	3650	1227	89.4	19.3	71.8	71.7	3.3
14	175	46	3825	1273	91.6	15.5	63.1	72.4	3.3
20	374	38.4	4199	1311	232	40	0	79.1	3.6
24	233	15.2	4432	1326	362.4	96.8	0	92.3	4.2
2	274	14	4706	1340	457.7	126.3	0	108.6	4.9
22	664	33.3	5370	1373	465.6	84	0	123.9	5.5
23	478	23.2	5848	1396	480.4	103.2	0	138.5	6.1
21	209	10.1	6057	1406	483	156.4	0	152.1	6.7
15	410	18	6467	1424	529.7	128.7	0	166.5	7.3
1	708	30	7175	1454	548	103.7	0	180.5	7.8
28	110	4.04	7285	1458	628.3	318.9	0	196.5	8.5
17	85	2	7370	1460	955.6	684.3	0	223.3	9.6

## 99GR72 Apatite

n (cryst.)	Ns	Ni	Sum Ns	Sum Ni	Grain age	± 1s	Chi-sq.	Sum age	± 1s
2	0	31	0	31	0	0	---		
1	0	31	0	62	0	0	---		
9	0	24	0	86	0	0	---		
4	0	23	0	109	0	0	---		
8	0	19	0	128	0	0	---		
5	0	18	0	146	0	0	---		
7	0	15	0	161	0	0	---		
10	0	14	0	175	0	0	---		
6	0	14	0	189	0	0	---		
13	0	10	0	199	0	0	---		
11	0	8	0	207	0	0	---		
19	0	7.18	0	214	0	0	---		
16	0	7.18	0	221	0	0	---		
12	0	7	0	228	0	0	---		
20	0	6.15	0	234	0	0	---		
14	0	6	0	240	0	0	---		
17	0	5.13	0	245	0	0	---		
18	0	4.1	0	249	0	0	---		
15	0	2.05	0	251	0	0	---		
3	1	32	1	283	7.8	7.9	99	0.9	0.9

## 99GR73 Zircon

n (cryst.)	Ns	Ni	Sum Ns	Sum Ni	Grain age	± 1s	Chi-sq.	Sum age	± 1s
1	82	25	82	25	93	21.5	---	93	21.5
12	111	32.3	193	57	97.5	19.8	87.2	96	14.9
25	139	36.4	332	93	108.1	20.5	86.1	101.1	12.4
16	8	2.08	340	95	108.9	84.9	95.8	101.4	12.3
27	49	12.6	389	107	110.5	35.2	98.2	103	11.8
18	25	6.24	414	113	113.4	50.9	99.3	103.8	11.6
29	53	12.6	467	125	119.4	37.7	99.4	105.8	11.3
5	26	5.15	493	130	142.6	69	99.2	107.4	11.2
2	103	19	596	149	153	38.6	92.4	113.2	11.1
28	49	8.79	645	157	157.3	57.9	90.6	116.3	11.1
9	120	21	765	178	161	38.5	80.4	121.6	11
19	60	6.24	825	184	268.9	113.5	51	126.8	11.3
14	60	6.24	885	190	268.9	113.5	30	131.7	11.5
21	41	4.16	926	194	275.5	142.1	22.1	134.9	11.7
7	50	5.05	976	199	276.7	129.6	14.7	138.6	11.8
24	128	12.5	1104	211	286.2	85.4	3	147.7	12.3
20	182	17.7	1286	228	287.3	72.3	0.3	178.6	14.3
13	76	7.28	1362	235	291.4	113.5	0.2	184.9	14.6
3	304	28	1666	263	302.8	60.7	0	191.2	14.4
23	92	8.32	1758	271	308.3	112.1	0	197.1	14.6
6	153	9.27	1911	280	454.9	154.7	0	209.6	15.3

17	165	9.36	2076	289	484.7	163.8	0	222.3	16
11	130	7.36	2206	296	485.6	184.8	0	234	16.7
26	299	16.3	2505	312	502.7	129	0	245.4	17.1
10	372	17.9	2877	329	568.6	139.2	0	258.7	17.6
8	378	14.7	3255	343	694.5	186.1	0	276	18.4
22	231	8.32	3486	351	747.8	265.2	0	294.1	19.5
4	559	20	4045	371	752.5	173.3	0	311	20.1
15	32	1.04	4077	372	823.7	821.3	0	329.4	21.3

====BinomFit Program v. 1.8=====

DATE\TIME: 03-09-2001\14:58:15 FILENAME:

C:\PROGRA~1\TRACKKEY\FTPEAKS\99GR73.FTZ

FILE HEADER:"99GR73"

FIT OPTION: Best-fit peaks using the binomial model of Galbraith and Green

-----INITIAL GUESS FOR MODEL PARAMETERS-----

NUMBER OF PEAKS TO FIT = 3

PEAK #)	PEAK AGE	THETA	FRACTION(%)	COUNT
1)	120.00	0.813	16.2	4.69
2)	300.00	0.917	21.6	6.25
3)	600.00	0.958	13.1	3.79

TOTAL RANGE FOR GRAIN AGES = 89.7 to 719.9 Ma

NUMBER OF GRAINS = 29

DEGREES OF FREEDOM FOR FIT = 24

AVERAGE OF THE SE(Z)'S FOR THE GRAINS = 0.37

ESTIMATED WIDTH OF PEAKS IN PD PLOT IN Z UNITS = 0.44

-----PARAMETERS FOR BEST-FIT PEAKS-----

{Standard error for peak age includes group error}

{Peak width is for PD plot assuming a kernel factor = 0.60}

PEAK NUMBER	MEAN	63% CI	95% CI	W(Z)	FRAC (%)	SE (%)	COUNT	
1)	118.0	( -10.8 +11.8)	( -20.2 +24.3)	0.31	35.5	10.0	10.3	
2)	301.1	( -45.2 +53.0)	( -82.4 +112.4)	0.38	32.8	13.3	9.5	
3)	579.1	( -65.3 +73.1)	(-121.2 +151.5)	0.36	31.7	12.7	9.2	
TOTAL:							100.0	29.0

LOG-LIKELIHOOD FOR BEST FIT = -9.0369E+01

CHI-SQUARED VALUE FOR BEST FIT = 2.4565E+01

REDUCED CHI-SQUARED VALUE = 1.0235E+00

DEGREES OF FREEDOM FOR FIT = 24

CONDITION NUMBER FOR COVAR MATRIX = 5.90

NUMBER OF ITERATIONS = 8

====BinomFit Program v. 1.8=====

99GR81 Zircon

n (cryst.)	Ns	Ni	Sum Ns	Sum Ni	Grain age	± 1s	Chi-sq.	Sum age	± 1s
12	231	92	231	92	65.8	8.4	---	65.8	8.4
2	128	50	359	142	67.1	11.4	92.6	66.2	7
19	75	29	434	171	67.8	15	99.1	66.5	6.4

11	99	38	533	209	68.3	13.2	99.8	66.8	5.9
21	63	23.2	596	232	71	17.4	99.9	67.3	5.7
1	194	66	790	298	77	11.3	97.7	69.4	5.3
7	44	14	834	312	82.2	25.4	98.2	70	5.3
13	188	56	1022	368	87.8	13.7	88.4	72.7	5.1
8	175	52	1197	420	88	14.2	82.4	74.6	5
3	105	31	1302	451	88.6	18.4	83	75.6	4.9
5	52	15	1354	466	90.7	26.8	86	76.1	4.9
4	180	50	1534	516	94.1	15.4	78.8	77.8	4.8
9	155	41	1689	557	98.8	17.7	70.8	79.4	4.8
16	161	38	1850	595	110.6	20.3	50.3	81.4	4.8
20	198	46	2048	641	112.4	18.8	30.4	83.6	4.8
22	750	162	2798	803	120.8	11.3	0.8	87	4.6
23	329	69.7	3127	872	123.1	16.8	0.2	89.1	4.6
18	533	106	3660	978	131.1	14.7	0	91.4	4.6
15	54	10	3714	988	140.7	48.7	0	94	4.7
6	229	40	3943	1028	149	26.1	0	96.8	4.8
17	145	25	4088	1053	151	33.1	0	99.4	4.9
10	93	10	4181	1063	240.4	80.4	0	105.9	5.2
14	68	6	4249	1069	291.8	124.7	0	114.1	5.6

====BinomFit Program v. 1.8====  
 DATE\TIME: 12-15-2002\17:44:33 FILENAME:  
 D:\TRACKK~1\FTPEAKS\99GR81.FTZ  
 FILE HEADER:"99GR81"

FIT OPTION: Best-fit peaks using the binomial model of Galbraith and Green

-----INITIAL GUESS FOR MODEL PARAMETERS-----

NUMBER OF PEAKS TO FIT = 2  
 PEAK #) PEAK AGE THETA FRACTION(%) COUNT  
 1) 80.00 0.758 38.7 8.91  
 2) 130.00 0.836 29.9 6.87

TOTAL RANGE FOR GRAIN AGES = 64.1 to 265.7 Ma  
 NUMBER OF GRAINS = 23  
 DEGREES OF FREEDOM FOR FIT = 20  
 AVERAGE OF THE SE(Z)'S FOR THE GRAINS = 0.22  
 ESTIMATED WIDTH OF PEAKS IN PD PLOT IN Z UNITS = 0.25

-----PARAMETERS FOR BEST-FIT PEAKS-----

{Standard error for peak age includes group error}  
 {Peak width is for PD plot assuming a kernel factor = 0.60}

PEAK NUMBER	MEAN	63% CI	95% CI	W(Z)	FRAC(%)	SE(%)	COUNT	
1)	77.0	( -5.2 +5.6)	( -9.9 +11.4)	0.20	50.0	13.7	11.5	
2)	123.3	( -7.7 +8.2)	( -14.6 +16.6)	0.18	50.0	13.7	11.5	
TOTAL:							100.0	23.0

LOG-LIKELIHOOD FOR BEST FIT = -8.3447E+01  
 CHI-SQUARED VALUE FOR BEST FIT = 2.5897E+01  
 REDUCED CHI-SQUARED VALUE = 1.2948E+00  
 DEGREES OF FREEDOM FOR FIT = 20  
 CONDITION NUMBER FOR COVAR MATRIX = 7.82  
 NUMBER OF ITERATIONS = 9

====BinomFit Program v. 1.8=====

## 00GR01 Apatite

n (cryst.)	Ns	Ni	Sum Ns	Sum Ni	Grain age	± 1s	Chi-sq.	Sum age	± 1s
14	0	15	0	15	0	0	---		
11	2	106	2	121	4.1	2.9	59.5	3.6	2.5
12	2	96	4	217	4.5	3.2	85.8	4	2
15	2	95	6	312	4.5	3.2	95.7	4.1	1.7
2	1	47	7	359	4.6	4.6	98.8	4.2	1.6
13	2	86	9	445	5	3.6	99.6	4.4	1.5
22	2	81.7	11	526	5.3	3.8	99.9	4.5	1.4
23	2	66.9	13	592	6.4	4.6	99.9	4.7	1.3
5	2	64	15	656	6.7	4.8	99.9	4.9	1.3
19	5	153	20	808	7.1	3.2	99.9	5.3	1.2
17	8	241	28	1049	7.2	2.6	99.9	5.8	1.1
6	3	83	31	1132	7.8	4.6	99.9	5.9	1.1
4	3	82	34	1214	7.9	4.6	99.9	6	1.1
10	3	74	37	1288	8.7	5.2	99.9	6.2	1.1
16	3	71	40	1359	9.1	5.4	100	6.3	1
9	3	71	43	1430	9.1	5.4	100	6.5	1
21	3	69.9	46	1499	9.3	5.5	100	6.6	1
18	5	115	51	1614	9.4	4.3	100	6.8	1
8	2	42	53	1656	10.3	7.4	100	6.9	1
24	7	137	60	1792	11	4.3	99.9	7.2	1
7	2	39	62	1831	11.1	8	99.9	7.3	1
3	5	95	67	1926	11.3	5.2	99.9	7.5	1
25	1	18.7	68	1944	11.5	11.8	100	7.5	1
20	5	82.7	73	2026	13	6	99.9	7.8	1
1	5	75	78	2101	14.4	6.7	99.7	8	1

## 00GR02 Zircon

n (cryst.)	Ns	Ni	Sum Ns	Sum Ni	Grain age	± 1s	Chi-sq.	Sum age	± 1s
14	100	54	100	54	39.4	6.8	---	39.4	6.8
1	147	70	247	124	44.7	6.6	57.2	42.4	4.9
12	82	37	329	161	47.1	9.5	76.2	43.5	4.4
23	180	78.9	509	239	48.5	6.7	80.2	45.3	3.8
24	201	85	710	323	50.3	6.7	82.1	46.7	3.5
2	183	77	893	400	50.5	7.1	87	47.5	3.2
4	81	33	974	433	52.2	10.9	91.4	47.8	3.2
8	83	33	1057	466	53.5	11.1	93.7	48.2	3.1
25	365	142	1422	607	54.8	5.7	87.9	49.8	2.9
22	68	26.3	1490	633	54.9	12.7	91.5	50	2.9
5	77	29	1567	662	56.4	12.4	93.4	50.3	2.8
10	154	56	1721	718	58.4	9.3	92.1	50.9	2.8
6	66	24	1787	742	58.4	14.1	93.7	51.2	2.8
16	97	34	1884	776	60.6	12.2	93.5	51.6	2.8
26	185	64.7	2069	840	60.7	9	91.1	52.3	2.7



3	206	71	2275	911	61.6	8.7	87.9	53.1	2.7
29	439	145	2714	1055	64.4	6.5	68.8	54.7	2.7
19	77	25.3	2791	1080	64.6	15	71.1	54.9	2.6
7	283	90	3074	1170	66.8	8.4	59.2	55.8	2.6
15	140	43	3214	1213	69.1	12.3	55.1	56.3	2.6
9	329	101	3543	1314	69.1	8.2	40.5	57.3	2.6
17	145	44.5	3688	1358	69.2	12.1	39	57.7	2.6
20	90	27.3	3778	1385	69.9	15.4	40.1	57.9	2.6
21	95	28.3	3873	1413	71.2	15.4	40.2	58.2	2.6
18	95	28.3	3968	1441	71.2	15.4	40.6	58.5	2.6
11	158	47	4126	1488	71.3	12.1	38	58.9	2.6
27	85	22.3	4211	1510	81	19.5	33.7	59.2	2.6
28	86	22.3	4297	1532	82	19.7	29.5	59.6	2.6
13	94	20	4391	1552	99.5	24.7	16.8	60.1	2.6

## 00GR03 Zircon

n (cryst.)	Ns	Ni	Sum Ns	Sum Ni	Grain age	± 1s	Chi-sq.	Sum age	± 1s
43	19	17.3	19	17	26	8.7	---	26	8.7
49	21	16.4	40	33	30.3	10	73.6	28.7	6.8
51	62	39	102	72	37.6	7.8	60.6	33.5	5.3
44	15	9.16	117	81	38.7	16.3	77	34.2	5.1
25	38	22.4	155	103	40.2	10.8	83.2	35.6	4.7
8	188	109	343	212	40.8	5.1	81.9	38.3	3.6
3	152	88	495	300	40.9	5.6	87.7	39	3.1
11	108	62	603	362	41.2	6.7	92.4	39.4	2.9
22	107	59	710	421	42.9	7.1	94.6	39.9	2.8
41	19	10.2	729	431	44.1	17.2	96.9	40	2.8
1	188	95	917	526	46.8	6.1	93.7	41.2	2.6
21	252	127	1169	653	46.9	5.3	90.9	42.3	2.5
17	137	69	1306	722	46.9	7.1	92.1	42.8	2.4
13	393	194	1699	916	47.9	4.5	88.6	43.9	2.3
20	308	151	2007	1067	48.2	5	88.2	44.5	2.2
32	46	22.4	2053	1089	48.6	12.6	91.2	44.6	2.2
38	67	32.6	2120	1121	48.6	10.5	93.4	44.7	2.2
23	80	38.6	2200	1159	49	9.7	95	44.9	2.2
6	59	28	2259	1187	49.8	11.5	96.2	45	2.2
56	89	42.1	2348	1229	50	9.5	96.9	45.2	2.2
7	49	23	2397	1252	50.4	12.8	97.7	45.3	2.2
26	78	36.6	2475	1288	50.4	10.2	98.2	45.4	2.1
55	62	28.8	2537	1316	51	11.6	98.6	45.6	2.1
31	71	32.5	2608	1348	51.6	11	98.9	45.7	2.1
9	178	81	2786	1429	51.9	7.2	98.7	46.1	2.1
4	119	54	2905	1483	52.1	8.7	98.7	46.3	2.1
24	65	29.5	2970	1512	52.1	11.7	99	46.4	2.1
40	45	20.4	3015	1532	52.3	14.1	99.2	46.5	2.1
12	69	31	3084	1563	52.6	11.5	99.4	46.6	2.1
50	122	53.4	3206	1616	54	9	99.3	46.9	2.1
16	66	27	3272	1643	57.7	13.3	99.2	47.1	2.1
15	69	28	3341	1671	58.2	13.2	99.1	47.3	2.1
48	61	24.6	3402	1695	58.5	14.1	99.1	47.4	2.1

18	156	63	3558	1758	58.5	8.9	98.2	47.8	2.1
37	99	39.7	3657	1797	58.9	11.2	97.7	48.1	2.1
47	109	43.1	3766	1840	59.7	10.9	96.9	48.4	2.1
19	57	22	3823	1862	61.2	15.5	96.7	48.5	2.1
33	307	116	4130	1977	62.5	7.1	87.2	49.4	2.1
10	76	27	4206	2004	66.4	15	84.2	49.6	2.1
53	38	13.5	4244	2017	66.7	21.3	84	49.7	2.1
28	93	32.5	4337	2049	67.5	13.9	78.8	50	2.1
2	118	41	4455	2090	67.9	12.5	70.6	50.4	2.1
39	36	12.2	4491	2102	69.6	23.2	70.3	50.5	2.1
27	91	30.5	4582	2132	70.4	14.9	62.9	50.8	2.1
29	51	16.3	4633	2148	74	21.2	59	51	2.1
46	16	5.09	4649	2153	74.2	37.8	60.7	51	2.1
35	90	28.5	4739	2181	74.6	16.2	50.8	51.4	2.1
5	102	32	4841	2213	75.2	15.4	39.6	51.7	2.1
42	39	12.2	4880	2225	75.3	24.8	38	51.8	2.1
36	99	28.5	4979	2253	82	17.6	24.8	52.2	2.2
45	18	5.09	4997	2258	83.4	41.9	25.2	52.3	2.2
14	172	48	5169	2306	84.5	14.1	8.4	53	2.2
54	31	8.21	5200	2314	89	35	7.5	53.1	2.2
52	71	18.5	5271	2332	90.5	23.8	4.3	53.4	2.2
30	164	41.7	5435	2373	92.7	16.4	0.7	57.5	2.3
34	60	13.2	5495	2386	106.8	32.6	0.3	58.4	2.4

=====  
 =====BinomFit Program v. 1.8=====

DATE\TIME: 12-15-2002\17:58:24 FILENAME:  
 D:\TRACKK~1\FTPEAKS\00GR03.FTZ  
 FILE HEADER:"00GR03"

-----INITIAL GUESS FOR MODEL PARAMETERS-----

NUMBER OF PEAKS TO FIT = 2

PEAK #)	PEAK AGE	THETA	FRACTION(%)	COUNT
1)	50.00	0.679	58.7	32.86
2)	70.00	0.748	29.8	16.69

TOTAL RANGE FOR GRAIN AGES = 25.9 to 103.8 Ma  
 NUMBER OF GRAINS = 56  
 DEGREES OF FREEDOM FOR FIT = 53  
 AVERAGE OF THE SE(Z)'S FOR THE GRAINS = 0.24  
 ESTIMATED WIDTH OF PEAKS IN PD PLOT IN Z UNITS = 0.28

-----PARAMETERS FOR BEST-FIT PEAKS-----

{Standard error for peak age includes group error}  
 {Peak width is for PD plot assuming a kernel factor = 0.60}

PEAK NUMBER	PEAK AGE & CONF. INTERVAL (MA)	PEAK WIDTH W(Z)	GRAINS IN PEAK
	MEAN (----63% CI---) (----95% CI---)		FRAC(%) SE(%) COUNT
1)	49.4 ( -2.6 +2.7) ( -5.0 +5.5)	0.20	67.9 15.8 38.0
2)	69.8 ( -6.3 +7.0) ( -11.9 +14.3)	0.24	32.1 15.8 18.0
		TOTAL:	100.0 56.0

LOG-LIKELIHOOD FOR BEST FIT = -1.7676E+02  
 CHI-SQUARED VALUE FOR BEST FIT = 5.1242E+01  
 REDUCED CHI-SQUARED VALUE = 9.6683E-01

DEGREES OF FREEDOM FOR FIT = 53  
 CONDITION NUMBER FOR COVAR MATRIX = 29.40  
 NUMBER OF ITERATIONS = 5  
 =====BinomFit Program v. 1.8=====

00GR04 Apatite

n (cryst.)	Ns	Ni	Sum Ns	Sum Ni	Grain age	± 1s	Chi-sq.	Sum age	± 1s
9	2	51	2	51	8.8	6.3	---	8.8	6.3
7	2	49	4	100	9.1	6.6	96.9	9	4.6
5	2	43	6	143	10.4	7.5	98.5	9.4	3.9
6	1	19	7	162	11.8	12.1	99.5	9.7	3.7
8	2	34	9	196	13.2	9.6	99.5	10.3	3.5
4	2	28	11	224	16	11.7	99.2	11	3.4
16	63	863	74	1087	16.3	2.2	93.8	15.2	1.9
21	5	68.4	79	1155	16.4	7.6	97	15.3	1.8
23	1	13.6	80	1168	16.4	17	98.6	15.3	1.8
15	19	254	99	1421	16.7	4	99.3	15.6	1.7
10	1	13	100	1434	17.2	17.9	99.7	15.6	1.7
2	3	37	103	1471	18.2	10.9	99.9	15.7	1.7
11	54	594	157	2065	20.3	3	98.2	17	1.5
24	2	21	159	2085	21.3	15.8	98.9	17.1	1.5
13	8	82.3	167	2167	21.8	8.1	99.1	17.3	1.5
12	11	112	178	2278	22	7	99.2	17.5	1.5
27	2	19.9	180	2297	22.4	16.7	99.5	17.5	1.5
25	3	28.3	183	2325	23.7	14.4	99.6	17.6	1.5
19	2	18.7	185	2343	24	17.9	99.8	17.7	1.5
3	1	9	186	2352	24.9	26.2	99.9	17.7	1.5
18	4	33.2	190	2385	27	14.3	99.9	17.8	1.5
22	10	79.8	200	2464	28	9.4	99.5	18.2	1.5
14	2	13.2	202	2477	33.9	25.7	99.5	18.3	1.5
20	4	24.9	206	2501	36	19.4	99	18.4	1.5
17	3	18.3	209	2519	36.7	22.9	98.6	18.6	1.5
1	5	30	214	2549	37.3	18	97.1	18.8	1.5
26	11	49.3	225	2598	49.8	16.7	69.2	19.4	1.5

00GR05 Zircon

n (cryst.)	Ns	Ni	Sum Ns	Sum Ni	Grain age	± 1s	Chi-sq.	Sum age	± 1s
4	64	57	64	57	27.5	5.1	---	27.5	5.1
13	26	22	90	79	29	8.4	88.1	27.9	4.4
6	32	27	122	106	29	7.6	98	28.2	3.9
8	56	45	178	151	30.5	6.2	98.6	28.9	3.3
17	46	30	224	181	37.5	8.9	88.2	30.3	3.2
33	142	84.7	366	265	41	5.8	49.4	33.8	2.9
16	72	42	438	307	42	8.3	48.1	34.9	2.8
26	73	42.4	511	349	42.2	8.3	49.5	35.9	2.7
5	14	8	525	357	42.8	19	58.5	36	2.7
27	106	58.5	631	415	44.3	7.4	52.9	37.2	2.6
12	31	17	662	432	44.6	13.5	58.8	37.5	2.6

23	82	43	744	475	46.7	8.9	55.5	38.3	2.6
19	303	158	1047	633	46.9	4.8	36.2	40.5	2.4
14	158	81	1205	714	47.7	6.7	34.1	41.3	2.4
30	84	42.4	1289	756	48.5	9.3	36.2	41.7	2.3
15	41	20	1330	776	50.1	13.8	40.2	41.9	2.3
22	60	25	1390	801	58.7	14.1	33.9	42.5	2.3
1	96	40	1486	841	58.7	11.2	24	43.2	2.3
21	65	27	1551	868	58.8	13.6	20.7	43.7	2.3
31	153	60.5	1704	928	61.8	9.6	8.9	44.9	2.3
29	74	29.3	1778	957	61.8	13.7	7.1	45.5	2.3
18	64	24	1842	981	65.1	15.7	5.4	45.9	2.3
25	57	19.2	1899	1000	72.6	19.3	3.4	46.5	2.4
11	67	20	1966	1020	81.7	21	1.3	47.2	2.4
3	86	20	2052	1040	104.7	26.2	0.1	51	2.6
2	59	13	2111	1053	110.5	34	0	53.3	2.7
10	263	54	2374	1107	118.5	18.1	0	55.7	2.7
28	40	8.07	2414	1115	120.6	46.7	0	58.1	2.8
9	31	5	2445	1120	150.5	72.7	0	61.3	3
24	68	10.1	2513	1130	163.6	55.5	0	64.7	3.1
32	86	12.1	2599	1142	172.2	53.2	0	68.2	3.3
7	60	8	2659	1150	181.6	68.6	0	71.8	3.4
20	87	7	2746	1157	298.2	117.5	0	78.7	3.8

====BinomFit Program v. 1.8====  
 DATE\TIME: 12-15-2002\18:41:42 FILENAME:  
 D:\TRACKK~1\FTPEAKS\00GR05.FTZ  
 FILE HEADER:"00GR05"

FIT OPTION: Best-fit peaks using the binomial model of Galbraith and Green

-----INITIAL GUESS FOR MODEL PARAMETERS-----

NUMBER OF PEAKS TO FIT = 3  
 PEAK #) PEAK AGE THETA FRACTION(%) COUNT  
 1) 30.00 0.550 14.3 4.73  
 2) 50.00 0.672 34.6 11.43  
 3) 140.00 0.852 9.7 3.21

TOTAL RANGE FOR GRAIN AGES = 27.5 to 280.3 Ma  
 NUMBER OF GRAINS = 33  
 DEGREES OF FREEDOM FOR FIT = 28  
 AVERAGE OF THE SE(Z)'S FOR THE GRAINS = 0.26  
 ESTIMATED WIDTH OF PEAKS IN PD PLOT IN Z UNITS = 0.30

-----PARAMETERS FOR BEST-FIT PEAKS-----

{Standard error for peak age includes group error}  
 {Peak width is for PD plot assuming a kernel factor = 0.60}

PEAK NUMBER	PEAK AGE & CONF. INTERVAL (MA)	PEAK WIDTH W(Z)	GRAINS IN PEAK
	MEAN (----63% CI---) (----95% CI---)		FRAC(%) SE(%) COUNT
1)	30.3 ( -4.7 +5.5) ( -8.5 +11.8)	0.25	9.8 7.5 3.2
2)	49.2 ( -2.8 +2.9) ( -5.3 +5.9)	0.22	61.8 10.3 20.4
3)	133.8 ( -13.2 +14.6) ( -24.6 +30.1)	0.32	28.5 8.3 9.4
TOTAL:			100.0 33.0

LOG-LIKELIHOOD FOR BEST FIT = -1.1955E+02  
 CHI-SQUARED VALUE FOR BEST FIT = 3.3437E+01  
 REDUCED CHI-SQUARED VALUE = 1.1942E+00

DEGREES OF FREEDOM FOR FIT = 28  
 CONDITION NUMBER FOR COVAR MATRIX = 15.85  
 NUMBER OF ITERATIONS = 9  
 =====BinomFit Program v. 1.8=====

00GR06 Apatite

n (cryst.)	Ns	Ni	Sum Ns	Sum Ni	Grain age	± 1s	Chi-sq.	Sum age	± 1s
11	0	4.9	0	4	0	0	---		
9	0	3.92	0	7	0	0	---		
2	0	5	0	12	0	0	---		
7	1	102	1	114	2.1	2.1	98.8	1.9	1.9
5	24	695	25	809	7.5	1.6	70.5	6.7	1.4
3	14	387	39	1196	7.8	2.1	80.9	7.1	1.2
4	6	146	45	1342	8.9	3.7	86.9	7.3	1.1
6	6	96	51	1438	13.5	5.7	73.6	7.7	1.1
8	1	9.79	52	1447	22.1	23.2	71.2	7.8	1.1
1	4	32	56	1479	27	14.4	27.5	8.2	1.1
12	1	5.87	57	1484	36.8	39.8	21.5	8.3	1.2
10	4	18.6	61	1502	46.4	25.6	1.2	8.8	1.2
13	8	28.6	69	1530	60.3	24.2	0	17.9	2.3

=====BinomFit Program v. 1.8=====

DATE\TIME: 12-15-2002\18:47:23 FILENAME:  
 D:\TRACKK~1\FTPEAKS\00GR06.FTZ  
 FILE HEADER:"00GR06"

FIT OPTION: Best-fit peaks using the binomial model of Galbraith and Green

-----INITIAL GUESS FOR MODEL PARAMETERS-----

NUMBER OF PEAKS TO FIT = 2

PEAK #)	PEAK AGE	THETA	FRACTION(%)	COUNT
1)	8.00	0.036	22.3	2.90
2)	40.00	0.156	12.8	1.66

TOTAL RANGE FOR GRAIN AGES = 3.2 to 63.0 Ma  
 NUMBER OF GRAINS = 13  
 DEGREES OF FREEDOM FOR FIT = 10  
 AVERAGE OF THE SE(Z)'S FOR THE GRAINS = 0.88  
 ESTIMATED WIDTH OF PEAKS IN PD PLOT IN Z UNITS = 1.02

-----PARAMETERS FOR BEST-FIT PEAKS-----

{Standard error for peak age includes group error}  
 {Peak width is for PD plot assuming a kernel factor = 0.60}

PEAK NUMBER	PEAK AGE & CONF. INTERVAL (MA)	PEAK WIDTH	GRAINS IN PEAK
	MEAN (----63% CI---) (----95% CI---)	W(Z)	FRAC(%) SE(%) COUNT
1)	8.0 ( -1.1 +1.3) ( -2.0 +2.7)	0.49	69.7 17.9 9.1
2)	42.5 ( -11.7 +16.2) ( -19.9 +37.4)	0.65	30.3 17.9 3.9
		TOTAL:	100.0 13.0

LOG-LIKELIHOOD FOR BEST FIT = -2.5710E+01  
 CHI-SQUARED VALUE FOR BEST FIT = 9.2473E+00  
 REDUCED CHI-SQUARED VALUE = 9.2473E-01  
 DEGREES OF FREEDOM FOR FIT = 10

CONDITION NUMBER FOR COVAR MATRIX = 5.46  
 NUMBER OF ITERATIONS = 8

====BinomFit Program v. 1.8=====

00GR06 Zircon

n (cryst.)	Ns	Ni	Sum Ns	Sum Ni	Grain age	± 1s	Chi-sq.	Sum age	± 1s
16	50	33.3	50	33	33.4	7.5	---	33.4	7.6
2	58	38	108	71	33.9	7.2	95.1	33.8	5.3
25	91	59.1	199	130	34.2	5.8	99.5	34	4
1	262	165	461	295	35.3	3.7	99.4	34.7	2.8
11	498	272	959	567	40.7	3.3	67.1	37.6	2.3
24	57	28.5	1016	595	44.4	10.3	72.1	37.9	2.3
4	40	20	1056	615	44.4	12.2	78.3	38.1	2.3
5	365	182	1421	797	44.5	4.3	59.8	39.6	2.2
21	304	151	1725	948	44.6	4.7	56.3	40.4	2.1
8	54	26	1779	974	46.1	11.1	63	40.6	2.1
14	21	10.1	1800	984	46.2	17.8	70.7	40.6	2.1
13	72	34	1872	1018	47	9.9	74.1	40.8	2.1
12	47	22	1919	1040	47.4	12.3	78.2	41	2.1
3	235	109	2154	1149	47.9	5.8	71.6	41.6	2
6	127	57	2281	1206	49.5	8	69.4	42	2
10	115	50	2396	1256	51	8.8	66.2	42.4	2
15	42	18.2	2438	1274	51.3	14.5	69.5	42.5	2
20	58	22.2	2496	1296	57.9	14.6	64.8	42.8	2
9	187	70	2683	1366	59.2	8.5	35.6	43.6	2
18	57	21.2	2740	1387	59.6	15.3	32.8	43.9	2
7	95	35	2835	1422	60.2	12.1	25.2	44.3	2
19	42	15.1	2877	1437	61.5	18.5	24.6	44.5	2
23	75	26.5	2952	1463	62.8	14.3	19.5	44.8	2
22	245	82.8	3197	1545	65.6	8.6	3.7	45.9	2.1
17	118	10.1	3315	1555	255.4	84.2	0	57.1	2.6

====BinomFit Program v. 1.8=====

DATE\TIME: 12-18-2002\11:12:22 FILENAME:  
 D:\TRACK~1\FTPEAKS\00GR06.FTZ  
 FILE HEADER:"00GR06"

FIT OPTION: Best-fit peaks using the binomial model of Galbraith and Green

-----INITIAL GUESS FOR MODEL PARAMETERS-----

NUMBER OF PEAKS TO FIT = 3  
 PEAK #) PEAK AGE THETA FRACTION(%) COUNT  
 1) 42.00 0.654 53.1 13.27  
 2) 55.00 0.713 45.2 11.29  
 3) 300.00 0.932 1.7 0.43

TOTAL RANGE FOR GRAIN AGES = 33.2 to 244.6 Ma  
 NUMBER OF GRAINS = 25  
 DEGREES OF FREEDOM FOR FIT = 20  
 AVERAGE OF THE SE(Z)'S FOR THE GRAINS = 0.22  
 ESTIMATED WIDTH OF PEAKS IN PD PLOT IN Z UNITS = 0.25

-----PARAMETERS FOR BEST-FIT PEAKS-----

{Standard error for peak age includes group error}  
 {Peak width is for PD plot assuming a kernel factor = 0.60}

PEAK NUMBER	----PEAK AGE & CONF. INTERVAL (MA)----				PEAK WIDTH	--GRAINS IN PEAK----		
	MEAN	(---63% CI---)	(---95% CI---)		W(Z)	FRAC(%)	SE(%)	COUNT
1)	42.7	( -2.4 +2.5)	( -4.6 +5.1)		0.16	62.4	23.4	15.6
2)	56.7	( -6.0 +6.7)	( -11.1 +13.8)		0.21	33.6	23.3	8.4
3)	257.7	( -71.6 +98.4)	(-121.7 +226.6)		0.38	4.0	3.9	1.0
					TOTAL: 100.0			25.0

LOG-LIKELIHOOD FOR BEST FIT = -8.4463E+01  
 CHI-SQUARED VALUE FOR BEST FIT = 2.1439E+01  
 REDUCED CHI-SQUARED VALUE = 1.0720E+00  
 DEGREES OF FREEDOM FOR FIT = 20  
 CONDITION NUMBER FOR COVAR MATRIX = 148.43  
 NUMBER OF ITERATIONS = 15  
 =====BinomFit Program v. 1.8=====

## Curriculum Vitae

Geoffrey, Modeste, Henri Ruiz

### Personal

Address Geological Institute  
Sonneggstrasse, 5  
ETH Zentrum  
8092 Zürich  
Switzerland.  
Tel: +41 1632 37 02 (fax: 10-80)  
Email: ruiz@erdw.ethz.ch

Date of birth: 8 May 1973  
Nationality: French  
Marital status: Married

### Education

- 1998-2002** Ph.D student at the Swiss Federal Institute of Technology, Institute of Geology, ETH Zürich, Switzerland. Thesis title: "Exhumation of the northern Sub-Andean Zone of Ecuador, and its source region: a combined thermochronological and heavy mineral approach". Supervised by P.D. W. Winkler, Dr. D. Seward, Prof. Burg J.P., and Dr. E. Jaillard.
- 1996-1997** D.E.A. (Diplôme d'Études Approfondies) 'Structure and Evolution of the Lithosphere: University Montpellier II Sciences et Techniques, Laboratory of Tectonics (Supervisor J.P. Petit).  
  
Title : « *Reactivation of calcitic joints into faults: application of the cathodoluminescence analysis to the Matelles area (Languedoc-France)* ».
- 1991-1996** DEUG A, Licence and Maîtrise des Sciences Physiques de la Terre Licence (Mathematics-Physics-Chemistry, Earth Sciences (Geology, Geochemistry, Geophysics): University Paris VII Jussieu-Institut de Physique du Globe de Paris (IPGP), 2 place Jussieu, 75251 Paris Cedex 5.
- 1988- 1991** Baccalauréat C (Mathematics-Physics-Chemistry)

Languages: English and Spanish